



JAEA-Review

2015-044

DOI:10.11484/jaea-review-2015-044

Proceedings of the 12th International Workshop on Beryllium Technology (BeWS-12)

(Eds.) Jae-Hwan KIM and Masaru NAKAMICHI

Sector of Fusion Research and Development

March 2016

Japan Atomic Energy Agency

日本原子力研究開発機構

JAEA-Review

本レポートは国立研究開発法人日本原子力研究開発機構が不定期に発行する成果報告書です。
本レポートの入手並びに著作権利用に関するお問い合わせは、下記あてにお問い合わせ下さい。
なお、本レポートの全文は日本原子力研究開発機構ホームページ (<http://www.jaea.go.jp>)
より発信されています。

国立研究開発法人日本原子力研究開発機構 研究連携成果展開部 研究成果管理課
〒319-1195 茨城県那珂郡東海村大字白方2番地4
電話 029-282-6387, Fax 029-282-5920, E-mail:ird-support@jaea.go.jp

This report is issued irregularly by Japan Atomic Energy Agency.
Inquiries about availability and/or copyright of this report should be addressed to
Institutional Repository Section,
Intellectual Resources Management and R&D Collaboration Department,
Japan Atomic Energy Agency.
2-4 Shirakata, Tokai-mura, Naka-gun, Ibaraki-ken 319-1195 Japan
Tel +81-29-282-6387, Fax +81-29-282-5920, E-mail:ird-support@jaea.go.jp

© Japan Atomic Energy Agency, 2016

JAEA-Review 2015-044

Proceedings of the 12th International Workshop on Beryllium Technology (BeWS-12)

(Eds.) Jae-Hwan KIM and Masaru NAKAMICHI

Sector of Fusion Research and Development
Japan Atomic Energy Agency
Rokkasho-mura, Kamikita-gun, Aomori-ken

(Received December 17, 2015)

The 12th International Workshop on Beryllium Technology (BeWS-12) was held on 10-11 September 2015, at the International Convention Center Jeju (ICCJEJU) in Jeju Island, South Korea. This workshop has been held every 2 years from 1993. The objective of this workshop is to disseminate results of research and technology development in areas relevant to beryllium utilization in fusion nuclear power systems. In this workshop, a lot of researchers and technicians engaged in R&D on beryllium related materials and fusion engineering attended and discussed. This report has been compiled the manuscripts and the presentation files in the BeWS-12.

Keywords : Beryllium, Fusion Engineering, Irradiation Effect, Health and Safety,
Beryllide Application

第 12 回ベリリウム技術に関する国際会議 (BeWS-12) 論文集

日本原子力研究開発機構 核融合研究開発部門

(編) 金 宰煥、中道 勝

(2015 年 12 月 17 日受理)

第 12 回ベリリウム技術に関する国際会議 (The 12th International Workshop on Beryllium Technology (BeWS-12)) は、平成 27 年 9 月 10 日 (木) 及び 11 日 (金) の 2 日間に渡り、韓国済州島の済州国際コンベンションセンター (ICCJEJU) にて開催された。本国際会議は、1993 年から 2 年毎に開催されており、今回で 12 回目となる。本国際会議では、世界におけるベリリウム関連材料 (ベリリウム金属及びその合金、金属間化合物など) と核融合炉工学研究開発に携わる研究者及び技術者が一同に会し、最新研究成果報告、討論及び情報交換を行うものであり、本テーマにおける研究活動の一層の活性化を図ることを目的としている。本報告書は、当該会議における論文及び発表資料を取りまとめたものである。

Content

1. Introduction	1
2. Manuscripts and Presentation Files	3
2.1 Agenda of BeWS-12	3
2.2 Plenary Session.....	7
2.2.1 Development and Qualification of Beryllium Materials for the EU HCPB Test Blanket Module: Strategy and R&D Achievements	7
M. Zmitko (F4E) <i>et al.</i>	
2.2.2 Status of R&D Activities on Beryllium for ITER Blanket First Wall Application in Russian Federation	20
I.B. Kupriyanov (JSC VNIINM) <i>et al.</i>	
2.2.3 Beryllium Production and Applications Overview at Materion	30
C.K. Dorn (Materion) <i>et al.</i>	
2.2.4 Recent Results on DEMO Activities and IFMIF/EVEDA under BA Program	52
T. Yamanishi (JAEA) <i>et al.</i>	
2.2.5 Material Development Strategy for HCCR-TBS in KO	62
Y.H.Park (NFRI) <i>et al.</i>	
2.3 Technical Session 1: Production, Forming and Joining	77
2.3.1 Development of Beryllium Casting Alloy for Instrument Application.....	77
I.Gvozdkov (JSC “Kompozit”) <i>et al.</i>	
2.3.2 Validation and Installation of Large Beryllium Structures at CERN	78
M.A. Gallilee (CERN) <i>et al.</i>	
2.3.3 Joining of Beryllium to CuCrZr and Ferritic-Martensitic Steels for Plasma Facing Components	81
J.Y. Park (KAERI) <i>et al.</i>	
2.3.4 Development of Beryllium Products in NGK	90
K. Nojiri (NGK)	

2.3.5 Distribution of Beryllium Pebble Size by Rotation Electrode Process	95
R. Fukatsu (NGK) <i>et al.</i>	
2.4 Technical Session 2: Irradiation Effects, High Heat Flux Performance, Modeling, Production.....	97
2.4.1 Experimental Investigation of Irradiation Effects in Beryllium Beam Window after Exposure in the NuMI Beamline: Preliminary Results and Plans	97
V. Kuksenko (University of Oxford) <i>et al.</i>	
2.4.2 Accounting of Neutron Irradiation in the Thermo-mechanical Computational Model of a Circular Beryllium Reflector	109
T. Trifonov (NIKIET)	
2.4.3 Tritium Bulk Distribution in Tritium Loaded Beryllium Pebbles	110
E. Pajuste (University of Latvia) <i>et al.</i>	
2.4.4 Effect of Hydrogen on Equilibrium Shape of Gas Bubbles in Beryllium	118
D. Bachurin (KIT) <i>et al.</i>	
2.4.5 Thermal Shock Performance Development of S-65 Grade Beryllium	131
B. Spilker (Forschungszentrum Jülich) <i>et al.</i>	
2.5 Technical Session 3: Composition Control and Characterization	141
2.5.1 Effect of Impurity and Grain Size on Mechanical Properties and Reactivity of Beryllium	141
Y. Akatsu (JAEA) <i>et al.</i>	
2.5.2 Microstructural Evolution and Adhesion of Thin Coatings in the Be-C-O and Be-W-O Systems under Annealing	144
R. Mateus (instituto superior técnico) <i>et al.</i>	
2.5.3 Surface Cleaning of Beryllium Parts from Be-containment Dust	152
A. Milkov (JSC “Kompozit”) <i>et al.</i>	
2.5.4 Experimental and Calculated Data of the Beryllium Oxide Slurry Formation Process	159
U. Zhapbasbayev (Kazakh-British Technical University) <i>et al.</i>	

2.6 Technical Session 4: Health and Safety Issues	173
2.6.1 Working Environment Control in Beryllium Handling Area	173
K. Yonehara (KAKEN) <i>et al.</i>	
2.6.2 An Overview of Current Beryllium Environmental, Health, and Safety Regulatory Activities	180
C.K. Dorn (Materion) <i>et al.</i>	
2.6.3 Recent Achievements and Related Safety Issues Concerning Beryllide Application	191
A. Goraieb (KBHF, GmbH) <i>et al.</i>	
 2.7 Technical Session 5: Beryllide Application.....	203
2.7.1 Recent Progress on R&D of Beryllides as Advanced Neutron Multipliers for DEMO Blanket in the Broader Approach Activities	203
M. Nakamichi (JAEA) <i>et al.</i>	
2.7.2 Extrusion of Be-Ti Powder at 650 °C	207
P. Kurinskiy (KIT) <i>et al.</i>	
2.7.3 Ab-initio Simulations of Intrinsic Defects in Be ₁₂ X (X=Ti,V,W,Mo)	210
M. L. Jackson (Imperial College) <i>et al.</i>	
2.7.4 Synthesis of Beryllides Powder for Advanced Neutron Multiplier	218
Y. Natori (KAKEN) <i>et al.</i>	
2.7.5 Preliminary Characterization of Beryllides as Advanced Neutron Multiplier	225
S. Nakano (JAEA) <i>et al.</i>	
2.7.6 Synthesis and Characterization of Ternary Beryllide	229
J.-H. Kim (JAEA) <i>et al.</i>	
2.7.7 Long-time Exposures of Be ₁₂ Ti to 1% Water Vapor at 1273 K	233
K. Munakata (Akita University) <i>et al.</i>	
2.7.8 Comparison of Tritium Release Behavior of Different Beryllium Materials	245
V. Chakin (KIT) <i>et al.</i>	
 Appendix Group Photos	259

目次

1. はじめに	1
2. 原稿（発表資料）	3
2.1 アジェンダ	3
2.2 プレナリーセッション	7
2.2.1 EU HCPB TBM におけるベリリウム材料の開発及びその資格：戦略と R&D 研究成果	7
M. Zmitko (F4E) <i>et al.</i>	
2.2.2 ロシアの ITER ブランケット第一壁におけるベリリウムの現状と R&D 研究 活動	20
I.B. Kupriyanov (JSC VNIINM) <i>et al.</i>	
2.2.3 核融合関連活動を含むベリリウム製造及び応用	30
C.K. Dorn (Materion) <i>et al.</i>	
2.2.4 BA 活動における DEMO 及び IFMIF/EVEDA 研究に関する最新結果	52
山西 敏彦(JAEA) <i>et al.</i>	
2.2.5 韓国の HCCR-TBS 開発における材料開発	62
Y. H. Park (NFRI) <i>et al.</i>	
2.3 テクニカルセッション 1：生産、成形、接合	77
2.3.1 機械応用におけるベリリウム鋳造合金の開発	77
I.Gvozdkov (JSC “Kompozit”) <i>et al.</i>	
2.3.2 CERN における大型ベリリウム構造材の実証及び設置	78
M.A. Gallilee (CERN) <i>et al.</i>	
2.3.3 プラズマ接触部分における CuCrZr 及びフェライト/マルテンサイト鋼へのベ リリウムの接合技術	81
J.Y. Park (KAERI) <i>et al.</i>	
2.3.4 NGK でのベリリウム製品の開発	90
野尻 敬午 (NGK)	
2.3.5 回転電極法によるベリリウム微小球サイズの分布	95
深津 遼平(NGK) <i>et al.</i>	

2.4	テクニカルセッション 2: 照射効果, 高熱流動, モデリング, 生産.....	97
2.4.1	NuMi ビームラインでの暴露後のベリリウムビームウィンドウにおける照射効果の実験的な調査.....	97
	V. Kuksenko (University of Oxford) <i>et al.</i>	
2.4.2	円形ベリリウム反射材の熱機械的計算モデルにおける中性子照射の評価.....	109
	T. Trifonov (NIKIET)	
2.4.3	トリチウムの暴露したベリリウム微小球におけるトリチウム分布.....	110
	E. Pajuste (University of Latvia) <i>et al.</i>	
2.4.4	ベリリウムにおけるガスバブルの平衡形状に与える水素の影響.....	118
	D. Bachurin (KIT) <i>et al.</i>	
2.4.5	S-65 グレードベリリウムの熱衝撃実証法の開発.....	131
	B. Spilker (Forschungszentrum Jülich) <i>et al.</i>	
2.5	テクニカルセッション 3: 組成制御, 特性評価.....	141
2.5.1	ベリリウムの機械的な特性及び反応性に及ぼす不純物や粒径の効果.....	141
	赤津 孔明(JAEA) <i>et al.</i>	
2.5.2	焼鈍下の Be-C-O と Be-W-O 系における微細構造変化及び薄膜コーティングの付着特性.....	144
	R. Mateus (instituto superior técnico) <i>et al.</i>	
2.5.3	Be-汚染ダストからのベリリウム部品の表面洗浄.....	152
	A. Milkov (JSC “Kompozit”) <i>et al.</i>	
2.5.4	材料プロセスにおけるベリリウム酸化物スラリの実験及び計算データ.....	159
	U. Zhapbasbayev (Kazakh-British Technical University) <i>et al.</i>	
2.6	テクニカルセッション 4: 健康、安全.....	173
2.6.1	ベリリウム取扱い場所における作業環境測定.....	173
	米原 和男 (KAKEN) <i>et al.</i>	
2.6.2	現在ベリリウム環境、健康、安全調整活動の概要.....	180
	C.K. Dorn (Materion) <i>et al.</i>	
2.6.3	ベリライド応用に関する最新成果及び安全性問題.....	191
	A. Goraieb (KBHF, GmbH) <i>et al.</i>	
2.7	テクニカルセッション 5: ベリライド応用.....	203
2.7.1	DEMO 炉における先進中性子増倍材の最新 R&D 成果.....	203
	中道 勝 (JAEA) <i>et al.</i>	

2.7.2	650°Cでの Be-Ti 粉末押し出し法.....	207
	P. Kurinskiy (KIT) <i>et al.</i>	
2.7.3	Be12X 系材料における固有欠陥とその移動に関する研究.....	210
	M. L. Jackson (Imperial College) <i>et al.</i>	
2.7.4	先進中性子増倍材におけるベリライド粉末の合成技術.....	218
	名取 ユリ(KAKEN) <i>et al.</i>	
2.7.5	先進中性子増倍材としてのベリライドの予備的な特性評価.....	225
	中野 優 (JAEA) <i>et al.</i>	
2.7.6	3 元系ベリライドの合成及び特性評価.....	229
	J.-H. Kim (JAEA) <i>et al.</i>	
2.7.7	長時間のベリライドの酸化挙動.....	233
	宗像 健三(Akita University) <i>et al.</i>	
2.7.8	トリチウム/水素混合ガスパージによる先進ベリリウム材料のトリチウム放 出特性.....	245
	V. Chakin (KIT) <i>et al.</i>	
付録	集合写真.....	259

1. Introduction

The 12th International Workshop on Beryllium Technology (BeWS-12) was held on 10-11 September at the International Convention Center Jeju (ICCJEJU) in Jeju Island, Korea within a framework created by the International Energy Agency (IEA) Energy Technology Initiative on Fusion Materials. This workshop has been held every 2 years from 1993. The objective of this workshop is to disseminate results of research and technology development in areas relevant to beryllium utilization in fusion nuclear power systems. In this workshop, a lot of researchers and technicians engaged in R&D on beryllium related materials and fusion engineering attended and discussed. This JAEA-Review has been compiled the manuscripts and the presentation files in the BeWS-12.

The BeWS-12 was divided into one plenary and five technical sessions. As to the plenary session, as unprecedented experiment, the joint session with the 18th International Workshop on Ceramic Breeder Blanket Interactions (CBBI-18) had been conducted including the panel session by the plenary speakers chaired by Dr. J. van der Laan who is engaged in ITER-IO. In the joint session, 5 presentations were delivered covering R&D for DEMO breeding blankets, development of TBMs and preparing their procurement in EU, JA and KO, as well as the qualification of bulk beryllium for ITER First Wall panels, accompanied by a capacity overview of the industrial beryllium supplier Materion. Discussion points for presenters and panel session had been provided as follows.

- 1) Materials production demand (quantities, delivery, quality)
- 2) Towards fusion power plants (multipliers and breeders behavior in TBM and DEMO)
- 3) Thermal-mechanical properties of pebble bed
- 4) Modeling for blanket design including safety and activation profiles

The five technical sessions consisted as follows.

- 1) Production, Forming and Joining
- 2) Irradiation Effects, High Heat Flux Performance, Modeling
- 3) Composition Control and Characterization
- 4) Health and Safety Issues
- 5) Beryllide Application

In this workshop, there were 30 oral presentations with 40 attendees of 14 persons from EU, 10 persons from Japan, 5 persons from Korea, 7 persons from Russia, 3 persons from US and one person from Kazakhstan.

Prof. Mario Dalle Donne Memorial Award (MDDMA) has been established at

previous BeWS-11 held in Barcelona for encouraging someone with outstanding achievements concerning beryllium-related research. It had been awarded to Dr. Vladimir Chakin who engaged in KIT and have a lot of outstanding scientific achievement in the beryllium-related fields.

2. Manuscripts and presentation files

2.1 Agenda of BeWS-12

12th International Workshop on Beryllium Technology



BeWS-12 Final program (10-11 September 2015)

Thursday, September 10

09:00 - 10:00 Registration open

Plenary Joint Session in conjunction with CBBI

(International Workshop on Ceramic Breeder Blanket Interactions)

Chair : Jaap van der Laan				
Opening Speech		10:10	10:20	
M. Zmitko (P0007)	F4E	10:20	10:40	Development and qualification of beryllium materials for the EU HCPB Test Blanket Module: Strategy and R&D achievements
I.B. Kupriyanov (P0027)	JSC VNIINM	10:40	11:00	Status and R&D Activities of beryllium for ITER blanket first wall application in Russia Federation
C.K. Dorn (P0023)	Materion, USA	11:00	11:20	Beryllium production and applications overview including fusion related activities
T. Yamanishi (M. Nakamichi) (P0016)	JAEA	11:20	11:40	Recent results on DEMO activities and IFMIF/EVEDA under BA program
S-Y. Cho (Y.H. Park) (P0022)	NFRI	11:40	12:00	Material development strategy for HCCR-TBS in KO
Panel (presenters) forum discussion		12:00	12:40	

12:40 - 14:00 Lunch break

Technical Session 1 : Production, forming and joining

Chair : V. Kuksenko				
I. Gvozdkov (P0010)	JSC "Kompozit"	14:00	- 14:20	Development of beryllium casting alloy for instrument application
M.A.Gallilee (P0024)	CERN	14:20	- 14:40	Validation and Installation of Large Beryllium Structures at CERN
J.-Y. Park (P0025)	KAERI	14:40	- 15:00	Joining of Beryllium to CuCrZr and Ferritic-Martensitic Steels for Plasma Facing Components
K. Nojiri (P0028)	NGK Insulators, LTD	15:00	- 15:20	Development of Beryllium products in NGK
R. Fukatsu (P0021)	NGK Insulators, LTD	15:20	- 15:40	Distribution of Beryllium Pebble Size by Rotation Electrode Process
		15:40	- 16:00	Coffee break

**Technical Session 2 :
Irradiation effects/High heat flux performance/Modeling/Production**

Chair : M. Zmitko				
V. Kuksenko (P0003)	University of Oxford	16:00	- 16:20	Experimental Investigation of Irradiation Effects in Beryllium Beam Window after Exposure in the NuMI Beamline: Preliminary Results and Plans
Y. Trifonov (P0008)	NIKIET	16:20	- 16:40	ACCOUNTING OF NEUTRON IRRADIATION IN THE THERMO-MECHANICAL COMPUTATIONAL MODEL OF A CIRCULAR BERYLLIUM REFLECTOR
E. Pajuste (P0018)	University of Latvia	16:40	- 17:00	Tritium bulk distribution in tritium loaded beryllium pebbles
D. Bachurin (P0005)	Karlsruhe Institute of Technology	17:00	- 17:20	Effect of hydrogen on equilibrium shape of gas bubbles in beryllium
B. Spilker (P0004)	Forschungszen- trum Jülich	17:20	- 17:40	Thermal Shock Performance Development of S-65 Grade Beryllium
		17:40	- 18:30	Coffee break and Industrial Exhibition
Workshop Banquet		19:00		Restaurant

Friday, September 11

Technical Session 3 : Composition control and characterization/production

Chair : P. Kurinskiy

Y. Akatsu (J.-H.Kim) (P0014)	JAEA	09:20 - 09:40	Effect of impurity and grain size on mechanical properties and reactivity of beryllium
E. Alves (P0017)	Instituto Superior Técnico	09:40 - 10:00	Microstructural evolution and adhesion of thin coatings in the Be-C-O and Be-W-O systems under annealing
A. Milkov (P0011)	JSC "Kompozit"	10:00 - 10:20	Surface cleaning of beryllium parts from Be-containment dust
G. Ramazanova (B. Assilbekov) (P0006)	Kazakh-British Technical University	10:20 - 10:40	Experimental and calculated data of the beryllium oxide slurry formation process

10:40 - 11:00 Coffee break

Technical Session 4 : Health and safety issues

Chair : C.K. Dorn

K. Yonehara (P0019)	Kaken Inc.	11:00 - 11:20	Working environment control in beryllium handling area
C.K. Dorn (P0027)	Materion, USA	11:20 - 11:40	An Overview of Current Beryllium Environmental, Health, and Safety Regulatory Activities
A. Goraieb (P0030)	KBHF, GmbH	11:40 - 12:00	Recent achievements and related safety issues concerning Beryllide application

12:00 - 13:40 Lunch break

Technical Session 5: Beryllide application

Chair : V. Chakin

M. Nakamichi (P0015)	JAEA	13:40 - 14:00	Recent progress on R&D of beryllides as advanced neutron multipliers for DEMO reactor
-------------------------	------	---------------	---

blanket in the Broader Approach activities				
P. Kurinskiy (P0009)	Karlsruhe Institute of Technology	14:00	- 14:20	Extrusion of Be-Ti powder at 650 C
M. L. Jackson (P0002)	Imperial College	14:20	- 14:40	Intrinsic defect accommodation and migration in the Be12X family of materials
Y. Natori (P0020)	Kaken Inc.	14:40	- 15:00	Synthesis of beryllides Powder for Advanced Neutron Multiplier
		15:00	- 15:20	Coffee break
Chair : E. Alves				
S. Nakano (J.-H.Kim) (P0013)	JAEA	15:20	- 15:40	Preliminary characterization of beryllides as advanced neutron multiplier
J-H. Kim (P0001)	JAEA	15:40	- 16:00	Synthesis and characterization of ternary beryllide
K. Munakata (P0029)	Akita University	16:00	- 16:20	Oxidation behavior of beryllides in long term
V. Chakin (P0012)	Karlsruhe Institute of Technology	16:20	- 16:40	Tritium Release from Advanced Beryllium Materials after Loading by Tritium/Hydrogen Gas Mixture
		16:40	- 16:50	Final Conclusion
		17:00		Adjourn

Sponsored by



2.2 Plenary session

2.2.1 Development and qualification of beryllium materials for the EU HCPB Test Blanket Module: Strategy and R&D achievements

**M. Zmitko¹, Y. Poitevin¹, P. Vladimirov², V. Chakin², P. Kurinskiy²,
A. Goraieb³, L. Magielsen⁴, A. Fedorov⁴, E. Alves⁵**

¹*Fusion for Energy (F4E), TBMs and Materials Development, Barcelona, Spain*

²*Institut fuer Materialforschung I, KIT, Karlsruhe, Germany*

³*KBHF GmbH, KIT - Campus Nord, Karlsruhe, Germany*

⁴*NRG Petten, Petten, The Netherlands*

⁵*Instituto Superior Técnico (IST), Universidade de Lisboa, Bobadela, Portugal*

E-mail: milan.zmitko@f4e.europa.eu

Europe has developed two reference breeder blankets concepts that will be tested in ITER under the form of Test Blanket Modules (TBMs) located in a common equatorial port of ITER: i) the Helium-Cooled Lithium-Lead (HCLL) concept which uses the eutectic Pb-15.7Li as both breeder and neutron multiplier, ii) the Helium-Cooled Pebble-Bed (HCPB) concept containing lithium ceramic pebbles as breeder and beryllium pebbles as neutron multiplier. Both concepts are using 9Cr-WVTa Reduced Activation Ferritic Martensitic (RAFM) steel as structural material, the EUROFER, and pressurized Helium technology for heat extraction.

The paper gives a brief general description of the European HCPB TBM design and the main design requirements including the requirements to beryllium multiplier material. The EU TBMs development and qualification plan with identification of the main milestones will be also presented.

The main part of the paper will be devoted to the presentation of beryllium materials development strategy, qualification plan and current status of research, development and characterization. The achieved results on fabrication technologies development, materials characterization and performance under TBM/DEMO relevant conditions, including the performance under neutron irradiation (e.g. HIDOBE irradiation experiments) and thermo-mechanical performance will be overviewed.



12th International Workshop on Beryllium Technology (BeWS-12),
Jeju Island, Korea, September 10-11, 2015

Development and qualification of beryllium materials for the EU HCPB Test Blanket Module: Strategy and R&D achievements



M. Zmitko, Y. Poitevin



P. Vladimirov, V. Chakin, P. Kurinskiy



A. Goraieb



L. Magielsen, A. Fedorov, S. van Til



E. Alves

Table of content



1. Introduction & Background
2. Beryllium materials for HCPB TBM concept
3. R&D achievements
4. Summary – Open issues

1. Introduction & Background

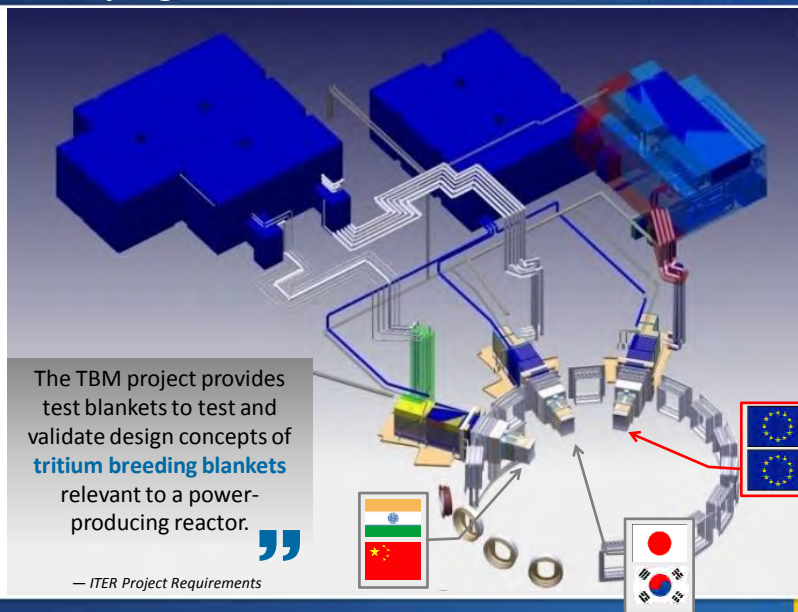
3rd ITER Council (2008) established the TBMs program in ITER



The TBM project provides test blankets to test and validate design concepts of **tritium breeding blankets** relevant to a power-producing reactor.



— ITER Project Requirements



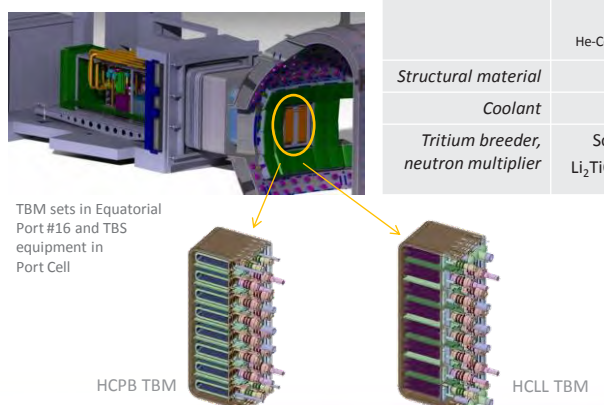
Two European BB concepts in ITER



Europe will test in ITER two DEMO breeder blankets concepts under the form of Test Blanket Modules (TBMs) Systems:

- Helium-Cooled Pebble-Bed (**HCPB**)
- Helium-Cooled Lithium-Lead (**HCLL**)

	HCPB	HCLL
	He-Cooled Pebble-Bed	He-Cooled lithium-Lead
<i>Structural material</i>	EUROFER97	
<i>Coolant</i>	Helium (8 MPa, 300-500°C)	
<i>Tritium breeder, neutron multiplier</i>	Solid pebbles $\text{Li}_2\text{TiO}_3 / \text{Li}_4\text{SiO}_4, \text{Be}$	Liquid Pb-15.7Li



TBM sets in Equatorial Port #16 and TBS equipment in Port Cell

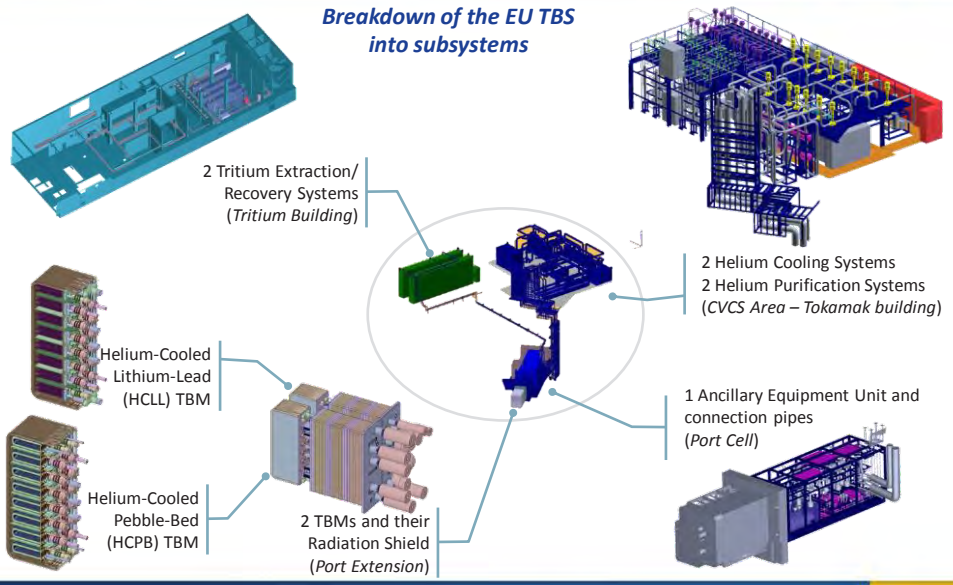
HCPB TBM
HCLL TBM

5

Two European TBM Systems in ITER



Breakdown of the EU TBS into subsystems



2 Tritium Extraction/Recovery Systems (Tritium Building)

2 Helium Cooling Systems
2 Helium Purification Systems (CVCS Area – Tokamak building)

1 Ancillary Equipment Unit and connection pipes (Port Cell)

2 TBM and their Radiation Shield (Port Extension)

Helium-Cooled Lithium-Lead (HCLL) TBM

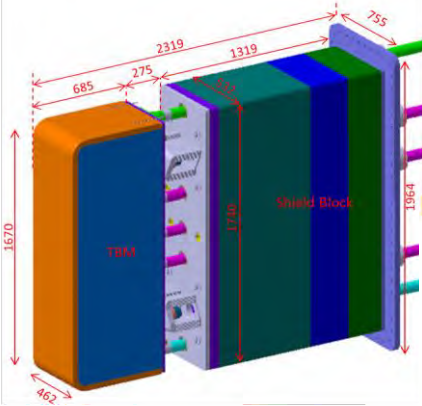
Helium-Cooled Pebble-Bed (HCPB) TBM

6

TBM-set design – global dimensions and materials

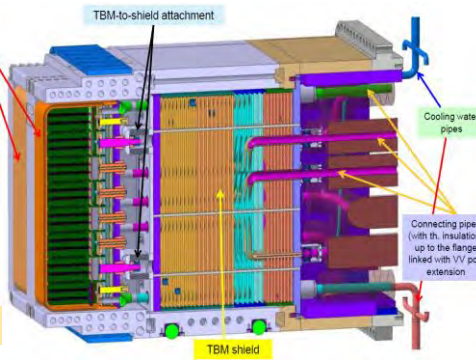


EU TBM dimensions



- TBMs structural material: **EUROFER-97 (X10CrWVTa9-1)**
- Shields material: **Stainless Steel SS-316L(N)-IG**

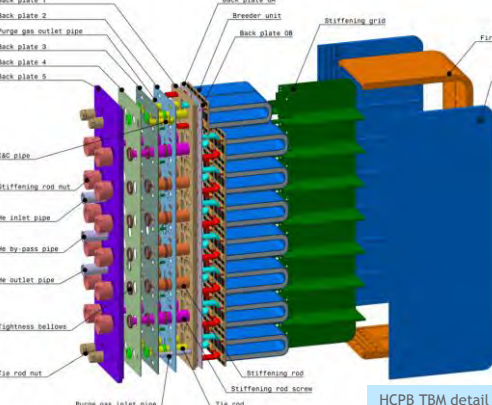
EU TBM-set global view



7

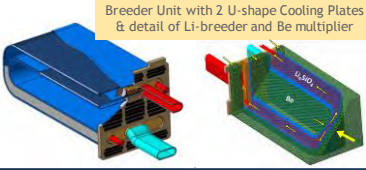
EU HCPB: Helium Cooled Pebble Bed TBM





HCPB TBM detail - front part

Breeder Unit with 2 U-shape Cooling Plates & detail of Li-breeder and Be multiplier



EUROFER-97 structural material

TBM total weight 1444 kg

Li-ceramic breeder (OSi / MTi) in the form of pebble beds (Li enriched at 90% in ⁶Li for the optimization of the tritium breeding ratio)

OSi total weight 76.5 kg
MTi total weight 105 kg

Beryllium neutron multiplier in the form of pebble beds

Be total weight 189 kg

Pressurized Helium coolant (8 MPa) for heat extraction (300-500 C)

Low-pressure Helium purge gas (0.4 MPa) for tritium extraction

8

2.

Beryllium materials for HCPB TBM concept

Beryllium multiplier materials

Tritium breeding ratio → ceramic breeder/Be volume ratio ~ 1/(3-4)

Single size beryllium pebble bed

Reference option for HCPB TBM:
1 mm Be pebbles produced by **Rotation Electrode Method (REM)** = **reference production route**

Alternative production routes for 1 mm Be pebbles – (i) **Fluoride Reduction Method (FRM)**; (ii) **fragmentation and milling of vacuum hot pressed Be ingots**

Alternative option for HCPB TBM:
 Advanced Be materials - **Beryllium alloys** (e.g. Titanium beryllide Be₁₂Ti)

- Better oxidation resistance
- Lower swelling
- Better tritium release characteristics
- Smaller reactivity with steel

HCPB BU

Be pebbles by REM

Be pebbles by fragmentation & milling

Be pebbles by FRM

Chemical composition of Be pebbles proposed for TBM application (in wt%)

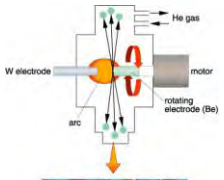
Be	BeO	Al	Fe	Mg	Si	Co	U
>99.5	<0.5	<0.09	<0.10	<0.08	<0.06	<0.001	<0.003

Beryllium materials: Functional Requirements

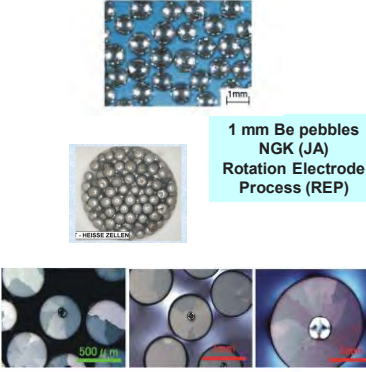


General requirements come from DEMO objectives with a short-term objective to characterize & qualify Functional Materials (Li-ceramics, Be) for a use in the ITER TBM

- **Neutronic performances** for T self-sufficiency ($TBR \geq 1.1$)
- **Temperature control** of the pebble beds during operation in the temperature window of ~300-650°C (PBTM issues/aspects)
- **Sufficient long lifetime** → (i) **neutron irradiation resistance** without significant changes of thermo-physical and mechanical properties; (ii) **to withstand stresses** induced under DEMO-relevant operating conditions without excessive fragmentation
- **Compatibility** between Be and EUROFER (up to max. T~550°C)
- **Low tritium retention** in the Be pebbles to minimize tritium inventory (safety aspect); efficient **tritium extraction**
- As **low as possible activation** under neutron irradiation (impurities level control; e.g. U, Co.) → for **recycling** (in the view of DEMO/future FPR) and **waste management**
- Limit/predict **hydrogen and passive heat release** during accidental conditions below safety limits (Be/steam/water interaction)



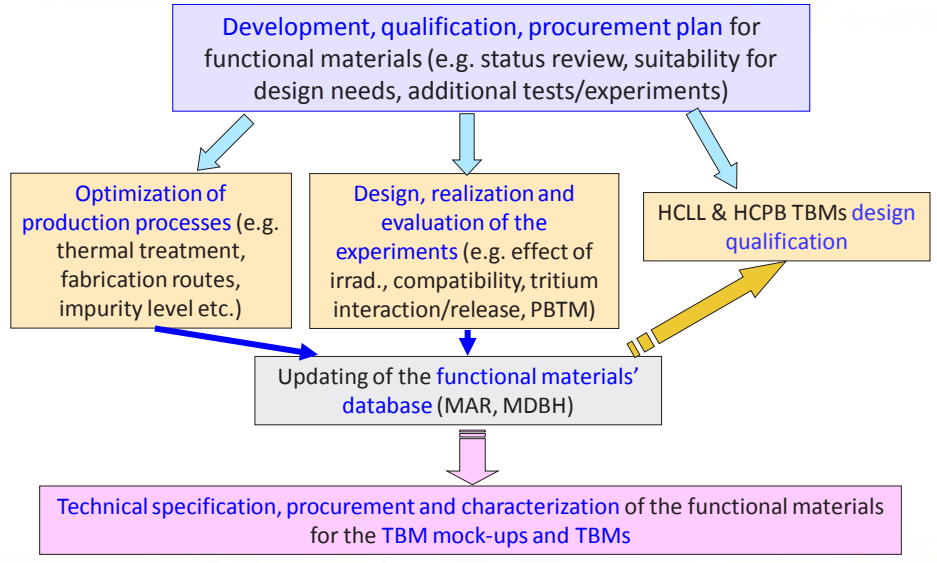
1 mm Be pebbles
NGK (JA)
Rotation Electrode Process (REP)



11

Functional Materials: Development strategy and future perspectives





```

graph TD
    A[Development, qualification, procurement plan for functional materials (e.g. status review, suitability for design needs, additional tests/experiments)] --> B[Optimization of production processes (e.g. thermal treatment, fabrication routes, impurity level etc.)]
    A --> C[Design, realization and evaluation of the experiments (e.g. effect of irradiation, compatibility, tritium interaction/release, PBTM)]
    A --> D[HCLL & HCPB TBMs design qualification]
    B --> E[Updating of the functional materials' database (MAR, MDBH)]
    C --> E
    D --> E
    E --> F[Technical specification, procurement and characterization of the functional materials for the TBM mock-ups and TBMs]
    
```

12



3. R&D achievements

Beryllium materials R&D activities: HIDOBE irradiation program & PIE



Objectives :

- (i) Beryllium behaviour under DEMO relevant He/dpa ratios and temperatures
- (ii) Tritium inventory as affected by microstructure, swelling, creep
- (iii) Pebble beds thermo-mechanical behaviour under neutron irradiation

HIDOBE-01 irradiation rig:

3000 appm He (DEMO: ~18,000 appm)
Irradiation completed - 665 FPD
Start of PIE in 2010, completed 2012 (F4E-GRT-030/A3)

HIDOBE-02 irradiation rig:

6000 appm He
Irradiation completed - 1274 FPD
PIE planned for 2015-16 (F4E-FPA-380/A3)



Post Irradiation Examination:

- Dimensional stability, porosity
- Microstructure (OM, SEM, TEM)
- Tritium release (TPD)
- Mechanical / thermal properties
- Interaction with air & steam

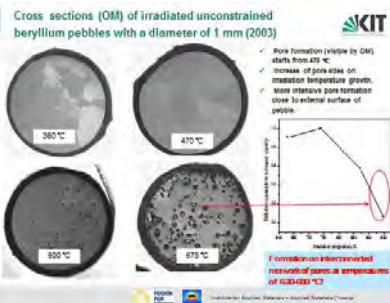
HIDOBE-01 PIE Plan

Unconstrained pebbles				He Pycno		Tritium release		SEM - OM		TEM	CREEP	Oxidation	Chem. Analysis
Grade	Supplier	name	specs	Temperatures	NRG	NRG	KIT	UL	NRG	KIT	KIT	ITN	ITN
7	EU-FZK	NGK pebbles	0.5 mm	425, 525, 650, 750	4	2	0	3	2	2		2	2
8	EU-FZK	NGK pebbles	1.0 mm (2003)	425, 525, 650, 750	4	4	2	2	2	4	4	2	2
9	EU-FZK	NGK pebbles	1.0 mm (2001)	425, 525, 650, 750	4	2	0	3	2	2	4	4	4
10	EU-FZK	NGK pebbles	2.0 mm	425, 525, 650, 750	4	0	0	2	2	2	4	4	4
Total amount of measurements					16	16	10	0	0	12	0	4	4
Constrained pebble beds				Dimensions + Mass		He Pycno		Tritium release		SEM - OM			
Grade	Supplier	name	specs	Temperatures	NRG	NRG	NRG	KIT	UL	NRG	KIT		
7	EU-FZK	NGK pebbles	0.5 mm	425, 525, 650, 750	4	4	4	4				1	1
8	EU-FZK	NGK pebbles	1.0 mm (2003)	425, 525, 650, 750	7	7	4	4				2	2
9	EU-FZK	NGK pebbles	1.0 mm (2001)	425, 525, 650, 750	3	3	4	4				1	1
10	EU-FZK	NGK pebbles	2.0 mm	425, 525, 650, 750	4	4	4	4				1	1
Total amount of measurements					18	18	0	0	0	0	0	5	5
Beryllides				Dimensions + Mass		He Pycno		Tritium release		Oxidation		Chem. Analysis	
Grade	Supplier	name	specs	Temperatures	NRG	NRG	NRG	KIT	ITN	ITN	ITN	ITN	XRD
11	JP-JAEA/IB	Be Electrode	08x2	425, 525, 650, 750	4	4	2	2	1	1	1	2	
12	JP-JAEA/IB	Be(171)Zr(1)	08x2	425, 525, 650, 750	0	0	2	2	1	1	1	4	
13	JP-JAEA/IB	Be(171)Zr(1)	08x2	425, 525, 650, 750	0	0	2	2	1	1	1	2	
Total amount of measurements					20	20	6	6	3	3	3	8	

Beryllium materials R&D activities: HIDOBE-01 PIE results (1/2)

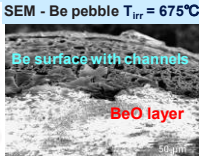


Cross sections (OM) of irradiated unconstrained beryllium pebbles with a diameter of 1 mm (2003)



• Pore formation (visible by OM) starts from 425 °C
 • Increase of porosity on irradiation temperature growth
 • More intensive pore formation close to external surface of pebble
 • Formation on unconstrained irradiation of pebbles at temperatures of 425-600 °C

SEM - Be pebble $T_{irr} = 675^\circ\text{C}$

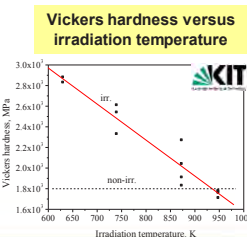


TEM
1mm Be pebble
 $T_{irr} 367^\circ\text{C}$
He bubbles size 8-15 nm

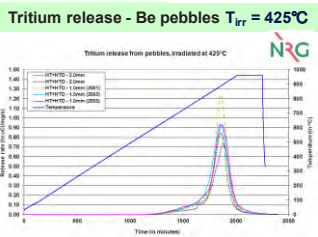
Table 1. Summary of the oxidation rate constant for the different oxidation studies

Sample	atmosphere	k (nm ² /h)	k (cm ² /y)
47 pc pebbles	60% O ₂ -40% N ₂	42 ± 9	1.2 ± 0.3 × 10 ⁻¹⁶
	relative humidity 55-60% H ₂ O	970 ± 27	27 ± 1 × 10 ⁻¹⁶
39 pc pebbles	relative humidity 55-60% H ₂ O	422 ± 60	12 ± 2 × 10 ⁻¹⁶
	Be5Ti	relative humidity 55-60% H ₂ O	4522 ± 847
Be7Ti	relative humidity 55-60% H ₂ O	1790 ± 848	50 ± 24 × 10 ⁻¹⁶

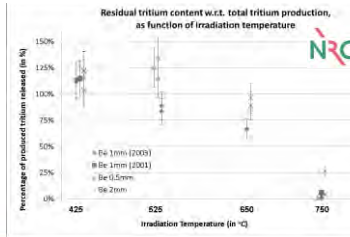
Vickers hardness versus irradiation temperature



Tritium release - Be pebbles $T_{irr} = 425^\circ\text{C}$



Residual tritium content w.r.t. total tritium production, as function of irradiation temperature



15

Beryllium materials R&D activities: HIDOBE-01 PIE results (2/2)



Summary of the main PIE results:

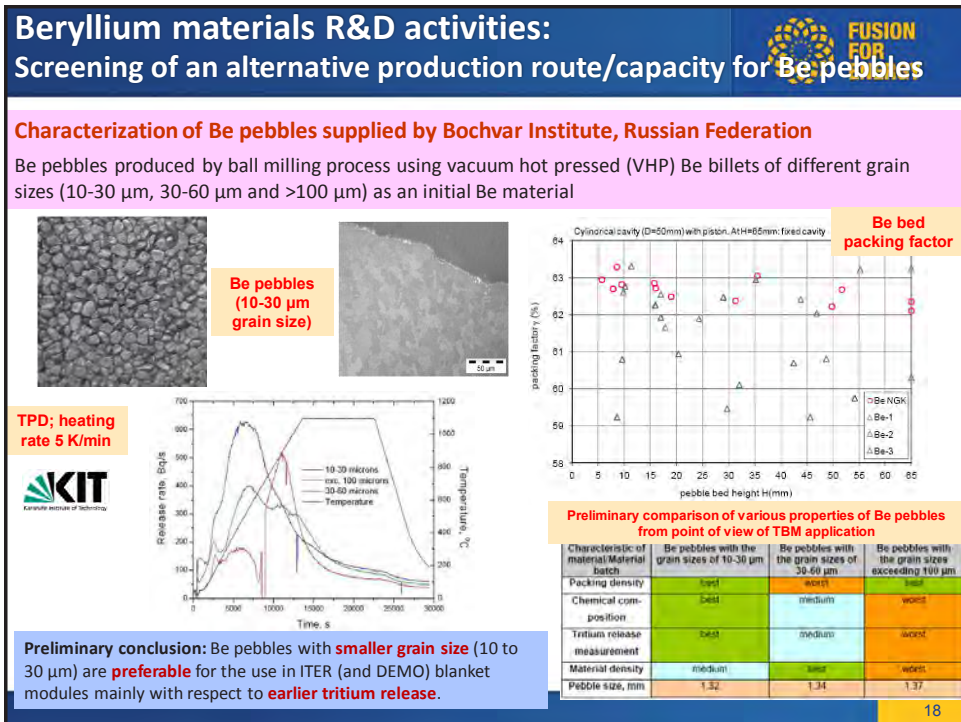
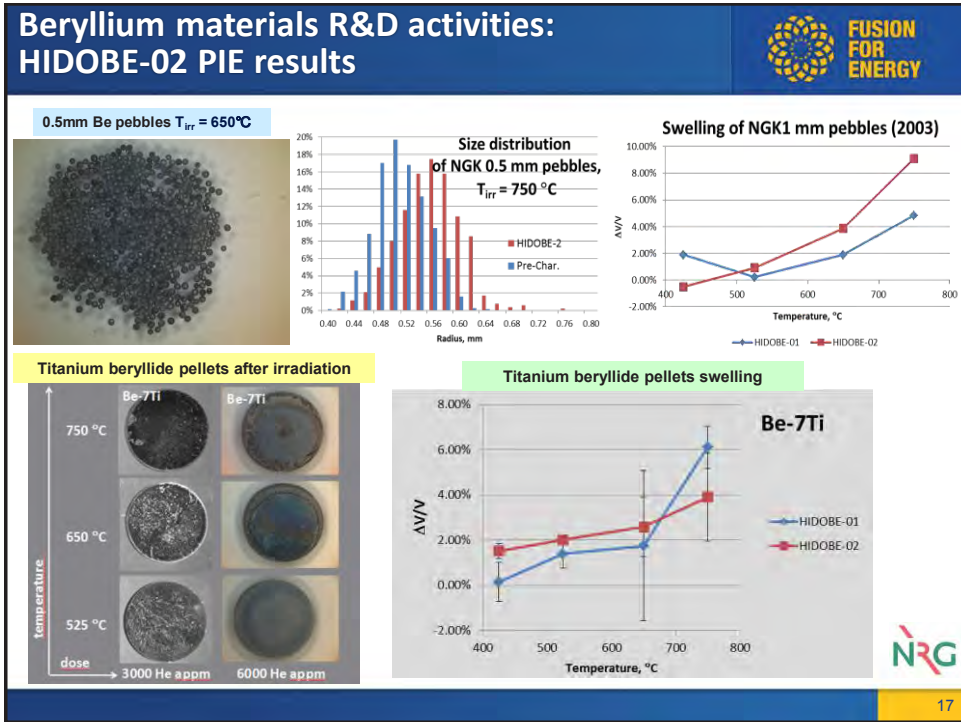
Microstructure:

- Strongly depends on irradiation temperatures independently for irradiated constrained/unconstrained Be pebbles. No significant pore or bubble formations occur at 425 and 525°C. Irradiations at 650 and 750°C lead to intensive pore formation resulting swelling up to the highest value of 7 %.
- No compact oxidation layer is observed on the surface regions at 425 and 525 °C. However, strong oxidation occurs after irradiation at 650 and 750°C where the thickness of BeO layers on the pebble surfaces can reach 10-25 µm.

Tritium release:

- One peak is observed (at TPD) in the temperature range ~900-1100°C independently to the irradiation temperature or the pebbles bed state (constrained/unconstrained).
- Tritium is released mainly in the form of HT.
- Irradiation temperature influences the amount of Tritium released/retained throughout irradiation: it increases significantly above 650°C; at 750°C, the residual Tritium measured in irradiated samples is 6 to 8 times lower than in samples irradiated at lower temperature.

16



Beryllium materials R&D activities: Material Assessment and Database Reports update

**Material Assessment Report (MAR) and
Material Database Report (MDBR) →
input for TBM and DEMO design activities**

KIT Document Ref. No.	Version	Date	Page
MAT-GEW-1238031-RD-016D01-01	1.0	29-May-15	2 of 113

Part 01: Intermediate Be MAR Update

Material Assessment Report
on
Be Pebble Beds for EU HCPB Test Blanket Module

Table of Content - continuation

- 4.1.1.5.1.1.7 HIDOBE-01 and HIDOBE-02
- 4.1.1.5.1.1.8 In-pile Results from HIDOBE-01 and HIDOBE-02
- 4.1.1.5.1.1.9 PIE results from HIDOBE-01
- 4.1.1.5.1.1.9.1 Dimension measurements
- 4.1.1.5.1.1.9.2 Density measurements
- 4.1.1.5.1.1.9.3 Microstructural analysis
- 4.1.1.5.1.1.9.4 Tritium release and retention
- 4.1.1.5.1.1.9.5 Discussion on Tritium Release in Beryllium
- 4.1.1.5.1.1.9.6 Crystallography (by X-Ray Diffraction)
- 4.1.1.5.1.1.9.7 Creep Measurements
- 4.1.1.5.1.1.9.8 Chemical Analysis and Oxidation Studies
- 4.1.1.5.2 Activation under 14-MeV Neutrons
- 4.1.1.5.3 Impact of Irradiation on Electrical Conductivity of Be Pebble Beds
- 4.1.1.5.4 Compatibility with Steels (EUROFER, etc.)
- 4.1.1.5.5 Air/Steam Interaction
- 4.1.1.6 Conclusions
- References

Table of Content

- 4.1.1.1 Introduction
- 4.1.1.2 Functional Requirements
 - 4.1.1.2.1 Reference HCPB DEMO Blanket Concept
 - 4.1.1.2.2 Reference ITER HCPB TBM Concept
 - 4.1.1.2.3 Safety Design Requirements
 - 4.1.1.2.4 Review of the design requirements for beryllium pebble beds
 - 4.1.1.2.5 Neutron performances for T self-sufficiency
 - 4.1.1.2.6 Thermal control
 - 4.1.1.2.7 Sufficiently long lifetime
 - 4.1.1.2.8 Material Compatibility
 - 4.1.1.2.9 Low tritium inventory in materials
 - 4.1.1.2.10 Activation
- 4.1.1.3 Properties of Be/Be-Ti Pebbles
 - 4.1.1.3.1 Fabrication Process
 - 4.1.1.3.2 Development of Fabrication Routes of Pebbles from Beryllides
 - 4.1.1.3.3 Chemical Composition
 - 4.1.1.3.4 Phase Composition and Microstructure
 - 4.1.1.3.5 Density, Porosity, Specific Surface
 - 4.1.1.3.6 Thermal Expansion Coefficient
 - 4.1.1.3.7 Mechanical Properties
 - 4.1.1.3.8 Commercial Availability
- 4.1.1.4 Properties of Pebble Beds
 - 4.1.1.4.1 Pebble Bed Density and Packing Factor
 - 4.1.1.4.2 Young's Pebble Bed Modulus
 - 4.1.1.4.3 Thermal Creep
 - 4.1.1.4.4 Friction Angles
 - 4.1.1.4.5 Heat Transfer Parameters
 - 4.1.1.4.5.1 Thermal Conductivity
 - 4.1.1.4.5.2 Heat Transfer Coefficient h
 - 4.1.1.4.6 Thermal Cycling/Shock of Pebble Beds
 - 4.1.1.4.7 Electrical Conductivity
- 4.1.1.5 Influence of In-Service Conditions
 - 4.1.1.5.1 Neutron Irradiation Effects
 - 4.1.1.5.1.1 Evolution of Microstructure and Physical-Mechanical Properties
 - 4.1.1.5.1.1.1 TPD setup at NRG
 - 4.1.1.5.1.1.2 EXOTIC-8 Experiments
 - 4.1.1.5.1.1.3 EXOTIC-8 PIE Results
 - 4.1.1.5.1.1.4 PBA Experiment
 - 4.1.1.5.1.1.5 In-pile Results from PBA
 - 4.1.1.5.1.1.6 Out-of-pile Results from PBA

19

4. Summary – Open issues

20

Beryllium Materials

Open technical issues (1/2)



Development and further optimization of fabrication routes

- **Optimization of Be pebbles fabrication processes** with respect to the production yield, pebbles' characteristics and mechanical properties
- Production of **Be pebbles with small grains** (tritium release)
- Development of an **alternative fabrication route for Be pebbles**
- Development of a suitable **fabrication route for Be-alloy material(s)** (e.g. Be₁₂Ti)
- **Control of undesired impurities** level in the functional materials (FM) (e.g. Co, U,...)
- In general, **availability of Be materials** for DEMO and future FPR

21

Beryllium Materials

Open technical issues (2/2)



Availability of the materials properties needed for a proper TBMs design

- **Effect of neutron irradiation on thermo-mechanical properties** of Be pebbles and Be pebble bed as function of irradiation temperature and neutron dose taking into account material swelling, thermal expansion and thermal creep
- **Tritium retention/release characteristics** as a function of irradiation temperature, neutron dose, purge gas chemistry, material properties (e.g. small grain Be pebbles)
- **Compatibility with structure material** under neutron irradiation
- **Interaction of air/steam** with Be/Be-alloy pebbles
- **Thermal conductivity** in pebble beds under compressive loads

22



Thank you for your attention

Follow us on:

 www.f4e.europa.eu

 www.twitter.com/fusionforenergy

 www.youtube.com/fusionforenergy

 www.linkedin.com/company/fusion-for-energy

 www.flickr.com/photos/fusionforenergy

2.2.2 STATUS OF R&D ACTIVITIES ON BERYLLIUM FOR ITER BLANKET FIRST WALL APPLICATION IN RUSSIAN FEDERATION

I.B. Kupriyanov¹, G.N.Nikolaev¹, G. Gorayev², R.Giniiatulin³

¹A.A. Bochvar High Technology Research Institute of Inorganic Materials (JSC VNIINM), Moscow, Russia

²FSUE Bazalt, Saratov, Russia

³ Efremov Research Institute, S.-Peterburg, Russia

Abstract

Beryllium will be used as a plasma facing material for the ITER Blanket first wall (FW). The primary reasons for the selection of beryllium as an armor material for the ITER first wall are its low Z and also high oxygen gettering characteristics. Three beryllium grades have been accepted for application as the first wall armor: S-65C (USA), TGP-56FW (Russian Federation) and CN-G01 (China). This selection is based on the results of a qualification program which includes material characterization and testing of their performance at transient heat loads. Russian Federation (RF) is responsible for manufacturing of 40 % of the FW panels of ITER Blanket. The 60 % of panels in the Russian share will be made of TGP-56FW beryllium grade that corresponds to ~2400 kg in form of final tiles (~180000 tiles with 50×16×8 mm in dimensions). It is expected, that mass production of beryllium tiles will start in 2016.

A status of R&D on the improvement of manufacturing technology of tiles made of TGP-56FW beryllium grade and also the activities aimed on the preparation of mass production are presented. Additionally, this paper presents the results of comparative study on influence of transient plasma heat loads with the energy density of 0.5-1.0 MJ/m² at 250-500°C (performed on QSPA-Be plasma gun facility), on the erosion, surface cracking and a microstructure of beryllium tiles made of TGP-56FW grade (RF) and S-65C grade (USA).

1. Introduction

Beryllium will be used as a plasma facing material for the ITER Blanket first wall (FW). The primary reasons for the selection of beryllium as an armor material for the ITER first wall are its low Z and also high oxygen gettering characteristics and also high thermal conductivity. For the first wall panels beryllium is used in form of flat tiles (of 8-mm in thickness) joined to a CuCrZr alloy heat sink. Present FW design assumes that a total quantity of beryllium tiles is about of 10 tons. Two types of FW panels will be armored by beryllium: the “normal” heat flux panels which will be loaded by stationary heat flux of $(1\div 2)$ MW/m² and “enhanced” heat flux (EHF) panels which will be loaded by heat flux ≤ 5 MW/m² respectively.

Three beryllium grades have been accepted for application as the first wall armour: S-65C (USA), TGP-56FW (Russian Federation) and CN-G01 (China). This selection is based on the results of the ITER

qualification program which includes material characterization and testing of their performance at transient heat loads [1, 2]. According to the ITER Procurement Agreement Russian Federation (RF) is responsible for manufacturing and delivering of 40 % FW panels of ITER Blanket. The 60 % of panels in the Russian share will be armored with Russian TGP-56FW beryllium that corresponds to ~2400 kg in form of final tiles (~180000 tiles with 50×16×8 mm in dimensions).

This report presents a status of R&D on the improvement of manufacturing technology of the TGP-56FW beryllium tiles and also the activities aimed on the preparation to mass production. In course of the preparation to mass production the production line for fabrication of a high purity beryllium powder has been upgraded, new pressing equipment for CIP and VHP has been mounted and commissioned, the electric discharge machine (EDM) has been installed and quality control procedures have been revised and improved. By this technology the experimental batches of billets and tiles have been manufactured which meet the ITER requirements.

Additionally, this report presents the recent results of comparative study on influence of transient plasma heat loads with energy density of 0.5-1.0 MJ/m² at 250-500°C on the erosion, surface cracking and microstructure of beryllium tiles made of TGP-56FW grade (RF) and S-65C grade (USA).

2. Beryllium armour for the enhanced heat flux (EHF) First Wall panels

In the FW beryllium is used in form of tiles joined to a CuCrZr alloy heat sink. According to the recent ITER estimations, ~50% (~350 m²) of FW surface will be exposed by scaled up stationary heat loads – up to 5 MW/m². All RF share is related to high loaded part of FW (EHF FW). During a few last years design of EHF FW panels was significantly changed.

Fig.1 shows the FW panel of a new design (1,a), which consists of individual fingers (1,b), with the rectangular-shaped hypervapotron-type cooling channels and beryllium armor tiles of decreased dimensions. By the moment the tiles (Fig.2) with dimensions of 16×50×8 mm³ and two transversal cut (7 mm deep) are considered as the main type of tiles for the EHF panels.



Fig.1. The views of a FW panel (a) and an individual finger (b)

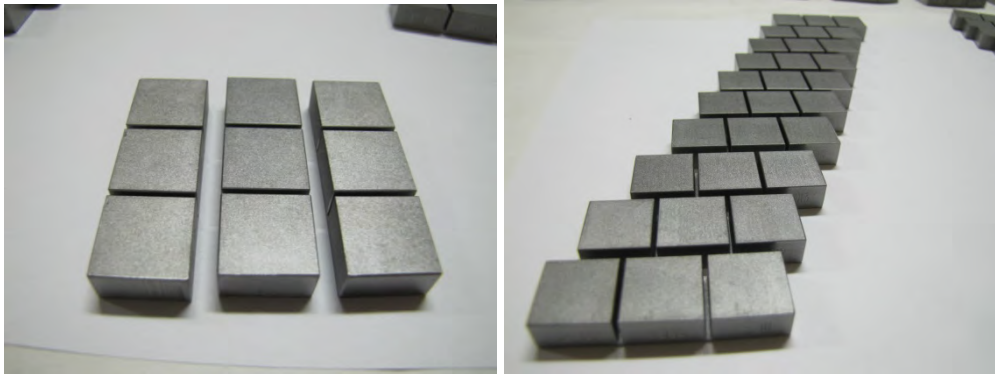


Fig.2. Beryllium tiles ($16 \times 50 \times 8$) mm³ of TGP-56FW grade for EHF FW panels

3. Selection of the beryllium grade

As the result of ITER EDA activities [3] the reference beryllium grade S-65C (USA, Brush Wellman) and DshG-200 grade (RF, A.A. Bochvar Institute) were selected for armor of ITER FW. The main criterion of this choice was the highest resistance against High Heat Flux loading, which was shown by the results of thermal fatigue/shock test experiments carried out in 1994-1997 in SNL (USA) [4] and FZJ (Germany) [5].

Later, Russian and Chinese ITER Parties proposed new grades for application in the ITER FW. Then, to assess the performance of new grades the qualification program was established [6]. This program included:

- Characterization of the main physical and mechanical properties and production technologies [7];
- Comparative thermal performance tests (thermal shock resistance, vertical displacement event (VDE) heat load simulation, thermal cyclic fatigue tests after VDE simulation testing) with respect to the reference grade S-65C [1-2, 8].

Both TGP-56FW and CN-G01 (China) grades successfully passed the qualification and were approved by the ITER IO for the application as an armor material of FW.

So, three beryllium grades are now available for the application as an armor material of FW: S-65, CN-G01 and TGP-56FW [1-2].

4. Technical requirements to TGP-56FW beryllium grade

According to the specification for the supply of beryllium blocks, chemical composition, density, grain size and mechanical properties of TGP-56FW grade have to meet the requirements listed in Table 1. The data of S-65C grade [3] are also included in Table 1 for comparison.

Table 1. Technical requirements to TGP-56FW [9]

Parameter	TGP-56 FW	S-65C [3]
Chemical composition, % wt		
Be (min)	99.0	99.0
BeO (max)	1.0	1.0
C (max)	0.1	0.1
Si (max)	0.02	0.06
Fe (max)	0.12	0.08
Al (max)	0.04	0.06
Ti (max)	0.04	n/d
Cr (max)	0.06	n/d
Mn (max)	0.04	
$\Sigma(\text{Mg}+\text{Cu}+\text{Ni})$ (max)	0.06	n/d
U (max)	0.003	0.003
Density (min), % of theoretical value	99.0	99.0
Average grain size (max), μm	25	20
Mechanical properties		
Ultimate Tensile Strength (RT), (min), MPa	300	290
Yield Strength (RT), (min), MPa	220	207
Total Elongation (RT), (min), %	2.0	3.0

5. Manufacturing of TGP-56FW beryllium grade

TGP-56FW grade has been developed by Bochvar Institute (JSC “VNIINM”), Russian Federation. The grade is manufactured by powder metallurgy and vacuum hot pressing techniques.

The basic components of the technology are:

- Fabrication of Be powder with required chemical composition and particle size by chipping of ingots into small pieces, grinding the chips by disk attrition and powder sizing;
- Cold isostatic pressing (CIP) or cold axial pressing (CP) of Be powder up to the 70-75 % of theoretical density;
- Vacuum hot pressing (VHP) of the required quantity of CIP or CP briquettes in a graphite mold up to > 99 % of theoretical density;
- Machining;
- Cutting of VHP beryllium blocks along the pressing direction to produce final beryllium tiles;
- Surface finishing by chemical etching 0.05 mm in the depth (optional).

Using this technology, several pilot batches of billets and tiles have been produced and investigated in Bochvar Institute (Fig. 3).

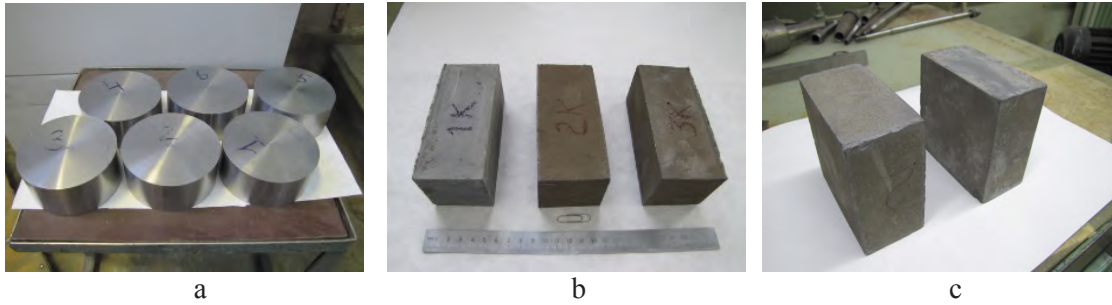


Fig.3 – The views of VHP Be billets of different sizes: a – \varnothing 125 mm, H= 60 mm; b – 135×60×60 mm; c - 106×106×54 mm

6. Preparation to industrial manufacturing of TGP-56FW beryllium billets and tiles

For mass production of billets and tiles at “Bazalt” plant (Saratov, RF) the following preparation has been performed:

- the line for fabrication of high purity beryllium powder has been modified;
- pressing equipment for CIP and VHP has been mounted and commissioned (Fig. 4);
- necessary quantity of the wire electric discharge machines (EDM) has been installed;
- quality control procedures have been revised and improved;
- the batch of vacuum-cast Be ingots has been procured (Fig. 5)

The experimental batches of billets and tiles meeting the ITER requirements have been already manufactured at “Bazalt” plant (Fig. 6-7).



a – CIP

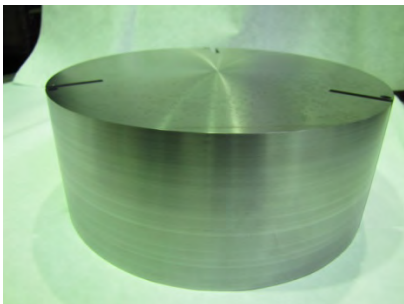


b - VHP

Fig.4 Pressing equipment



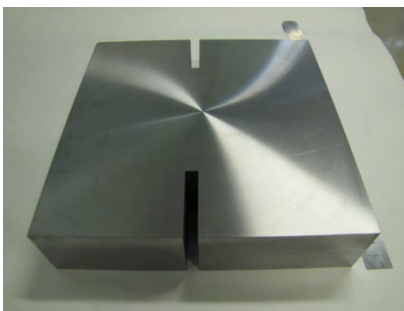
Fig. 5 Vacuum-cast Be ingots



a



b



c



d

Fig. 6. The views of VHP Be billets of different sizes: a – $\text{Ø} 300 \text{ mm}$, $H= 120 \text{ mm}$; b - $\text{Ø} 300 \text{ mm}$, $H=60 \text{ mm}$; c-d - $220 \times 220 \times 60 \text{ mm}$

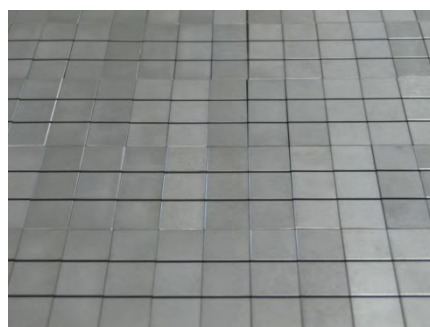


Fig. 7. Beryllium tiles with $50 \times 16 \times 8 \text{ mm}$ in dimensions

One of the important requirements for beryllium application in ITER is a low content of uranium. Uranium content has a strong impact on a total inventory of the activation products in fusion reactor due

to the formation of long-lived actinides (e.g. ^{239}Pu , ^{241}Am). From the safety point of view the maximum U concentration in beryllium for ITER application is specified as 0.0030 weight %.

Therefore it is necessary to carry out a special inspection of uranium impurity content in beryllium. Since the main factor influencing the content of U in Be billets and tiles is a composition of initial raw materials used in the ingots melting, the incoming control of uranium content in vacuum-cast Be ingots have been organized. The results of U measurements in the batch of 18 vacuum-cast Be ingots are shown in Fig. 8. These data demonstrate that uranium content does not exceed 10 ppm.

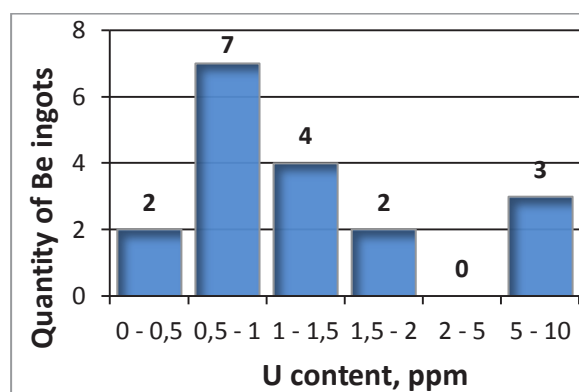


Fig. 8. U content in batch of vacuum-cast Be ingots

Given the fact that during machining up to 70-90% of beryllium could turn into chips, the consumption of material and manufacturing cost of Be tiles could vary significantly depending on the billet shape. For this purpose, the influence of beryllium billet shape (round or square) on the efficiency of the metal utilization in wire EDM machining has been estimated using two and three-dimensional modeling with "Compass" program. The dimensions of billet after finishing were taken as follows:

1. 216 mm × 216 mm × 55 mm (square);
2. Ø 292 mm and H1 = 55 mm (round).

The thickness of cut in the wire EDM machining was 0.4 mm. In the simulation the losses associated with cutting the samples required for the certification of billets (mechanical properties, density, and chemical analysis) were taken into account. The mass of a tile is 0.011 kg. The results of 3D modeling are presented in Fig. 9 and Table 2.

As follows from these data, the square billets result in higher yield (0.76 against 0.72).

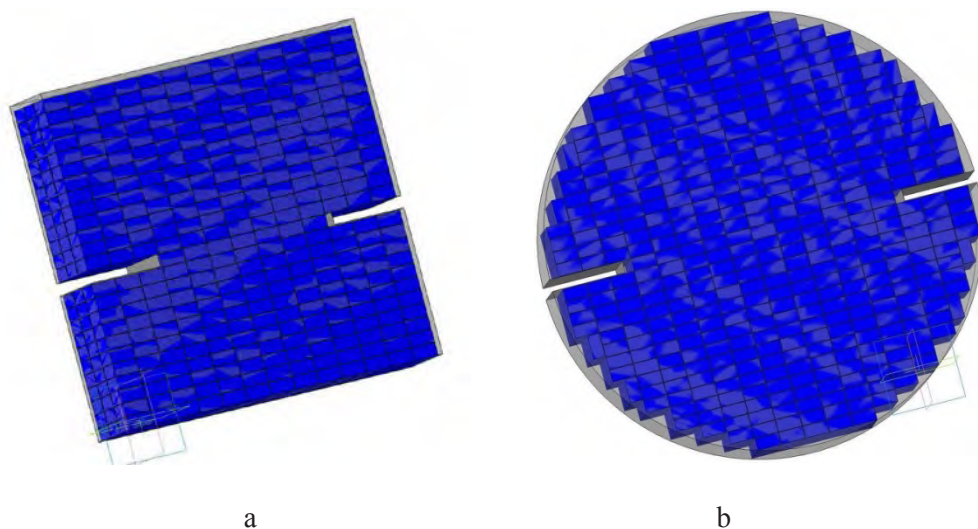


Fig. 9. The 3D modeling: a) square (216 mm × 216 mm × 55 mm) Be billet, b - round (Ø 292 mm H1 = 55 mm) Be billet

Table 2. Estimated metal utilization factor (MUF) in manufacture of beryllium tiles from billets of different shapes

	Shape and dimensions of billet	
	Square (216 mm×216 mm×55 mm)	Round (Ø 292 mm and H ₁ = 55 mm)
Weight of billet, kg	4.618	6.63
Tiles quantity (max), pieces/kg	319/3.51	437/4.807
Yield (max)	0.76	0.72

7. Behavior under transient plasma heat loads

In ITER the edge-localized modes (ELMs) and disruptions will result in large thermal transient loads on beryllium components of FW. These loads cause rapid heating of beryllium surface and can result in some changes in surface and near-surface regions such as material loss, melting, cracking, evaporation and formation of beryllium dust as well as hydrogen isotopes retention both in the armour and in the dust. Erosion of beryllium under transient plasma loads such as ELMs and disruptions will mainly determine a lifetime of ITER first wall.

The study of influence of transient plasma heat loads with the energy density of 0.5-1.0 MJ/m² at 250-500°C on the erosion, surface cracking and a microstructure of beryllium tiles made of TGP-56FW grade (RF) and S-65C grade (USA) was performed on QSPA-Be plasma gun facility in Bochvar Institute [10,11]. The surfaces of mockups made of TGP-56FW beryllium grade and S-65C beryllium grade after 100 shots of plasma irradiation with energy of 0.55 MJ/m² and 1 MJ/m² is shown in Fig.10.

Typical damages of both beryllium grades are: mass loss (erosion) (Fig.11), surface melting, displacement and splashing of molten layer, formation of the erosion products, the gradual filling of gaps between the Be tiles with molded beryllium, and slight surface cracking. Performances of both grades are very similar

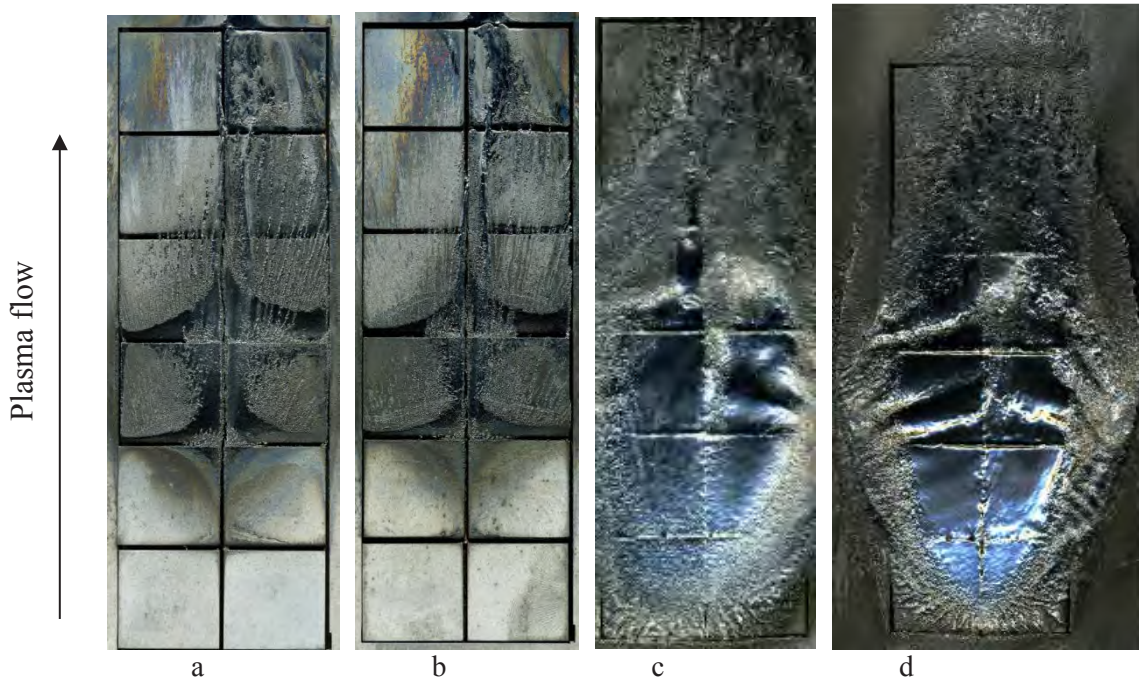


Fig. 10 – Surfaces of mockups made of TGP-56FW beryllium grade (a,c) and S-65C beryllium grade (b,d) after 100 shots, where a-b: $Q_{max}=0.55 \text{ MJ/m}^2$ at 250°C , c-d: $Q_{max}=1 \text{ MJ/m}^2$ at 500°C

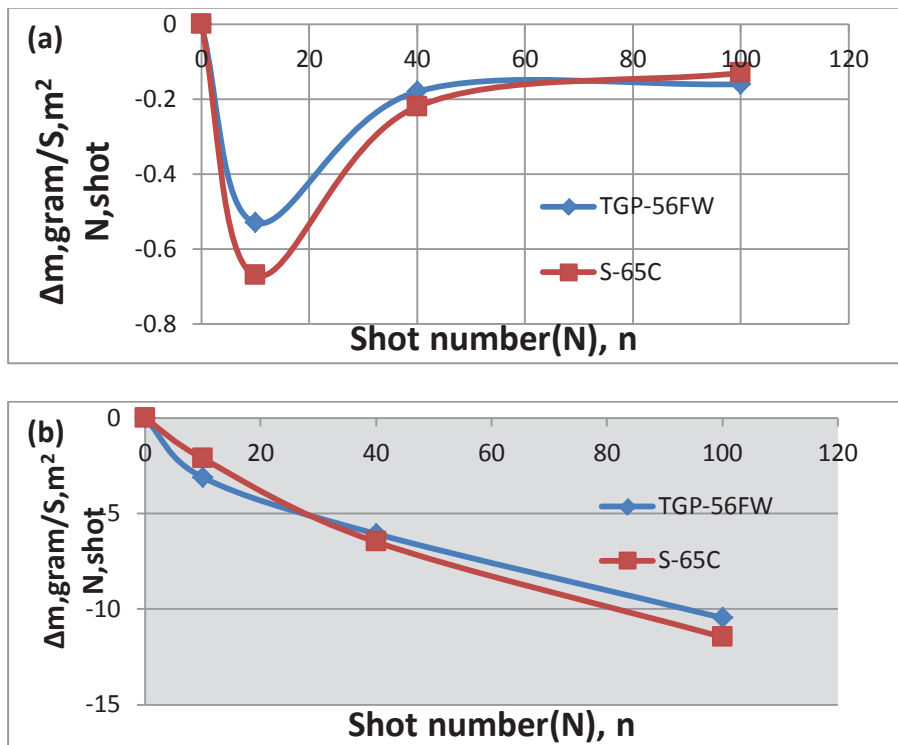


Fig.11. The weight loss of the FW prototypes coated with beryllium of the TGP-56FW grade and the S-65C grade, depending on number of shots: a - at maximum absorbed energy of 0.55 MJ / m^2 , and the preheating temperature $\sim 250^\circ\text{C}$, b – at maximum absorption energy of 1MJ/m^2 , and the preheating temperature $\sim 500^\circ\text{C}$

8. Conclusions

Russian beryllium of TGP-56FW grade has been accepted for the ITER first wall application.

Experimental technology of TGP-56FW billets and tiles developed in Bochvar Institute, has been adapted and successfully introduced to the industry at “Bazalt” plant.

Prior to the serial production of tiles in 2019-2020, further R & D will be directed on the cost reduction and increasing the efficiency of production, as well as on studying the behavior of beryllium at various heat and radiation loads, expected in ITER

References

- [1] V. Barabash, R. Eaton, T. Hirai, I. Kupriyanov, G. Nikolaev, Z. Wang, X. Liu, M. Roedig, J. Linke, *Physica Scripta*, 2011, T. 145, 014007.
- [2] I. Kupriyanov et al., *Physica Scripta*, T145 (2011) 014063 (5p).
- [3] ITER Materials Assessment Report (MAR), ITER Final Design Report 2001.
- [4] R. Watson, D. Youchison, D. Dombrovski, R. Giniyatulin, I. Kupriyanov, Low cycle thermal fatigue testing of berylliums, *Fusion Engineering and Design* 37 (1997) pp.553-579.
- [5] M. Rodig, R. Duve, A. Gervash, A. Khomutov, J. Linke, A. Schuster, Thermal Shock Tests with Beryllium Coupons in the Electron Beam Facility JUDITH, Proc. 2nd IEA Int. Workshop on Beryllium Technology for Fusion, Sept. 6-8, 1995, pp. 39-56.
- [6] Test program for qualification of RF Be (27SUCU_v1_0), ITER Report, 2008.
- [7] I.B. Kupriyanov, G.N. Nikolaev, M. Roedig, J. Linke, L.A. Kurbatova et al., Status of RF beryllium characterization for ITER first Wall, *Journal of Nuclear Materials JNM* 417 (2011) pp.756-760.
- [8] M. Rodig, I. Kupriyanov, J. Linke, X. Liu, Zh. Wang, Simulation of transient heat loads on high heat flux materials and components *Journal of Nuclear Materials JNM* 417 (2011) pp.761-766.
- [9] Material specification for the supply of beryllium blocks made of TGP-56FW grade to be used for manufacturing of beryllium tiles for the ITER First Wall (2015)
- [10] JSC VNIINM Report, 2013.
- [11] JSC VNIINM Report, 2014.

2.2.3 Beryllium Production and Applications Overview at Materion

C.K. Dorn, E.E. Vidal, and K.J. Smith

*Materion Beryllium &
Composites*

*14710 West Portage River South Road, Elmore, Ohio 43416-
9500 U.S.A.*

E-mail:

chris.dorn@materion.com

Materion Corporation is the world's largest producer of beryllium metal. Beryllium (Be) metal and other beryllium-containing materials are known for their unusual combination of properties. This accounts for the long-standing interest in these materials since the 1930s. Important fields of application for beryllium metal, beryllium composites, and beryllium compounds include acoustics, aerospace structures, x-ray transmission, motion control, nuclear test reactors, laser-based optical systems, high-energy particle physics research, high-performance automotive applications, and thermal management. Beryllium-containing alloys, which typically contain less than 2% Be, are used extensively in commercial electronics, telecommunications infrastructure, automotive electronics, oil and gas equipment, tooling for plastic molding, and medical equipment applications. This paper will describe the processes used at Materion to make beryllium as well as highlighting important end-use applications, including nuclear fusion.

**12th International Workshop on
Beryllium Technology
Jeju Island, Korea**



**BERYLLIUM PRODUCTION
&
APPLICATIONS OVERVIEW
INCLUDING
FUSION-RELATED
ACTIVITIES**

**Christopher Dorn
Edgar Vidal
Keith Smith**

**Materion Beryllium & Composites
Elmore, Ohio, U.S.A.**

September 2015

Materion Beryllium & Composites

Beryllium Overview – BeWS-12, Korea

Presentation Outline

- What is Beryllium?
 - Brief History
 - Materion Overview
- Properties & Product Forms
- How are Beryllium Products Made?
 - Mining, Ore & Refining
 - Casting, Powder & Consolidation
 - Finished Parts & Assemblies
- Applications Overview
 - Aerospace & Defense
 - Commercial & Medical
 - Nuclear including Fusion Activities
- Summary & Conclusion



Beryllium & Composites

Beryllium Overview – BeWS-I2, Korea

What is Beryllium?

- Metallic Element
- Discovery & Isolation
- Alkaline Earth Metal
- Precious Gem Forms
- Beryllium-Bearing Ores
- Industrialization & Commercialization
 - Over 100 Years to Begin Study
 - First Commercial Production
 - C.F. Brush II & C.B. Sawyer



Beryl Ore



Beryllium & Composites

3

Beryllium Overview – BeWS-I2, Korea

Global Footprint



- 2400**
Employees serving
our customers
- 50**
In more than 50
countries
- 30**
From more than
30 facilities
- 10**
In 10 countries
around the world

Corporate Office
Mayfield Heights, Ohio

Manufacturing Facilities

Albuquerque, New Mexico
Bloomfield, Connecticut
Brewster, New York
Buffalo, New York
Delta, Utah
Elmore, Ohio
Fremont, California
Limerick, Ireland

Lincoln, Rhode Island
Lorain, Ohio
Milwaukee, Wisconsin
Newburyport, Massachusetts
Reading, Pennsylvania
Santa Clara, California
Singapore
Subic Bay, Philippines

Suzhou, China
Taipei, Taiwan
Tucson, Arizona
Tyngsboro, Massachusetts
Westford, Massachusetts
Wheatfield, New York
Windsor, Connecticut

Service Centers
Elmhurst, Illinois
Warren, Michigan
Singapore
Stuttgart, Germany
Theale, England
Tokyo, Japan



Beryllium & Composites

4

Beryllium Overview – BeWS-12, Korea

Materion Product Portfolio

- Precious & Non-Precious Specialty Metals
- Precision Optical Filters
- Inorganic Chemicals & Powders
- Specialty Coatings
- High-Performance Engineered Alloys
 - Beryllium-Containing
 - Non-Beryllium
- Beryllium & Metal Matrix Composites
- Engineered Clad & Plated Metal Systems



Copper-Beryllium & Copper-Nickel-Tin Aerospace Bushing & Bearing Components



Beryllium & Composites

5

Beryllium Overview – BeWS-12, Korea

Physical Properties of Beryllium

- Density
- Modulus
- Thermal
- Melting Point
- Nuclear
- Acoustic
- Optical
- Electrical
- Magnetic



Beryllium & Composites

6

Beryllium Overview – BeWS-12, Korea



Beryllium Mill Products
& Near-Net Shapes

Why Would You Use High-Performance Metals and Composites?

- Improve Performance
- Reduce Cost
- Minimize Risk
- Ensure Reliability

**“Unusual Combination
of Attributes”**



Beryllium & Composites

7

Beryllium Overview – BeWS-12, Korea

Materion Be&C Product Offerings

- Beryllium Metal, Compounds & Chemicals
- Aluminum-Beryllium Composites (AlBeMet®)
- Beryllium Oxide & Aluminum Oxide Ceramic Products
- Aluminum-Based Metal Matrix Composites (SupremEX®)
- Be-BeO Metal Matrix Composites (E-Materials)
- Electrofusion Products (Beryllium Foil & X-Ray Windows)



Beryllium & Composites

8

Beryllium Overview – BeWS-12, Korea

Product Forms & Other Services

- Beryllium Metal
 - VHP, HIP, CIP, Cold-Pressed
 - Rod, Bar, Tube, Sheet & NNS
- AlBeMet® I62 Composite
 - HIPed Bar & Plate
 - Extrusions & Rolled Sheet
 - Castings & EB-Welded NNS
- BeO & High-Purity Al₂O₃ Ceramics
- SupremEX® Al-Based Metal Matrix Composites
- E-Materials: Be-BeO Metal Matrix Composites
- Bulk Metallic Glasses: Zr-Based Cast Materials
- Special Products & Applications Development Engineering



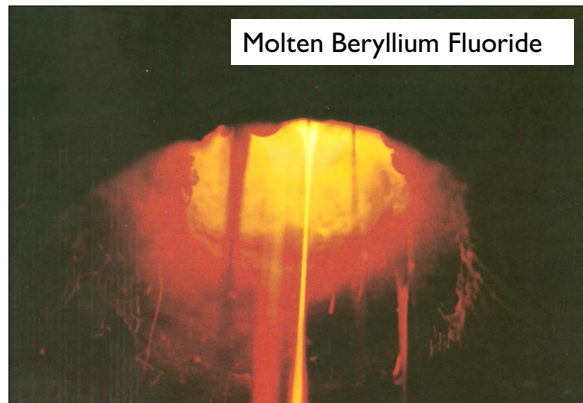
Beryllium-Aluminum Investment Castings



Beryllium Overview – BeWS-12, Korea

How is Beryllium Made?

- Multi-Step Mfg. Process
 - Mining & Extraction
 - Reduction (Be Pebbles)
 - Vacuum Casting
 - Powder Making
 - Consolidation
 - Machining & Cutting
 - Recycling
- MBe&C as Fully-Integrated Supplier



Beryllium Overview – BeWS-12, Korea

Materion Resources – Delta, Utah, U.S.A.



- Be Hydroxide Capacity Increase Announced Nov-2013
- New Mine Pit Opened in First Quarter of 2014



Beryllium & Composites

11

Beryllium Overview – BeWS-12, Korea

Mining & Extraction – Mine Operations



Beryllium & Composites

12

Beryllium Overview – BeWS-12, Korea

Mining & Extraction – Mill Operations



Beryllium & Composites

13

Beryllium Overview – BeWS-12, Korea

Elmore, Ohio, U.S.A. Beryllium & Composites Production Facility



Beryllium & Composites

14

Beryllium Overview – BeWS-12, Korea

Primary Beryllium Manufacturing Vacuum Casting

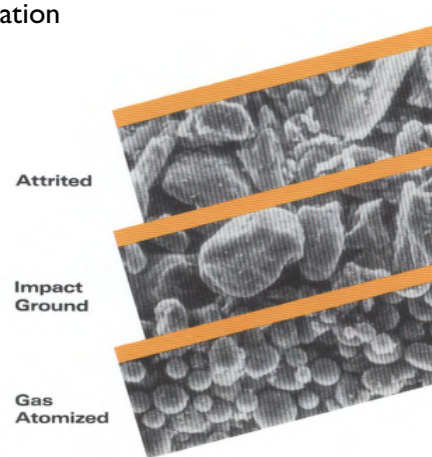
- Technical Reason for Casting
- Virgin Material & Recycle Input
- Next Step: Powder Making



Beryllium Overview – BeWS-12, Korea

Primary Beryllium Manufacturing Powder Making

- Two Types of Powder
- Next Step: Consolidation



Beryllium Overview – BeWS-12, Korea

Primary Beryllium Manufacturing Consolidation

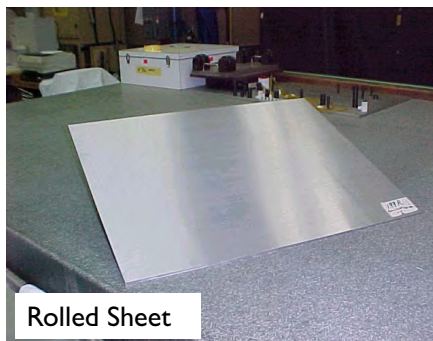
- Principal & Alternative Methods
- Next Step: Secondary Manufacturing



Beryllium Overview – BeWS-12, Korea

Secondary Beryllium Manufacturing "Special Products"

- Machining, Cutting, Sawing, Grinding, EDM
- Rolling, Extrusion, Forging, etc.
- Forming & Shaping



Beryllium Overview – BeWS-12, Korea



Aerospace & Defense

- Airborne FLIR & Targeting Systems
- Land-Based Fire Control & Laser Range-Finders
- Satellite & Missile Structures & Instrumentation



Beryllium & Composites

19

Beryllium Overview – BeWS-12, Korea

Optical Properties & End-Uses

- Bare & Plated Beryllium Mirrors
 - Reflectivity in Infrared
 - Nickel & Copper Plated
- Plated AlBeMet® Mirrors
 - CTE Match with Nickel



- Optical Benches & Housings
- Telescopes & Assemblies
- FLIRs & Other Fire Control Systems
- Polygon & Galvanometer Scanner Systems



Beryllium & Composites

20

Beryllium Overview – BeWS-12, Korea

Semiconductor Handling Equipment

- X-Y Stage Components (AM162)
 - AlBeMet® I62 (Machined)
 - BeO Ceramic
 - SupremEX® MMCs
- End-Effectors & Arm Components
 - AlBeMet® I62 (Machined)
 - BeO Ceramic
 - SupremEX® MMCs
- Wafer Chucks
 - BeO Ceramic
 - SupremEX® MMCs
- Wire Bonding Equipment
 - Flex-Link Parts (AlBeCast®)



Beryllium Overview – BeWS-12, Korea

Other Commercial Applications

- Acoustics & Loudspeakers
- Medical (non-X-Ray)
 - Blood Glucose Meter Parts
 - Defibrillator Components
 - Radiation Dosimeter Parts
- Acoustics & Loudspeakers
- Historical Miscellaneous
 - Data Storage
 - Sporting Goods



Beryllium Overview – BeWS-12, Korea

X-Ray Transmission Window Applications

- Medical Diagnostic
 - CT, Mammography, etc.
- Industrial / Analytical
 - X-Ray Fluorescence & Diffraction
- Synchrotron & Scientific Research



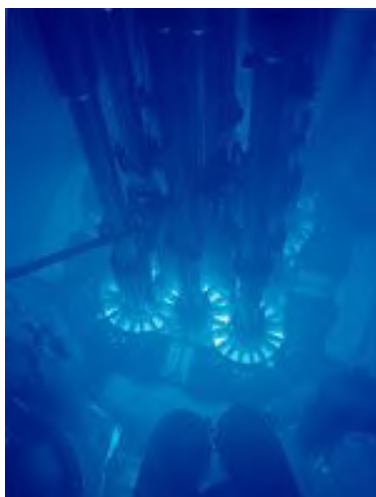
Medical X-Ray Source Tubes
Photo Courtesy Varian Medical Systems



National Synchrotron
Light Source (U.S.A.)
Water-Cooled Beryllium
Window Assemblies



Beryllium Overview – BeWS-12, Korea



Core of the
Advanced Test Reactor

Fission Test Reactors

- Traditional Functions
 - Materials Research
 - Accelerated Life-Testing
 - Weapons Research
 - Fuel Production & Research
- New Functions
 - Medical Radioisotope Production
 - Nuclear Medicine (BNCT, etc.)



Beryllium Overview – BeWS-12, Korea

Fission Test Reactor Programs (Current & New)

- ATR – Advanced Test Reactor (Idaho, U.S.A.)
- HFIR – High Flux Isotope Reactor (Tennessee, U.S.A.)
- MURR – Missouri University Research Reactor (U.S.A.)
- JMTR – Japan Materials Testing Reactor (Japan)
- JRR-3 – Japan Research Reactor (Japan)
- HFR – High Flux Reactor (Netherlands)
- BR2 – SCK-CEN Test Reactor (Belgium)
- SAFARI-I – NECSA Test Reactor (South Africa)
- OPAL – ANSTO Test Reactor (Australia)
- JRTR – Jordan Research & Training Reactor (Jordan)
- RJH – Jules Horowitz Reactor (France)
- KJRR – Ki-Jang Research Reactor (Korea)



Beryllium Overview – BeWS-12, Korea

HFR Machined S-200F Beryllium Reflector Assemblies



Beryllium Overview – BeWS-I2, Korea

Materion Beryllium Reflector Materials Specification vs. Typical

Factor	Grade	Be Assay		YS		UTS		Elongation		GS
		min	typ	min	typ	min	typ	min	typ	max
		(%)		(MPa)		(MPa)		(%)		(µm)
Reference	S-200F	98.5	99.1	241	260	324	380	2.0	3.0	20
Purity	S-65	99.2	99.4	206	230	289	386	3.0	5.2	20
Isotropy	S-65-H	99.0	99.4	206	280	345	450	2.0	5.1	15
	I-70-H	99.0	99.4	207	290	345	460	2.0	5.4	12
	O-30-H	99.0	99.5	297	302	400	425	3.0	3.1	15
Strength	S-200F-H	98.5	99.1	296	336	414	450	3.0	4.6	12
	I-220-H	98.0	98.6	345	498	448	577	2.0	3.2	15



Beryllium Overview – BeWS-I2, Korea

Fusion Test Reactors

- Fusion Technologies
 - Origin
 - Magnetic Confinement
 - Inertial Confinement (also called Laser)
- Potential Benefits
 - No CO₂ Emissions
 - Unlimited Fuel Supply
 - Minimal Waste Products



Beryllium Overview – BeWS-12, Korea

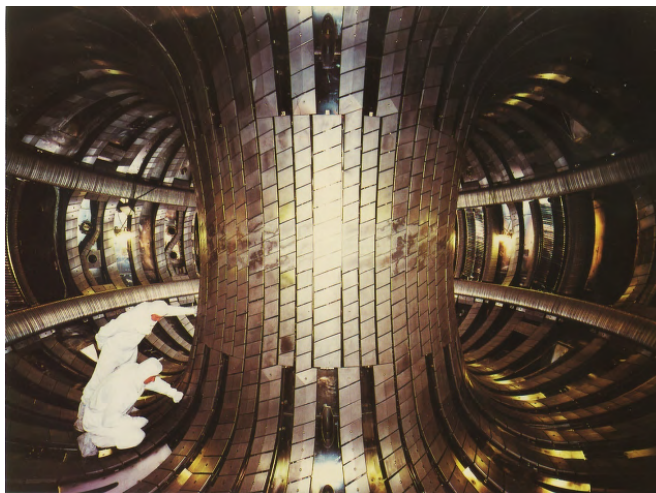
Fusion Test Reactor Programs

- JET – Joint European Torus (England)
 - RF Antenna & Belt Limiter Tiles; ITER-Like Wall Project
- ITER – Int’l Thermonuclear Experimental Reactor (France)
 - First Wall Tiles & TBM Neutron Multiplier Option
- DEMO – Demonstration Fusion Reactor (Future)
 - High-Temperature Neutron Multiplier Material
- NIF – National Ignition Facility (California, U.S.A.)
- LIFE – Laser Inertial Fusion Energy (Future)
 - Molten-Salt Coolant & Neutron Multiplier Possibilities



Beryllium Overview – BeWS-12, Korea

Joint European Torus – Historical Use of S-65 Be

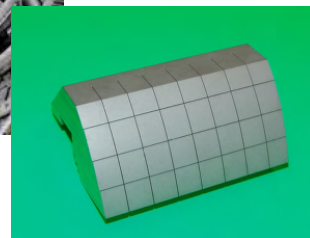
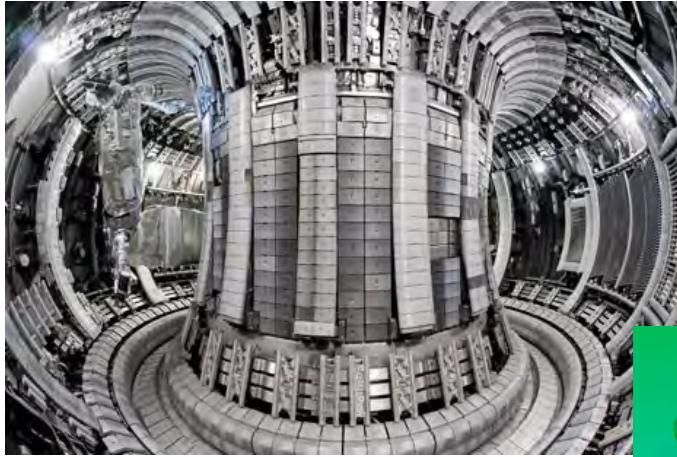


JET Reactor & Beryllium RF Antenna Tiles



Beryllium Overview – BeWS-12, Korea

ITER-Like Wall Project at JET – New Use of S-65-H Be



Machined Be Tile for ITER-Like Wall Project
Photo Courtesy of Axsys Technologies PMP



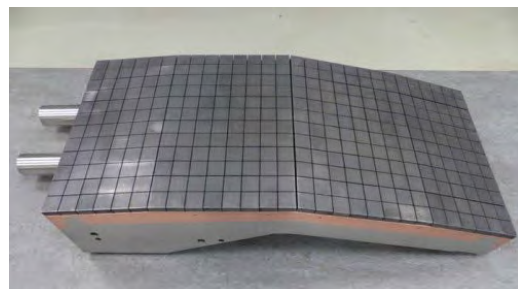
Beryllium Overview – BeWS-12, Korea

International Thermonuclear Experimental Reactor

- First Wall Tile Assemblies
 - EU, Russia & China
 - S-65 Be ITER Ref Grade
 - Russia & China Also Qualified
 - 680m² – Multiple Tile Sizes
 - Semi-Prototypes 2013-2015
 - Full-Scale Prototypes by 2017
 - First Plasma 2021 or Beyond



ITER First Wall Be Tile Mock-up
Photo Courtesy of Sandia Nat'l Lab



ITER FW Semi-Prototype Panel
Photo Courtesy of AREVA NP

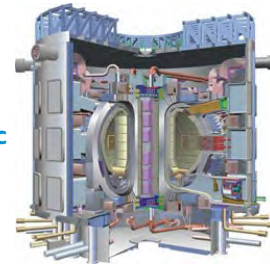


Beryllium Overview – BeWS-I2, Korea

International Thermonuclear Experimental Reactor

- Test Blanket Modules
 - Solid vs. Liquid Breeder
 - Neutron Multiplier
 - Cooperative Agreement – KIT/KBHF (Germany)
 - Imm-OD Mini-Spheres
 - Rotating Electrode Process
 - Fluoride Reduction Process
 - Shotting Method
 - Impact-Ground Material

ITER Schematic



Beryllium Overview – BeWS-I2, Korea

Summary & Conclusion

- Beryllium Metal & Other Beryllium-Containing Materials
 - Long History from Discovery to Commercialization
 - Unusual Combination of Properties
- Extensive Historical Use in High-Performance Applications
 - Aerospace, Defense & Optics
 - Commercial, X-Ray Transmission & Medical
 - Wide Range of Nuclear End-Uses including Fusion
- Ongoing Development of New Applications in All Fields





MATERION BUSINESSES
Advanced Chemicals
Barr Precision Optics & Thin Film Coatings
Brush Beryllium & Composites
Brush Performance Alloys
Ceramics
Electrofusion
Large Area Coatings
Microelectronics & Services
Natural Resources
Technical Materials

www.materion.com



**REFERENCE SLIDES &
ADDITIONAL
INFORMATION**

Materion Beryllium & Composites

Beryllium Overview – BeWS-I2, Korea

Comparison of Typical Physical & Mechanical Properties

Property	Beryllium S-200F AMS7906	AlBeMet® AM162H AMS7911	SupremEX® S640XA (Non-Be)	E-Material E-60	Magnesium AZ80A T6	Aluminum 6061 T6	Titanium Grade 4
Density (g/cm³)	1.85	2.10	2.90	2.51	1.80	2.70	4.50
Modulus (GPa)	303	193	140	331	45	69	105
UTS (MPa)	380	305	570	273	340	310	660
YS (MPa)	260	226	480	N/A	250	275	590
Elongation (%)	3.0	4.7	2.5	<0.05	5.0	12.0	20.0
Fatigue Strength (MPa)	261	138	271	N/A	100	95	N/A
Thermal Cond. (W/m-°K)	216	210	130	210	76	180	16.9
Heat Capacity (J/g-°C)	1.95	1.56	N/A	1.26	1.05	0.896	0.54
CTE (ppm/°C)	11.3	13.9	13.4	6.1	26	24	8.6
Elec. Resistivity (ohm-cm)	4.2 E-06	3.5 E-06	N/A	N/A	14.5 E-06	4 E-06	60 E-06



Beryllium & Composites

37

Beryllium Overview – BeWS-I2, Korea

Comparison of Typical Ceramics Properties

	BeO	AlN	Al ₂ O ₃ 96%	Al ₂ O ₃ 99.8%
Density (g/cm³)	2.85	3.28	3.75	3.94
CTE (ppm/°C)	6.3	4.7	7.1	7.1
Thermal Conductivity (W/m-°K)	285	180	21	28
Specific Heat (J/g-°K)	1.046	0.75	--	--
Flexural Strength (MPa)	232	186	276	414
Young's Modulus (GPa)	345	320	380	390



Beryllium & Composites

38

Beryllium Overview – BeWS-12, Korea

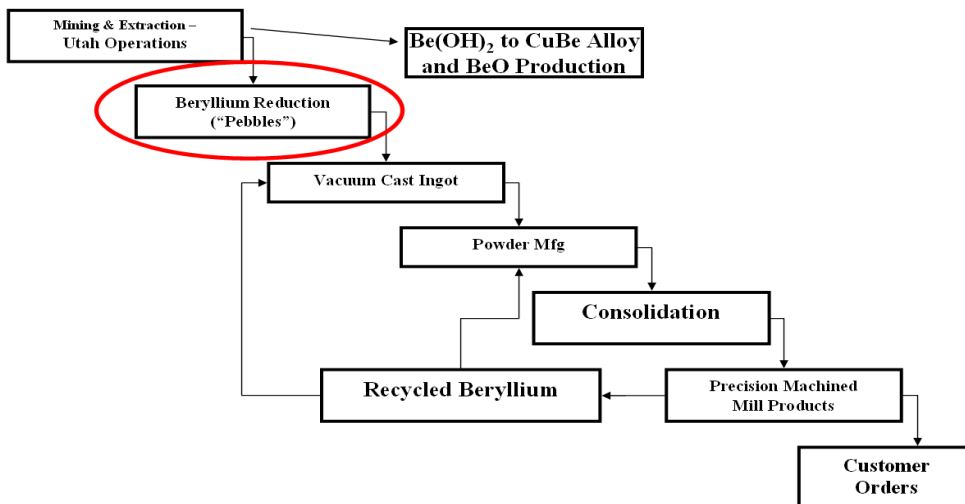
Comparison of Materion Ceramics Key Properties

	BeO Thermalox 995	BeO BW1000	BeO BW3250	Al ₂ O ₃ Durox AL	Al ₂ O ₃ Durox UHP
Density (g/cm ³)	2.85	2.90	2.95	3.94	3.95
Thermal Conductivity (W/m-°K)	285	270	325-340	30	35
Flexural Strength (MPa)	221	345	221	379	379
Purity (%)	99.5	99.5	99.7	99.8	99.9
Grain Size (µm)	15	9	25	1	2



Beryllium Overview – BeWS-12, Korea

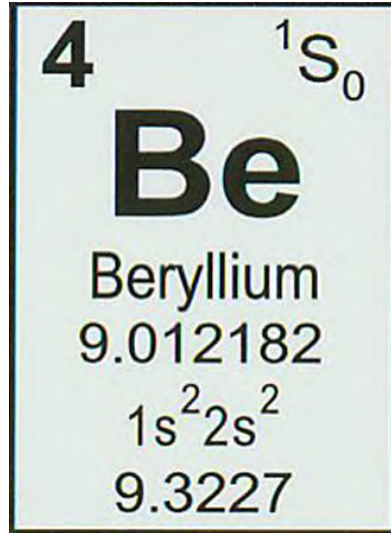
Process Flow Chart for Making Beryllium



Beryllium Overview – BeWS-I2, Korea

Why Beryllium? – Relevant Properties for Nuclear Uses

- Nuclear Properties
 - Low Atomic Number “Z”
 - Low Mass Absorption Coefficient
 - Neutron Reflection, Moderation, Donation & Multiplication
- Thermal Conductivity
- Melting Point



Beryllium & Composites

41

Beryllium Overview – BeWS-I2, Korea

Environmental, Health & Safety (EH&S) Basics

- All Beryllium Materials Must Be Treated Alike
- Solid Forms Pose No Special Hazards
- Necessary Conditions
 - Allergic Reaction
 - Airborne & Ultra-Fine
- All Materials Recyclable
 - Buy-Back Program



Beryllium & Composites

42

2.2.4 Recent results on DEMO activities and IFMIF/EVEDA under BA program

T. Yamanishi¹, M. Nakamichi¹, N. Asakura¹, K. Tobita¹, S. Ohira¹, G. Federici², R. Heidinger³, J. Knaster⁴, S. Clement⁵, N. Nakajima⁶, and other BA IFERC and IFMIF/EVEDA contributors

¹ *Japan Atomic Energy Agency, Rokkasho, Aomori, Japan*

² *EFDA Close Support Unit, Garching, Germany*

³ *Fusion for Energy, Garching, Germany*

⁴ *BA IFMIF/EVEDA Project Team, Rokkasho, Aomori, Japan*

⁵ *Fusion for Energy, Barcelona, Spain*

⁶ *BA IFERC Project Team, Rokkasho, Aomori, Japan*

yamanishi.toshihikko@jaea.go.jp

In the Broader Approach (BA) activities, the International Fusion Energy Research Center (IFERC) project, the International Fusion Materials Irradiation Facility/Engineering Validation and Engineering Design Activities (IFMIF/EVEDA) project are implemented aiming at early realization of the fusion energy from 2007 to 2017 at Rokkasho Fusion Institute of JAEA.

DEMO design activity has been conducted as joint work between EU and Japan, in order to establish DEMO design bases. Divertor designing is regarded to be a critical issue on engineering and material. A conceptual design of the tungsten armor and two cooling units, i.e. copper-alloy and reduced activation ferritic martensitic (RAFM) steel pipes for the different heat and neutron conditions, was investigated on the basis of neutronic analysis in a 1.5 GW fusion power DEMO.

In the DEMO R&D activities, following five R&D tasks related blanket materials and technology are carried out intensively according to the common interests of the EU and Japan for DEMO; R&D on RAFM steels as structural material, SiCf/SiC composites as a flow channel insert material and/or alternative structural material, advanced tritium breeders and neutron multipliers, and tritium technology relevant to the DEMO operational condition. As a recent major activity, the compatibility of SiC/SiC composites with liquid metal breeding materials has been carried out to design a liquid metal breeding blanket. A series of analysis studies for dust and tile samples of JET has also been started: the tritium inventory and surface characteristics of the samples.

Development of the software for the remote experiment has been started, and the Remote Experimental Center room will be made from 2015. A super computer, Helios, has been operated from 2012, and has been used heavily by EU and JA users; a weekly averaged operation rate has reached to 97%.

Regarding the IFMIF/EVEDA Project, the validation test using EVEDA Lithium Test Loop (ELTL) was completed successfully in 2014 the end of October, achieving an integrated operation time more than 1,300 hours with a stable lithium flow at a 15 m/s, which was more than the goal of the operation time (1,000 h), and within specified thickness tolerance of the lithium screen of +/-1 mm. Installation of the LIPAc injector and auxiliary equipment delivered by F4E has been done and the first proton beam extraction was successfully performed in November 2014.

A series of post BA activities from 2017 has been started between EU and JA. A neutron source using the IFMIF/EVEDA prototype accelerator and the IFMIF/EVEDA lithium target test loop is under discussion as one of the major activities after 2017.

The 12th International Workshop on Beryllium Technology (BeWS-12),
 ICC JEJU, Jeju Island, Korea, 10 September 2015.

1

Recent results on DEMO activities and IFMIF/EVEDA under BA program

Masaru NAKAMICHI,
 instead of Toshihiko YAMANISHI

Japan Atomic Energy Agency

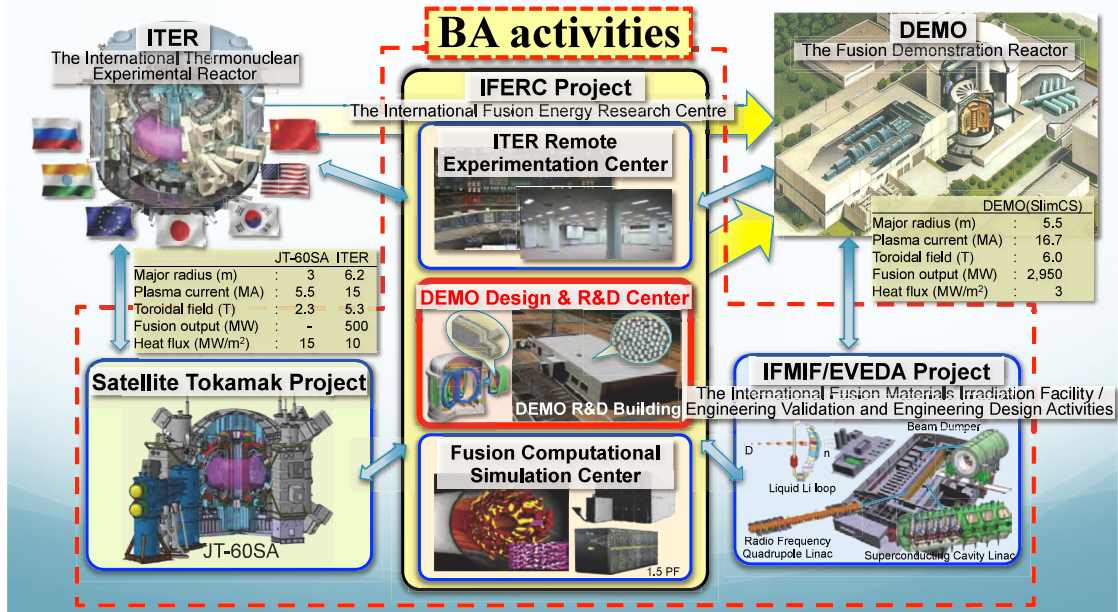


Broader Approach (BA) Activities



2

In parallel to the ITER program, BA activities are being implemented by the EU and JA, aiming at early realization of the fusion energy. BA activities comprise as follows,

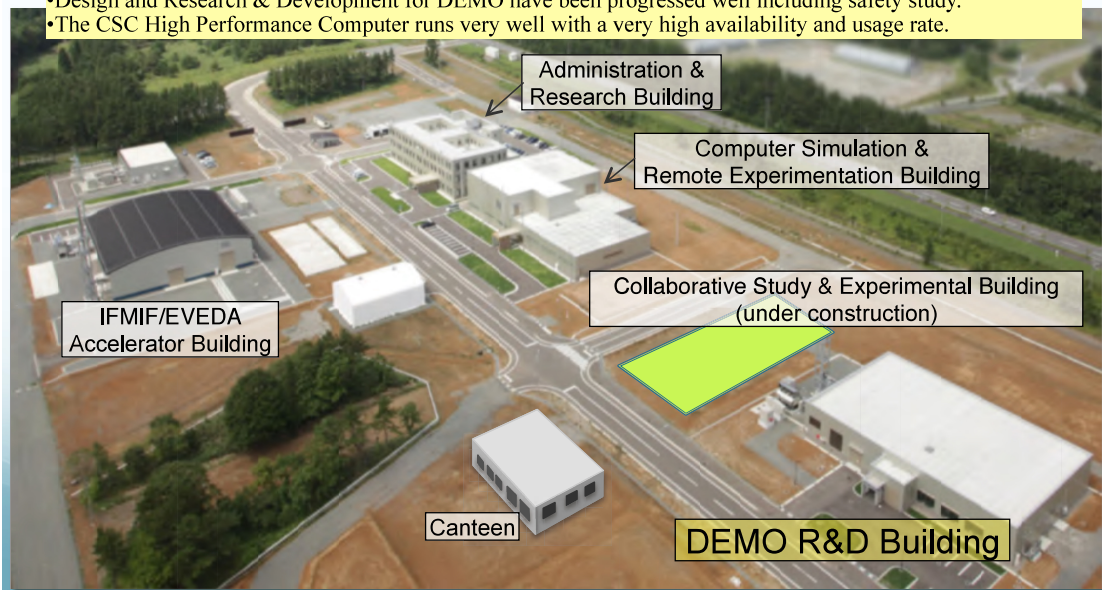


International Fusion Energy Research Centre (IFERC)³



Rokkasho BA site⁴

- Those research buildings have been completed in March 2010 and a cafeteria and utilities for IFMIF/EVEDA Prototype Accelerator (LIPAc) have been constructed during 2011 - 2012.
- Installation of the LIPAc injector and auxiliary equipment delivered by F4E has been done and the first proton beam extraction was successfully performed in November 2014.
- Design and Research & Development for DEMO have been progressed well including safety study.
- The CSC High Performance Computer runs very well with a very high availability and usage rate.



DEMO Design and R&D Coordination Centre

5

The purpose of the DEMO Design Activities (DDA) under BA is to provide a technical perspective of a Demonstration Fusion Reactor (DEMO) based on relevant technologies. The DDA has addressed design features of fusion DEMO reactors, critical design issues found through gap study between ITER and DEMO, and various efforts for resolving the issues.

- Forty technical meetings have been held to address various DEMO design issues as of May 2015.
- Joint work between DEMO design and R&D has started to consolidate materials database for DEMO design in 2014.
- Intermediate Report was compiled in Feb. 2015, highlighting the BA DEMO Design Activities in the period of 2011-2014 .



(130 pages, unpublished)

Intermediate Report
of BA DEMO Design

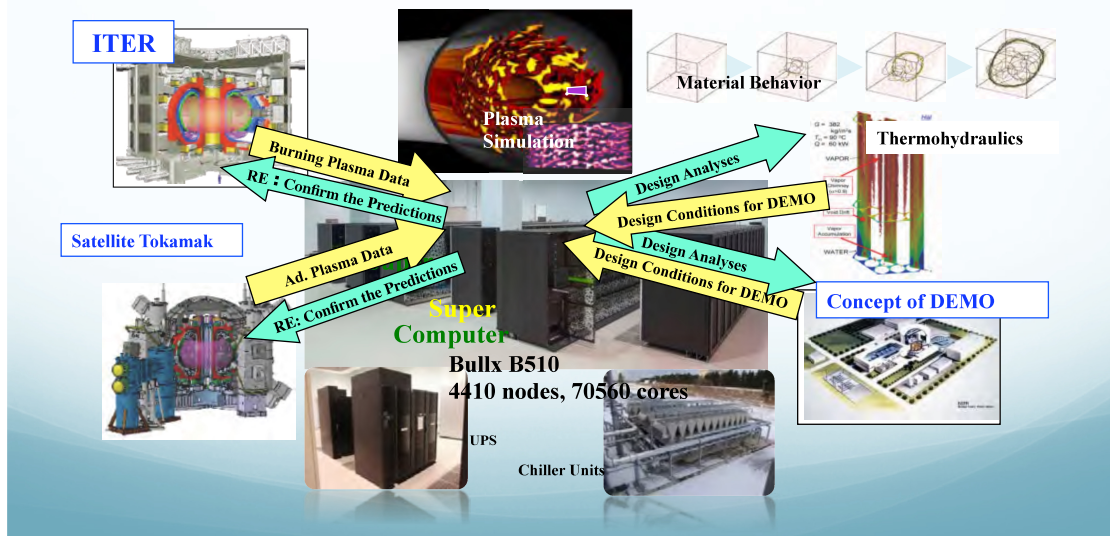


20th Design Task mtg. (Garching, Nov. 2014)

BA Computational Simulation Center

6

- ◆ BA Computational Simulation Center is established for the simulation and modeling of ITER and the other fusion experiments, and for the design of future fusion power plants.
- ◆ It will be a powerful tool not only for the plasma physics but also fusion nuclear technology, such as multi-scale modeling of the irradiation effect on the blanket materials.



ITER Remote Experimental Centre (REC)

7

- The REC aims to facilitate a broad participation of scientists in ITER experiments.
- Prior to the demonstration of the ITER remote experimentation, the functions of the REC will be tested on existing machines, such as the Satellite Tokamak (JT-60SA).
- JA and the EU started discussion on the overall plan of the REC.

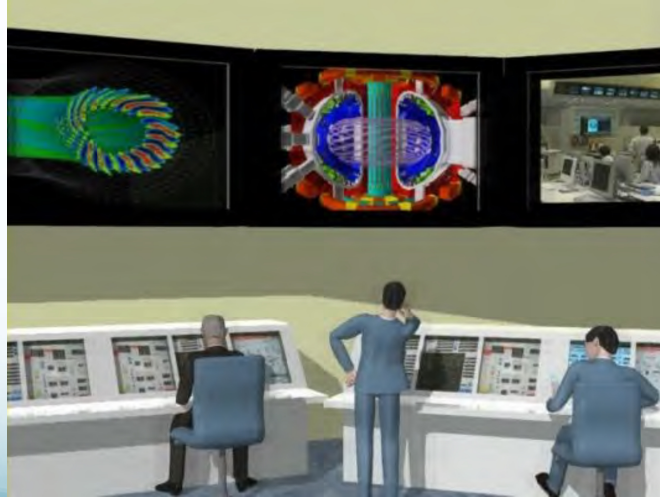
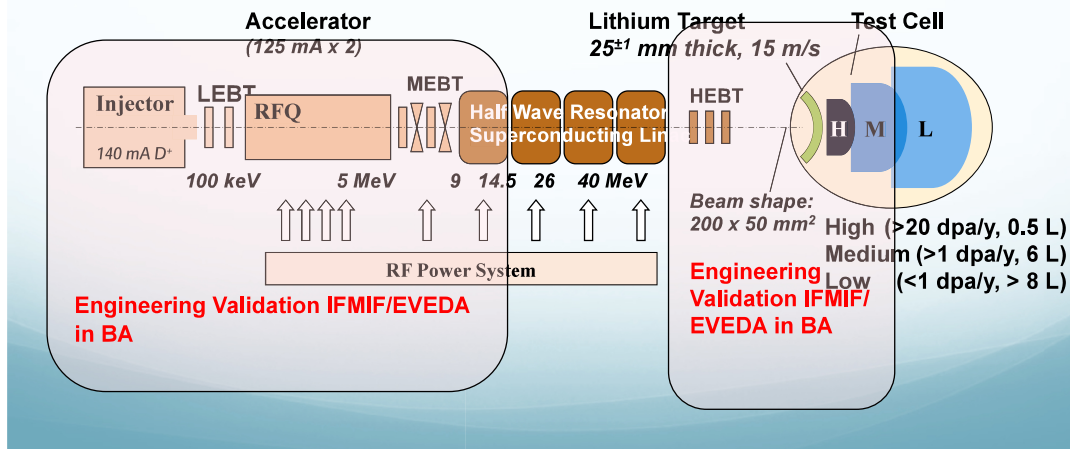


Image of the ITER Remote Experimental Centre

IFMIF/EVEDA

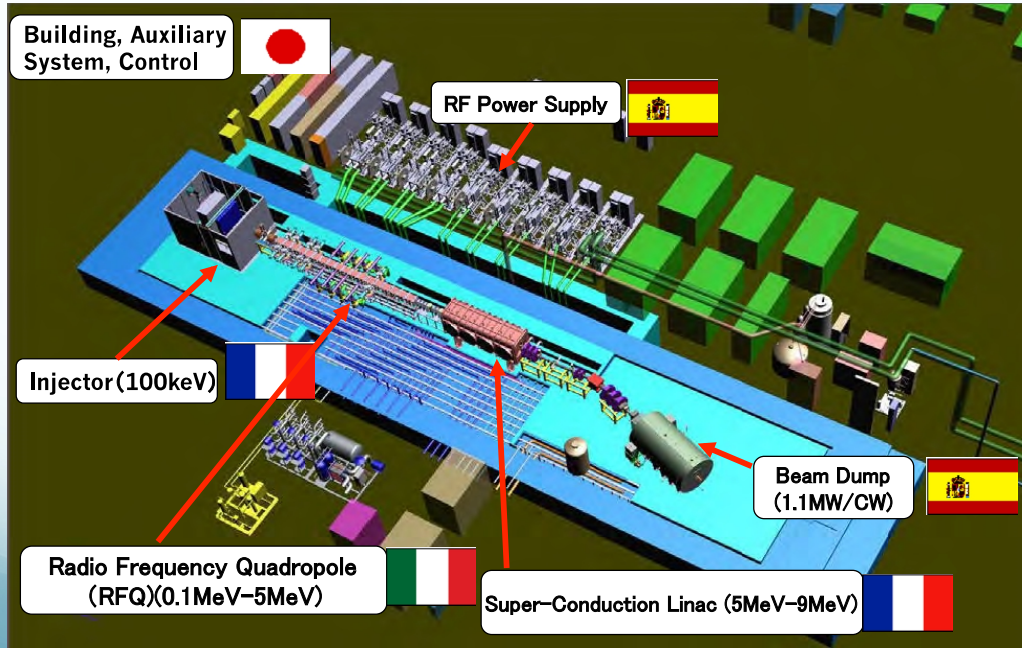
8

- ◆ IFMIF is an accelerator based neutron source using $\text{Li}(d,n)$ reactions aiming at providing a material irradiation database for the design, construction, licensing, and safe operation of DEMO.
- ◆ IFMIF consists of two deuteron linear accelerators, free surface liquid lithium target, test cell, and the post irradiation examination facility.



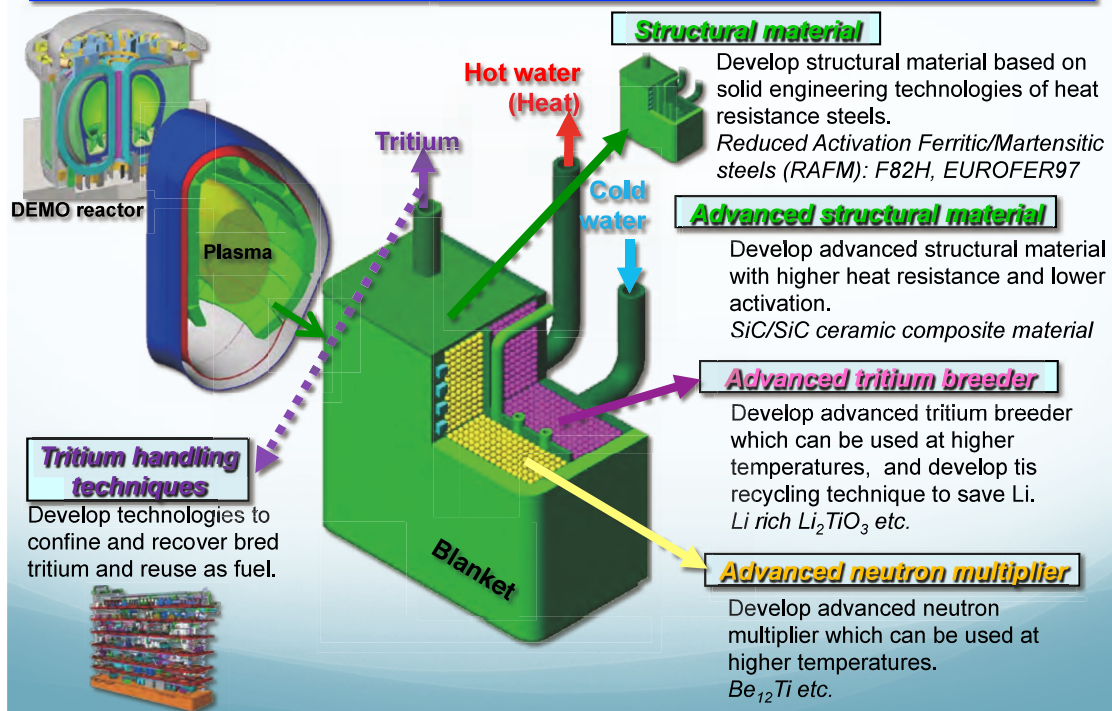
Linear IFMIF Prototype Accelerator: LIPAC

9



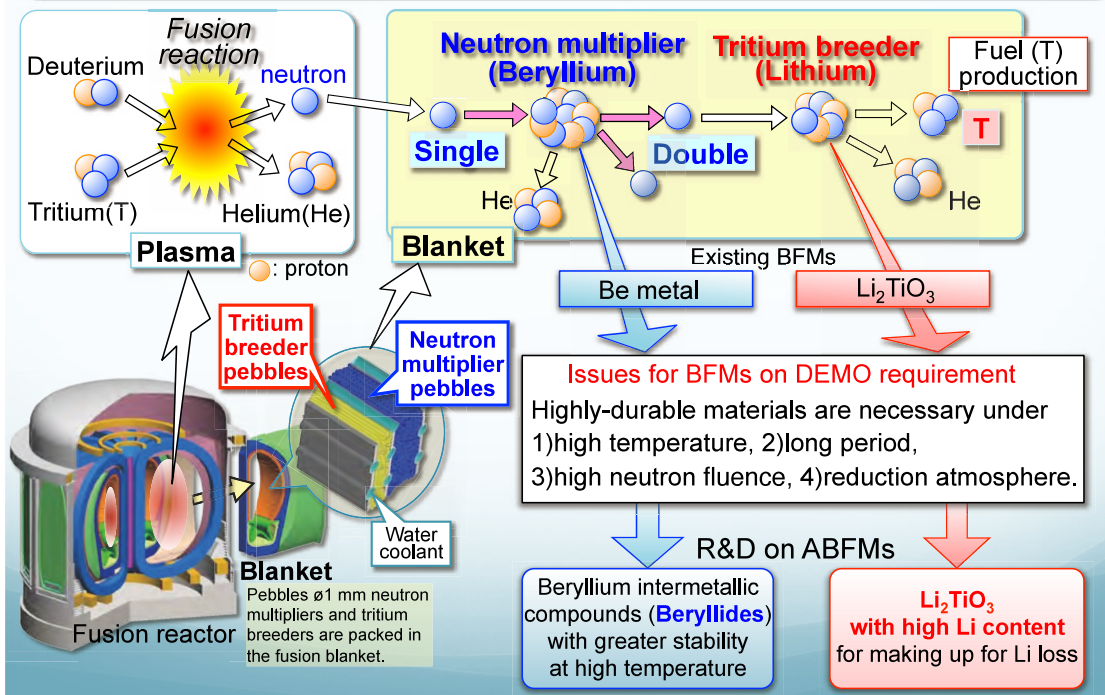
DEMO R&D Activities

10



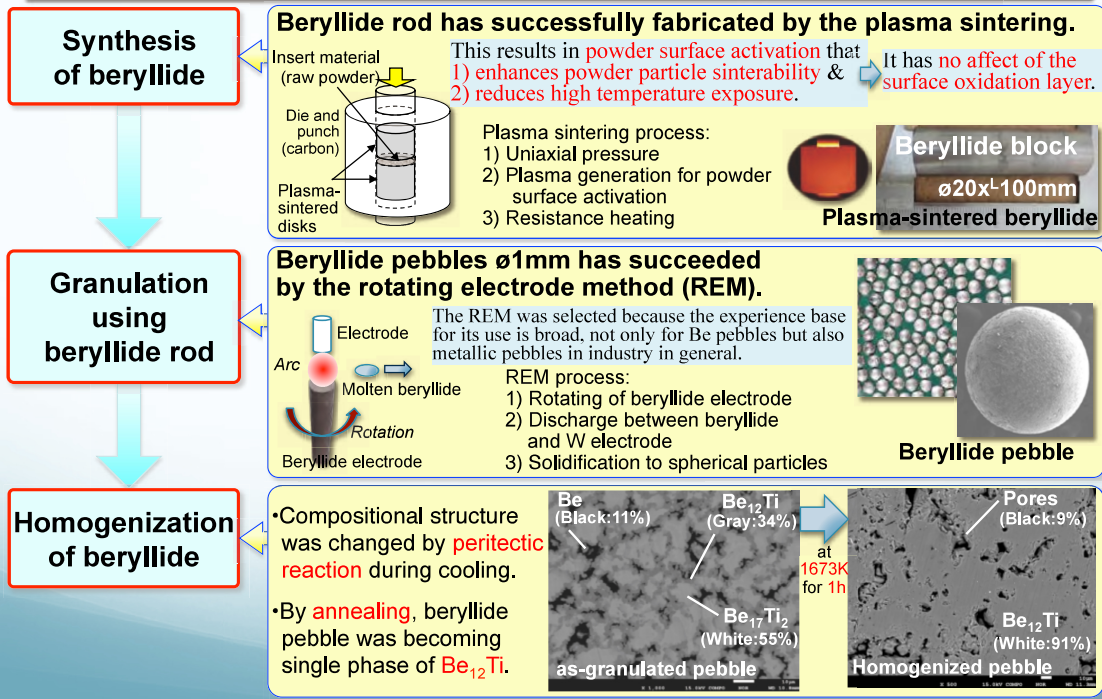
Advanced Tritium Breeding Functional Materials

Necessity of Advanced Breeding Functional Materials (ABFMs)¹²

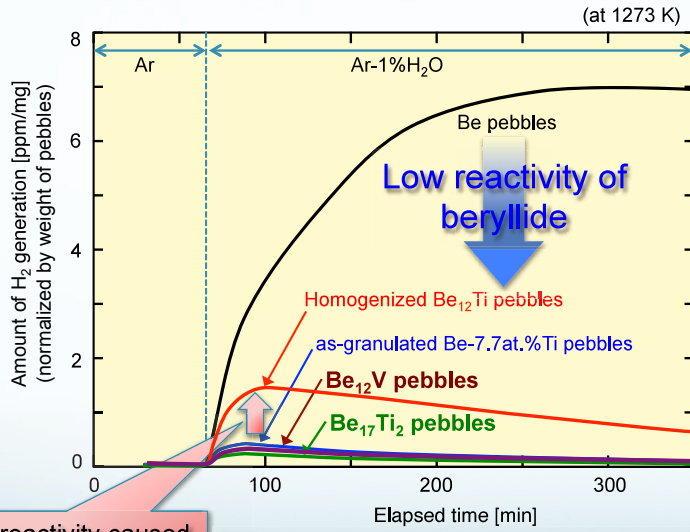


Advanced Neutron Multipliers

Novel granulation flow scheme of Be₁₂Ti beryllide



Reactivity with water vapor of Beryllides pebbles



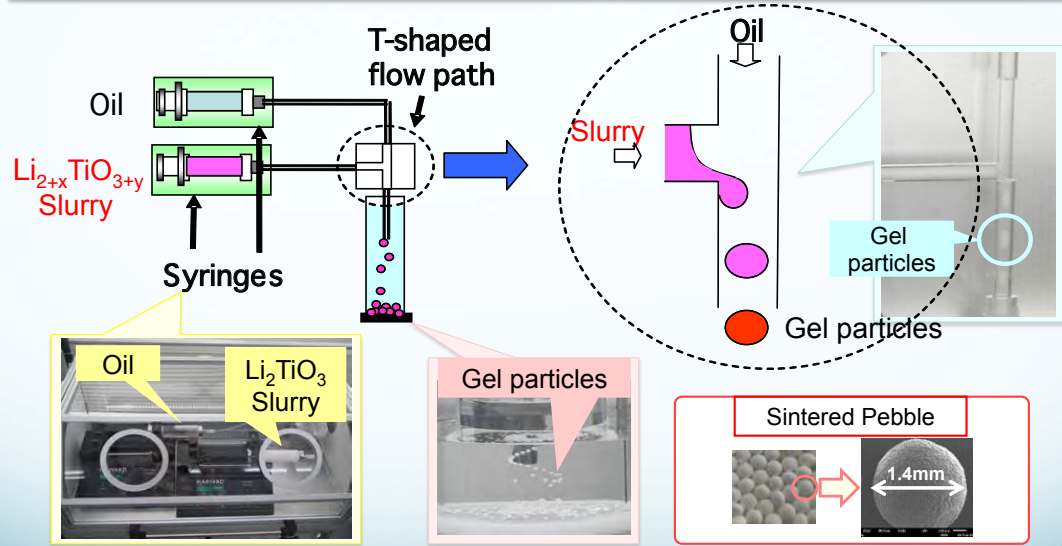
Increased reactivity caused by the increased specific surface area by homogenization treatment

- Beryllides pebbles indicated the lower reactivity with water vapor than Be pebbles.
- However, homogenized Be₁₂Ti pebbles demonstrated increased reactivity relative to as-granulated pebbles.
- It was clarified that the increased hydrogen generation was caused by the increased specific surface area of the homogenized Be₁₂Ti pebbles.

Advanced Tritium Breeders

Novel granulation method – Emulsion method -

17



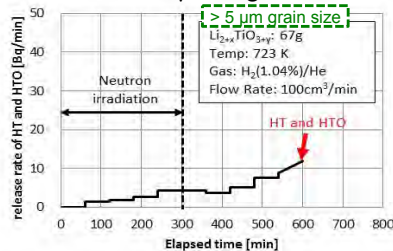
This granulator consisted of two syringes arranged in a T-shaped flow path. One syringe was filled with oil and the other with a $\text{Li}_{2+x}\text{TiO}_{3+y}$ slurry. The two flow lines from the syringes were connected in a T-shaped flow path. This arrangement allowed cutting the slurry flow with oil from the oil-filled syringe. The size of the tritium breeder gel particles was controlled by the flow speeds of oil and slurry. The gel particles were placed in an oil-filled container.

Ref.: T. Hoshino, et. al, Fusion Science and Technology, 67, 146-149, (2015)

Tritium Release Properties

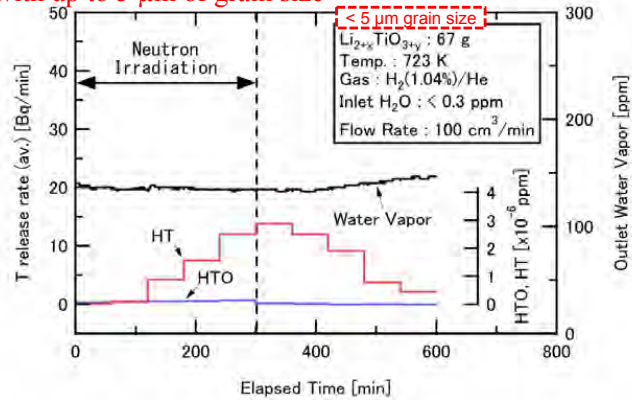
18

Trial pebbles of $\text{Li}_{2+x}\text{TiO}_{3+y}$ with more than $5 \mu\text{m}$ of grain size



Tritium release speed was gradually increased because cross-sectional grain size was large ($5\text{--}10 \mu\text{m}$). The ratio of released tritium chemical form of HT and HTO was 50 : 50. Finally, the tritium recovery was about 40%, and a large amount of tritium remained.

Optimized $\text{Li}_{2+x}\text{TiO}_{3+y}$ pebbles with up to $5 \mu\text{m}$ of grain size



The optimized pebbles exhibited good tritium release behavior from viewpoints of not only chemical form of released tritium but also tritium recovery rate.

- 1) 95% of released tritium was HT chemical form. : Good tritium handling & treatment
- 2) Tritium recovery was about 90%. : Good tritium release property

Ref.: T. Hoshino, et. al, Fusion Science and Technology, 67, 146-149, (2015)

2.2.5 Material Development Strategy for HCCR-TBM in KO

Yi-Hyun Park¹, Seungyon Cho¹, Mu-Young Ahn¹ and Young-Bun Chun²

¹*National Fusion Research Institute, Daejeon, Republic of Korea*

²*Korea Atomic Energy Research Institute, Daejeon, Republic of Korea*

E-mail: yhpark@nfri.re.kr

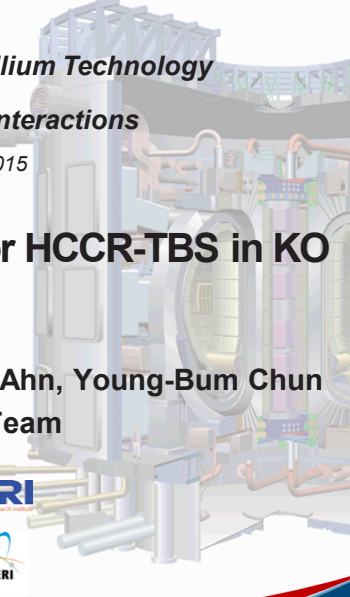
The first experimental data on a tritium breeding blanket in fusion environment will be provided by the ITER Test Blanket Module (TBM) Program. Korea has developed a Helium Cooled Ceramic Reflector (HCCR) TBM in order to acquire experimental results and verify a breeding blanket concept for demonstration power reactor (DEMO) under the ITER TBM Program. The HCCR TBM is adopting a four sub-module concept considering the manufacturability and the post irradiation examination including the transfer of irradiated TBM. The HCCR TBM structure is made from the reduced activation ferritic/martensitic (RAFM) steel. The breeding zone of each sub-module consists of seven layers which are three neutron multiplier layers, three tritium breeder layers, and one neutron reflector layer. Beryllium and lithium ceramic pebbles are used as neutron multiplier and tritium breeder materials, respectively. The HCCR TBM has a unique concept among the ITER TBMs that graphite is employed as neutron reflector in order to reduce the beryllium amount. It means to have several advantages from the viewpoint of safety and cost.

The Advanced Reduced Activation Alloy (ARAA) is being developed as a structural material of the HCCR TBM. The total number of 91 model alloys were designed, fabricated, and evaluated. The commercial scale ARAA, which was 5 ton scale, was successfully fabricated by industrial company. The material properties database for unirradiated ARAA has been constructed. The neutron irradiation test up to 3 dpa has been planned using HANARO research reactor in KAERI. Lithium metatitanate is primary candidate material for tritium breeder of HCCR TBM. The slurry droplet wetting method was developed to fabricate the pebble shape with 1 mm diameter by NFRI. The automatic slurry dispensing system was manufactured for mass-production of breeder pebble. The production rate of this system for Li₂TiO₃ pebble was estimated at more than 40 kg/year. Fabrication conditions for mass-production system, such as needle size, dispensing pressure, sintering temperature, and so on, were investigated and established. The beryllium pebble and nuclear grade graphite will be purchased from industrial company for neutron multiplier and reflector in the HCCR TBM, respectively. Especially, in accordance with the radioprotection requirement limit of ITER and the activation product inventory in the irradiated TBM, the uranium content in beryllium pebble has to be strictly controlled. The properties database of functional materials will be built up not only by Korean TBM team but also by international collaborators including industrial companies.

Joint Session between
12th International Workshop on Beryllium Technology
and
18th Ceramic Breeder Blanket Interactions
Jeju Island, September 10, 2015

Material Development Strategy for HCCR-TBS in KO

Seungyon Cho, Yi-Hyun Park, Mu-Young Ahn, Young-Bum Chun
on behalf of KO TBM Team



Outline

- I** Introduction
- II** Status of Structural Material Development
- III** Status of Functional Material Development
- IV** Summary



BeWS-12, Jeju Island, 10-11 Sep., 2015

1

1. Introduction

◆ **Helium Cooled Ceramic Reflector (HCCR) TBM**
(DEMO-relevant Breeding Blanket Concept)

Main design parameters and materials

Parameter	Values
FW heat flux	0.3 MW/m ²
Neutron wall load	0.78 MW/m ²
Structural material	KO-RAFM (ARAA) (< 550 °C)
Breeder	Li ₂ TiO ₃ (< 920 °C) 70% enrichment Li-6
Multiplier	Be (< 650 °C)
Reflector	Graphite (<1200 °C)
Size	1670(P) x 462(T) x 605(R) (mm)
Coolant	8 MPa He
	1.14 kg/s (Nominal)
	300 °C inlet 500 °C outlet
Purge gas	He with 0.1 % H ₂

- Four sub-module Concept
 - Manufacturability, PIE & Transportation of Irradiated TBM
 - EM Force Reduction, Endurance of Internal Over-Pressure
- Graphite as Neutron Reflector
 - Reduce the Amount of Be Multiplier
 - Decrease of Cost
 - Comparable Nuclear Performance for tritium breeding and shielding

NFRI KAERI BeWS-12, Jeju Island, 10-11 Sep., 2015 2

1. Introduction

◆ **Materials Procurement Strategy** for HCCR TBM

- **Structural Material**
 - Develop KO own RAFM (ARAA)
 - Establish material property Data Base up to 2~3 dpa
 - Follow ITER Material Qualification Process (Particular Material Appraisal)
- **Breeder Material**
 - Develop KO own Li₂TiO₃ pebbles
 - Establish material property Data Base for pebble and pebble-bed
 - Comparison with other fusion breeder materials (No-qualification)
- **Multiplier Material**
 - Purchase pure beryllium pebbles developed by companies
 - Utilize the available material property Data Base
- **Reflector Material**
 - Purchase commercially available nuclear grade graphite block from companies
 - Utilize the available material property Data Base established by companies

NFRI KAERI BeWS-12, Jeju Island, 10-11 Sep., 2015 3

Outline

- I Introduction
- II Status of Structural Material Development**
- III Status of Functional Material Development
- IV Summary


 BeWS-12, Jeju Island, 10-11 Sep., 2015 4

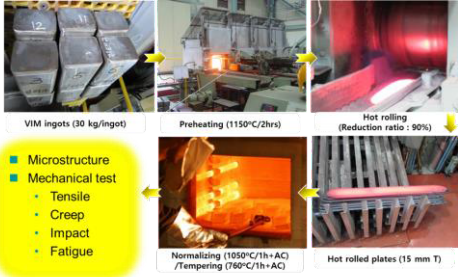
2. Status of RAFM Development

ISFNT-12 : O2B.3

- ◆ Advanced Korean RAFM steel development with:
 - Improved creep and impact resistances
 - Good irradiation resistance under neutron



Advanced Reduced
Activation Alloy



- Microstructure
- Mechanical test
 - Tensile
 - Creep
 - Impact
 - Fatigue

2. Status of RAFM Development

- ◆ Alloy Design : Strategy
 - Basic guidelines
 - 8~9 Cr – 1~2 W base (good resistance to irradiation embrittlement)
 - Minimized induced-activity: (Nb, Mo, Ni, Co, Cu, Al)-free
 - Full-martensitic structure (delta-ferrite free)
 - Approaches
 - Optimal combination of the amounts of alloying elements commonly used in the RAFM steels
 - Cr, W, Ta, V, Ti, ...
 - Addition of new alloying elements
 - Zr or Sc, or both



BeWS-12, Jeju Island, 10-11 Sep., 2015

6

2. Status of RAFM Development

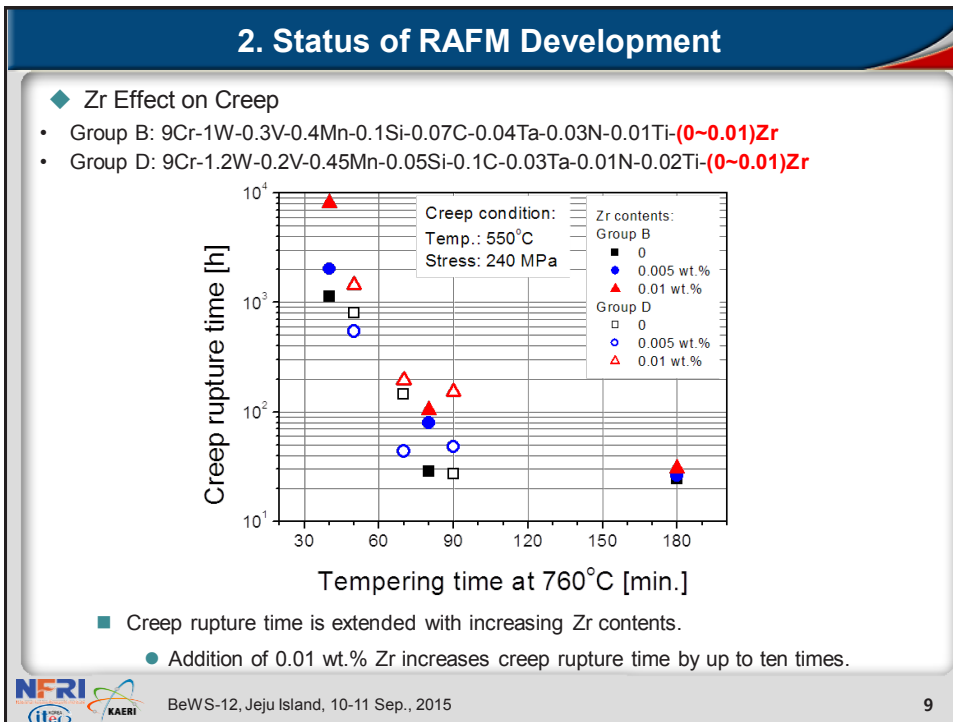
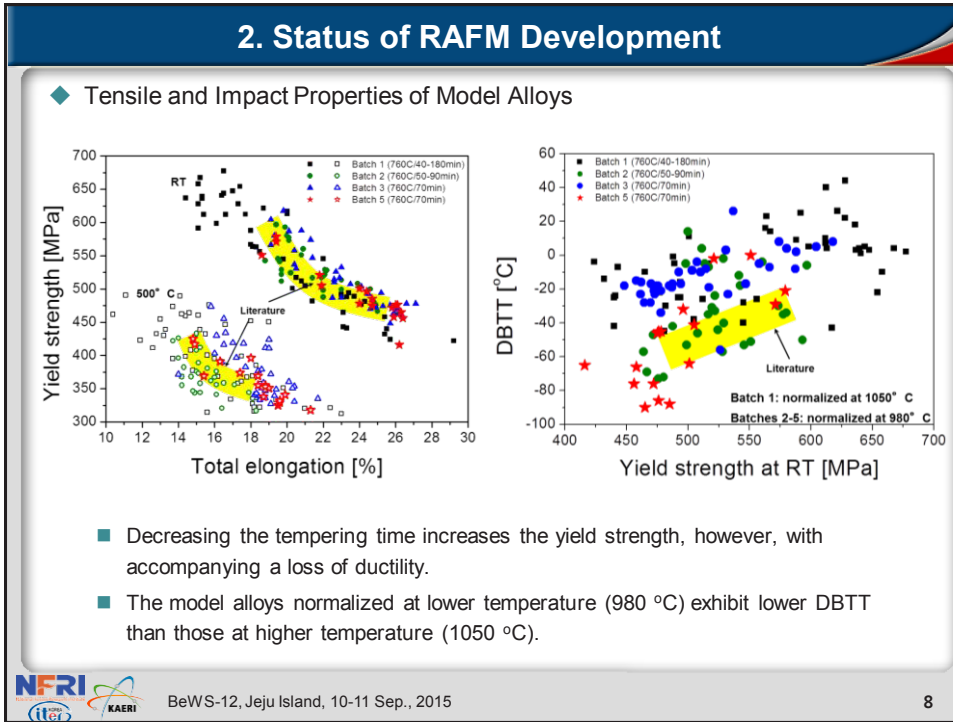
◆ Total of 98 alloys were designed, fabricated and evaluated

Group	C	Si	Mn	Cr	W	V	Ta	N	B	Ti	Zr	Sc
Batch 1												
Group A (10 alloys)	0.07	0.10	0.40	9.0	1.0 - 2.0	0.2 - 0.3	0.04 - 0.12	0.03	-	-	-	
Group B (12 alloys)	0.07	0.10	0.40	9.0	1.0	0.2 - 0.6	0.02 - 0.10	0.03	0 - 0.005	0.01	0 - 0.01	
Batch 2												
Group C (8 alloys)	0.07	0.05	0.4	8.0- 9.0	1.0 - 1.5	0.2	0.05	0.03	-	0 - 0.01		
Group D (7 alloys)	0.1	0.05	0.45	9.0	1.2	0.2	0.03	0.01	-	0 - 0.02	0 - 0.01	
Batch 3												
Group E (21 alloys)	0.07	0.05	0.4	8.0- 10.0	0.8 - 1.6	0.2	0.07	0.04	-	0.01 - 0.02	0 - 0.04	0 - 0.05
Group F (15 alloys)	0.07	0.05	0.5	8.5	1.4	0.15 - 0.35	0.03 - 0.1	0.05	-	0.01 - 0.02	0 - 0.04	0 - 0.05
Batch 5												
Group G (17 alloys)	0.1	0.1	0.45	9	1.2	0.2	0.07	-		0.01	0 - 0.05	0 - 0.05



BeWS-12, Jeju Island, 10-11 Sep., 2015

7



2. Status of RAFM Development

◆ Production of Commercial-scale ARAA



- 5-ton scale
- January 2014
- POSCO Specialty Steel
- VIM + ESR process
- Normalizing : 980 °C, 40 min
- Tempering : 750 °C, 70 min
- Mock-up fabrication, DB establishment

■ Chemical composition of Commercial-scale ARAA

wt.%	C	Si	Mn	Cr	W	V	Ta	N	Ti	Zr
Target	0.10	0.10	0.45	9.0	1.2	0.20	0.07	0.01	0.01	0.01
Allowance	0.08-0.12	0.05-0.15	0.30-0.60	8.70-9.30	1.00-1.40	0.10-0.30	0.05-0.09	0.005-0.015	0.005-0.020	0.005-0.020
Analysis	0.089	0.057	0.43	8.98	1.20	0.19	0.07	0.011	0.010	0.012



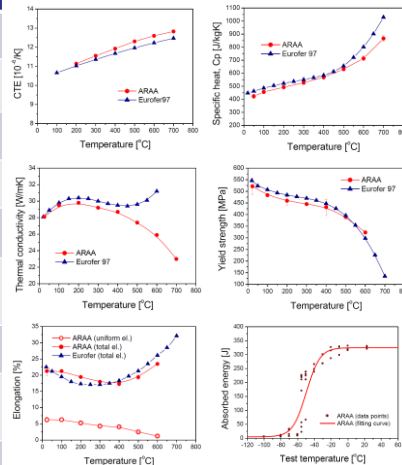
BeWS-12, Jeju Island, 10-11 Sep., 2015

10

2. Status of RAFM Development

◆ Properties of Commercial-scale ARAA (1st Heat, 5 ton-scale)

Properties	Values
Density	$\rho(T) = 7,792 - 2.8 \times 10^{-1}T - 2.9 \times 10^{-5}T^2$
Young's Modulus	$E(T) = 208.4 - 7.1 \times 10^{-2}T + 1.7T^2 - 3.5T^3$
Coefficient of Thermal Expansion (CTE)	$CTE(T) = 9.3 + 9.4 \times 10^{-3}T - 6.2 \times 10^{-6}T^2$
Specific Heat	$C_p(T) = 358.8 + 1.1 \times 10^{-1}T - 2.7 \times 10^{-3}T^2 + 6.7 \times 10^{-6}T^3$
Thermal Conductivity	$\kappa(T) = 27.3 + 1.4 \times 10^{-2}T - 3.1 \times 10^{-5}T^2$
Magnetic Properties	Coercive Field (H_c) : 680 A/m Remanent Magnetization (M_r) : 189 Gauss Saturated Magnetization (M_s) : 19,907 Gauss
Yield Strength	522 MPa at room temperature 390 MPa at 500 °C
Total Elongation	21.2 % at room temperature 17.3 % at 400 °C 19.4 % at 500 °C
DBTT	- 50 °C

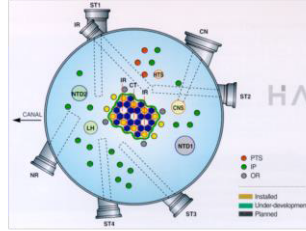


BeWS-12, Jeju Island, 10-11 Sep., 2015

11

2. Status of RAFM Development

◆ Irradiation Test using HANARO



Location	Hole		Inside Dia. (cm)	Neutron Flux (n/cm ² · sec)		Remarks
	Name	No.		Fast Neutron (E>1.0 Mev)	Thermal Neutron (<0.625 eV)	
Core	CT	1	7.44	2.10×10^{14}	4.39×10^{14}	Fuel/material isotope production
	IR	2	7.44	1.95×10^{14}	3.93×10^{14}	
	OR	4	6.00	2.23×10^{13}	3.36×10^{14}	
Reflector	LH	1	15.0	6.62×10^{11}	9.77×10^{13}	Fuel/material Isotope, semi-conductors
	HTS	1	10.0	9.44×10^{10}	4.79×10^{13}	
	IP	17	6.0	1.45×10^9	2.40×10^{13}	
				$\sim 2.10 \times 10^{12}$	$\sim 1.95 \times 10^{14}$	

- Neutron irradiation test will be performed using HANARO at KAERI.
- The test has been designed up to 3 dpa at 320 °C. (will be adjusted)



BeWS-12, Jeju Island, 10-11 Sep., 2015

12

2. Status of RAFM Development

◆ Material DB for ARAA in Progress

Categories	Properties	un-irradiated	irradiated
Thermal	Thermal conductivity	○	-
	Thermal diffusivity	○	○
	Specific heat	○	-
	CTE (Coefficient of Thermal Expansion)	○	-
Physical	Density	○	-
	Elastic modulus	○	-
	Poisson's ratio	○	-
Mechanical	Yield strength (0.2% proof)	○	○
	Ultimate tensile strength	○	○
	Uniform elongation	○	○
	Charpy impact energy (DBTT)	○	○
	Fatigue & creep-fatigue	○	-
	Creep	○	-
Electrical	Electrical resistivity	○	-
Magnetic	Magnetic permeability	○	-



BeWS-12, Jeju Island, 10-11 Sep., 2015

13

2. Status of RAFM Development

- ◆ Near-term Schedule (ARAA Development)
 - 2015.05 : 2nd commercial scale production (2nd Heat : 6 ton-scale)
 - 2015.12 : Establishment of material properties DB for un-irradiated material
 - 2016.05 : 3rd commercial scale production (3rd Heat : 12 ton-scale)
 - 2016.12 : Irradiation test using HANARO
(Postponed due to wall reinforcement after Fukushima accident)

- ◆ Near-term Schedule (Fabrication Technology)
 - 2015.03 : Development of Welding Procedure Specification
 - 2015.07 : Validation of fabrication procedure (Small Mockup)
 - 2015.12 : DB for welded materials
 - 2016.03 : Fabrication of a full Sub-module mockup
 - 2016.12 : Compatibility between structural/functional materials

ISFNT-12 : P3.061
ISFNT-12 : P2.061

Outline

- I Introduction
- II Status of Structural Material Development
- III Status of Functional Material Development**
(Breeder Pebble, Li_2TiO_3)
- IV Summary

3. Status of Functional Materials Development

◆ Fabrication Process of Li_2TiO_3 Pebble

- Slurry Droplet Wetting Method based on the Cross-linking Reaction between PVA and Boric-acid

Fabrication Process

```

graph TD
    A[Li2TiO3 Powder] --> C[Mixing]
    B[PVA Solution] --> C
    C --> D[Dropping into Glycerin including Boric Acid]
    D --> E[Drying]
    E --> F[Sintering]
        
```

BeWS-12, Jeju Island, 10-11 Sep., 2015
16

3. Status of Functional Materials Development

◆ Parameter Study

- Effect of Sintering Time (1200°C, Air atmosphere)

Sintering Time : 1 h	Sintering Time : 2 h	Sintering Time : 3 h	Sintering Time : 4 h
Avg. Dia. : 1.03 mm	Avg. Dia. : 1.01 mm	Avg. Dia. : 1.00 mm	Avg. Dia. : 0.98 mm
Grain Size : 8 μm	Grain Size : 10 μm	Grain Size : 20 μm	

- Grain size was increased with increasing sintering time.
- The whole pore of the sintered pebble was open type.
- The open porosity was about 10 %. (Sintering Time : 3 h)

BeWS-12, Jeju Island, 10-11 Sep., 2015
17

3. Status of Functional Materials Development

◆ Crush Load and Fracture Surface

■ Crush Load of Sintered Pebble

Sintering Time (min)	PVA : 10 wt.% (N)	PVA : 15 wt.% (N)
60	~65	~35
120	~75	~35
180	~85	~60
240	~80	-

Experimental Conditions

- Equipment : INSTRON 5969
- Crosshead Speed : 0.1 mm/min
- Experimental Mode : Single Compression
- Number of Specimens : 15 EA

■ Fracture Surface (PVA : 10 wt.%)

Sintering Time : 1 hr Sintering Time : 3 hr Sintering Time : 4 hr

50µm 50µm 50µm

NFRI KAERI BeWS-12, Jeju Island, 10-11 Sep., 2015 18

3. Status of Functional Materials Development

◆ Development of Mass-production System

ISFNT-12 : P1.108

➢ Funded by SMBA (Small and Medium Business Administration)

- Period : 2013.11.01 ~ 2015.10.31
- Support Fund : 500 million won

- Automatic Dispensing System
- Target Production Rate : 40 kg/yr.
- Diameter of Sintered Pebble : 1.00 ± 0.05 mm
- Sphericity of Sintered Pebble : < 1.05

NFRI KAERI BeWS-12, Jeju Island, 10-11 Sep., 2015 19

3. Status of Functional Materials Development

◆ Development of Mass-production System

BeWS-12, Jeju Island, 10-11 Sep., 2015
 20

3. Status of Functional Materials Development

◆ Establishment of Fabrication Conditions for Mass-production

■ Effects of Sintering Temp. ■ Effects of Needle Size ■ Effects of Sintering Position

Sintering Temperature (°C)	Crush Load (N)	Diameter (mm)
1000	~75	~1.55
1050	~65	~1.50
1100	~50	~1.45
1150	~35	~1.40
1200	~30	~1.35

Needle Size (Gauge)	Green Body Diameter (mm)	Sintered Body Diameter (mm)
20G	~2.0	~1.5
25G	~1.6	~1.2
27G	~1.3	~1.0
30G	~1.1	~0.9

Sintering Position	Crush Load (%)	Diameter (mm)
Top	~35	~1.05
Middle	~35	~1.00
Bottom	~35	~1.00

Needle (Gauge)	Min. Dia. (mm)	Avg. Dia. (mm)	Max. Dia. (mm)
20	1.42	1.54	1.61
25	1.21	1.25	1.31
27 (0.4MPa)	1.01	1.03	1.06
27 (0.5MPa)	1.01	1.03	1.06

BeWS-12, Jeju Island, 10-11 Sep., 2015
 21

3. Status of Functional Materials Development

◆ Impurities of Li_2TiO_3 Powder and Pebble

■ Analysis Results by ICP-OES

(unit : ppm)

Element	Powder	Green Body (Before Sintering)	Pebble (After Sintering)
Al	5.49	10.71	4077.56
B	N.D.	2555.05	N.D.
Ca	70.07	58.85	290.71
Co	629.11	515.98	662.61
Cr	34.57	28.87	38.09
Fe	6.54	6.57	12.63
K	N.D.	N.D.	N.D.
Mg	20.92	17.07	52.77
Na	144.40	102.03	41.46

- The boron, which was used as hardening agent of the PVA, was perfectly removed during the final sintering process.
- The development of high purity starting powder is necessary and important.

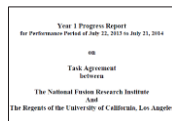


3. Status of Functional Materials Development

◆ International Collaboration

■ with US (UCLA-INL)

- Task 1 : COMET - Ceramic Optimal Material Experiment for Thermomechanics
- Task 2 : Deuterium and Tritium Transport, Permeation Experiments, Modeling and Code Validation
- Task 4 : MELCORE Analysis for KO TBS and GAMMA code V&V



■ with IEA NTFR Solid Breeder Subtask – WG_P

- Round Robin Test for Ceramic Breeder Pebbles



■ with JA TBM Collaboration (Biannual Meeting)

■ with CN TBM Collaboration (Annual Meeting)



3. Status of Functional Materials Development

◆ Near-term Schedule (Li_2TiO_3 Pebbles Development)

ISFNT-12 : P3.103
ICFRM-17

- 2015.10 : Powder synthesis technology
- 2015.12 : Improvement of mass-production technology
- 2015.12 : Validation of thermal/mechanical performance
- 2016.12 : Establishment of material properties DB for pebble/pebble-bed

	Properties	Remarks
Pebble	Morphology	Diameter, Sphericity
	Porosity	Open, Closed
	Grain Size	
	Chemical Composition	including U and halogen
Pebble-bed	Crush Load	
	Effective Thermal Conductivity	
	Thermal Expansion	
	Stress-strain Curve	
	Creep Rate	

Outline

- I Introduction
- II Status of Structural Development
- III Status of Functional Material Development
- IV Summary

4. Summary

- ◆ Alloy design has been performed based on ferritic-martensitic steel containing 8-9 wt.% Cr and 1-2 wt.% W.
- ◆ As a candidate of HCCR TBM structural material, ARAA was selected and **1st Heat of 5 ton-scale and 2nd heat of 6 ton-scale** was manufactured for DB establishment and mock-up fabrication.
- ◆ **DB** for physical and mechanical properties of **un-irradiated ARAA** will be established by the end of 2015.
- ◆ **Irradiation test** for commercial-scale ARAA is to be done in 2016 using HANARO.
- ◆ **Li₂TiO₃ pebbles** were fabricated by slurry droplet wetting method. Fabrication parameters were investigated to establish suitable process conditions for high-quality ceramic breeder pebbles.
- ◆ The automatic dispensing system for the high viscosity ceramic slurry is being developed for **mass-production** of the ceramic breeder pebbles. The production rate for **Li₂TiO₃ pebbles** was estimated at **50 kg/year**.
- ◆ **Physical and mechanical properties** of breeder pebble and pebble bed have being evaluated not only by KO TBM Team but also by collaborators. Especially, database of thermo-mechanical properties will be established by UCLA under KO-US TBM collaboration program in the near term.

Thank you for your attention!

2.3 Technical session 1: Production, Forming and Joining

2.3.1 Development of beryllium casting alloy for instrument application

I. Gvozdikov¹, B. Belikov¹, V. Sizenev¹, P. Bryantsev²

¹*JSC “Kompozit”, Korolev, RF*

²*Moscow Institute of Steel and Alloys, Moscow, RF*
beryllium@kompozit-mv.ru

Development space instruments requires material with a high specific stiffness, high thermal conductivity and low coefficient of linear thermal expansion (CTE). The unique combination of these requirements can be implemented in beryllium-silicium alloys (Table 1). The specific stiffness of Be-Si alloys is 2,5 times higher than Ti or Al alloys, CTE is 2 times lower than pure beryllium. Low CTE will provides thermal agreement with optical glasses in lightweight reflectors. From the other hand alloys close to eutectic composition will have good casting properties, which is more technologically.

Table 1 – Physical properties of Be-Si alloy (39% mass Be)

	Be-Si	Be	Ti	Al
Elastic modulus E, GPa	180	300	103	70.6
Density ρ , g/cm ³	2.15	1.85	4.50	2.69
Specific stiffness E/ ρ , m	$8.5 \cdot 10^7$	$16.2 \cdot 10^7$	$2.3 \cdot 10^7$	$2.6 \cdot 10^7$
Thermal conductivity λ , W/m/K	130	180	21.9	220
CTE α , 1/K	$6.5 \cdot 10^{-6}$	$11.3 \cdot 10^{-6}$	$9.2 \cdot 10^{-6}$	$23.3 \cdot 10^{-6}$
λ/α , W/m	$2 \cdot 10^7$	$1.6 \cdot 10^7$	$0.2 \cdot 10^7$	$0.9 \cdot 10^7$

Ternary system Be-Si-Al is characterized by ternary eutectic reaction and absence of compounds. The combination of binary and ternary eutectics in alloy expects to provide good mechanical properties.

The selected system Be-Si-Al is promising from the point of view of combination required physical and mechanical properties with possibility of using investment casting. Experimental binary and ternary alloys were prepared by vacuum induction melting, samples were prepared by investment casting. Microstructure and CTE in temperature range 293-773 K were investigated.

2.3.2 Validation and Installation of Large Beryllium Structures at CERN

M.A. Gallilee¹, P. Costa Pinto¹, and C.K. Dorn²

¹CERN, Route de Meyrin 385, CH-1217 Meyrin, Switzerland

²Materion Beryllium & Composites, 14710 West Portage River South Road, Elmore, Ohio 43416-9500 U.S.A.

E-mail: mark.antony.gallilee@cern.ch

Abstract

Beryllium is a key material for the central beam vacuum chambers for the CERN (European Organization for Nuclear Research) LHC (Large Hadron Collider) experiments. Three new beryllium chambers have been delivered by Materion Electrofusion and installed in the LHC experiments ATLAS, CMS and LHCb during the shutdown between 2013 and 2014. Upon arrival at CERN these chambers underwent rigorous testing campaigns and thin film Non Evaporable Getter coating (NEG coating) to ensure that they could meet the strict ultra-high vacuum and secondary electron emission requirements for installation in the LHC. In accordance with the LHC design report, components installed in the machine must be able to reach base pressures between 10^{-10} and 10^{-11} mbar and maximal secondary electron yields below 1.3. This paper will present the validation, thin film coating and installation of these chambers.

deviation of less than 0.2mm was within specification and therefore compatible with the extremely strict requirements to install this hardware in the LHC machine.

VACUUM VALIDATION AT CERN

Vacuum compatibility is essential for any accelerator component that will be in contact with vacuum. The required base pressure in the LHC of between 10^{-10} and 10^{-11} mbar necessitates that the material of the inner surface of the chamber must be extremely clean and contain no contamination, especially hydrocarbons and halogens (for details, see section on thin film coating). To achieve the required base pressure, the technical requirements are based on the residual outgassing rate of the chamber measured 48

INTRODUCTION

Having been manufactured and delivered to CERN by Materion [1], three new beryllium chambers have been further processed at CERN and installed in the LHC. These chambers formed part of an upgrade known as Long Shutdown 1 (LS1). Before any component can be installed in contact with the LHC machine ultra-high vacuum, it must undergo a series of acceptance tests to ensure machine compatibility, both for vacuum and mechanical aspects.

Between 2012 and 2014 three new beryllium chambers were qualified at CERN and then installed during LS1.

DIMENSIONAL INSPECTION AT CERN

When a new vacuum chamber is conceived, the compatibility with the LHC proton beam must be verified, specifically the manufacturing and installation tolerances [2]. To take one example, the ATLAS experiment requested a new central vacuum chamber in beryllium. Their request was for an aperture reduction from 58 mm internal diameter to 47 mm internal diameter over their 7.3 m long central chamber. In order to meet this request, the deviation from the perfect cylinder over 7.3m needed to be less than 1.95mm [2]. Figure 1 shows the dimensional inspection results for the ATLAS example measured at 25 positions and rotated to account for gravity. A

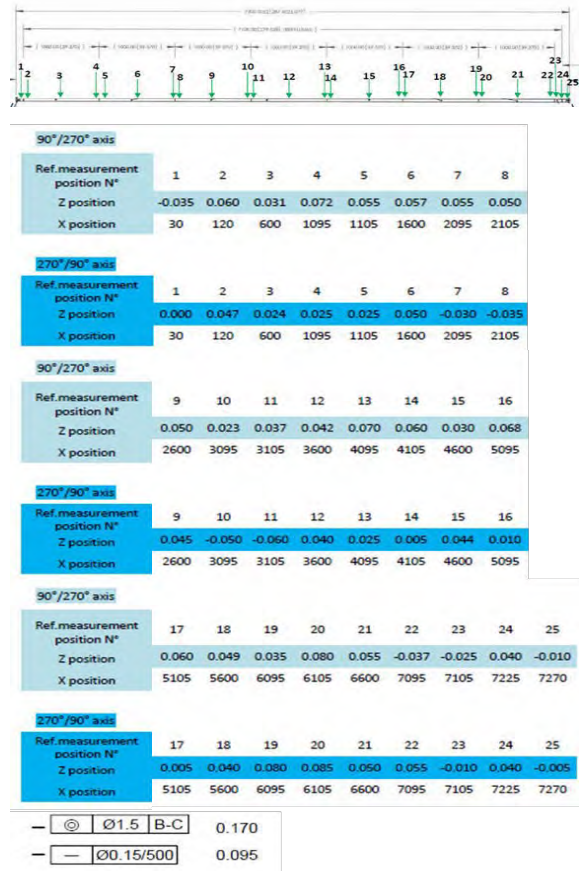


Figure 1: ATLAS Beryllium Chamber Metrology

hours after a 24-hour bake at 250 C. The distribution of gas species is measured with a Residual Gas Analyser (RGA).

Figure.2 shows a new beryllium chamber for the LHCb experiment on a vacuum test bench. The internal along the chamber (up to 1 ls cm for H₂ and 10 ls cm cleanliness of this chamber was specified at an outgassing rate of better than 3.0×10^{-12} mbar·l·s⁻¹·cm⁻² after bake-out. The measured outgassing rate from the internal surfaces of this chamber was 2.9×10^{-13} mbar·l·s⁻¹·cm⁻², which is one order of magnitude better than requirements showing that, in a cleaned form, beryllium has excellent compatibility with the LHC vacuum requirements.



Figure 2: Vacuum Test for LHCb Beryllium Chamber

THIN FILM COATING

To cope with the low vacuum pressure demanded by the experiments, (to minimize the background noise due to beam-gas interactions), the internal surface of the beryllium tubes is coated with a NEG [3] thin film. This coating provides two functionalities to the beam pipe: distributed vacuum pumping and a Secondary Electron Yield (SEY) below 1.3. The first is necessary due to the length of the tubes (the closest conventional vacuum pumps are installed approximately 20 meters away from the core of the experiments, resulting in limited effective pumping speed), and the second to avoid electron multi-pacting [4]

The NEG coating, made of Ti, Zr and V, was developed at CREN to have a low activation temperature, compatible with the materials commonly used in the construction of vacuum chambers for particle accelerators. Activation is achieved after heating at a temperature between 180 C and 250 C for about 24 hours. During the activation process, the oxide layer is dissolved into the bulk and the resulting metallic surface can react chemically with most of the gas species present in ultra-high vacuum systems. Noble gases and methane are exceptions and not pumped by the NEG. Halogens are of particular importance because they bind with the getter activation sites. Heating afterwards will not overcome the binding

energy, thus rendering the getter useless. NEG provides a pumping speed distributed along the chamber (up to 1 ls·lcm⁻² for H₂ and 10 ls·lcm⁻² for CO). The dissolution of the oxide layer also leads to the decrease of the SEY from ~1.8 before activation, to 1.1 afterwards.



Figure 3: Installation Preparation for Thin Film Coating

The coating is applied by DC magnetron sputtering in cylindrical configuration from a target, made of intertwined wires of Ti, Zr and V. The chamber is supported in a dedicated cradle, and the target insertion takes place using a horizontal bench. The assembly is then lifted up with a crane (Figure 3) and inserted in an 8m-long solenoid with a 60cm diameter. The setup is then evacuated by an ultra-high vacuum pumping station and baked at 200°C for 8 hours. The temperature of the system is then stabilized at 100°C. If no leaks or any contaminants are found in the residual gas, (total pressure~10⁻⁹ mbar), the discharge gas (krypton), is injected to a pressure of about 5×10^{-3} mbar. The target is polarized to-500 V and the coating process takes about 10 hours with a power density of 100 W/m. After coating, the chamber cools down to room temperature and is vented to dry air. The film quality is controlled on samples installed at the extremities of the chambers: the stoichiometry by energy dispersive x-ray analysis (EDX) and the activation performance, (reduction of the surface oxides), by x-ray photoelectron spectroscopy (XPS).

INSTALLATION AND OPERATION

Given the nature of the LHC experiments, the vacuum chambers are difficult to access and need to be installed in close-fitting environments. Precision installations are key to safeguard chamber and detector integrity, and to ensure that the accurate aperture of the chamber is available for accelerator operation. Figure 4 shows the installation of the CMS central vacuum chamber with the CMS detector in the open position. This chamber was slid into the detector on specially constructed tooling. The chamber was then transferred gradually to the detector supports. The tooling was finally released. Over several days, theodolites were used to measure survey targets located on the vacuum chamber. Gradually the chamber was brought into alignment with the detector to achieve sub-millimetre precision on an object in excess of 6m long.

Figure 5 shows the CMS measurements from installation compared to those taken from first physics data. The two types of measurements correlate very well, showing the good precision of the installation relative to the particle beam position of the LHC machine; within 0.8mm in the horizontal direction and 0.2mm in vertical for all measured values. In fact, the measured value by interactions is the mean of the measured values at installation. The point at which the interactions are measured is the centre, in the z direction, of the two points measured at installation.



Figure 4: Installation in CMS

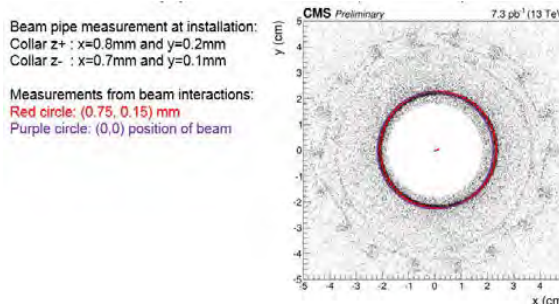


Figure 5: First Interactions in CMS

CONCLUSIONS

Beryllium has excellent characteristics to achieve geometrical, mechanical, vacuum, thin film coating and operational compatibility with the LHC machine at CERN. Beryllium's compatibility with the vacuum system and mechanical constraints means that optimised vacuum chambers become a key component to maximise the LHC experimental performance for data taking. First interactions from the CMS example validate the installation and measurement techniques and provide confidence for future exchange or upgrade the vacuum chambers in the experimental areas of the LHC. CERN is currently working on the next generation of beryllium chambers to be installed during the next long shutdown.

ACKNOWLEDGEMENTS

This work was possible with inputs from many colleagues. The authors would like to specifically acknowledge the work of the CERN Metrology team, the data provided by the experiments. Also current and previous colleagues from the vacuum group for data, images and feedback, specifically Giuseppe Bregliozzi, Giulia Lanza, Patrick Lepeule, Gerhard Schneider and Josef Sestak.

REFERENCES

- [1] M. Gallilee, G. Simmons, Fabrication Considerations for Large Beryllium Structures, BeWS-11 (2015)
- [2] R. Veness et al., Specification of New Vacuum Chambers for the LHC Experimental Interactions, PAC11 (2011)
- [3] P. Chiggiato, P. Costa Pinto, Ti-Zr-V non evaporable getter films: From development to large scale production for the Large Hadron Collider, Thin Solid Films 515 (2006) 382 – 388
- [4] Fritx Caspers, Giovanni Rumulo, Walter Scandale, Franck Zimmermann, Beam-Induced Multipactoring and Electron-Cloud Effects in Particle Accelerators, International Workshop in Multipactor, Corona and Passive Intermodulation (MULCOPIM'08), Valencia 24-26 September (2008)

2.3.3 Joining of Beryllium to CuCrZr and Ferritic-Martensitic Steels for Plasma Facing Components

Jeong-Yong Park¹, Yang-Il Jung¹, Hyun-Gil Kim¹, Byoung-Kwon Choi¹, Jung-Suk Lee¹, Yong-Hwan Jeong¹, Suk-Kwon Kim¹, Dong-Won Lee¹ and Seungyon Cho²

¹*Korea Atomic Energy Research Institute, 989-111 Daedeokdaero, Yuseong, Daejeon 305-353, Republic of Korea*

²*National Fusion Research Institute, 169-148 Gwahangno, Yuseong, Daejeon 305-806, Republic of Korea*

E-mail: parkjy@kaeri.re.kr

The joining of beryllium (Be) to structural materials has been a critical issue in the fabrication of plasma facing component. We have developed the joining technology for Be using a hot isostatic pressing (HIP) method for the fabrication of ITER first wall and test blanket module (TBM). The effects of different interlayer types and temperature have been investigated in order to optimize the HIP joining conditions of Be to CuCrZr. Ti/Cu and Cr/Cu interlayers were coated onto a Be surface before a HIP joining. HIP temperature was changed from 580 to 620 °C. The joining strength was higher in the joint specimen with Ti/Cu interlayers when compared to that with Cr/Cu interlayers and it was increased with an increase of the HIP temperature from 580 to 620 °C. Three types of the mock-ups consisting of Be, CuCrZr and stainless steel (SS) were fabricated to demonstrate the fabricability of the ITER first wall. The effects of the mock-up design and the interlayer type on the joining strength of the Be/CuCrZr joint were investigated on the basis of the shear test results for the Be/CuCrZr joint specimens. The joining strength of the Be/CuCrZr ranged from 78MPa to 204MPa depending on the types of mock-ups and interlayers. The effect of the size and the number of Be tiles used in the mock-ups was not as significant as the interlayer selection. The joining of Be to ferritic-martensitic steels (FMS) was carried out to develop the fabrication technology of ITER TBM. The diffusion barrier layers together with the coated interlayer were applied to the HIP joining of Be and FMS. Multiple layers formed due to an excessive diffusion of elements in the interface region in the absence of a diffusion barrier layer. Such a complicated interface structure consisting of brittle phases in part would be very prone to fracture even at low stress levels. A Cu foil or a HIPed CuCrZr layer applied as a diffusion barrier was effective to retard the diffusion between Be and FMS.

References

- [1] J.Y. Park et al., *Fusion Engineering and Design* **82**, 2497 (2007)
- [2] J.Y. Park et al., *Fusion Engineering and Design* **84**, 1468 (2009)
- [3] J.Y. Park et al., *Fusion Science and Technology* **60**, 422 (2011)

Joining of Beryllium to CuCrZr and Ferritic-Martensitic Steels for Plasma Facing Components

Jeong-Yong Park¹, Yang-Il Jung¹, Hyun-Gil Kim¹, Byoung-Kwon Choi¹, Jung-Suk Lee¹, Yong-Hwan Jeong¹, Suk-Kwon Kim¹, Dong-Won Lee¹, Seungyon Cho²

¹Korea Atomic Energy Research Institute
²National Fusion Research Institute

12th International Workshop on Beryllium Technology (BeWS-12)
 ICC, Jeju, Korea, 10 Sep 2015

Joining technology development for ITER first wall

Phase 1		Phase 2		
2005	2006	2007	2008	2009
Cu/SS HIP joining technology - Cu/SS joint block fabrication and sample test - Optimization of Cu/SS joining condition		Mock-up fabrication for NDT and HHF test - Small Cu/SS and Be/Cu mock-ups - Pre-qualification mock-ups		
Be/Cu HIP joining technology - Be/Cu joint block fabrication and sample test - Optimization of Be/Cu joining condition (HIP temperature, pressure and interlayer)		Qualification mock-up fabrication - Qualification mock-up fabrication - HHF test for qualification mock-up		
		Semi-prototype fabrication technology development		

- ITER first wall was designed to consist of the Be armor, the CuCrZr heat sink layer and the stainless steel (SS) plate.
- The joining of three different materials has been the critical issue in the fabrication of ITER first wall.

Be handling facility in KAERI

- Government-approved facilities was installed for the Be processing.
(Permissible Exposure Limit (PEL): $2 \mu\text{g}/\text{m}^3$ as an 8-hour time-weighted average.)

Preparation Room



- Preparation room
- clothes for protection
 - shower booth
 - equipments



Processing Room



- Processing room
- cutting
 - polishing
 - coating

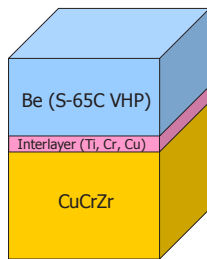
*hood and duct system
glove boxes



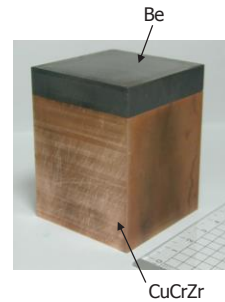
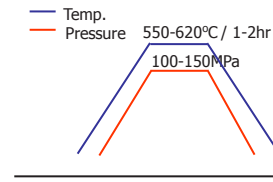
3

Be/Cu HIP joining technology

- Fabrication of Be/CuCrZr joint by HIP



- HIP conditions



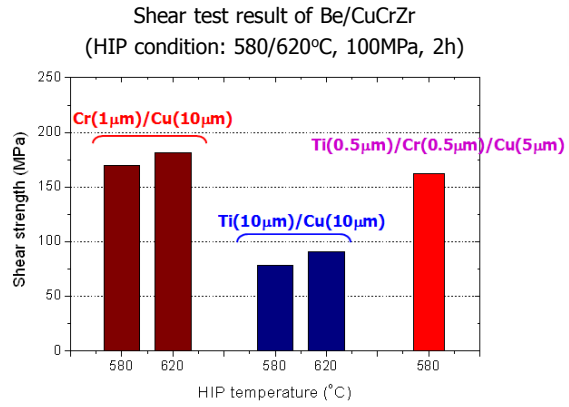
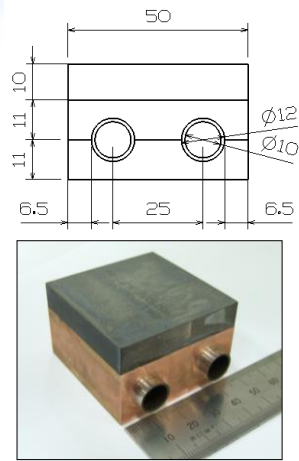
Variables

- Surface preparation conditions
- Interlayer type
- Interlayer thickness
- HIP condition (temp. & pressure)

Optimize the joining condition

4

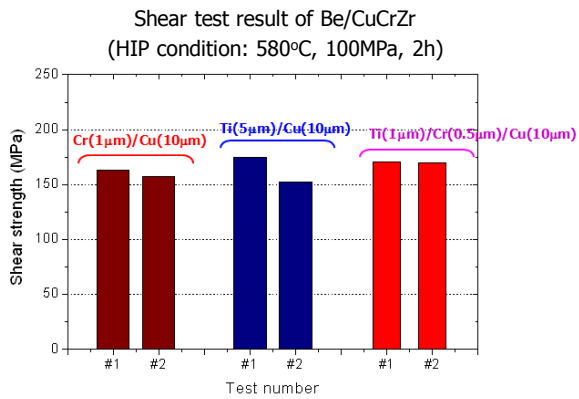
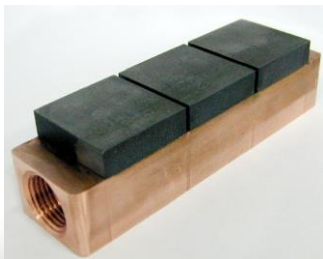
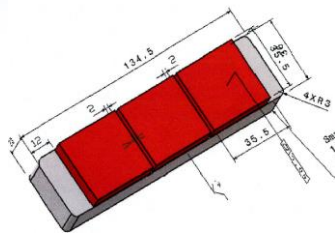
Fabrication of small mock-up



- Joint specimens with Cr/Cu interlayer showed a higher strength as compared to the samples with Ti/Cu interlayer.
- The strength of the joint specimens with Ti/Cr/Cu interlayer was comparable to that with Cr/Cu interlayer.

5

Fabrication of middle-sized mock-up



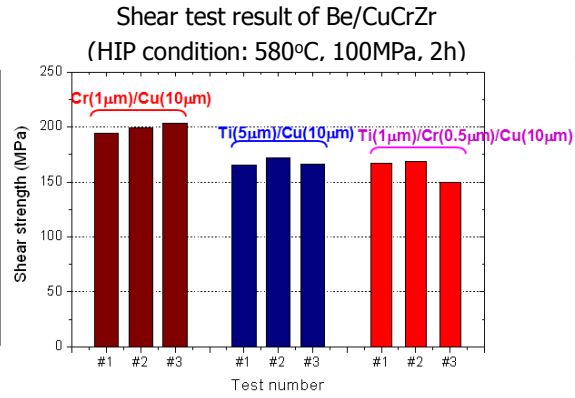
- The strength of the joint specimens was comparable to each other.

6

Fabrication of pre-qualification mock-up

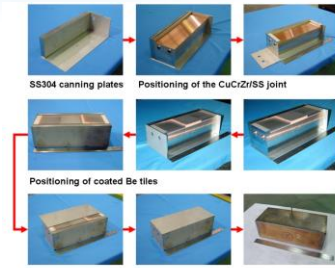
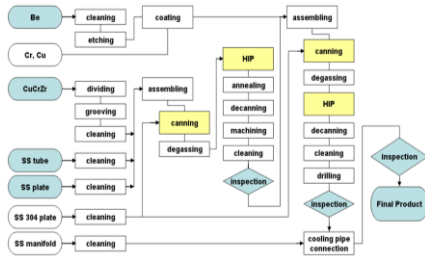
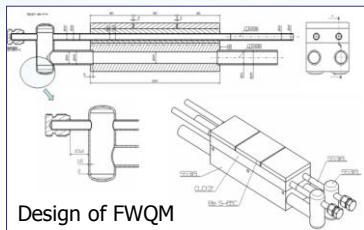


Pre-qualification mock-up

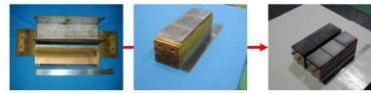


- The strength of the joint specimens was comparable to each other.

Fabrication process of FWQ mock-up



Canning process before HIP



Decanning process after HIP



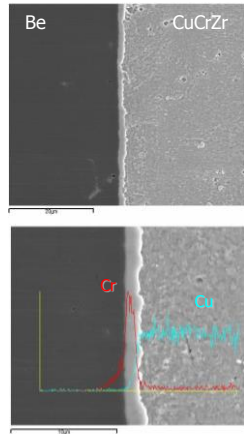
Welding manifold and cooling pipes

Fabrication process of the KO qualification mock-up

- HIP condition for CuCrZr/SS: 1050°C, 100MPa, 2h
- HIP condition for Be/CuCrZr: 580°C, 100MPa, 2h

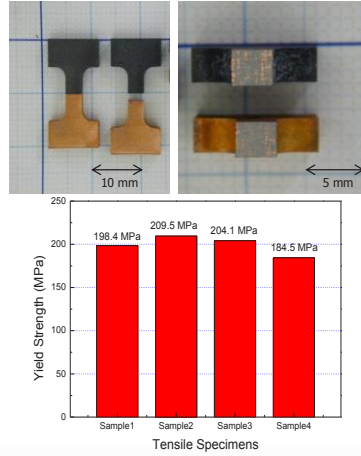
Destructive examination of Be/CuCrZr joint

Microstructures



- No cracks and pores were observed at the interface

Tensile test



- Average YS was 199.1 MPa; in between the YS of Be and CuCrZr base metal

9

High heat flux test for FWQM



FWQM before HHF test



Be surface appearance after the HHF test



KoHLT-1(Korea Heat Load Test facility)

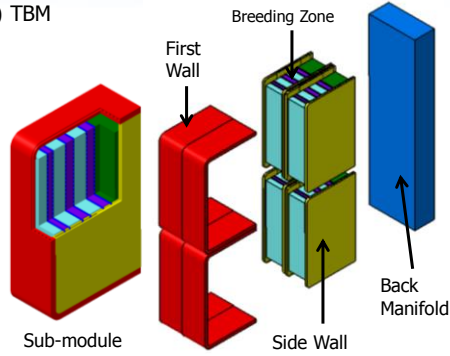
- Two KO FWQMs were survived after 12,000 cycles at 0.625MW/m² in KoHLT-1.
- KO FWQMs passed the HHFT tests performed in EU and US test facilities.

10

Joining technology development for TBM

KO Helium Cooled Ceramic Reflector (HCCR) TBM
(DEMO-relevant breeding breeder concept)

Parameter	Values
FW heat flux	Average 0.3 MW/m ² Peak 0.5 MW/m ²
Neutron wall load	0.78 MW/m ²
Thermal Power	1.01 MW ^t
Structural material	KO-RAFM (ARAA) (< 550 °C)
Breeder	Li ₄ SiO ₄ pebble bed or Li ₂ TiO ₃ pebble bed < 920 °C
Multiplier	Be pebble bed < 650 °C
Reflector	Graphite pebble bed
Size	1670(P) x 462(T) x 600(R) (mm)
Coolant	8 MPa He 1.14 kg/s (Nominal) FW (300 °C/390 °C) Breeding Zone(390 °C/500 °C)
Purge	He with 0.1 % H ₂

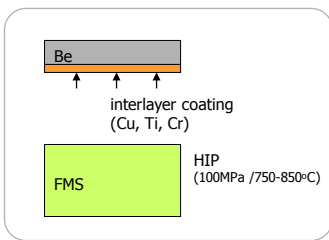


- Four-sub-module concept
 - Manufacturability
 - PIE & Transportation of Irradiated TBM
- Graphite pebbles as neutron reflector
 - Reduce the amount of Be multiplier
 - Decrease of cost
 - Comparable nuclear performance

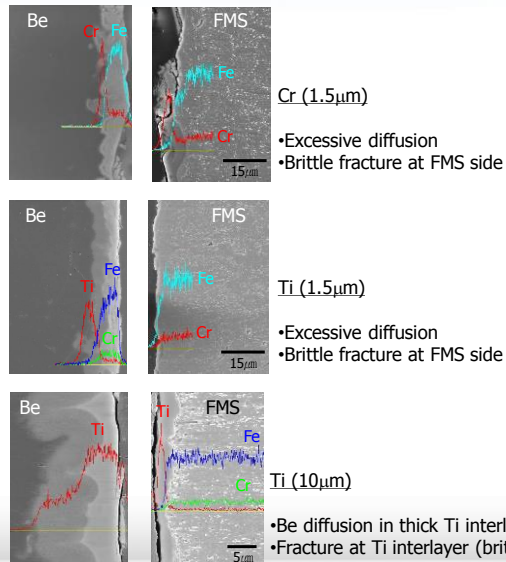
11

HIP joining of Be/FMS with interlayer coating

Approach:
to make diffusion bonding



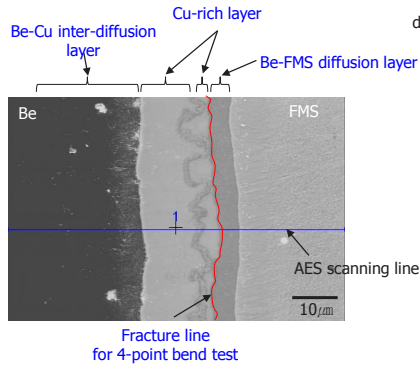
- In the interface region, many layers formed due to the excessive diffusion of elements.
- Such a complicated interface structure consisting of the brittle phases would be very prone to failure even at the extremely low stress level.



12

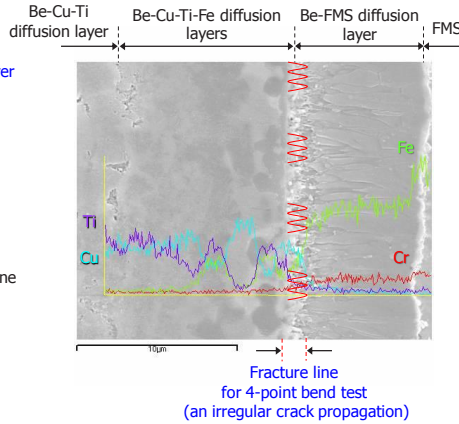
HIP joining of Be/FMS with interlayer coating

Cr (3 μ m) / Cu (10 μ m)



- Cu as a compliant layer
- Inter-diffusion of Be-Cu
- Diffusion layer of Be in FMS
- **Successful joining: 156MPa**

Ti (5 μ m) / Cu (15 μ m)

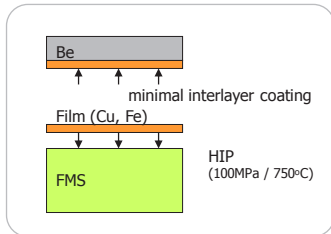


- Complex diffusion layer of Be-Cu-Ti-Fe
- Diffusion layer of Be in FMS
- **Successful joining: 257MPa**

13

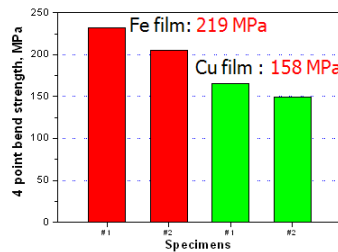
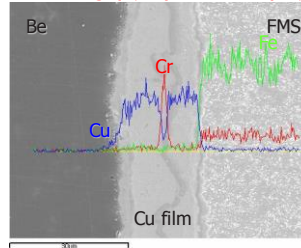
HIP joining of Be/FMS with interlayer coating and diffusion barrier film

Approach:
to prevent excessive diffusion



- Applying the film as a diffusion barrier was effective to retard the diffusion between Be and FMS, making the interface have an appreciable bonding strength.

Cr coating (2 μ m) / Cu film (10 μ m)

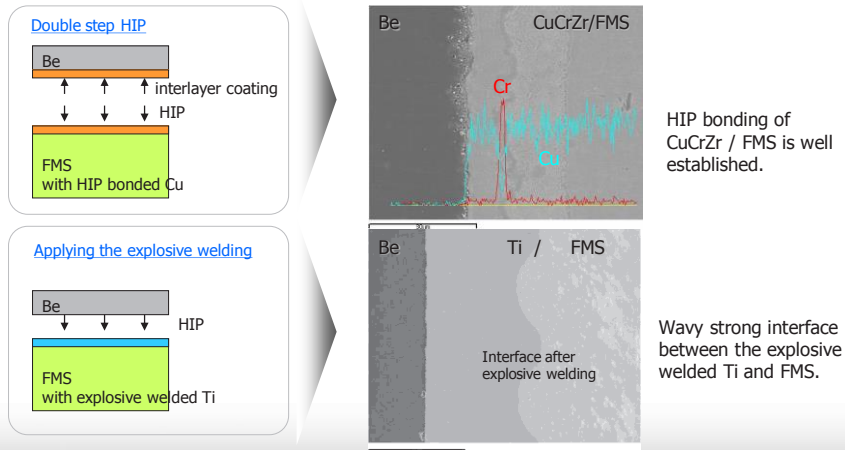


HIP condition: 100MPa / 750°C / 2hr

14

HIP joining of Be/FMS (Double step HIP and Explosive welding)

Approach: to prevent brittle fracture at FMS side



15

Summary

- The joining of beryllium (Be) to structural materials has been a critical issue in the fabrication of plasma facing component.
- We have developed the joining technology for Be to CuCrZr using a hot isostatic pressing (HIP) method for the fabrication of ITER first wall.
- The effects of different interlayer types and temperature have been investigated in order to optimize the HIP joining conditions of Be to CuCrZr.
- The joining of Be to ferritic-martensitic steels (FMS) was carried out to develop the fabrication technology of ITER TBM.
- The diffusion barrier layers together with the coated interlayer were applied to the HIP joining of Be and FMS.

16

2.3.4 Development of Beryllium Products in NGK

K. Nojiri

New Metal Division, NGK Insulators, Ltd, Nagoya, Japan

E-mail: nojiri@ngk.co.jp

NGK is one of the world leader companies in the field of fine ceramic products. The new metal division specialises in metal products specially beryllium and beryllium containing alloys. Beryllium has unique and excellent characteristics like low density, high rigidity, high heat resistance, high sound speed, high X-ray penetration, interesting nuclear properties, etc. NGK's beryllium business has wide variety of business field with fusions between beryllium's characteristics and NGK's metal working technologies. The beryllium products are always required very severe specification because of their extremely limited usage. The R&D of new products has a quality target which is more difficult. NGK has some development items, which could provide better human life, for example, galvano scanner mirrors, the target for BNCT, X-ray windows, etc.

The details will be presented in the workshop.



10 September 2015, Jeju Island, Korea

Development of Beryllium Products in NGK

Keigo Nojiri

NGK Insulators, Ltd
Aichi Japan

NGK INSULATORS, LTD.

1

Contents



- (1) NGK Insulators, Ltd
- (2) NGK's Beryllium business
- (3) Topics of Beryllium Application
 - 3-1 Mirror of Laser Machine
 - 3-2 Target of BNCT
 - 3-3. Sub Marine Cable Repeater Housing

NGK INSULATORS, LTD.

2

NGK Insulators, Ltd



Company Name

NGK INSULATORS, LTD.

Date of Establishment

May 5, 1919

Paid-in Capital

69,800 Million Yen

Number of Employees

16,217 (consolidated)

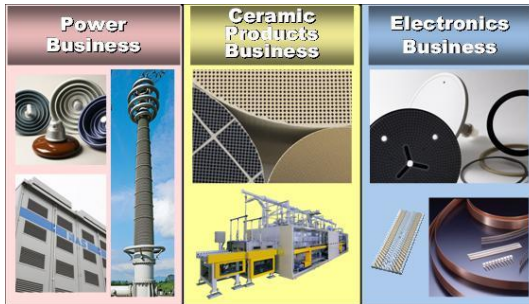
Consolidated Subsidiaries

58 companies

World Network



Main Products



As of March 31, 2015

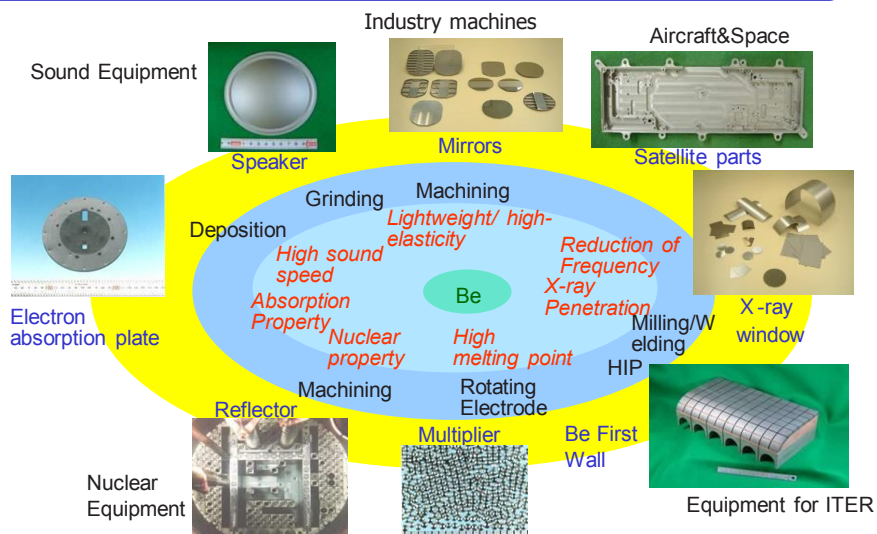
NGK INSULATORS, LTD.

3

NGK's Beryllium business



The most important usage of beryllium is the additive for alloying. But Pure Be also has many interesting applications,,,



NGK INSULATORS, LTD.

4

3-1 Mirror of Laser Machine



NGK INSULATORS, LTD.

5

3-2 Target of BNCT



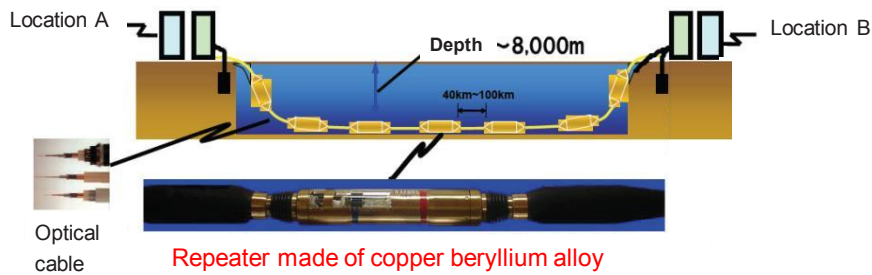
NGK INSULATORS, LTD.

6

3-3. Sub Marine Cable Repeater Housing



Be is mainly used as an additive for Cu base alloys. Popular applications are electric and electronic parts such as switches, relays, etc. Optical cable network system is also hot issue of the beryllium alloys.



Thank you for your attention



2.3.5 Distribution of Beryllium Pebble Size by Rotation Electrode Process

R. FUKATSU and K. NOJIRI

NGK Insulators Ltd.

Abstract

Beryllium pebble is one of the candidates as a neutron multiplier in ITER. The manufacturing process of this beryllium pebble is the Rotation Electrode Process. Conventional manufacturing depends on the worker’s skills and experience. In this experiment, the out of specification was reduced by half by changing to automated adjustments of the distance between the tungsten and beryllium.

1. Introduction

Beryllium metal is used in various industrial and R&D processes due to its unique and extremely excellent properties. One of the representative properties is a nuclear reaction. When a neutron collides with the beryllium, (n, 2n) neutron reaction is caused. Therefore, beryllium releases more neutrons than it absorbs.

Beryllium is a candidate as a neutron multiplier in ITER. A beryllium neutron multiplier will be used in the form of pebble, a small sphere of high quality. “BP-1” beryllium pebble (Fig.1) is the reference material for the multiplier in the ITER project. The specifications of “BP-1” shall contain a minimum beryllium content of 99.0 %. The chemical composition of “BP-1” is shown in Table 1, and it should be a sphere made by REP (Rotation Electrode Process) with a diameter of 0.8–1.2 mm. REP is a method to produce metal spheres. High voltage electric power is charged between both electrodes. The rotating beryllium electrode ejects beryllium droplets by centrifugal force. The melted beryllium drops form spherical shapes before solidification. The schematic is shown in Fig. 2

Table 1 : The chemical composition of “BP-1” specifications

Chemical Composition (wt.%)	
Beryllium	≥ 99.0
Beryllium Oxide	≤ 0.50
Aluminum	≤ 0.09
Cobalt	≤ 0.001
Iron	≤ 0.10
Magnesium	≤ 0.08
Silicon	≤ 0.06
Uranium	≤ 0.005

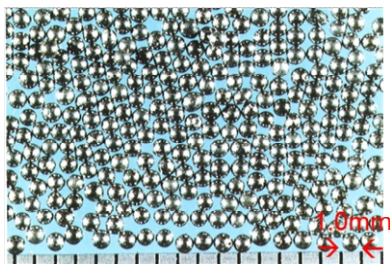


Fig. 1 : Products of “BP-1”

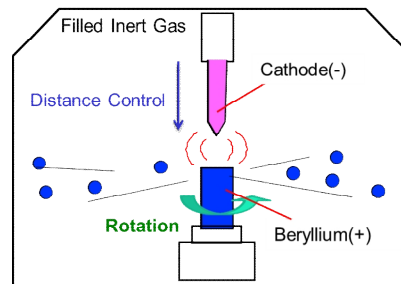


Fig.2 : The schematic of Rotation Electrode Process

2. Experiments

First, our conventional manufacturing data was reviewed. It was found that the distribution of beryllium pebble size made by the previous REP process was not symmetrical. Therefore, it was out of specification by 16%. This is because the previous manufacturing process depended on worker’s skills and experience.

In this experiment, due to the decrease of the out of specification, it was tried to reduce the dependence on workers and changed to automated adjustments of the distance between the tungsten and beryllium. This experiment method included changing the rotation speed some times. And then the production condition was adjusted.

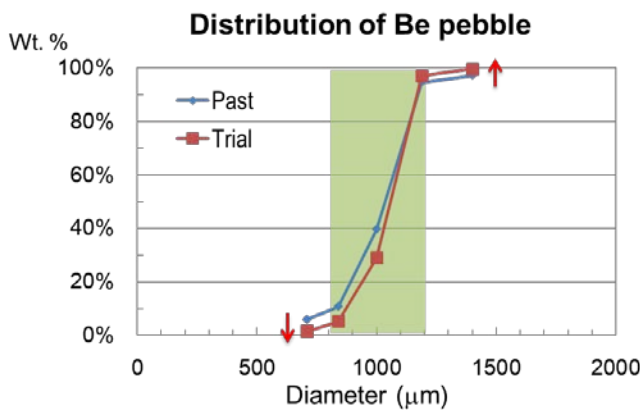
3. Results

The distribution of beryllium pebble size at this time is shown in fig. 3 and table 2. The distribution curve of this trial test is narrower than that of the past test. The out of specification, both over range and under range, was decreased by half. As a result, it is out of specification by only 8%.

4. Conclusion

Looking at Fig. 3, it is found that 50% of this distribution curve is pointed at 1070µm. The distribution curve can be adjusted to the center, and it is possible to reduce the out of specification result by adjusting the manufacturing conditions.

Two steps for future examinations are being planned. First, the distribution curve of the optimum manufacturing condition must be found. The distribution curve is adjusted to center for it to be narrower. After that, we will move to the mass production step. The new equipment for mass production will be introduced.



Pebble Size	Past	Trial
-800 µm	10.7 %	5.3%
800-1000 µm	28.9%	23.6%
1000-1200µm	55.0%	68.1%
1200 µm-	5.4%	2.6%

Table 2 : The ration of each pebble size of this trial test

Fig. 3 : The distribution of pebble size of this trial test

2.4 Technical session 2 : Irradiation effects, High heat flux performance, Modelling, Production

2.4.1 Experimental Investigation of Irradiation Effects in Beryllium Beam Window after Exposure in the NuMI Beamline: Preliminary Results and Plans

V. Kuksenko¹, B. Hartsell², K. Ammigan², C. Densham³, P. Hurh², S. Roberts¹

¹ *University of Oxford, Oxford, UK,*

² *Fermi National Accelerator Laboratory, Batavia, USA*

³ *Rutherford Appleton Laboratory, Didcot, UK*

E-mail: viacheslav.kuksenko@materials.ox.ac.uk

Progress in the development of high intensity particle sources is closely linked to the abilities of materials to sustain the increased demands from the severe working conditions. Beryllium is among the leading candidate materials for beam windows and target components in near-future multi-megawatt accelerator particle sources. An international collaboration - “RaDIATE” - was recently launched in order to explore radiation damage issues in materials under the relevant environment, including investigation of beryllium.

A beryllium beam window (grade PF60) from the NuMI beamline has been irradiated by 120GeV protons over 7 years of beam exposure at 70°C up to an integrated damage level of 0.5 dpa and now is available for analysis. Up to 2000 appm of He and 1800 appm of H have been generated during the irradiation.

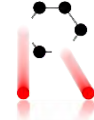
The evolution of microstructure of the beam window during irradiation has been investigated at different scales by microscopy and through nanoscale investigation of the evolution of impurity distributions using Atom Probe Tomography. Descriptions of the experimental programme and the results of the current activities will be presented.

*Work supported by Fermi Research Alliance, LLC under Contract No. DE-AC02-07CH11359 with the United States Department of Energy.

Experimental Investigation of Irradiation Effects in Beryllium Beam Window after Exposure in the NuMI Beamline: Preliminary Results and Plans

V. Kuksenko¹, B. Hartsell², K. Ammigan², C. Densham³, P. Hurh², S. Roberts¹

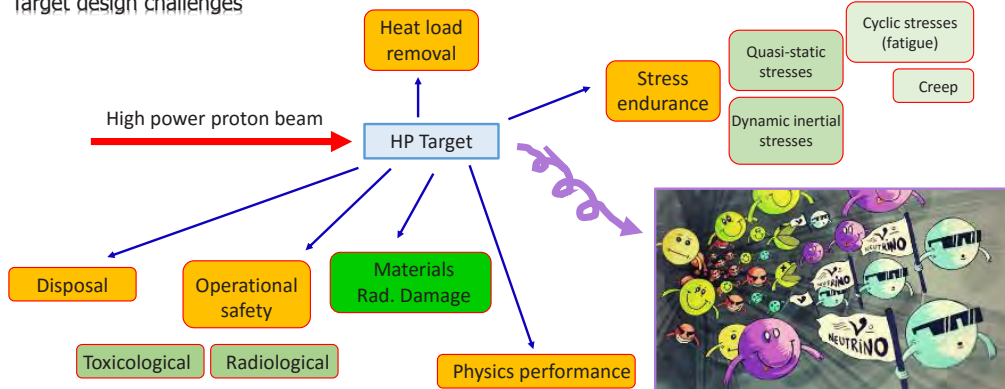
¹ University of Oxford, UK
² Fermi National Accelerator Laboratory, USA
³ Rutherford Appleton Laboratory, UK



12th International Workshop on Beryllium Technology
 September 10, 2015

1

Target design challenges



After Otto Caretta, HTPW, May 2014



Investigation of the radiation response of structural window and target materials in new highly intensity proton accelerator particle sources for future neutrino sources

2

Beryllium

- is extensively used as a material of neutrino targets parts, for example – beam window
- is a promising candidate for future high-power neutrino sources

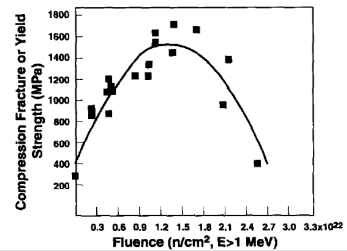
For example, the expected working conditions for some parts of the Long-Baseline Neutrino Facility (LBNF)

Application	Operating conditions					Proton beam parameters
	Avg. T (°C)	Peak T (°C)	Total DPA	Gas production (appm/DPA)		
				He	H	
Beam window (vacuum to air)	200	300	~ 0.23/yr	>2000	>2000	700 kW; 120 GeV; ~1 Hz; $\sigma_{rms} = 1.3$ mm
Target	375	450	~ 0.23/yr	>2000	>2000	700 kW; 120 GeV; ~1 Hz; $\sigma_{rms} = 1.3$ mm

Environment: elevated temperature + radiation + pulsing loads

What can we expect?

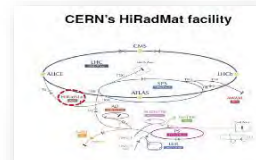
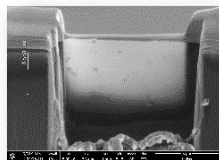
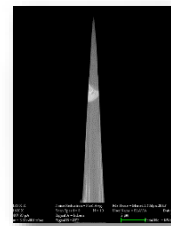
Examples form n-irradiation
 - reduction induced embrittlement
 - irradiation induced hardening



Compressive fracture or yield strength as a function of fluence (E > 1 MeV) for beryllium specimens irradiated at 75-125°C. D.S. Gelles et al. /Journal of Nuclear Materials 212-215 (1994) 29-3X

Experimental investigation

- o [Investigation of the as-received Be](#)
- o [Investigation of the proton Be window \(NuMI\)](#)
- o Ion irradiation experiments
- o Thermal shock experiments
- o Micromechanical tests



Materials

PF-60	
Max impurities, appm	
Al	170
C	450
Fe	130
Mg	810
O	2900
Si	130
N	195
Be	balance

S-200-F	
Max impurities, appm	
Al	335
C	1130
Fe	210
Mg	130
O	5445
Si	195
Be	balance

S-65	
Max impurities, appm	
Al	170
C	680
Fe	130
Mg	15
O	3260
Si	145
Be	balance

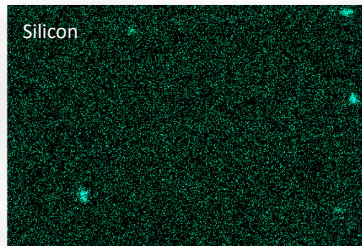
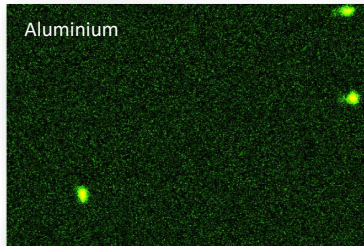
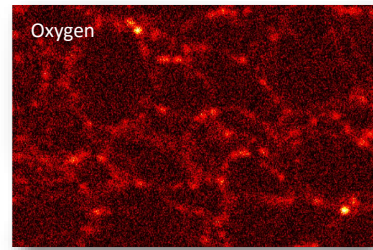
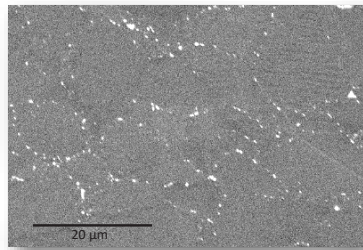
Method of manufacture: vacuum hot pressing

Beryllium is of industrial purity

5

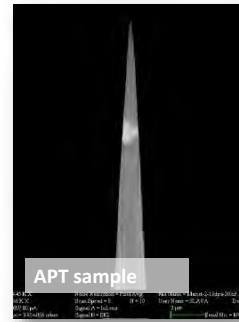
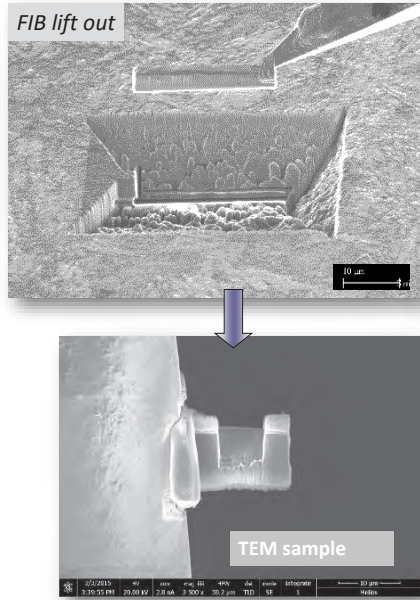
Pre- and post-irradiation experiments

Example:
PF-60/VHP



6

preparation of samples



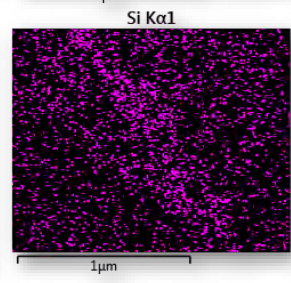
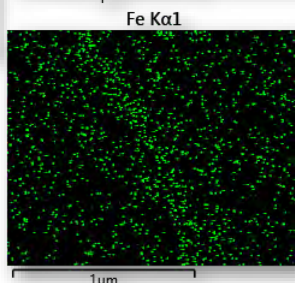
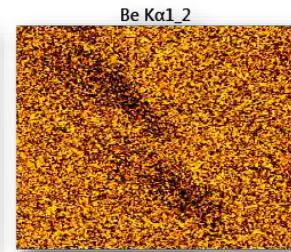
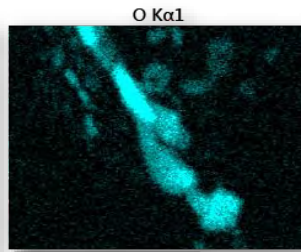
Culham Materials Research Facility



- FIB lift-out**
- investigation of localized microstructure and properties
 - minimize activity of samples
 - minimize toxicity of samples

7

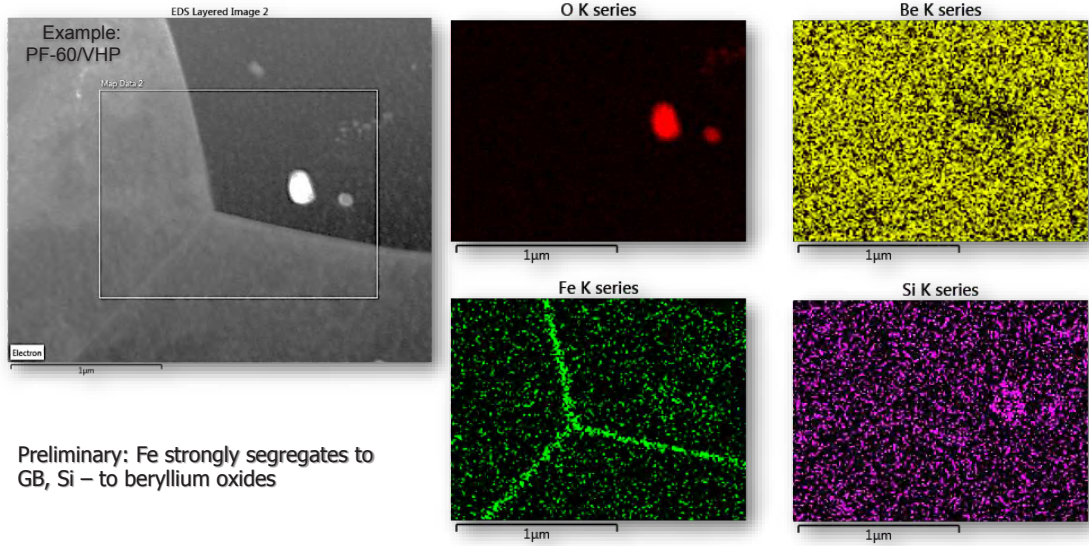
Pre- and post-irradiation experiments



Preliminary: Fe and Si segregates to beryllium oxides

8

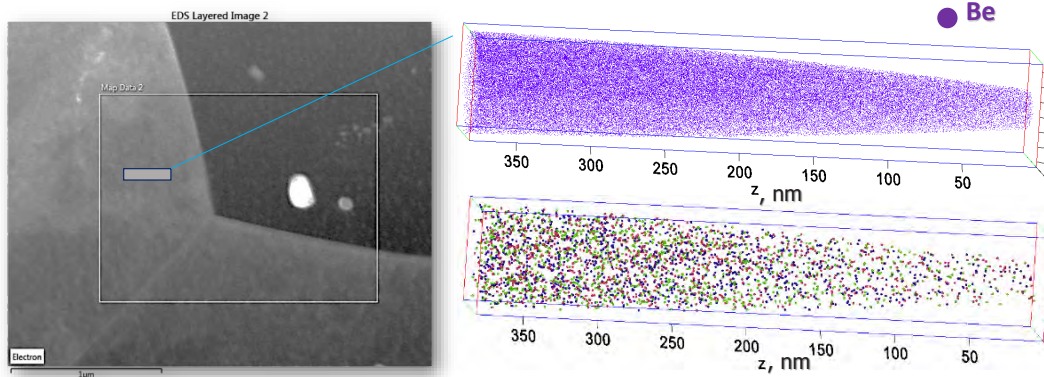
Pre- and post-irradiation experiments



Preliminary: Fe strongly segregates to GB, Si – to beryllium oxides

9

Pre- and post-irradiation experiments



Preliminary: small quantity of Fe, Cu, Ni and O are homogeneously distributed inside Be grains

● Fe ● Ni ● O

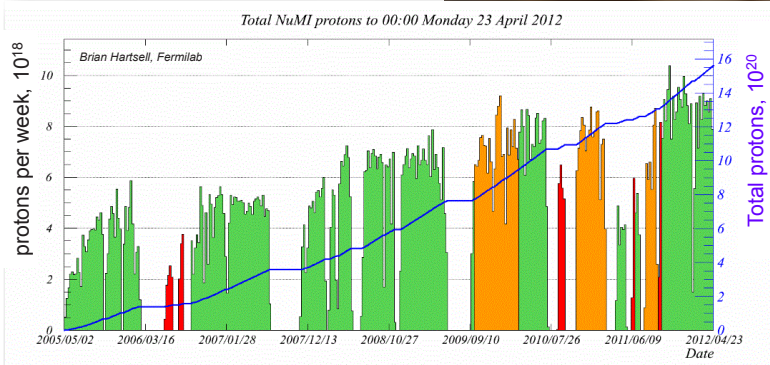
Impurities in Beryllium matrix (preliminary)		
Fe, appm	Cu, appm	Ni, appm
55±10	15±10	30±10

10

NuMI beam window experiments

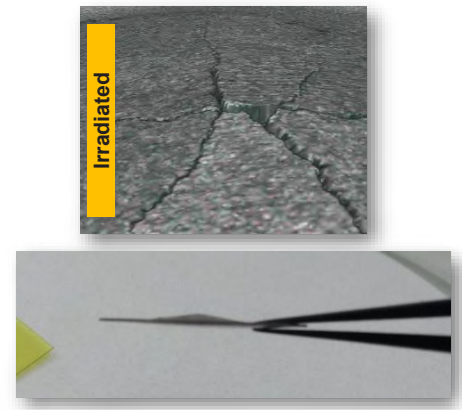
300 kW NuMI beam window
 (MARS calculations of Brian Hartsell, Fermilab)

- 120GeV proton beam
- about 3×10^{13} protons per pulse, 0.5 Hz
- 1.57×10^{21} protons during its lifetime
- 1.1mm beam sigmas, X and Y
- $T \approx 50^\circ\text{C}$



11

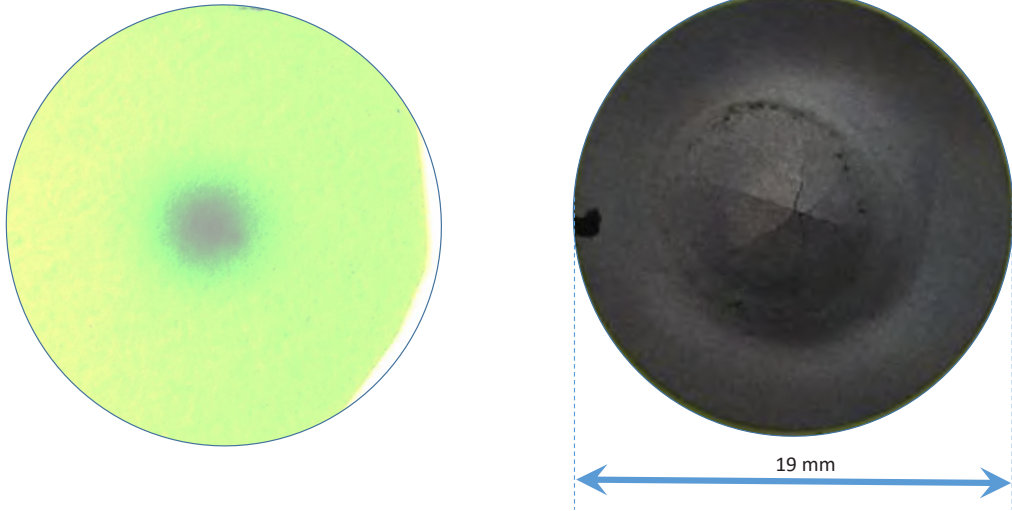
NuMI beam window experiments



Radiation embrittlement?

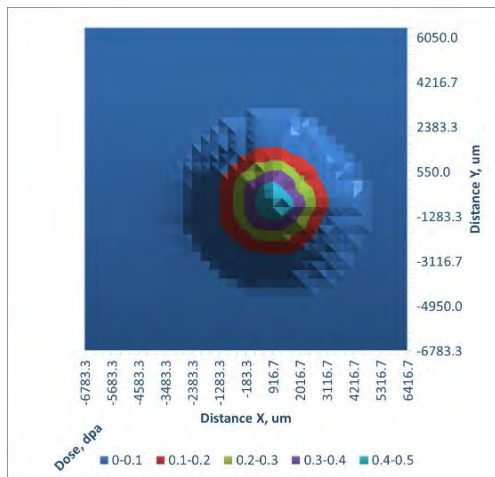
12

Dosimetry film, 5 days of exposure

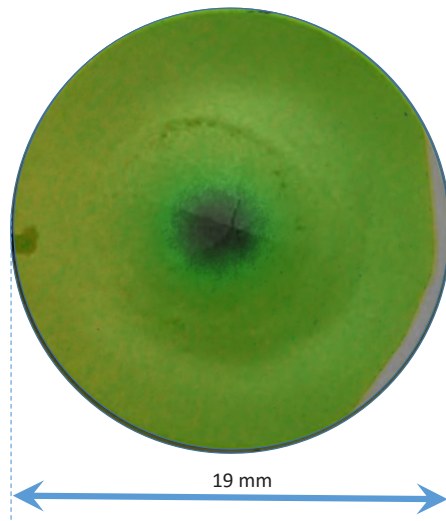


13

MARS calculations map



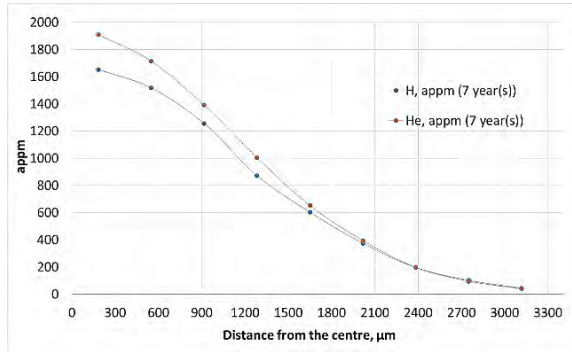
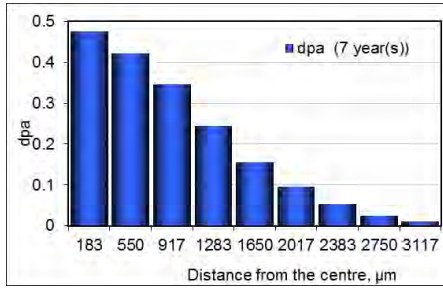
Dosimetry map



14

NuMI beam window experiments

The main transmutation products are He and H



Irradiation Source	He gas production in Be (appm/DPA)
Mixed spectrum fission reactor	10-500
Fusion reactor	550
High energy proton beam (NuMI)	~ 4000

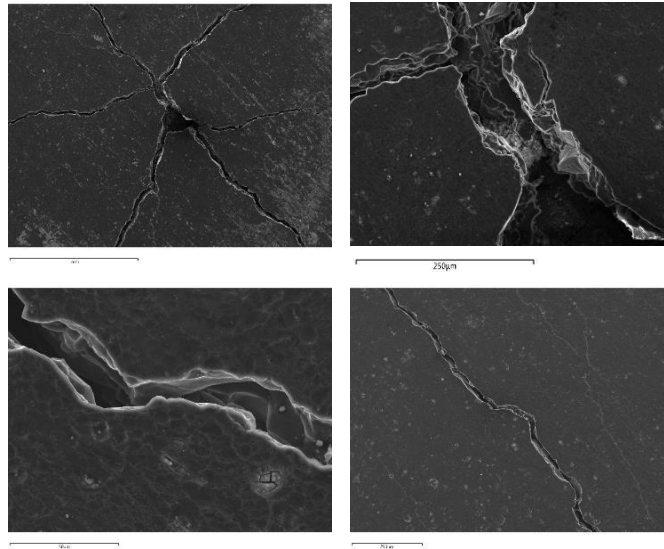
Large difference of dpa and transmutants production is likely to produce non-homogeneous changes across the surface of Be window.

15

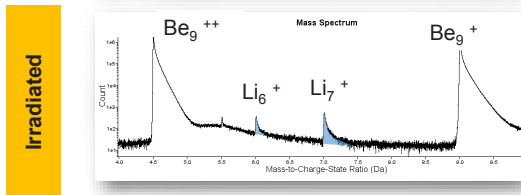
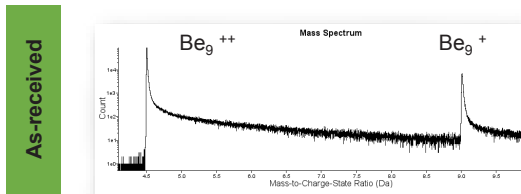
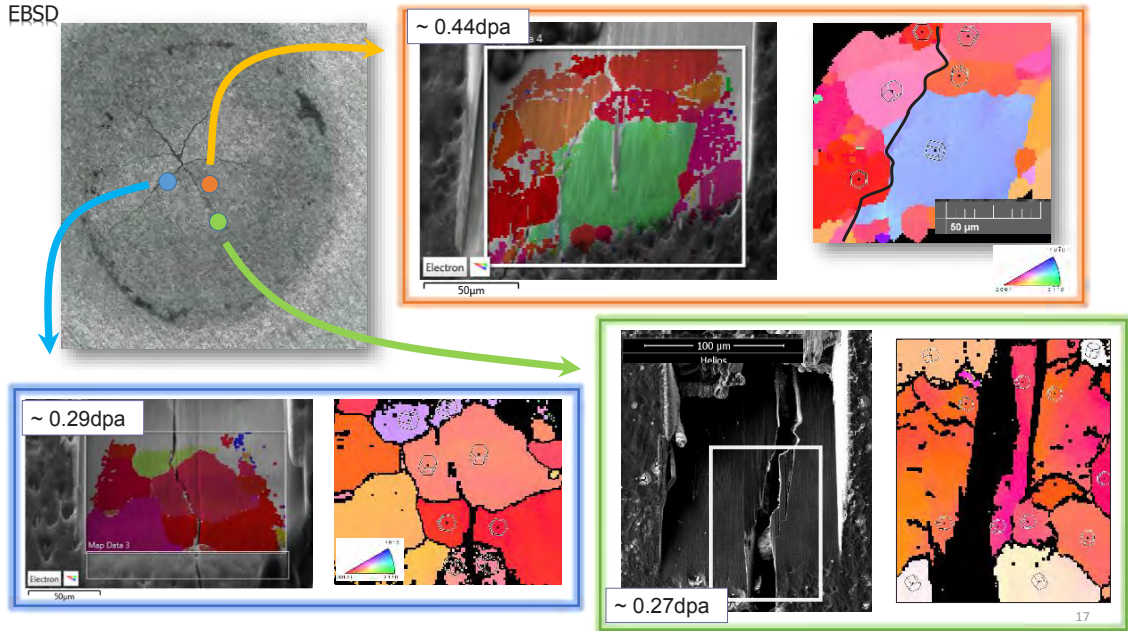
NuMI beam window experiments



What is the crack propagation mechanism?

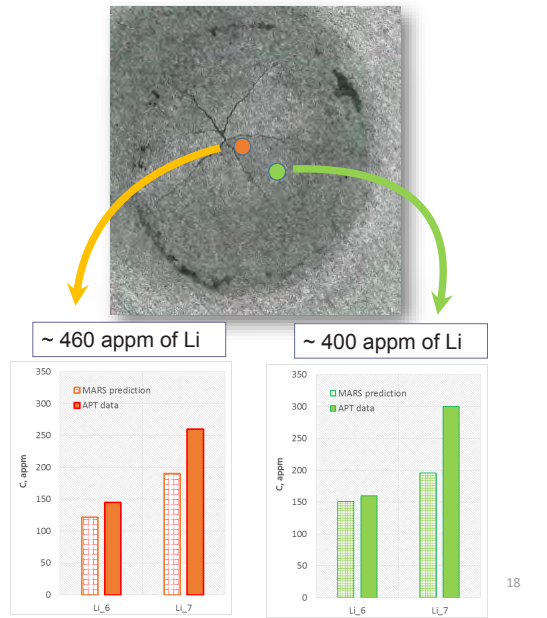


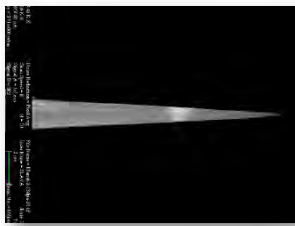
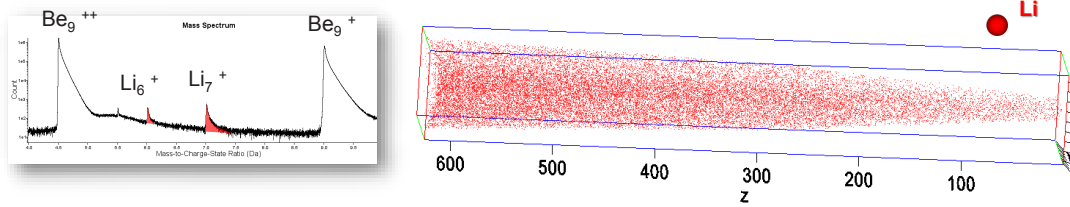
16



- New peaks on mass-spectrum – transmutation products
- Good agreement between the MARS model and APT data on Lithium production

Li is not soluble in Be. Will it segregate?

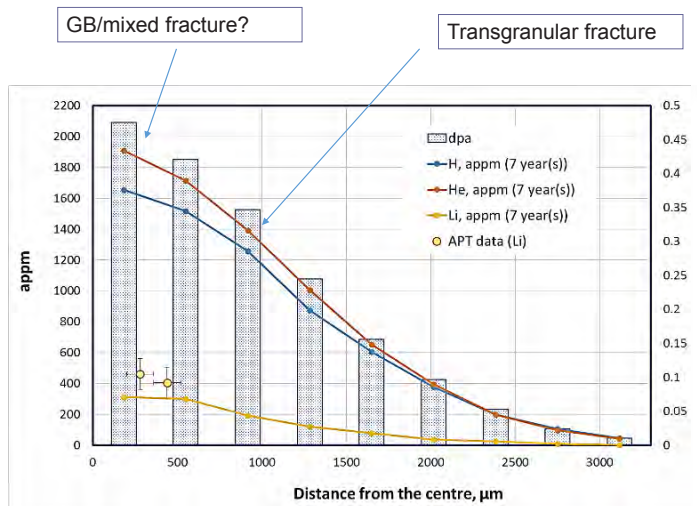




After irradiation inside grains:

- Transmutant Li is homogeneously distributed
- Impurities (Fe, Ni, Cu, O) are homogeneously
- ...but the temperature was low (50°C), and the behaviour can be different under new working conditions (>200°C). Ion implantation/annealing experiments are needed

19



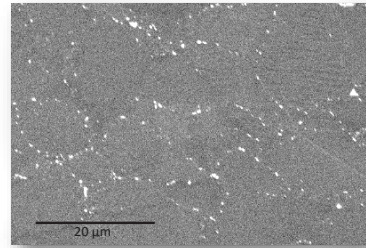
Transmutant Li can be one of the reasons of properties degradation under proton irradiation

But TEM and He/H transmutants distribution analysis is needed

20

Conclusions

- Industrial beryllium is an impure alloy: relatively pure grains and strongly "alloyed" GB
- Impurities strongly create GB precipitates and segregations, segregate to BeO
- Beryllium matrix has some quantity of homogeneously distributed oxygen, iron, nickel and copper
- Proton irradiation cause Li production, which is homogeneously distributed (T=50°C)
- Signs of irradiator induced embrittlement and change in fracture mode (from intra- to inter-granular) under high energy proton irradiation



21

Thank you for your attention!

2.4.2 ACCOUNTING OF NEUTRON IRRADIATION IN THE THERMO- MECHANICAL COMPUTATIONAL MODEL OF A CIRCULAR BERYLLIUM REFLECTOR

Y. Trifonov

JSC “NIKIET”, Moscow, RF

trifonov@nikiet.ru

Abstract

Earlier developed was the thermo-mechanical computational model of a circular beryllium reflector for a small-sized nuclear power facility operating under high heat and neutron fluxes. This model has been supplemented with a computational estimation of thermal conductivity variation of reflector material under high temperature irradiation. Such estimation permits to take into account an increase of thermal stresses and to accomplish the analyses of serviceability for a beryllium reflector during the whole term of its operation.

Being essentially a computational, the model developed was based on the experimental results of mechanical testing and thermo-physical measurements. It was intended to describe stress-strain state (SSS) of the reflector material at the beginning of its steady state operation as a part of nuclear power facility when the micro-structural changes are still negligible. To analyze serviceability of the reflector material during the whole term of its operation some corrections have been introduced into the model under consideration linked with the influence of neutron irradiation upon mechanical and thermo-physical properties of beryllium.

An analyses of the most probable structural changes of beryllium reflector operating at temperature above 450°C and integral neutron flux up to 10^{22} 1/cm² has determined a gas accumulation resulting from nuclear-physical reactions as a main process affecting micro-structural evolution at operating parameters indicated above. Therefore the thermo-mechanical model has been supplemented with computation heat conductivity variation resulting in the increase of thermal stresses and stress-strain state changes.

Computation of stress-strain state with regard to neutron irradiation has been carried out for all textural types of beryllium half-finished products that became the basis for the assessment of beryllium reflector serviceability at the final phase of its operation.

2.4.3 Tritium bulk distribution in tritium loaded beryllium pebbles

E. Pajuste¹, V. Chakin², G.Kizane¹, A. Matiko¹, P.Vladimirov², R. Rolli²

¹ Institute of Chemical Physics, University of Latvia, Kronvalda blvd.4, LV-1010, Riga, Latvia

² Karlsruhe Institute of Technology, Institute for Applied Materials, Herman-von-Helmholtz-Platz 1, 76344 Eggenstein - Leopoldshafen, Germany

Abstract

Tritium inventory in beryllium as a result of neutron-induced transmutations is a significant safety and technological issue for the operation of the breeding blanket. For evaluation of tritium behavior in beryllium without intricate and expensive neutron irradiation experiments, tritium gas loading at elevated temperatures is considered.

Tritium bulk distribution by the dissolution method has been evaluated for two kinds of beryllium pebbles (produced by the rotating electrode method and the fluoride reduction method) loaded with hydrogen and tritium gas mixture at the Karlsruhe institute of Technology [1].

The results revealed that after loading samples with tritium, its distribution is uneven – the higher amount of tritium is concentrated in the near-surface layers up to 0.1 mm of the pebbles, however, other peaks of high tritium concentration were found also deeper in the bulk of the pebbles (up to 0.4 mm).

Tritium distribution in the loaded pebbles was compared to its distribution in neutron irradiated beryllium pebbles.

1. Introduction

In the EU Helium Cooled Pebble Bed (HCPB) breeding blanket concept, beryllium is planned to be used as a neutron multiplier. The reference material was chosen to be pebbles with a diameter of 1 mm fabricated by NGK Insulators, Japan using the rotating electrode method (REM) [2]. As an alternative, Materion, USA suggests to use the 1 mm beryllium pebbles produced by fluoride reduction method (FRM).

As a result of neutron-induced transmutations of beryllium, helium and tritium atoms are produced in considerable amounts in the pebbles. In the frame of the European Power Plant Conceptual Study, the peak integral gaseous atom production in beryllium, at the End-Of Life (EOL) of the HCPB modules (40 000 h operation), has been assessed as 25 700 appm helium and 640 appm tritium, taking account in-pile tritium decay. According to the previous studies, the complete tritium release from the 1 mm beryllium pebbles occurs at higher temperatures than operation temperature of beryllium pebble bed [4-6]. To simulate the breeding blanket conditions, several neutron irradiation tests with beryllium have been performed in the past [7-10]. However, these experiments are very expensive and time consuming. Moreover, beryllium pebbles after irradiation become highly active due to the formation

of radioactive isotopes (^{60}Co , etc.) from the impurities in beryllium. Therefore, a simpler method for preliminary estimation of the tritium behavior trends in different kinds of beryllium samples without irradiation is highly desirable. Tritium gas loading at elevated temperatures is considered as an alternative way to saturate beryllium pebbles with tritium. This method was proposed for a long time ago (F. Scaffidi-Argentina, R. Rolli), but was always questioned if tritium is present at the surface only or tritium is absorbed in material bulk. Only in the latter case the features of tritium release curves would reflect properties of intrinsic tritium traps existing in material bulk. In this study, the tritium bulk distribution in beryllium pebbles after the tritium-hydrogen gas loading was investigated. These results were compared with data obtained on the pebbles after neutron irradiation.

2. Experimental/Methodological

Two kinds of 1 mm beryllium pebbles (produced by NGK and Materion) were loaded by $\text{H}_2 + 500$ appm T_2 gas mixture at temperatures of 600 and 850 °C for 15 h at the pressure of 4 bar at Karlsruhe Institute of Technology, Karlsruhe, Germany [1].

The method of dissolution (Fig. 2-1) developed in the Institute of Chemical Physics of the University of Latvia has been used. This method is based on dissolution of beryllium samples in the solution of diluted sulphuric acid and simultaneous registration of hydrogen and tritium in the purge gas [11].

Calculations of the tritium distribution in the pebble bulk are based on the controlled dissolution process of a pebble in $2 \text{ mol} \cdot \text{L}^{-1} \text{H}_2\text{SO}_4$ and simultaneous tritium measurements. The following

reactions occur during dissolution of a beryllium pebble containing tritium:



The rate of the hydrogen evolution was measured with a katharometer. Molecular and atomic tritium (T_2 and T^0) present in a Be sample transfer as $\text{T}_2 + \text{HT}$ into a flow of carrier gas, where the tritium activity released was measured with tritium monitor TEM 2100A with a proportional gas flow-through detector DDH 32. Molecular tritium is assumed to be localized in the helium bubbles, whereas atomic exists as an interstitial atom. Chemically bonded tritium (T^+) remains in the solution, and the tritium activity was measured with the liquid scintillation method. Chemically bonded tritium most likely is localized in the beryllium oxide layer on the pebble surface or in its inclusion in the bulk of the pebble. Solution containing tritium was distilled and 5 mL aliquot mixed with 15 mL of *Ultima Gold* scintillation cocktail and analysed for total tritium with the TRi-Carb 2910TR counter [PerkinElmer, Inc].

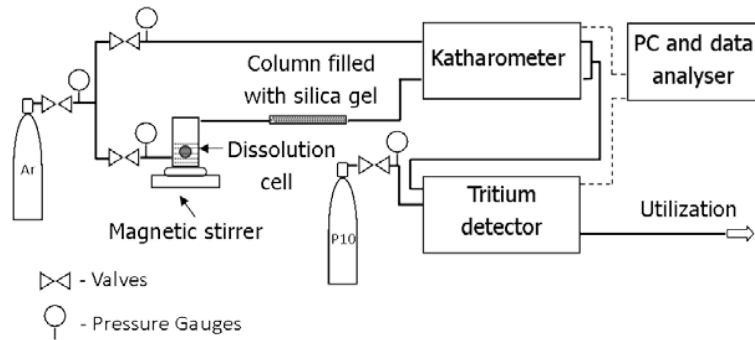


Fig. 2-1 Scheme of the set-up for dissolution of beryllium samples.

One hydrogen molecule corresponds to one beryllium atom and the dissolution rate of beryllium (and hereby also the thickness of dissolved layer for the estimation of the tritium bulk distribution) can be calculated from the hydrogen measurements (see Fig. 2-2). If dissolution process of a beryllium pebble starts at $t = t_0$ and the pebble radius at this moment is r_0 , it could be calculated as follows:

$$r_0 = \sqrt[3]{\frac{3m_0}{4\pi\rho_{Be}}}, \quad (2.5)$$

where, r_0 – the theoretical radius of the pebble, cm;

m_0 – mass of the pebble, g;

ρ_{Be} – the beryllium density, g/cm³.

The radius of the pebble r_t at a moment t can be calculated as follows:

$$r_t = \sqrt[3]{\frac{3(m_0 - \Delta m_t)}{4\pi\rho_{Be}}}, \quad (2.6)$$

where Δm_t is a mass of the dissolved beryllium at the moment t and can be calculated from the released hydrogen amount N_{H_2} (tritium gas contribution is negligible and, therefore, it is not taken into account):

$$\Delta m_t = \frac{N_{H_2}}{N_A} \cdot M_{Be} \quad (2.7)$$

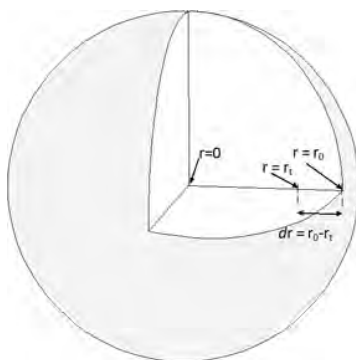


Fig. 2-2 Estimation of the dissolved layer.

In this method, the pebble is regarded as a perfect sphere and is assumed that tritium concentrations in all points of the sphere with radius r_1 are equal and theoretical density of beryllium ($9,018 \text{ g/cm}^3$) is used in the calculations. Finally, only an overall tendency of tritium distribution is obtained.

3. Results and discussion

The pebbles loaded at both 600 and 850 °C were dissolved. The gas phase was not detected in the pebbles loaded at the lower temperature. Probably, the amount of the gaseous tritium released during the dissolution of the pebble loaded at 600 °C was below the detection limit of the equipment. Therefore, the tritium distribution was measured and compared each other only for the pebbles loaded at 850 °C.

The total amount of tritium differs for each investigated sample. For the REM pebbles, it varies from 0.74 to 2.57 MBq/g, whereas for the FRM pebbles, this range is narrower: 0.46 to 0.69 MBq/g. The average values of tritium concentration in the gas and liquid phases of the REM and the FRM beryllium pebbles are shown in Fig. 3-1.

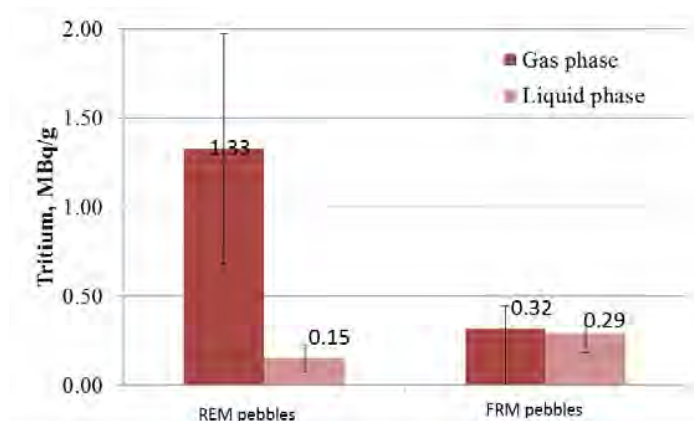


Fig. 3-1 Average tritium concentration in the 1 mm beryllium pebbles loaded at 850 °C.

The most interesting here is the considerably higher tritium concentration in gas phase for the REM pebbles compared to the FRM pebbles. This indicates the presence of comparatively larger amount of microstructure traps in the REM pebbles which can effectively capture the molecular tritium. Likely,

tritium exists in the pores in the molecular form T_2 [11]. Pores which are always present in both kinds of the pebbles (in the “as received” state) can be considered as the effective microstructure traps [12]. Examples of tritium distribution measured in gas phase in the REM pebbles are shown in Fig. 3-2. A little differing for each individual pebble, tritium was detected in the depth up to 0.4 mm from the pebble surface, i.e. practically to the pebble center. There are many peaks with different heights. The highest peaks are located near the surface within 0.04 mm. It can be supposed, the lower peaks in the pebble bulk correspond to the tritium release from the pores. The amount and location of the peaks differ for all three pebbles tested due to variation of microstructure (different pore size, amount and distribution) formed during the pebble production by REM.

Examples of tritium distribution measured in gas phase in the FRM pebbles are shown in Fig. 3-3. This distribution is significantly different from that for the REM pebbles. Despite of the largest peaks located approximately within the same near the surface layer up to 0.04 mm of beryllium (excluding BeO layer), the other peaks are much smaller than that for the REM pebbles. Moreover, all these peaks have tritium concentration less than 0.2 relative units and appear very often. This means, the pores in the FRM pebbles should have comparatively smaller sizes and higher density in the pebble bulk. In this case, tritium under loading can easier penetrate through the matrix between pores reaching the pebble center. However, under cooling, the most part of the tritium may easy move by the same path backward to the near-surface layers. It seems that the FRM pebble microstructure is practically transparent to the tritium penetration. After loading, only a small part of the tritium remains in these pores. The most part of the tritium moves to the surface and is concentrated there.

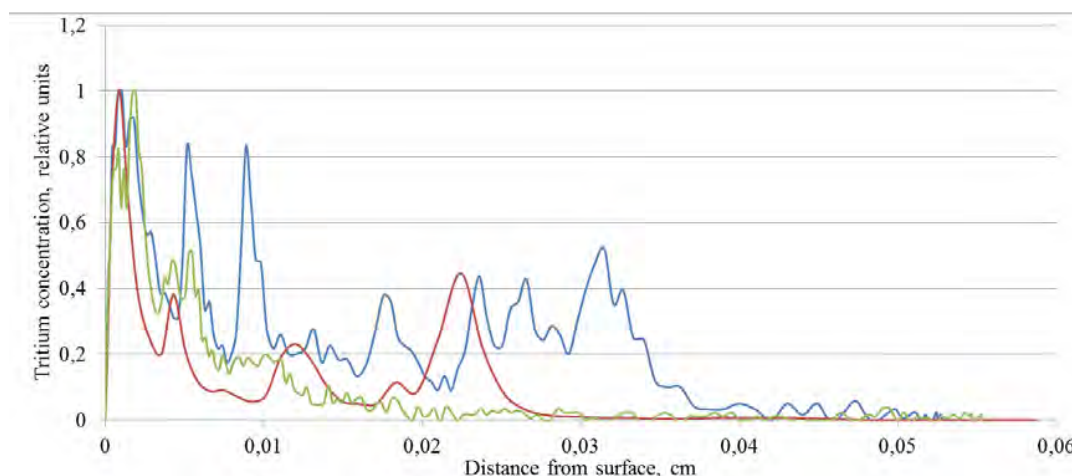


Fig. 3-2 Tritium distribution in the three (blue, red, green) tested 1 mm REM pebbles loaded at 850 °C (tritium concentration is given in relative units for the better comparison of each other).

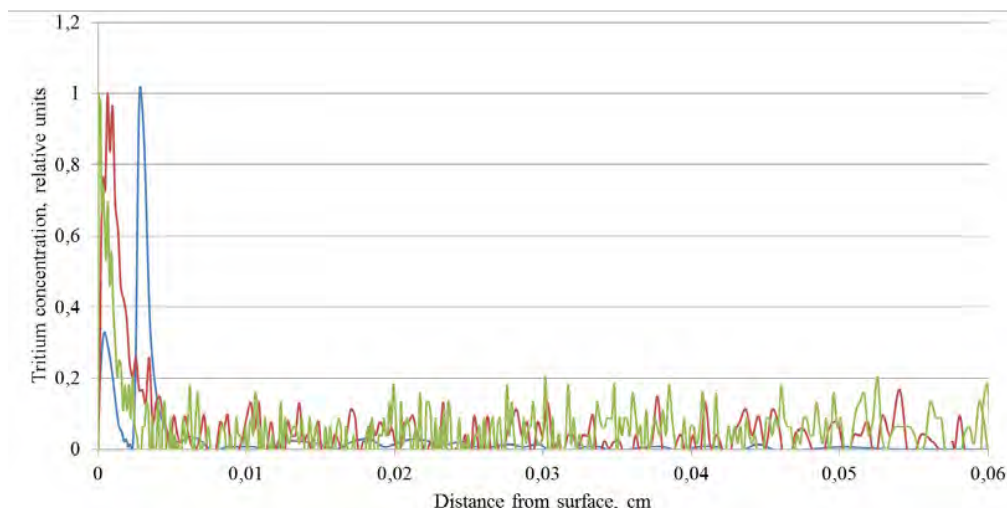


Fig. 3-3 Tritium distribution in the three (blue, red, green) tested 1 mm FRM pebbles loaded at 850 °C (tritium concentration is given in relative units for the better comparison of each other).

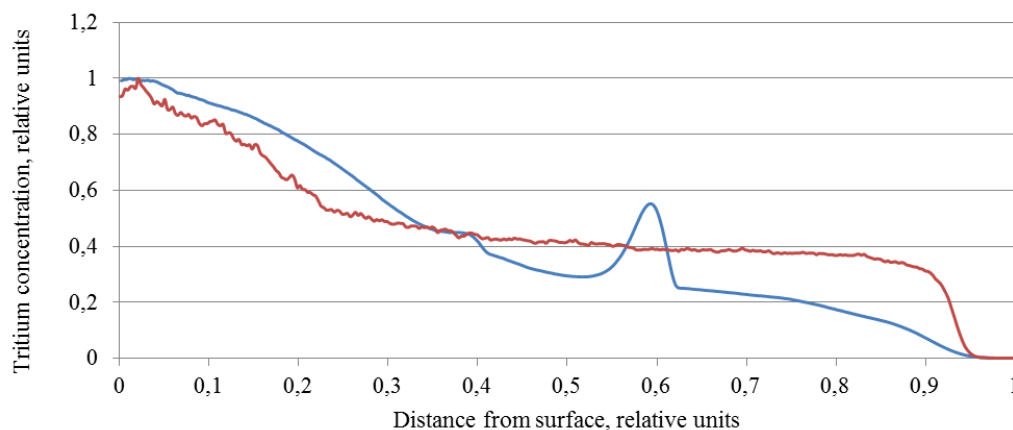


Fig. 3-4 Tritium distribution in neutron irradiated pebbles – irradiation experiments BERYLLIUM (blue) and PBA (red) (tritium concentration is given in relative units for the better comparison, distance from the surface also given in relative units as a ratio to the pebble radius).

On the pebble surface, beryllium oxide (BeO) layer always exists. Its thickness can reach 0.15 μm for REM pebbles [1]. The BeO layer can be a strong barrier to the tritium escaping outside the pebble because it has much lower tritium diffusivity than that in the pure beryllium. Therefore, tritium might be concentrated in the beryllium matrix close to the interface with the oxide layer under cooling after the loading at 850 °C.

Examples of tritium distribution in neutron irradiated pebbles are given in Fig. 3-4. Pebbles irradiated in the PBA experiment were produced by the REM process, whereas pebbles from the BERYLLIUM experiment – FRM. In contrast to thermal loading, neutron irradiation results in homogeneous tritium generation over pebble bulk. Therefore, compared to the loaded beryllium pebbles, tritium is much

more evenly distributed through the pebble matrix for the irradiated pebbles. However, even here, an increase of tritium concentration is visible within the near-surface layers up to 0.3 relative units depth. The release peak around the 0.6 relative units on the curve for pebble irradiated in BERYLLIUM experiment might be related to T₂ release from a large pore.

4. Conclusions

The method of dissolution developed in the Institute of Chemical Physics of the University of Latvia was applied for investigations of tritium distribution in beryllium pebbles of two kinds (produced by REM and FRM) after loading by H₂ + 500 appm T₂ gas mixture at temperatures of 600 and 850 °C for 15 h at the pressure of 4 bar. The loading at 600 °C was not used in the investigations because the tritium amount in the gaseous phase was below the detection limit of the equipment.

In both types of pebbles tritium was detected up to the center of pebble. This fact clearly shows that tritium loading procedure results in tritium absorption in the bulk of beryllium pebbles. The details of tritium distribution in the loaded pebbles depend on the pebble type (production method, structure, etc.). Comparatively lower tritium retention in the FRM pebbles than in the REM pebbles should be attributed to the differences in their microstructure. Except of one sample, in the majority of the FRM pebbles, the most part of tritium is trapped near the surface within 0.04 mm. In the REM pebbles, tritium was found up to 0.5 mm from the surface, i.e. all over the pebble bulk. These peaks in the pebble bulk might correspond to the tritium retention in small pores which are formed during production of the pebbles. In the both kinds of the pebbles, peaks with the higher tritium concentration were observed; however, the peaks in the FRM pebbles occur more frequently and have smaller heights.

Tritium concentration peaks were observed also in neutron irradiated pebbles. Although irradiation creates additional tritium traps, traps existing before irradiation, like, e. g., fabrication induced porosity, are still present. Therefore, the method of tritium loading gives a possibility for preliminary evaluation of the beryllium pebble performance regarding tritium retention.

References

- [1] V. Chakin, A. Moeslang, P. Kurinskiy, R. Rolli, H.C. Schneider, E. Alves, L.C. Alves, *Fusion Engineering and Design*, 86 (2011) 2338-2342.
- [2] L.M. Giancarli, M. Abdou, D.J. Campbell, V.A. Chuyanov, M.Y. Ahn, M. Enoeda, C. Pan, Y. Poitevin, E. Rajendra Kumar, I. Rikapito, Y. Strebkov, S. Suzuki, P.C. Wong, M. Zmitko, *Fusion Engineering and Design*, 87 (2012) 395-402.
- [3] E. Rabaglino, C. Ronchi, A. Cardella, *Fusion Engineering and Design*, 69 (2003) 455-461.
- [4] A. Vitiņš, G. Kizane, A. Matiss, E. Pajuste, V. Zubkovs, *Journal of Nuclear Materials*, (2013) S490-S493

- [5] P. Kurinskiy, P. Vladimirov, A. Moeslang, R. Rolli, M. Zmitko, *Fusion Engineering and Design*, 89 (2014) 1455-1458.
- [6] V. Chakin, R. Rolli, P. Vladimirov, A. Moeslang, *Fusion Engineering and Design*, 95 (2015) 59-66.
- [7] A.V. Fedorov, M.M. Peeters, J.G. van der Laan, in: A.J.Magielsen (Ed.), NRG, Petten, 2008, p. 109.
- [8] J.G. van der Laan, L.V. Boccaccini, R. Conrad, J.H. Fokkens, M. Jong, A.J. Magielsen, B.J. Pijlgroms, J. Reimann, M.P. Stijkel, S. Malang, *Fusion Engineering and Design*, 61-62 (2002) 383-390.
- [9] J.B.J. Hegeman, J.G.v.d. Laan, H. Kawamura, A. Möslang, I. Kupriyanov, M. Uchida, K. Hayashi, *Fusion Engineering and Design*, 75-79 (2005) 769-773.
- [10] S. van Til, J.B.J. Hegeman, H.L. Cobussen, M.P. Stijkel, *Fusion Engineering and Design*, 86 (2011) 2258-2261.
- [11] E. Pajuste, A. Vitins, G. Kizane, V. Zubkovs, P. Birjukovs, *Fusion Engineering and Design*, 86 (2011) 2125-2128.

2.4.4 Effect of hydrogen on equilibrium shape of gas bubbles in beryllium

Dmitry Bachurin, Pavel Vladimirov

Institute for Applied Materials – Applied Materials Physics, Karlsruhe Institute of Technology,
76344 Eggenstein-Leopoldshafen, Germany

Abstract

In fusion environment hydrogen isotopes can be either produced inside beryllium bulk or adsorbed on beryllium surface. In the present work the effect of hydrogen surface concentration on the properties of five principal hexagonal close-packed beryllium surfaces (basal, prismatic type I and II, pyramidal type I and II) was studied by first-principle calculations. The configurations with high hydrogen coverage were studied for all considered surfaces. It was shown that the presence of adsorbed hydrogen atoms significantly changes the energy of all surfaces with except the prismatic type II surface. Relaxation of outermost atomic layers at critical coverage drastically differs from that found for pure beryllium. Influence of hydrogen surface concentration on the equilibrium shape of hydrogen covered bubbles was investigated by means of the Wulff polyhedron construction.

1. Introduction

Beryllium is very promising material for fusion energy applications due to its ability for neutron multiplication [1-2]. The Helium Cooled Pebble Bed Blanket with beryllium pebbles is the advanced concept of the tritium breeding blanket for the future demonstration fusion reactor DEMO. In this concept lithium ceramic is used as tritium breeding material, while beryllium acts as neutron multiplier. High-energy fusion neutrons result in transmutation of beryllium atoms into beta-radioactive tritium and helium and, as a consequence, to formation of gas bubbles and degradation of the material properties. Tritium is captured by vacancies and gas bubbles. Assessment of the radioactive inventory of tritium trapped inside beryllium pebbles is very important from the safety point of view during operation and for handling of the radioactive beryllium waste after the end-of-life of the blanket. On the other hand, the concept of ITER considers beryllium as plasma facing material for the first wall. Under such conditions interaction of hydrogen isotopes with beryllium surfaces is also unavoidable.

Experimental studies and first-principle calculations show that the presence of hydrogen atoms on beryllium surface leads to a considerable change of its properties. A significant interplanar relaxation of the outermost atomic layers accompanied by the change of the structural and energetic characteristics takes place [3-10]. Note, that majority of the available first-principles studies consider mainly the basal and prismatic type I planes only [3,5,7,9,11-14]. In order to investigate an equilibrium shape of gas filled bubbles it is necessary, however, to extend our knowledge about the energetics of the principal hcp surfaces with and without hydrogen.

For understanding of the presented results it is necessary to mention that: (i) hydrogen molecule undergoes dissociative adsorption on beryllium surface; (ii) hydrogen atoms can desorb from the surface only as a molecule; (iii) hydrogen atoms repel each other on the surface thus preventing their desorption from the surface until high hydrogen surface concentration is reached or the temperature is high enough to overcome desorption barrier; (iv) there exist upper limits for hydrogen concentrations on beryllium surfaces above, which athermal desorption of hydrogen molecules occurs (these concentrations will be referred as maximum or 100% coverage below); (v) significant hydrogen surface concentration can be accumulated on the inner surface of helium bubbles, which will result in notable changes of surface energies of various bubble facets and will lead to the change of the equilibrium gas bubble form.

Gas bubbles in beryllium are often formed after neutron irradiation at elevated temperatures (above 400–500°C). In this case both helium and tritium are produced due to nuclear transmutation. Small bubbles are usually faceted having a form of a hexagonal prism extended on basal plane. These bubbles are mainly filled with helium as far as about ten times more helium than tritium is produced in typical mixed spectrum nuclear reactor [15]. On the other hand, bubbles formed after annealing of hydrogen implanted beryllium at 400–600°C have completely different shape [16].

The main goal of the present work is to study the effect of hydrogen surface concentration (coverage) on beryllium surface energies via first-principle calculations. The obtained results are used for construction of the equilibrium shape of bubbles covered with hydrogen and compared with experimental data after neutron irradiation or hydrogen implantation.

2. Modeling

Static first-principles calculations were performed using the Vienna Ab initio Simulation Package (VASP) [17-18]. The projector augmented wave potentials (PAW) were used to describe the interactions between ions and electrons. The PAW potentials for beryllium (with two valence electrons) and hydrogen were taken from the VASP depository [19-20]. The generalized gradient approximation (GGA) of Perdew and Wang [21] was employed to determine the exchange-correlation energy.

Hydrogen effects were studied for five principal close-packed beryllium surfaces: basal (0001), prismatic type I ($1\bar{1}00$) and II ($2\bar{1}\bar{1}0$) as well as pyramidal type I ($1\bar{1}01$) and II ($2\bar{1}\bar{1}2$) (see Fig. 2-1). For the prismatic type I and pyramidal type I surfaces, which can be terminated in two possible ways, only the most energetically favorable "short" termination was considered. A vacuum gap of 17–23Å, equivalent to four atomic layers and sufficient to avoid interaction between the top and the bottom of the simulation box due to periodic boundary conditions was used. During energy minimization both volume and shape of the simulation box were fixed, while no restrictions on the relaxation of atoms were imposed. The optimized lattice constants for pure beryllium were $a=2.265\text{Å}$, and $c=3.562\text{Å}$. A Fermi broadening of 0.2 eV and the cut-off energy of the plane waves of 450 eV

were chosen after extensive verification. The atomic structures were visualized using the Jmol program [22].

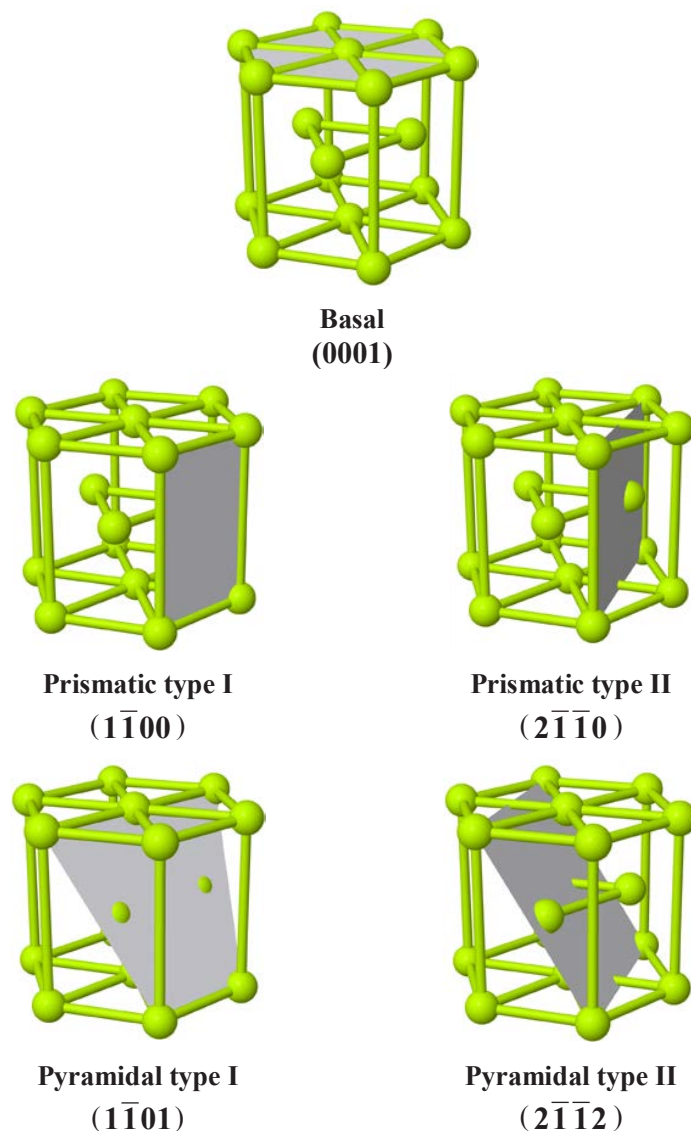


Fig. 2-1. Principal hcp crystallographic planes shown in unit cell.

For surface energy calculations five different configurations with the free surface area large enough to avoid the interaction of the hydrogen atom with its periodic images were created (see Table 2-1). This imposes certain restrictions on the thickness of the slab, since the number of atoms should not be too large to get reasonable calculation times. For convenience of surface energy calculation hydrogen atoms in the initial configurations were placed symmetrically on both free surfaces at the most energetically favorable adsorption sites found for single hydrogen on otherwise hydrogen-free surface: hcp hollow site for basal plane; bridge site at the 'surface ridge' for prismatic type I and II as well as pyramidal type II planes; a middle of triangle formed by two beryllium atoms at the 'surface ridge' and one atom at the 'surface valley' (see Ref. [10] for details).

Table 2–1. Surface energies of hydrogen free and 100% H-covered principal close-packed beryllium surfaces. N_{Be} is the number of beryllium atoms in the slab. N_H^{\max} is the number of hydrogen atoms corresponding to 100% of coverage. The fourth column indicates the number of beryllium atomic layers in the simulated slab. $N_s^{0\%}$ and $N_s^{100\%}$ are the energies (J/m²) of hydrogen-free and 100% covered beryllium surfaces, respectively.

Surface	cell size	N_{Be}	Be layers	N_H^{\max}	k -points	$E_s^{0\%}$	$E_s^{100\%}$
(0001)	3×3×4	72	8	9	18×18×5	1.71	1.64
(1 $\bar{1}$ 00)	2×3×6	72	12	12	14×15×5	1.80	1.53
(2 $\bar{1}$ $\bar{1}$ 0)	3×3×3	108	6	18	9×10×8	2.02	1.88
(1 $\bar{1}$ 01)	3×2×6	72	12	12	15×12×5	1.83	1.08
(2 $\bar{1}$ $\bar{1}$ 2)	3×2×4	96	8	24	11×15×8	2.40	0.76

The surface energy of beryllium slab covered by n hydrogen atoms was defined as

$$E_s = \frac{E_{total}^{Be+nH} - E_{total}^{Be} - nE_{ref}^H}{2S}, \quad (2.1)$$

where E_{total}^{Be+nH} is the total energy of the beryllium system with n hydrogen atoms; E_{total}^{Be} is the total energy of the hydrogen-free beryllium slab; $E_{ref}^H = -3.3590$ eV is the energy per hydrogen atom in H₂ molecule; S is the surface area. Factor two in Eq. (2.1) corresponds to the fact that the slab has two surfaces with equivalent hydrogen configurations on both sides.

It should be noted that our *ab initio* molecular dynamics runs reveal that there is an upper limit for hydrogen coverage on (0001) surface of beryllium in equilibrium with molecular hydrogen gas phase above which hydrogen molecules cannot be adsorbed. For basal surface this critical coverage corresponds to one hydrogen atom per beryllium surface atom (or equivalently one hydrogen per surface lattice unit cell). In order to determine the critical hydrogen occupations for other surfaces, the stability of configurations with increasing number of hydrogen atoms adsorbed was checked by performing static VASP relaxations. This procedure was performed by placing hydrogen at different adsorption sites for each of the five considered beryllium surfaces. Thus, the following maximum surface coverage per surface unit cell was obtained: one hydrogen atom on basal plane; two hydrogen atoms on prismatic type I, type II and pyramidal type I planes; four hydrogen atoms on pyramidal type II plane (see Table 2–1).

Knowledge of the surface energy for various close packed surfaces allows us to determine an equilibrium shape of a gas bubble by means of the Gibbs-Wulff construction [23]. This procedure consists in minimization of the total surface free energy. The Wulff theorem states that the distance from a polyhedron face to its center should be proportional to the surface energy of this face. The Wulff shape of bubble was determined by construction of Voronoi polyhedron according to this rule.

3. Results

3.1. Beryllium surfaces at critical hydrogen coverage

Configurations with 100% hydrogen coverage are shown in Fig. 3–1. It was found that at high concentrations hydrogen prefers to have two-fold coordination with beryllium surface atoms in contrast to lower coverages, where in half of the cases hydrogen is three-fold coordinated. Atop-like positions for hydrogen adsorption were not observed in our simulations.

At high coverage the bridge position turns into a stable adsorption site and is the most energetically favorable (see Fig. 3–1a), although at low coverage it corresponds to a saddle point between hcp and fcc adsorption sites [10]. At high coverage the hcp and fcc hollow sites do not correspond to the energy minima anymore. For example, the energy difference of the fcc and the bridge sites on the fully covered surface is 0.22 J/m^2 . The distance between the first neighboring hydrogen atoms is 2.27 \AA .

For prismatic type I plane the stable hydrogen sites are along the surface 'ridge' and 'valley' as illustrated in Fig. 3–1b. All hydrogen atoms are located at bridge positions. The first neighboring hydrogen atoms are located at the distance of 2.27 \AA along the surface 'ridge' and surface 'valley'.

For prismatic type II plane hydrogen atoms can be located at bridge positions along surface ridges and valleys as shown in Fig. 3–1c, which is similar to stable hydrogen sites of single atom. However, different hydrogen occupations of the 3×3 surface results in quite different results: (i) the configuration with 3 hydrogen in the valleys and 6 on the ridges is stable; (ii) the configuration with 6 hydrogen in the valleys and 3 on the ridges results in formation of Be-H chains and surface disordering, while (iii) the configuration with 6 hydrogen in the valleys and 6 on the ridges reveals formation of BeH_2 chains detaching from the surface during relaxation. The length of the H-Be bonds are 1.47 \AA for surface 'ridge' and 1.71 \AA for surface 'valley' similar to those for single hydrogen atom. The distance between the first neighboring hydrogen atoms located at the surface 'ridge' and surface 'valley' is 2.74 \AA .

For pyramidal type I plane the half of hydrogen atoms are located at the bridge sites, while the other half is close to be three-coordinated with beryllium surface atoms (see Fig. 3–1d). Note that both stable sites found for single hydrogen atom are three-coordinated [10]. The length of the H-Be bonds varies from 1.40 to 1.52 \AA . The first neighboring hydrogen atoms are located at the distance of 2.10 \AA .

For pyramidal type II plane all stable adsorption sites are bridge-like positions with the bonds which are in the range of 1.41 to 1.45 \AA . Figure 3–1e demonstrates that there is a certain asymmetry in the position of hydrogen atoms along the surface valley suggesting that the energy difference between them supposed to be insignificant. The first neighboring hydrogen atoms are located at the distance of 2.06 \AA along the surface 'ridge' and surface 'valley'.

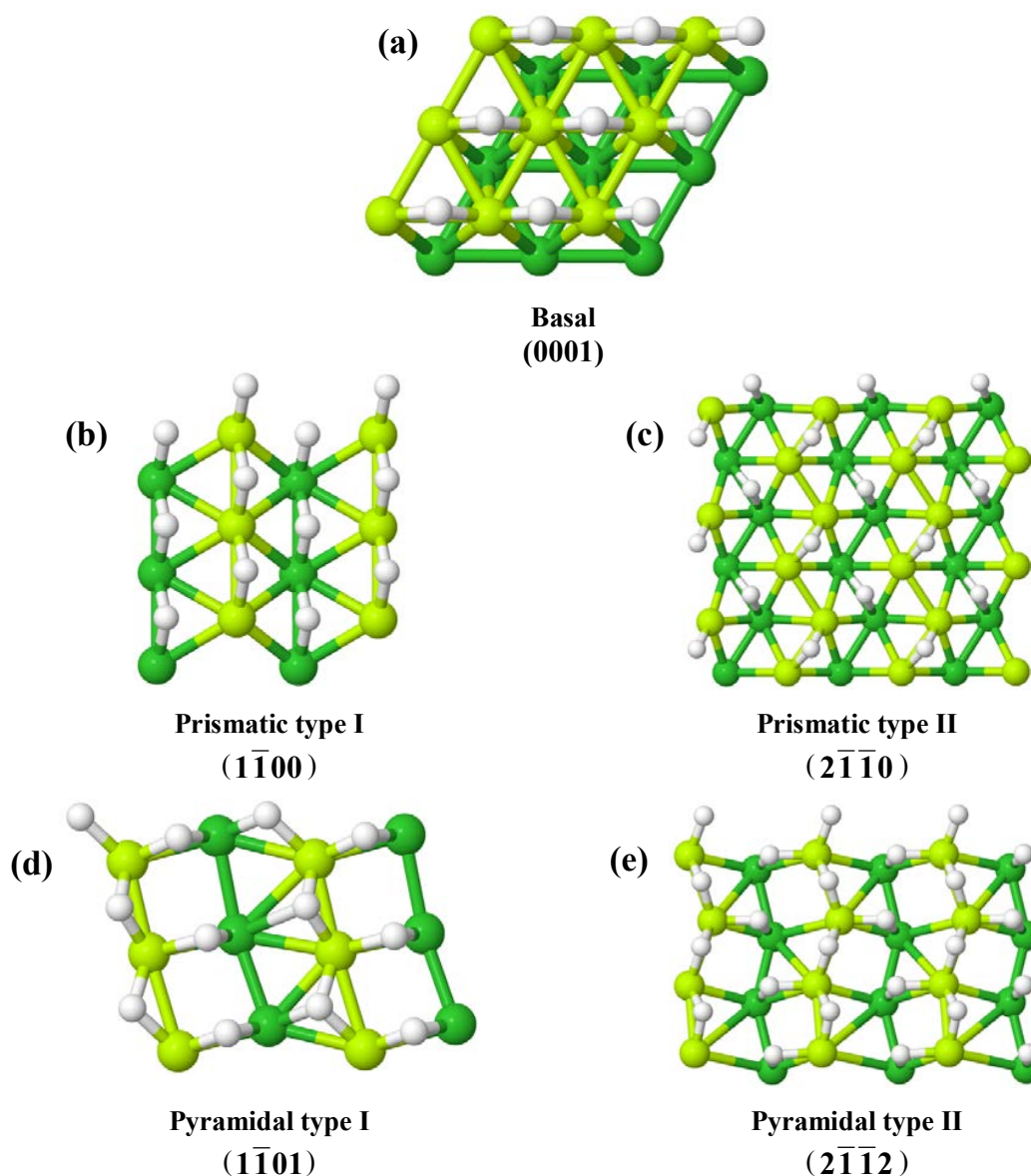


Fig. 3-1. Minimum energy configurations of beryllium surfaces with a critical (100%) hydrogen coverage. The top outermost layer (green) and the layer beneath it (dark green) are shown. The top atoms are also called as a surface 'ridge', the layer beneath it as a surface 'valley'.

3.2 Beryllium surface energy vs. hydrogen coverage

The effect of sequential addition of hydrogen atoms on surface energies of various orientations is presented in Fig. 3-2. Generally, the surface energy first reduces, reaches a minimum and then raises with the increase of hydrogen coverage. Thus, from a certain point, which is different for different beryllium surfaces, further hydrogen adsorption is energetically unfavorable. The energy of all considered beryllium surfaces covered with hydrogen atoms is always smaller than that of the corresponding clean surface. The energies of prismatic type I and pyramidal type I surfaces at zero coverage are almost equal, but they differ by 0.4 J/m^2 in the case of critical coverage. The presence of

hydrogen changes drastically the energy of pyramidal type II surface from 2.4 down to 0.8 J/m². In this way the most unfavorable surface turns out to be the most favorable after hydrogenation. On the other hand, the prismatic type II surface is not very sensitive to the presence of adsorbed hydrogen showing the surface energy changes in the range of 0.2 J/m² (~10% with respect to the pure surface energy). It is interesting to note that when the coverage exceeds 40%, the pyramidal type II surface becomes the most energetically favorable one (see Fig. 3–2), while the energy of basal surface is 0.4–0.8 J/m² higher.

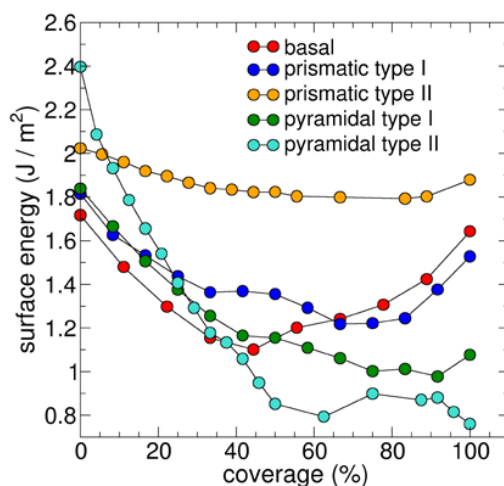


Fig. 3–2. Surface energy of beryllium surfaces as a function of hydrogen coverage. Zero coverage corresponds to the energy of beryllium surface without hydrogen atoms. Lines connecting the data points are guides to the eye.

3.3. Effect of hydrogen on interplanar relaxation

Figure 3–3 demonstrates how the presence of hydrogen on beryllium surfaces changes the relaxation pattern at critical hydrogen coverage in comparison with pure beryllium surface. Only the top layer of basal plane exhibits noticeable expansion, while the interplanar spacings for all other inner atomic planes are very close to the ideal hcp lattice value (see Fig. 3–3a). In other words, hydrogen 'tears' the top beryllium layer from the bulk, which is a good illustration of hydrogen embrittlement of the surface. An oscillatory relaxation (interchanging stretching and compression between layers) occurs for prismatic type I and pyramidal type I and II surfaces. Moreover, the compression of interlayer distances of beryllium surfaces without hydrogen is replaced by the tension of these distances at critical hydrogen coverage and vice versa as shown in Fig. 3–3b, 3–3d, 3–3e. Expansion of the 'short' interlayer distances $d_{12}, d_{34}, d_{56}, \dots$ and contraction of the 'long' distances $d_{23}, d_{45}, d_{67}, \dots$ is observed for prismatic type I plane with critical coverage in contrast to the pure surface. Generally the 'short' distances relax more significantly (>50%) than the 'long' ones. Furthermore, tension of the topmost short-terminated distance d_{12} takes place, while the other 'short' distances d_{34} and d_{56} are under contraction as seen in Fig. 3–3d. The relaxation patterns of fully covered and pure prismatic type II plane are relative similar (see Fig. 3–3c).

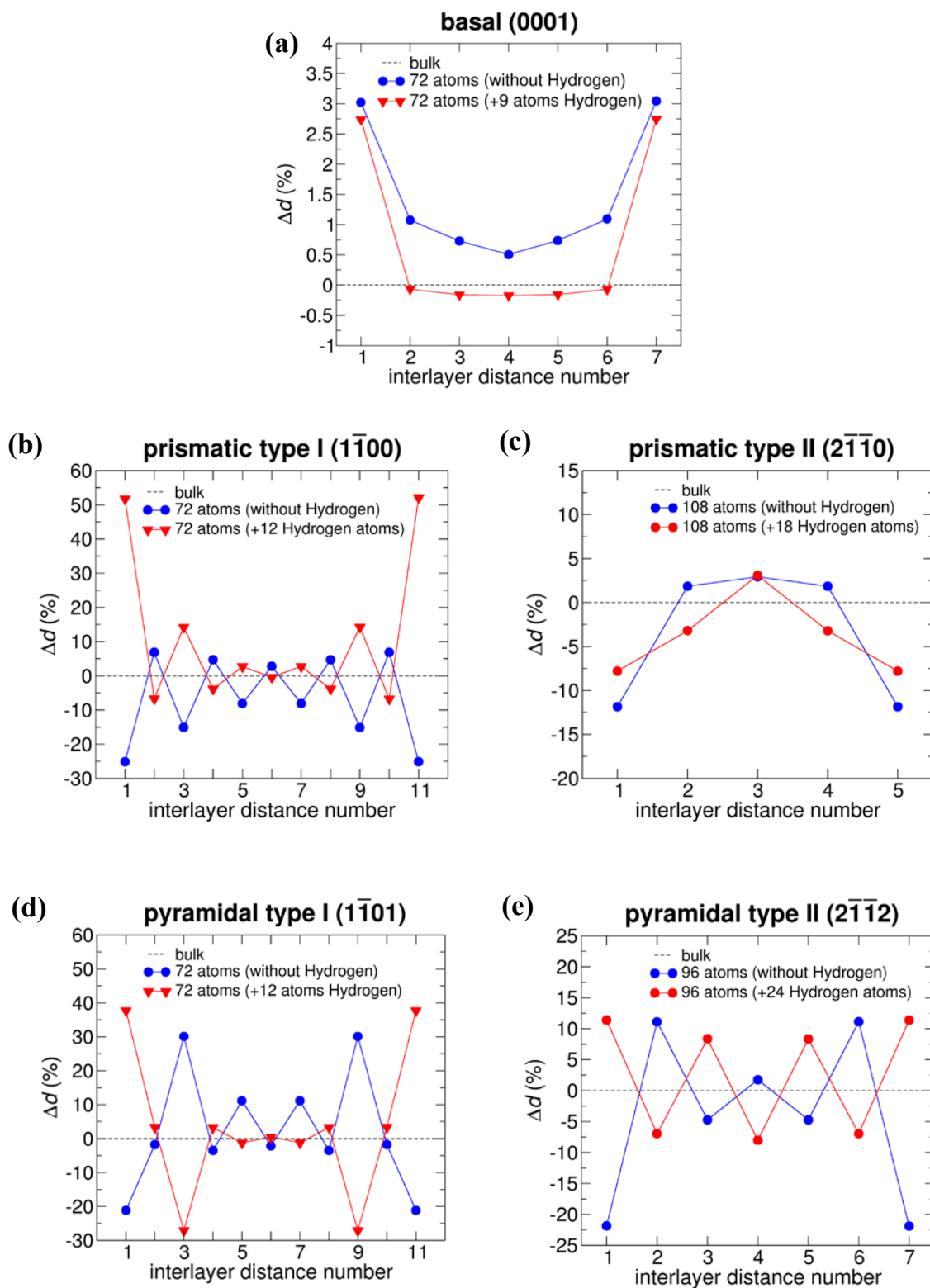


Fig. 3–3. Comparison of relaxation of outermost surface layers in pure beryllium and with 100% hydrogen coverage for five principal hcp surfaces. The relative distance between the surface layers i and j in % as compared with the interlayer spacing in the bulk, d , was calculated as $\Delta d_{ij} = (d_{ij} - d)/d$. Lines connecting the data points are guides to the eye.

3.4. Equilibrium shape of hydrogen covered bubbles in beryllium

As a first approximation Gibbs-Wulff construction was performed assuming that hydrogen concentration is the same for different beryllium surfaces, although this assumption might be not necessarily valid. Figure 3–4 illustrates the computed equilibrium shapes of a bubble in hcp beryllium crystal without hydrogen (0% of coverage), which is composed mainly of basal, prismatic type I and pyramidal type I faces. Similar equilibrium shapes were obtained for other hcp materials [24-27]. The only difference from the previous works is the presence of a small fraction of prismatic type II face (orange) which cuts an edge formed between two adjacent prismatic type I faces. Since hydrogen considerably decreases the beryllium surface energy, the change of equilibrium shape of bubbles is expected with the increase of hydrogen coverage. Indeed, a full disappearance of prismatic type II, a slight decrease of the area of prismatic type I and an increase of the fraction of pyramidal type I facets are seen at 17% of coverage. Further increase of hydrogen concentration leads to a significant increase of the area of pyramidal type II facets. At 46% of coverage the bubble is faceted with basal and pyramidal type II planes, while at 100% coverage only pyramidal type II facets are present.

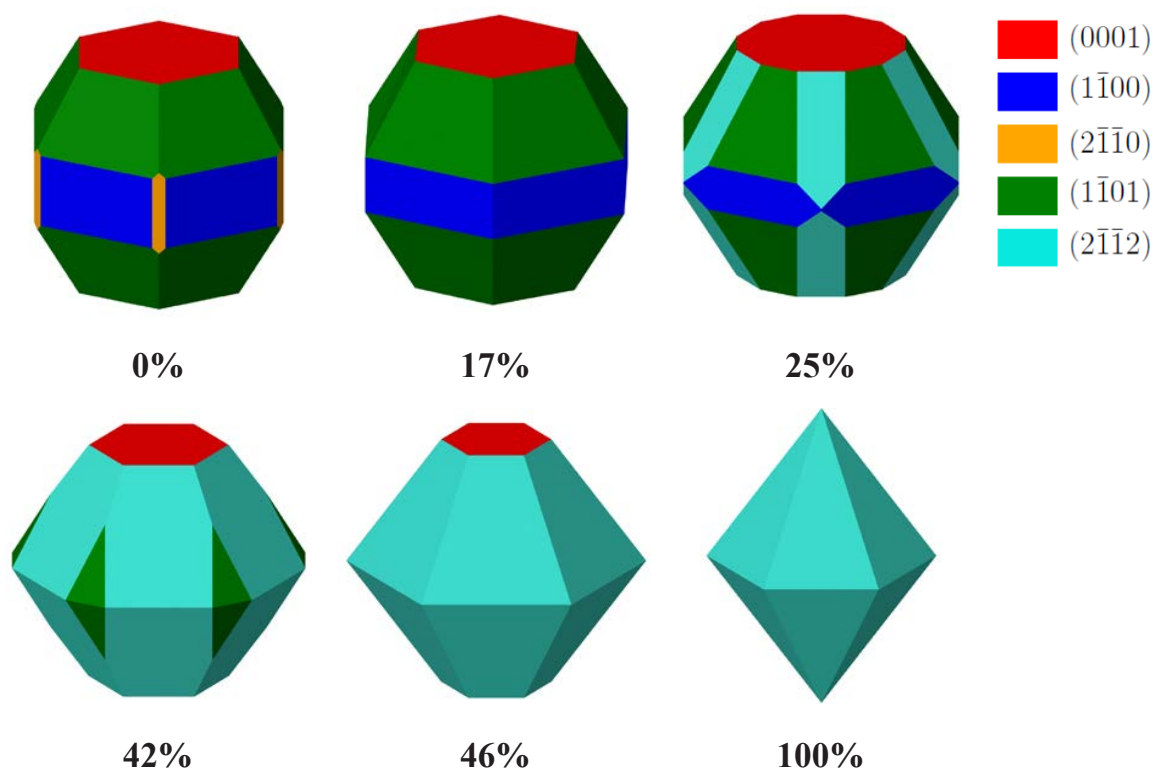


Fig. 3–4. Calculated three-dimensional equilibrium shape of bubble in an hcp beryllium single crystal at 0 K as a function of hydrogen coverage (shown below).

4. Discussion

As we learned for the basal surface, the stable hydrogen adsorption sites at high coverage can noticeably differ from those with lower coverage. At high coverage, in the majority of the cases, hydrogen atoms prefer to occupy bridge sites and to be two-fold coordinated (see Fig. 2–1). A number of early first-principle calculations [4,28] have revealed that on the basal plane the bridge position above the middle of the Be-Be bond is a stable adsorption site for one hydrogen atom in the smallest 1×1 simulation cell. Our study confirmed that these results were not artifacts related to the small size of the simulation cells common at that time: stable bridge adsorption sites were repeatedly reproduced with larger simulation cells at high hydrogen coverages.

More recent study [29] of Be(0001) surface reported higher hydrogen coverage than that found in this work suggesting that 3×3 cell, which includes 9 beryllium surface atoms, is completely covered, when 12 hydrogen atoms are present. As can be seen from the Fig. 3c therein most of the hydrogen atoms are two-fold coordinated and form a kind of disordered Be-H chains on the surface. As was mentioned earlier, our attempt to put two hydrogen atoms per one beryllium (corresponds to 18 H per 9 Be) on the basal surface ended with athermal desorption of several hydrogen molecules, while no desorption was observed with one hydrogen per surface beryllium. Formation of similar distorted Be-H chains was also observed in the latter case. It seems that the critical coverage above which molecular adsorption stops is below the maximum hydrogen coverage, which can be reached by atomic hydrogen adsorption or diffusion of hydrogen from the bulk. Moreover, probably the maximum coverage will be reached with two hydrogen atom per beryllium corresponding to the formation of complete BeH_2 chains. Therefore our findings are complementary to the previous results from [29].

Relaxation of surface layers of basal plane with the coverage corresponding to one hydrogen atom per beryllium surface atom was given in Refs. [4,7]. The first layer was found to be under contraction with $d_{12} \approx -0.27\%$ of the bulk value [4], while it was under stretching with 10 times higher value of $d_{12} \approx 2.7\%$ in work [7]. Unfortunately, it is difficult to explain the difference of one order of magnitude (and even opposite sign) between the results obtained by the same author within slightly different frameworks. However, the latter result is in a good agreement with our findings (see Fig.3–3a). We are not aware of the works, where the relaxation of outermost surface layers of other principal close-packed beryllium surfaces at high hydrogen coverage was investigated.

There are plenty of experimental investigations of helium bubbles growing as a result of ion or neutron irradiation at elevated temperatures in beryllium. It is commonly accepted that helium bubbles in beryllium have a form of prism with hexagonal base laying on the basal plane of hcp lattice, which height is smaller than width (see, e.g. [30]). The side faces of the prism are assumed to be rectangle $(01\bar{1}0)$ facets. Recently Klimenkov et. al. [15] have confirmed the hexagonal form of bubbles and showed that height to width ratio varies with the irradiation temperature. However, the prism was often truncated by one of the pyramidal planes instead of prismatic.

Sometimes quite different shape of bubbles was reported after hydrogen implantation at elevated temperatures. Implantation with deuterium ions at 500 and 700 K led to formation of faceted bubbles elongated along [0001] direction [31]. The study of hydrogen-implanted beryllium at temperature below 50°C and then annealed for 15 min at 500–600°C has revealed the elongated shape along [0001] direction and truncated by pyramidal planes [16].

Our model calculations predict change of the faceting shape of bubble with increase of hydrogen surface coverage on its walls. The area of the most energetically favorable without hydrogen basal surface is decreasing until it disappears, while the area of the pyramidal type II plane is dominating at high hydrogen coverage until other facets disappear finally.

The discrepancy between our predictions of equilibrium shape of bubbles with the mentioned above experimental studies in beryllium can have the following reasons:

- Faceting under irradiation or implantation conditions is kinetic process which stages can be far from the expected equilibrium shape.
- Presumably the hydrogen coverage can be different on different beryllium surfaces. Moreover, the coverage of the surfaces probably depends on hydrogen gas pressure in the bubble or hydrogen production rate in the bulk.
- Temperature slightly changes the bubble morphology. For instance, bubbles with argon gas in hcp zinc after bombardment in heavy-ion accelerator at 300°C were bounded by basal, pyramidal type I and prismatic type I facets, while at lower temperature of 130°C the dominating facets were basal and prismatic type I [26].

5. Conclusions

The critical hydrogen coverage above which hydrogen molecular adsorption stops was found for all studied principal close-packed beryllium surfaces. At this coverage hydrogen prefers to be two-fold coordinated with beryllium atoms, i.e. occupies mainly the bridge site above the middle of Be-Be bond. Addition of hydrogen on pure beryllium surface results in a significant reduction of surface energy for all surfaces except prismatic type II, which energy changes only moderately. Above ca. 40% coverage a pyramidal type II plane was found to be the most energetically favorable, while the energies of other surfaces are noticeably higher. Relaxation of outermost atomic layers considerably differs from that found for pure beryllium surfaces. Interchanging stretching and compression between layers occurs for prismatic type I and pyramidal type I and II surfaces. An equilibrium shape of hydrogen covered bubbles in beryllium was studied using Gibbs-Wulff construction. The bubble without hydrogen is bounded by basal, prismatic type I and pyramidal type I planes with a small fraction of prismatic type II facet. Our model predicts drastic changes of faceting with hydrogen coverage so that at critical coverage all faces are pyramidal type II planes.

Acknowledgments

This work has been carried out within the framework of the EUROfusion Consortium and has received funding from the Euratom research and training programme 2014-2018 under grant agreement No 633053. The views and opinions expressed herein do not necessarily reflect those of the European Commission. Computational resources were provided by the IFERC Computational Simulation Centre (Rokkasho, Japan) and the Steinbuch Centre for Computing (Karlsruhe, Germany).

References

- [1] Y. Poitevin, L.V. Boccaccini, M. Zmitko, I. Ricapito, J.F. Salavy, E. Diegele, F. Gabriel, E. Magnani, H. Neuberger, R. Lasser, L. Guerrini, *Tritium breeder blankets design and technologies in Europe: Development status of ITER Test Blanket Modules, test & qualification strategy and roadmap towards DEMO*, Fusion Eng Des **85** (2010) 2340-2347.
- [2] P. Vladimirov, D. Bachurin, V. Borodin, V. Chakin, M. Ganchenkova, A. Fedorov, M. Klimenkov, I. Kupriyanov, A. Moeslang, M. Nakamichi, T. Shibayama, S. Van Til, M. Zmitko, *Current status of beryllium materials for fusion blanket applications*, Fusion Sci Technol **66** (2014) 28-37.
- [3] A. Antonelli, S.N. Khanna, P. Jena, *Interplanar relaxation at the (0001) surface of Be*, Surf Sci **289** (1993) L614-L616.
- [4] P.J. Feibelman, *Structure of H-covered Be(0001)*, Phys Rev B **48** (1993) 11270-11276.
- [5] M. Lazzeri, S. de Gironcoli, *Ab-initio dynamical properties of the Be(0001) surface*, Surf Sci **402** (1998) 715-718.
- [6] M. Lazzeri, S. de Gironcoli, *First-principles study of the thermal expansion of Be(10 $\bar{1}$ 0)*, Phys Rev B **65** (2002) 245402.
- [7] R. Stumpf, P.J. Feibelman, *Interaction of hydrogen with the Be(0001) surface*, Phys Rev B **51** (1995) 13748-13759.
- [8] S.J. Tang, H.T. Jeng, C.S. Hsue, Ismail, P.T. Sprunger, E.W. Plummer, *Surface state influence on the surface lattice structure in Be(10 $\bar{1}$ 0)*, Phys Rev B **77** (2008) 045405.
- [9] E. Wachowicz, A. Kiejna, *Bulk and surface properties of hexagonal-close-packed Be and Mg*, J Phys-Condens Mat **13** (2001) 10767-10776.
- [10] D.V. Bachurin, P.V. Vladimirov, *Ab initio study of hydrogen on beryllium surfaces*, Surf Sci **641** (2015) 198-203.
- [11] P. Hofmann, K. Pohl, R. Stumpf, E.W. Plummer, *Geometric structure of Be(10 $\bar{1}$ 0)*, Phys Rev B **53** (1996) 13715-13719.
- [12] Ismail, P. Hofmann, A.P. Baddorf, E.W. Plummer, *Thermal expansion at a metal surface: A study of Mg(0001) and Be(10 $\bar{1}$ 0)*, Phys Rev B **66** (2002) 245414.
- [13] Y.F. Li, Y. Yang, B. Sun, Y.H. Wei, P. Zhang, *Dissociation of hydrogen molecules on the clean and hydrogen-preadsorbed Be(0001) surface*, Phys Lett A **375** (2011) 2430-2436.

- [14] X.Z. Wu, R. Wang, S.F. Wang, *Generalized-stacking-fault energy and surface properties for HCP metals: A first-principles study*, Appl Surf Sci **256** (2010) 3409-3412.
- [15] M. Klimenkov, V. Chakin, A. Moeslang, R. Rolli, *TEM study of beryllium pebbles after neutron irradiation up to 3000 appm helium production*, J Nucl Mater **443** (2013) 409-416.
- [16] S.P. Vagin, P.V. Chakrov, B.D. Utkelbayev, L.A. Jacobson, R.D. Field, H. Kung, *Microstructural study of hydrogen-implanted beryllium*, J Nucl Mater **258** (1998) 719-723.
- [17] G. Kresse, J. Hafner, *Ab initio molecular-dynamics for liquid-metals*, Phys Rev B **47** (1993) 558-561.
- [18] G. Kresse, J. Furthmuller, *Efficient iterative schemes for ab initio total-energy calculations using a plane-wave basis set*, Phys Rev B **54** (1996) 11169-11186.
- [19] P.E. Blöchl, *Projector augmented-wave method*, Phys Rev B **50** (1994) 17953-17979.
- [20] G. Kresse, D. Joubert, *From ultrasoft pseudopotentials to the projector augmented-wave method*, Phys Rev B **59** (1999) 1758-1775.
- [21] J.P. Perdew, Y. Wang, *Accurate and simple analytic representation of the electron-gas correlation-energy*, Phys Rev B **45** (1992) 13244-13249.
- [22] Jmol: an open-source Java viewer for chemical structures in 3D. <http://www.jmol.org/>.
- [23] G. Wulff, *Zur Frage der Geschwindigkeit des Wachstums und der Auflösung der Krystallflächen*, Zeitschrift für Kristallographie und Mineralogie **34** (1901) 449-530.
- [24] A. Hashibon, J. Adler, G. Baum, S.G. Lipson, *Roughening transitions and surface tension in an hcp lattice with higher neighbor interactions*, Phys Rev B **58** (1998) 4120-4129.
- [25] P. Kaghazchi, T. Jacob, *Structure-activity relation of Re nanoparticles*, Phys Rev B **86** (2012) 085434.
- [26] W.A. Miller, G.J.C. Carpenter, G.A. Chadwick, *Anisotropy of interfacial free energy of some hexagonal close-packed metals*, Philos Mag **19** (1969) 305-319.
- [27] M. Touzani, M. Wortis, *Simple-model for the equilibrium shape of He-4 crystals*, Phys Rev B **36** (1987) 3598-3602.
- [28] R. Yu, P.K. Lam, *1st-Principles total-energy study of hydrogen adsorption on Be(0001)*, Phys Rev B **39** (1989) 5035-5040.
- [29] A. Allouche, *Density functional study of hydrogen adsorption on beryllium (0001)*, Phys Rev B **78** (2008) 085429.
- [30] V.P. Chakin, Z.Y. Ostrovsky, *Evolution of beryllium microstructure under high-dose neutron irradiation*, J Nucl Mater **307** (2002) 657-663.
- [31] V.N. Chernikov, V.K. Alimov, A.V. Markin, A.E. Gorodetsky, S.L. Kanashenko, A.P. Zakharov, I.B. Kupriyanov, *Gas-induced swelling of beryllium implanted with deuterium ions*, J Nucl Mater **233** (1996) 860-864.

2.4.5 Thermal Shock Performance Development of S-65 Grade Beryllium

B. Spilker, J. Linke, G. Pintsuk, M. Wirtz

Forschungszentrum Jülich GmbH, Institut für Energie- und Klimaforschung, 52425 Jülich, Germany

**Corresponding author: b.spilker@fz-juelich.de*

ITER, the experimental fusion reactor, will apply beryllium as plasma facing material (PFM) for the first wall (FW). The plasma compatibility, the oxygen getter capability, and the excellent thermal conductivity of beryllium make it well suited for this utilization. However, the low melting point (1287 °C) and the rather high erosion rate are serious drawbacks that limit the lifetime of FW panels armored by beryllium. The demanding environment in ITER puts enormous requirements onto the PFMs, e.g. withstanding high steady state and transient heat fluxes. Transient events like edge localized modes (ELMs) deposit up to 25 % of the plasma energy loss in the non divertor regions of present machines. Therefore, it remains essential to simulate and quantify the damages induced by ELMs on the beryllium armor tiles. In the last two decades, significant progress has been made in the development and improvement of hot pressed beryllium grades that can be applied as PFM. The beryllium grade S-65 represents the reference grade for the ITER FW application and is characterized by a low impurity content together with a high resistance against cyclic thermal loading. Within this work, S-65C and S-65E are subjected to ELM-like thermal loads with power densities in the range of 200 – 700 MWm⁻² and a pulse duration of 1 ms in the electron beam facility JUDITH 1. The samples were exposed to 100 thermal loads each, with a base temperature at RT. The cracking threshold for S-65C was determined to be between 400 MWm⁻² and 500 MWm⁻², while it rises to be between 500 MWm⁻² and 600 MWm⁻² for S-65E. For both materials, no damage was detected up to the absorbed power density of 200 MWm⁻². Once the cracking threshold is exceeded, both materials exhibit small and isolated cracks distributed over the loaded surface area, in addition with significant roughening that was quantified using the arithmetic mean roughness parameter. For the entire range of absorbed power densities, the induced surface roughness is slightly higher in the case of S-65E. In contrast, the amount of thermally induced cracks is greater for S-65C. Consequently, we conclude that S-65E demonstrates a superior ductility over S-65C at RT, which is accompanied by a lower yield strength. This slight difference in the damage behavior might be related to the decrease in average grain size of the loaded surface from 14 µm (S-65C) to 11 µm (S-65E). The higher cracking threshold and the lower amount of thermally induced cracks indicate that S-65E exhibits an improved thermal shock performance over S-65C and may serve as reference grade for future thermal shock investigations on beryllium for the ITER FW application.

Keywords: ITER, first wall, beryllium, ELMs, thermally induced damage

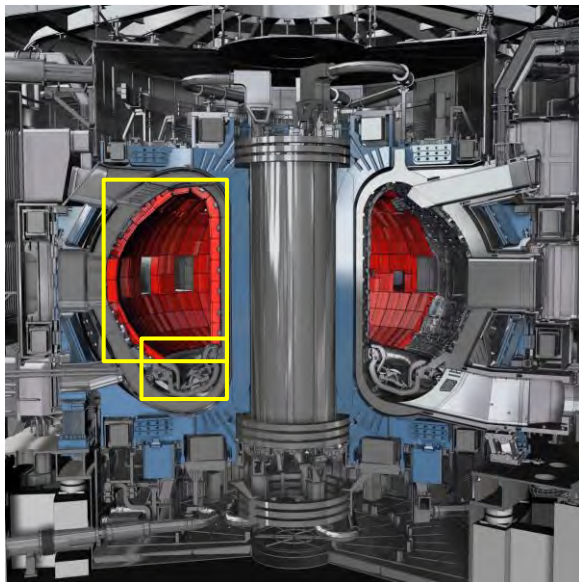
Thermal Shock Performance Development of S-65 Grade Beryllium

10. September 2015 B. Spilker, J. Linke, G. Pintsuk, M. Wirtz

Forschungszentrum Jülich GmbH
Institut für Energie- und Klimaforschung (IEK-2)

12th International Workshop on Beryllium Technology | 10-11 September 2015
International Convention Center Jeju | South Korea

Introduction – ITER



Fusion power output
500 MW

Major plasma radius
6.2 m

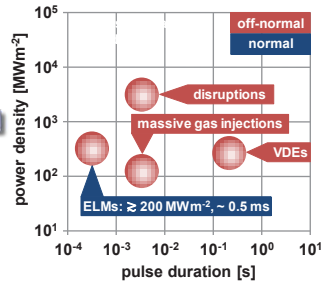
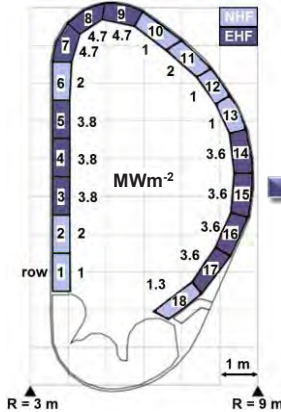
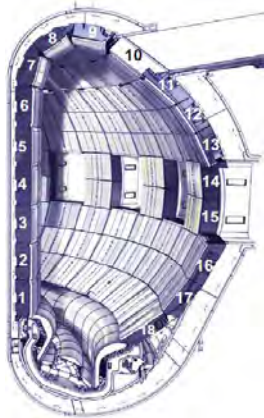
Average plasma temp.
~ 13 keV

Pulse duration
~ 400 s

Plasma facing materials

- Beryllium (First wall, ~ 620 m²)
- Tungsten (Divertor)

Introduction – Power loads to the FW



ITER first wall (FW):
Be armour tiles

Expected maximum
steady state power loads
per row

Additional transient
power loads (thermal
shocks, TS)

M. Kočan et al., J. Nucl. Mater. (2015), <http://dx.doi.org/10.1016/j.jnucmat.2014.11.130>
A.R. Raffray et al., Nucl. Fusion 54 (2014), 033004 (18pp)
A. Loarte et al., Phys. Scr. T128 (2007), 222-228

Benjamin Spilker 12th International Workshop on Beryllium Technology | 10-11 September 2015 | Jeju Island | South Korea 2

Experimental – TS testing of Be in Jülich



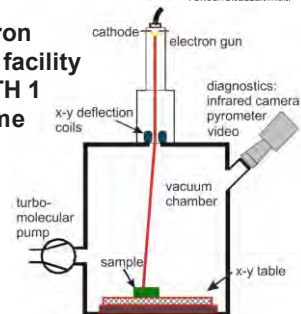
ELM like heat loading

- JUDITH 1
 - Threshold determination
 - Surface finish influence
 - Cracking behavior
- JUDITH 2
 - High pulse number investigations
 - Threshold development
- 1064 nm Nd:YAG laser
 - Comparison to e-beam experiments (e⁻ penetration depth influence)

MGI like heat loading

- JUDITH 1
 - Influence of the pulse duration

Electron beam facility JUDITH 1 scheme

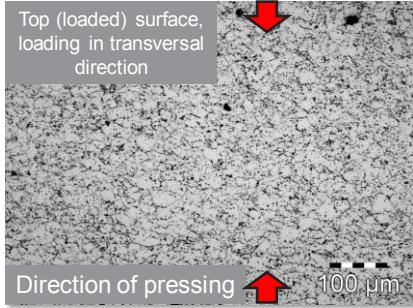


Electron beam parameters

- Max. power: 60 kW
- Max. acc. voltage: 150 kV
- Pulse duration: ≥ 1 ms
- Beam diameter: ~ 1 mm
- Sweeping freq.: ≤ 100 kHz
- Beam is swept over loaded area
- Capable of handling toxic/radioactive materials

Benjamin Spilker 12th International Workshop on Beryllium Technology | 10-11 September 2015 | Jeju Island | South Korea 3

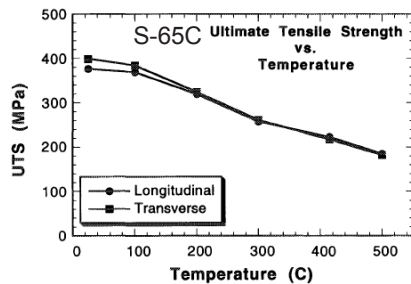
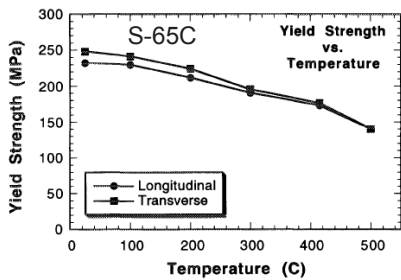
Experimental – Beryllium S-65 rev. E



S-65E Beryllium (Materion Brush Inc.)

- Vacuum hot pressed
- Density = 99.8 % theor.
- Average grain size ~ 13 µm (circular equivalent diameter)
- BeO content = 0.6 wt%
- Mech. strength comparable to S-65C

S.H. Goods et al., Proceedings of the third IEA international workshop on beryllium technology for fusion (1998), 39-52



Benjamin Spilker 12th International Workshop on Beryllium Technology | 10-11 September 2015 | Jeju Island | South Korea

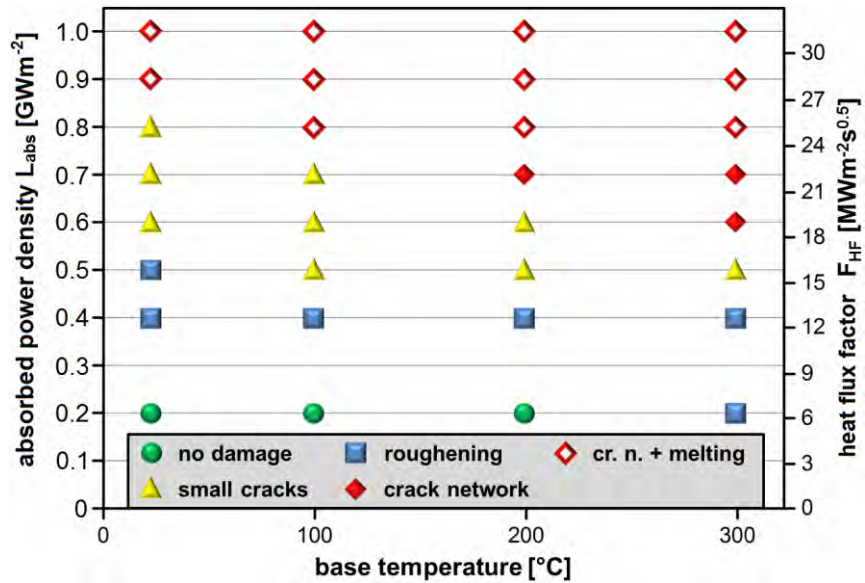
4

Results – Damage mapping



Pulse length = 1 ms, 100 pulses for each data point

$$F_{HF} = L_{abs} \times t^{0.5}$$



Benjamin Spilker 12th International Workshop on Beryllium Technology | 10-11 September 2015 | Jeju Island | South Korea

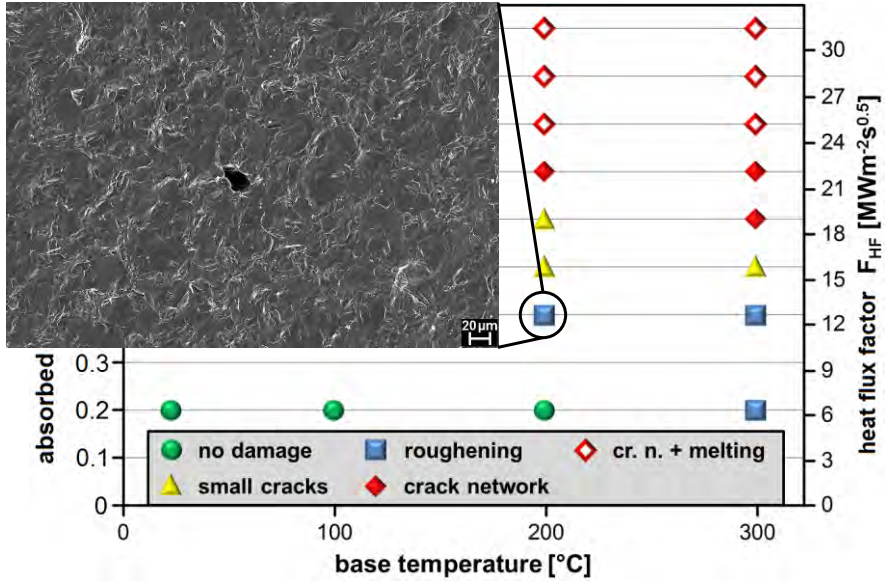
5

Results – Damage mapping



Pulse length = 1 ms, 100 pulses for each data point

$$F_{HF} = L_{abs} \times t^{0.5}$$



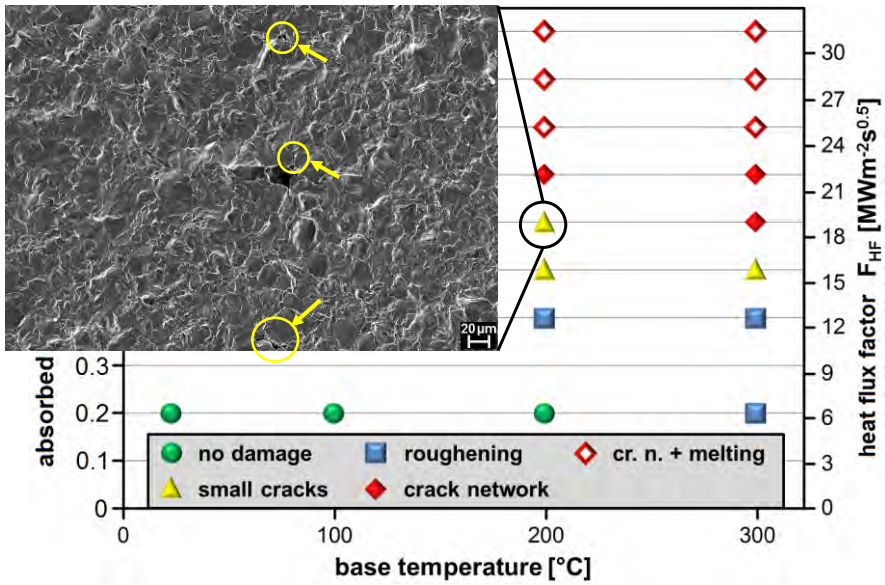
Benjamin Spilker 12th International Workshop on Beryllium Technology | 10-11 September 2015 | Jeju Island | South Korea 5

Results – Damage mapping



Pulse length = 1 ms, 100 pulses for each data point

$$F_{HF} = L_{abs} \times t^{0.5}$$



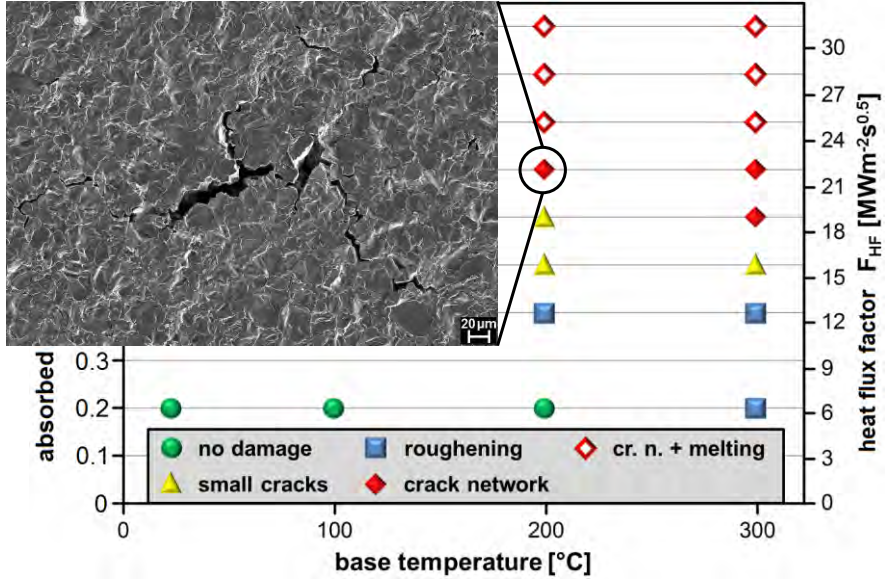
Benjamin Spilker 12th International Workshop on Beryllium Technology | 10-11 September 2015 | Jeju Island | South Korea 5

Results – Damage mapping



Pulse length = 1 ms, 100 pulses for each data point

$$F_{HF} = L_{abs} \times t^{0.5}$$



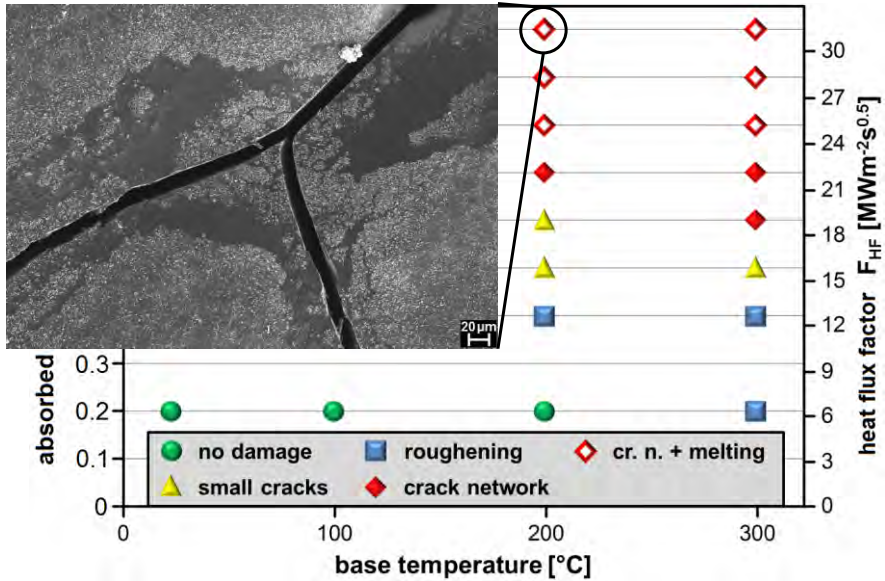
Benjamin Spilker 12th International Workshop on Beryllium Technology | 10-11 September 2015 | Jeju Island | South Korea 5

Results – Damage mapping



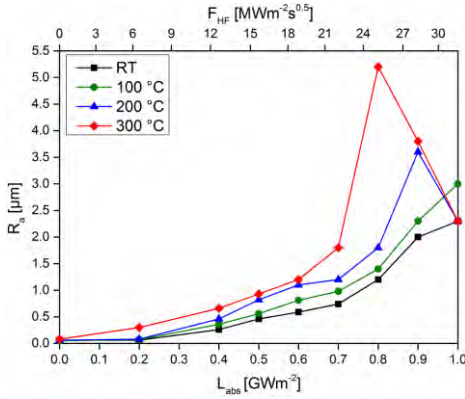
Pulse length = 1 ms, 100 pulses for each data point

$$F_{HF} = L_{abs} \times t^{0.5}$$



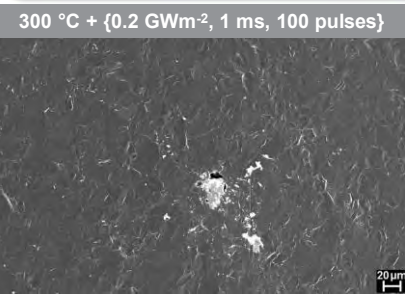
Benjamin Spilker 12th International Workshop on Beryllium Technology | 10-11 September 2015 | Jeju Island | South Korea 5

Results – Temperature dependent R_a



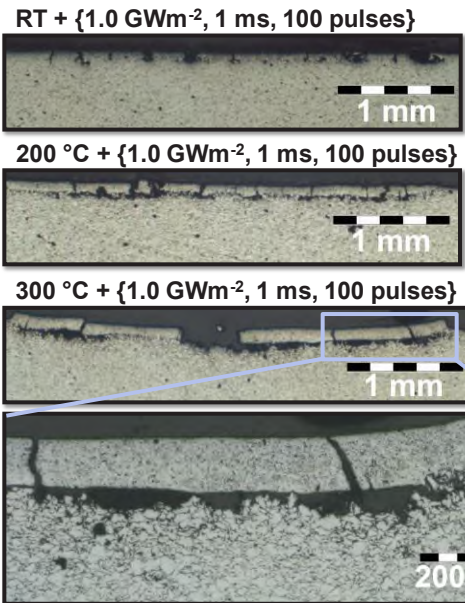
- Decreasing yield strength leads to more strongly pronounced roughening for higher base temperatures
- Decreasing tensile strength leads to a crack formation at lower L_{abs} for higher base temperatures

Damage threshold drops below $F_{HF} \sim 6 \text{ MWm}^{-2}\text{s}^{0.5}$ @ 300 °C



Member of the Helmholtz Association

Results – Cross sections



Cracks and lost grains (preparation) down to $\sim 100 \mu\text{m}$

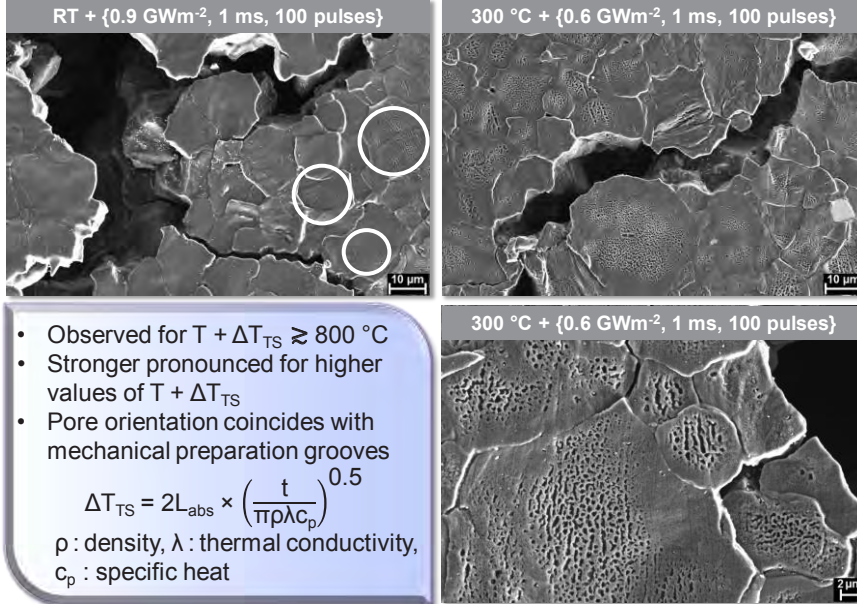
Formation of molten/solidified "plates" with poor cohesion to bulk

Loss of plate during preparation; not seen in SEM

Black area under the plates: Either lost material during careful preparation or cavity formed during TS loading

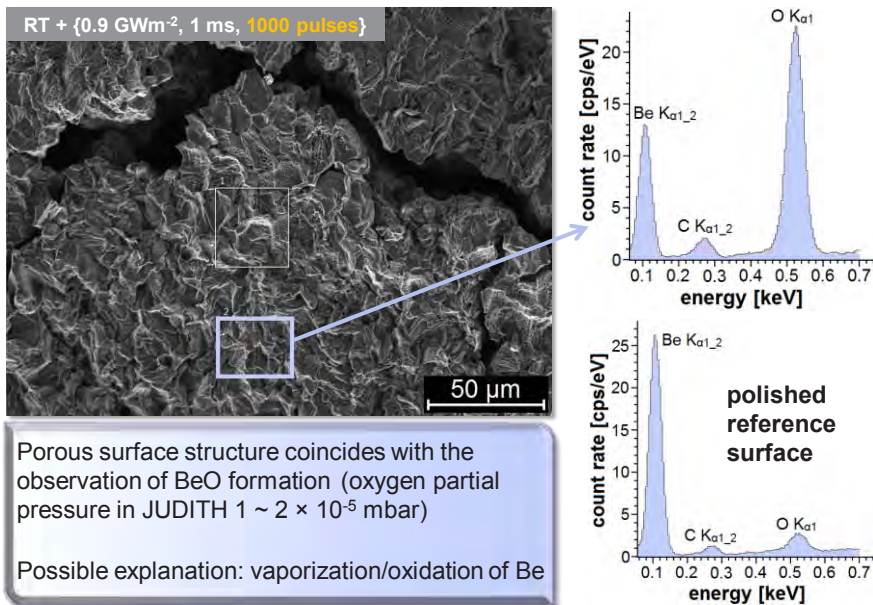
Member of the Helmholtz Association

Results – Porous surface structure



Benjamin Spilker 12th International Workshop on Beryllium Technology | 10-11 September 2015 | Jeju Island | South Korea 8

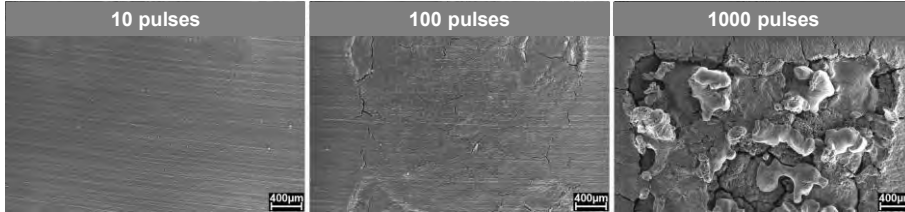
Results – Porous surface structure



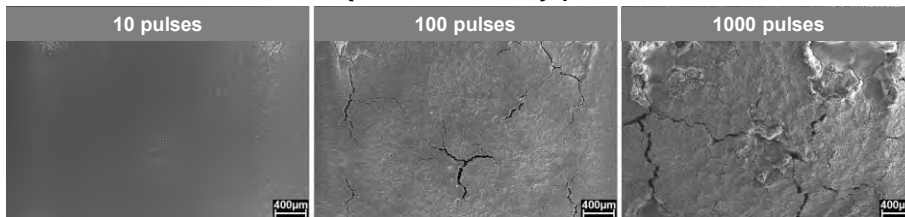
Benjamin Spilker 12th International Workshop on Beryllium Technology | 10-11 September 2015 | Jeju Island | South Korea 9

Results – Surface finish influence

RT + {0.9 GWm⁻², 1 ms}, surface ground with SiC paper (particle diameter 82 μm)



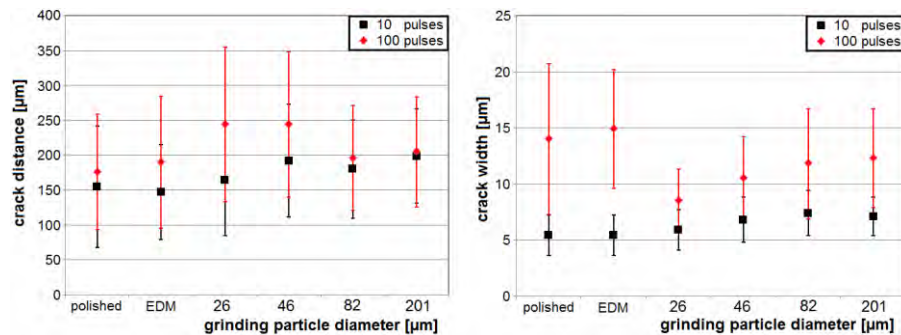
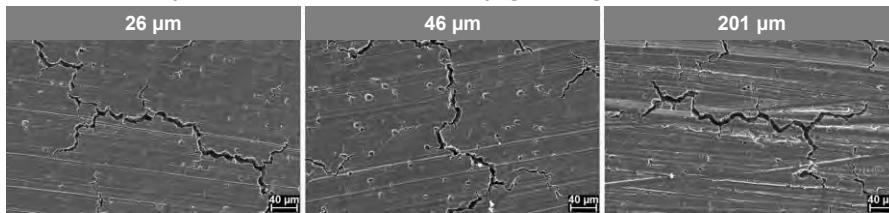
RT + {0.9 GWm⁻², 1 ms}, polished



Member of the Helmholtz Association

Results – Surface finish influence

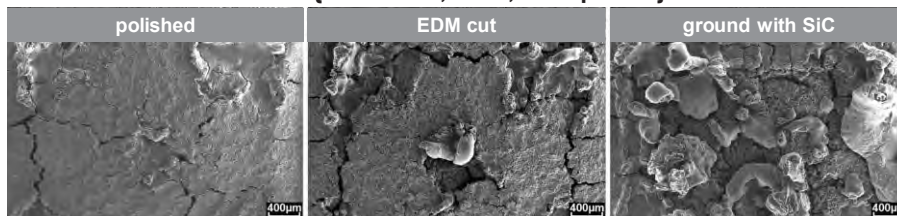
RT + {0.9 GWm⁻², 1 ms, 10 pulses}, grinding particle diameter:



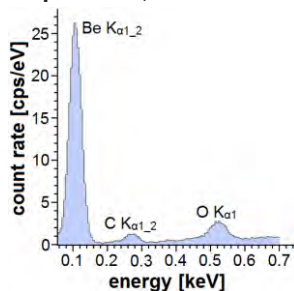
Member of the Helmholtz Association

Results – Surface finish influence

RT + {0.9 GWm⁻², 1 ms, 1000 pulses}

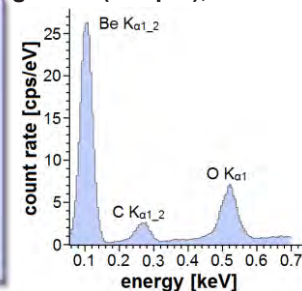


polished, unloaded



- Grinding process increases surface / amount of Be available for oxidation
- Larger surface / more BeO present accelerates crucial destruction of Be

ground (201 µm), unloaded



Member of the Helmholtz Association

Summary

- TS loading of Be yields valuable thresholds and results for the operation of ITER
- The decreasing yield strength and tensile strength with increasing temperature exacerbate the plastic deformation and crack formation of Be
- TS loading with $T + \Delta T_{TS} \gtrsim T_{Be_melt}$ leads to the formation of molten plates with a poor cohesion to the bulk
- TS loading with $T + \Delta T_{TS} \gtrsim 800$ °C leads to the formation of a porous surface structure that can influence surface sensitive processes (erosion / absorption / retention)
- The cracking behavior of Be is not influenced by the surface finish
- After 1000 pulses, a crucial destruction of the loaded area was observed for all ground surfaces (linked to the enlarged surface area / BeO content)

Member of the Helmholtz Association

2.5 Technical session 3: Composition Control and Characterization

2.5.1 Effect of impurity and grain size on mechanical properties and reactivity of beryllium

J-H. Kim, Y. Akatsu, M. Nakamichi

Sector of Fusion Research and Development, Japan Atomic Energy Agency, JAEA,

2-166 Omotedate, Rokkasho-mura, Kamikita-gun, Aomori, 039-3212, Japan

E-mail: kim.jaehwan@jaea.go.jp

Abstract

Great interests on not only beryllium but beryllium intermetallic compound have been increasing as a promising neutron multiplier material in a fusion power reactor. In this study, plasma-sintered beryllium with different grain size and impurity was fabricated and then examined as evaluations of mechanical property and reactivity.

1. Introduction

A fusion power reactor requires functional materials such as a tritium breeder and a neutron multiplier, planning to be loaded as a pebble type in a blanket in water cooled solid breeder concept to produce tritium as a fuel and multiply neutron, respectively. In specific, beryllium materials, such as beryllium, beryllium intermetallic compounds have been extensively studied as the neutron multiplier on a variety of aspects, mechanical properties, reactivity, irradiation properties, synthesis methods and so on. For granulation of Be metal, rotating electrode method (or Fluoride reduction process) has been considered as promising method. But, degradation of He (or Tritium) release as well as reactivity may be occurred due to large grain (500~1000 μ m)

In this study, the effect of grain size and impurity on mechanical property and reactivity at 1073, 1273 and 1473 K in dry air and Ar gas with 1 % H₂O in the plasma-sintered beryllium was investigated.

2. Experimental

Beryllium specimens used in this study were prepared to compare their reactivity. For comparison of the reactivity, two different beryllium grades, S65C grade (NGK Co. Ltd.) and S65E grade (Materion Co. Ltd.), were prepared by hot pressing method. In parallel to two beryllium specimens, the plasma-sintered beryllium (PS-Be) was fabricated. In parallel to this, four beryllium specimens fabricated by starting powders with different size were prepared to understand the grain size effect on mechanical and reactivity of a plasma-sintered beryllium. For clarity for impurity, all beryllium powders with

purity of 99.5% (Materion, USA) were sintered using plasma sintering method under the identical conditions [1]. The disc-type of plasma-sintered beryllium was cut to $3.0 \times 3.0 \times 5.0 \text{ mm}^3$ and polished using polishing disc with up to #2400 SiC paper for the measurements. For evaluation of sinterability, sintering density was measured by He pycno-meter and water immersion. SEM and optical microscopic observation were carried out to confirm grain size and surface morphology. To understand grain size and impurity effect on the reactivity of the beryllium specimens, thermal-gravimetric analysis with gas chromatography was used.

3. Results and discussion

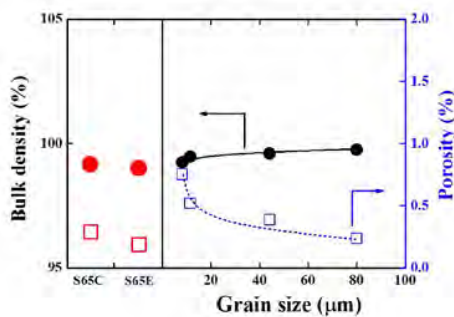


Fig.1 Density and porosity

Fig.1 shows density and porosity of each beryllium specimens, indicating that the PS-Be was fabricated with high sintering density and low fraction of open pore. In addition, the surface observation result clearly clarified that the plasma sintering led to synthesis of the beryllium with not only smaller grain size but less impurity.

As results of reactivity, under dry air, oxidation behavior is mainly associated with grain size and oxygen ions move along grain boundary. Therefore, the smaller grain size it has, the larger weight gain it has as shown in Fig.2. However, a smaller increase in weight is observed when PS-Be20, with small grain size, is heated in the presence of Ar and 1% H₂O at 1273 K (Fig.3). This is in

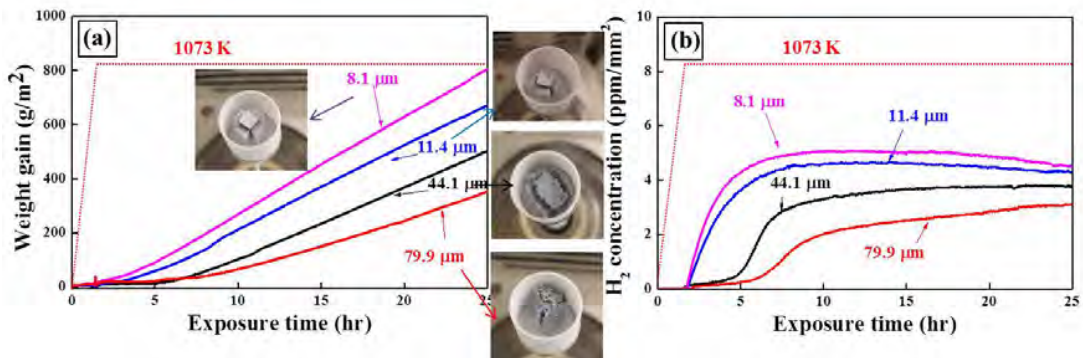


Fig.2 Weight gain and H₂ concentration at 1073 K in 1%H₂O/Ar

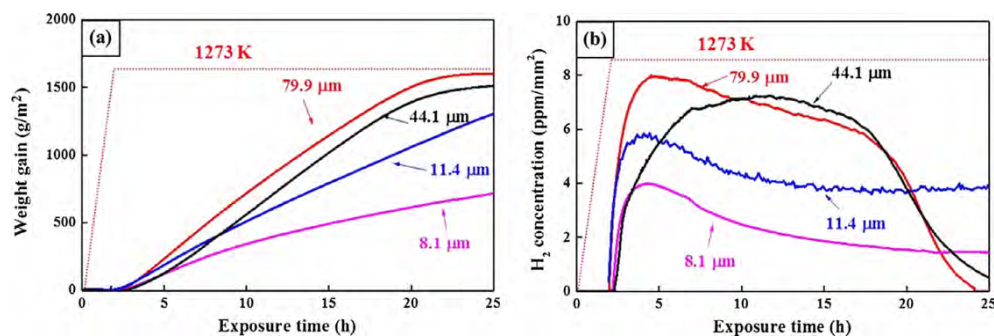


Fig.3 Weight gain and H₂ concentration at 1273 K in 1%H₂O/Ar

contrast to the observation made when PS-Be samples are oxidized in dry air at 1273 K and in Ar gas with 1% H₂O at 1073 K. This is attributed to the decomposition of H₂O to OH and H⁺, which results in the formation of the unstable Be(OH)₂, and consequently cracks. Oxidation through the cracks occurs at a catastrophic rate and is not limited to grain boundaries, but impacts the bulk. Moreover, outward diffusion of Be²⁺ ions through the oxide film accompanied with the inward proton diffusion facilitates the formation of cracks.

Additionally, chemically adsorbed protons on the surface can facilitate oxidation by rupturing the protective oxide film. Thus when catastrophic oxidation occurs through the bulk of Be at 1273 K in 1% H₂O, grain boundaries appear to hinder oxygen diffusion.

4. Conclusion

(1) As results of comparative examination, PS-Be was fabricated with high sintering density, low fraction of open pores and less impurities.

(2) Regarding the reactivity, it was concluded that PS-Be exhibited larger weight gain as well as H₂ gas generation during oxidation at 1073 K and during the initial stages of oxidation at 1273 K. With regards of grain size effect on reactivity, oxidation at 1273 K in dry air reveals that the lower grain sizes in PS-Be₂₀ and PS-Be₄₅ permit the penetration of oxygen deeper into the layers of Be. With a decrease in the grain size, oxidative stress concentrated at the boundaries of grain leads to generation of cracks. Therefore, it is inferred that a larger grain size in PS-Be offers a better resistance against oxidation.

(3) Reactivity of Be with H₂O at 1073 K follows a trend that is similar to that observed for its oxidation in dry air, i.e., a smaller grain size results in greater weight gain and higher H₂ generation. Reactivity of Be with H₂O at a higher temperature, 1273 K, results in catastrophic oxidation with increase of weight gain and H₂ generation, since outward diffusion of Be²⁺ ion through the oxide film is accompanied by an inward diffusion of proton and facilitates the formation of cracks. At lower temperature (<1273 K), the grain boundary protects underlying Be from being oxidized; however, catastrophic bulk oxidation occurs at 1273 K in Ar with 1% H₂O as a rate determining reaction. In conclusion, the smaller grain size Be has, the lower weight gain and H₂ concentration it shows.

Reference

[1] Jae-Hwan Kim, Masaru Nakamichi, Journal of nuclear materials, 453 (2014) 22-26.

2.5.2 Microstructural evolution and adhesion of thin coatings in the Be-C-O and Be-W-O systems under annealing

R. Mateus^{1,*}, C. Porosnicu², C.P. Lungu², E. Alves¹

¹Instituto de Plasmas e Fusão Nuclear, Instituto Superior Técnico, Universidade de Lisboa, Av. Rovisco Pais, 1049-001, Lisboa, Portugal

²National Institute for Lasers, Plasma and Radiation Physics, Bucharest 077125, Romania

Abstract

During reactor operation chemical composition of exposed surfaces will evolve over time due to erosion, re-deposition and heat-load events. The main materials considered for plasma facing components (PFC) in the reactor chamber will be beryllium and tungsten. From the present work we conclude that this option will highly mitigate the re-emission of co-deposits to the main plasma compared with previous carbon wall machines. The experiment was carried out by analysing Be, C and W layers deposited on pure Be, graphite and W plates after annealing in vacuum up to 1073 K. In the Be-C-O system, the formation of beryllium carbide and beryllium oxide is enhanced at temperatures higher than 873 K, leading to strong delamination of the films. In opposition, the formation of intermetallics in the Be-W-O system mitigates the occurrence of these events and recovers the delaminated zones.

*Corresponding author: rmateus@ipfn.ist.utl.pt

1. Introduction

In ITER, beryllium (Be) will cover the primary wall, tungsten (W) will be the only plasma facing material at the divertor and carbon (C) was definitively removed from the selected list of materials for plasma facing components (PFCs) due to the imposed fuel retention limitations [1]. Nevertheless, carbon facing components were foreseen to be used at the strike point plates in ITER divertor [1] and obviously, it will be always present as contaminant. Therefore, the implications of C reactivity under reactor operation should remain under investigation and compared to those ones of W.

During reactor operation, the exposed PFC surfaces will become eroded in some preferential locations of the vessel walls, and dust will be guided by the magnetic field to other areas [1,2]. Be eroded from the main wall will be preferentially deposited at the divertor, while impurities eroded from the W

divertor will remain deposited nearby the divertor region. In full metallic wall designs, oxygen (O) will act as a natural contaminant (mainly for Be at high temperature), and therefore, mixed Be-W-O compounds will evolve spontaneously as superficial deposits in PFCs under irradiation and annealing. If the presence of C is significant, and due to the affinity of O to react with Be [2], the additional study of the Be-C-O system assumes particular importance.

Previous experiments signaled the flaking of deposits in tokamak walls [3]. In mixed deposited layers, the flaking mechanism depends of microstructural changes imposed to the deposits under annealing, while the formed compounds present distinct crystallographic structures and thermal expansion coefficients. Two intermetallic compounds are identified in the Be-W diagram up to 1073 K: Be_2W and Be_{12}W [4]. Pure Be, Be_2W and beryllium oxide (BeO) have hexagonal structures with distinct lattice parameters, Be_{12}W is tetragonal, pure W has a body-centered cubic (BCC) material and finally, beryllium carbide (Be_2C) has an anti-fluorite cubic structure [4,5]. Besides the lattice structure, the toughness of the deposits also depends of the nature of the chemical bonding itself. Covalent materials such as metallic carbides are very hard and fragile, ionic compounds like BeO are stable and inert, and intermetallic compounds lead to good cohesion and mechanical strength [6]. Therefore, we could expect a better toughness of the materials formed within the Be-W-O system relatively to those ones obtained from Be-C-O.

The emission of dust will result in radiation losses and it is detrimental to the plasma performance, especially when high-Z materials are involved [1,2]. In order to predict the influence of compound formation in this process, in the present work we followed the microstructural changes observed from pure Be, C and W films deposited on Be, graphite and W plates under annealing up to 1073 K and compared the corresponding delamination behaviour in each set of samples.

2. Experiment

The investigation of the Be-C-O system was carried out with two sets of samples: C films with thicknesses close to 100 nm were evaporated on polished Be plates, and: Be plates with thicknesses of about 150 nm were deposited afterwards on polished graphite plates. For the study of the two Be-W reverse systems, W and Be films were deposited on Be and W polished plates, respectively. In this case, the films presented nominal thicknesses of 100 and 200 nm in order to evaluate the influence of this parameter in the final delamination process. All the Be and W films were prepared using the thermionic vacuum arc (TVA) method at the INFLPR institute, in Romania [7]. The samples were annealed with a base pressure of 1×10^{-7} mbar up to 1073 K and analysed afterwards by Rutherford backscattering (RBS) for elemental depth profiling, by scanning electron microscopy (SEM) using both secondary (SE) and backscattered electron (BSE) imaging as well as energy-dispersive X-ray spectroscopy (EDS) for topographic inspection and local chemical analysis, and by glancing X-ray diffraction (XRD) involving a geometry with the purpose to enhance the analysis of the superficial layers and a X-ray Cu-K α 1 source.

3. Results and discussion

3.1 Be-C-O system

Carbon films deposited on beryllium plates

The SEM images of Fig. 1 follow the chemical and structural modifications observed in the first batch of samples. The only modification induced by annealing over 90 min at temperatures up to 773 K is the buckling of the C layers (Fig. 1(a)). At 873 K a reaction front becomes apparent along the edge of the blisters (Fig. 1(b)), and by comparing the corresponding SE and BSE images at this temperature we conclude that O is absent of the flat zones of the film, but not on the blisters [8]. The result can be explained by the higher volume of the hexagonal unit-cell of BeO. The oxide phase needs free space to growth and find it in the blistered zone. After annealing at temperatures higher than 873 K the reaction zone becomes spread out over the entire blisters as in Fig. 1(c) and 1(d), and a discontinuous precipitation structure including the distinct Be₂C and BeO phases leads to cracking and to the delamination of the blisters from the films. This is confirmed by BSE analysis and elemental EDS mapping [8]. From both XRD and RBS spectra (not included on the document) it becomes evident that the formation of the carbide and oxide compounds at the surface is highly enhanced at 873 K [8].

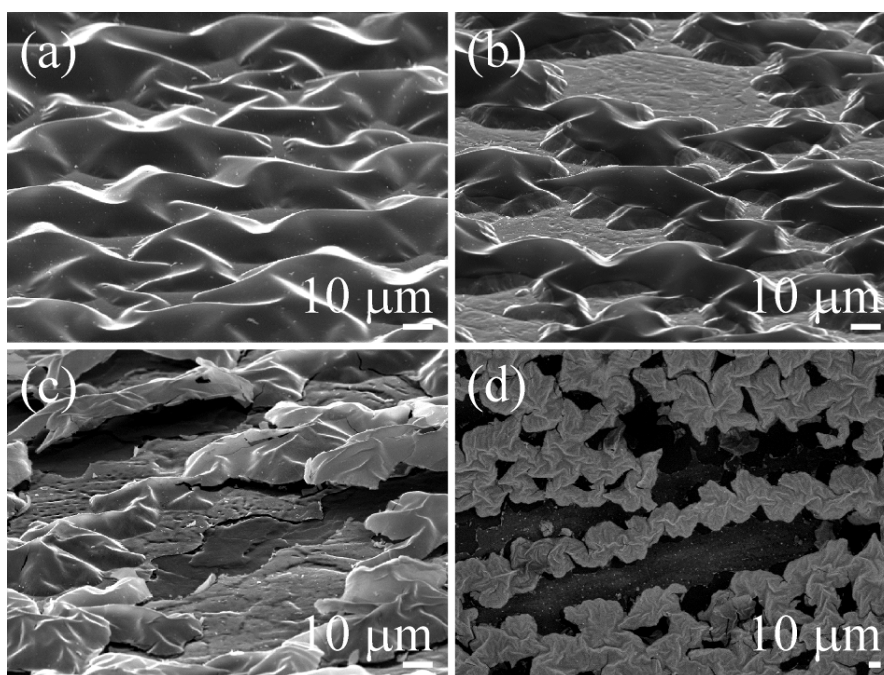


Fig. 1. SE images (tilted views) of C films deposited on Be plates after annealing over 90 min at 773 (a), 873 (b) and 973 K (c), and corresponding BSE image (top view) at 1073 K (d).

Beryllium films deposited on graphite plates

The results obtained from the Be films deposited on graphite are typically the same revealed from the reverse system (C deposited on Be). Due to the mechanical strength of the Be films, the blistering effect is not observed at this time. Anyway, equivalent cracks and delamination events are observed after

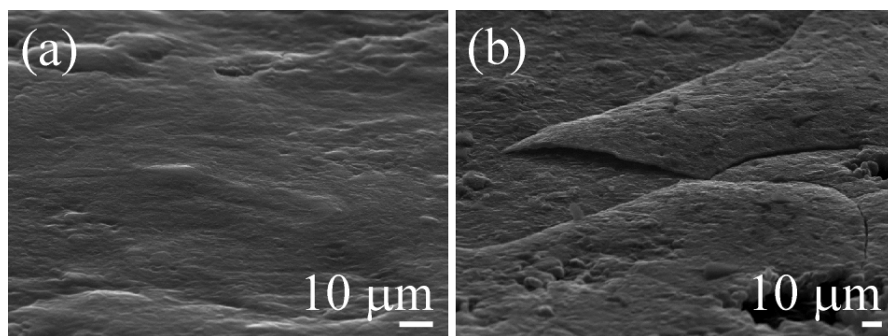


Fig. 2. SE images (tilted view) of an as-deposited Be film grown on a graphite plate (a) and corresponding crack events after annealing at 973 K during 90 min (b).

annealing at 973 K, as in Fig. 2b. Once again, the formation of the carbide and oxide phases is enhanced at 873 K, where BeO evolves easily at the surface, leading the carbide component to the deeper regions in the films. These assumptions are easily visualized by the Be₂C and BeO patterns in the diffractograms at 35.8° or at 38.5 and 41.5°, respectively (Fig. 3a), and by the increment of the O yield and recoil of the C yield towards the low energy region in the RBS spectra from 973 to 1073 K. In the RBS spectra, the energies corresponding to the presence of Be, C and O at the superficial layer are signaled by the vertical arrows (Fig. 3b) [8].

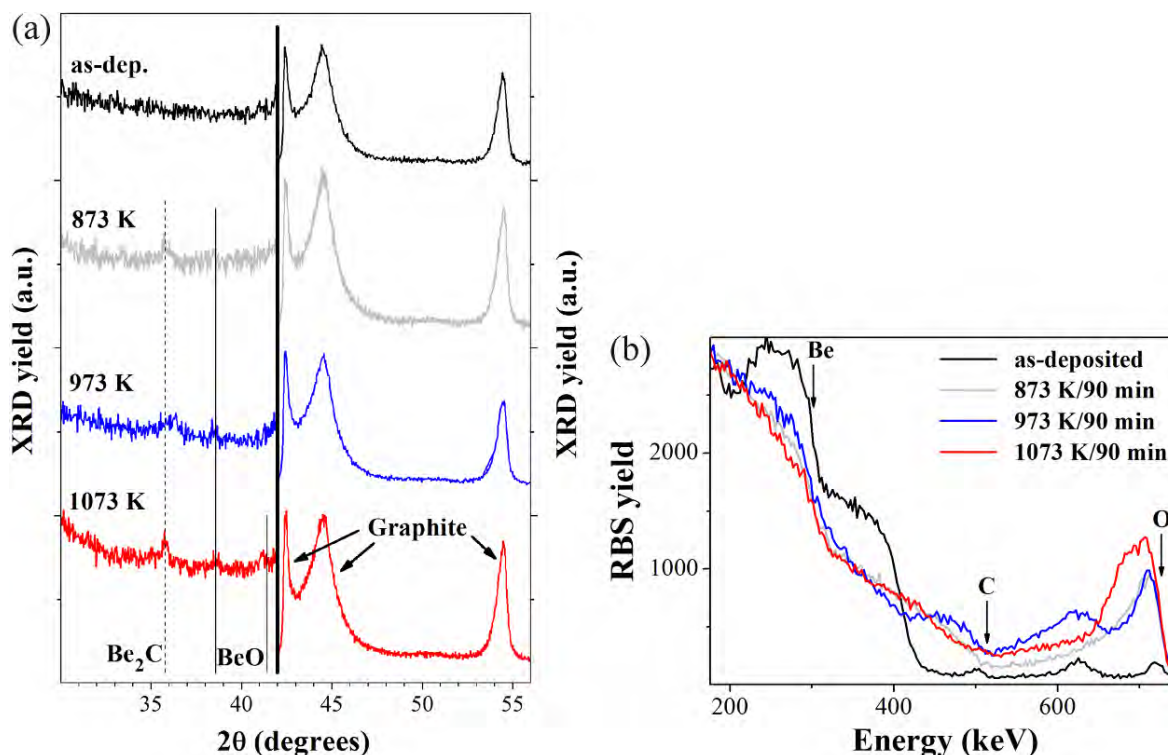


Fig. 3. Study of Be films deposited on graphite: XRD (a) and respective RBS spectra obtained from 2.0 MeV ⁴He⁺ beams (b).

3.2 Be-W-O system

Tungsten films deposited on beryllium plates

The diffractograms and RBS spectra of Fig. 4a were collected from the 100 nm W films deposited on Be plates after the annealing procedure with periods of 10 h. From the analysis of the thicker W films (with 200 nm) it is observed a time delay in the Be-W intermixing and reactivity. Nevertheless, the final conclusions are the same. Any significant reaction occurs up to 973 K. Afterwards, the Be_{12}W pattern is easily identified at 17.0, 24.3 and 34.5° and this is the principal intermetallic composition formed at 1073 K. Weaker peaks relative to the formation of Be_2W are also identified from the pattern at 39.5 and 43.5° and the BeO content is identified at 41.5 and 44.1°. At the end of the annealing procedure, almost the W reacted with Be, as it is observed from the decrease of the W peak at 40.3°. The XRD data are confirmed by ion beam analysis. The RBS spectra of the as-deposited sample and of the sample annealed at 973 K are quite similar, while the Be-W intermixing is not significant in this temperature range. At 1073 K, a strong Be-W intermixing is observed. As in the examples within the Be-C-O system, it is also observed at this temperature a firm diffusion of pure Be from the bulk towards the surface, were Be oxidizes. Once again, the mechanism is identified by the increment of the O yield and by the recoil of the W yield in the RBS spectra from 973 to 1073 K (Fig. 4b). From SEM imaging and EDS analysis, and in opposition with the results of the Be-C-O system, we confirm the absence of a delamination behaviour up to 1073 K.

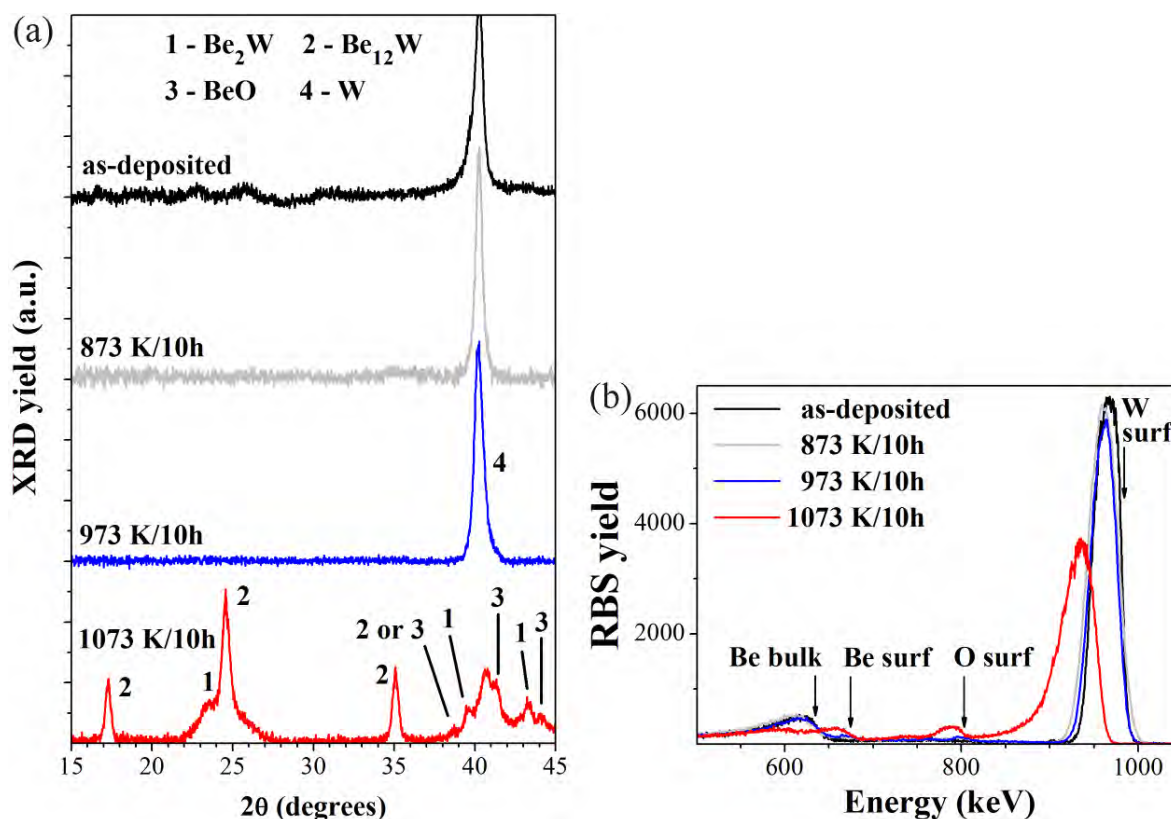


Fig. 4. Study of W films (100 nm) deposited on Be: XRD (a) and respective RBS spectra obtained from 1.0 MeV H^+ beams (b).

Moreover, a similar and homogeneous depth composition of the films is observed after annealing at this temperature. In resume, the present data evidence that metallic bonding and the growth of Be-W alloys prevents the occurrence of delamination events.

Beryllium films deposited on tungsten plates

The SEM images from Fig. 5a to 5c relates to the deposition of thicker Be films on W (200 nm Be films), where a slight delamination mechanism becomes more evident at a narrow temperature window. In opposition to the reverse system (W deposition on Be), the lower mechanical strength of Be relatively to W promotes the formation of some few cavities on the films after annealing at 873 and 973 K, and sometimes a slight and complete limited removal of the deposited Be layer is also observed, as it in the example of Fig. 5b, where the flat W bulk becomes visible. Anyway, and due to the high diffusion of metallic ions, the same image also evidences the beginning of the recovery of the

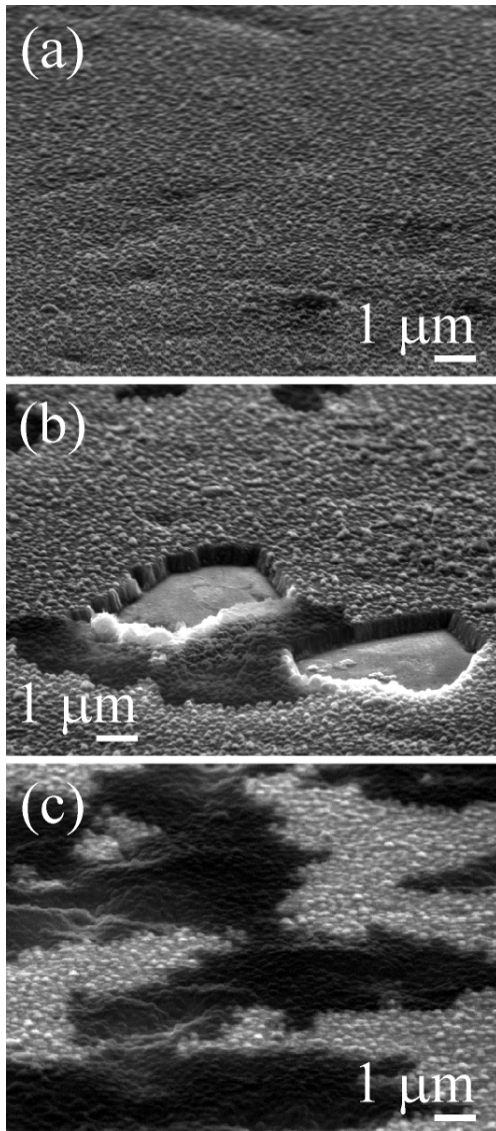


Fig. 5. SE images (tilted views) of delaminated zones in Be films deposited on W plates after annealing over 4h at 873 (a), 973 (b) and 1073 K (c).

delaminated zone at the edge of this area, which is visible by the formation of the dark component. After annealing at 1073 K over 4 h all the recovery of cavities and delaminated zones is complete, as it visible in Fig. 5c. The mechanism is confirmed by comparing the corresponding SE and BSE images at 973 and 1073 K, while a homogeneous W content is observed along the recovered areas [9].

The Be-W intermixing and reactivity at higher temperatures is also confirmed by the complementary chemical analyses. From the XRD diffractograms in Fig. 6a we identify the formation of the same compositions previously observed in the reverse system (W deposited on Be). In the RBS spectra of Fig. 6b it is visible the W yield relative to the presence of W in the bulk and the growth of the diffused W yield toward the surface at higher temperatures. Once again, the (diffused) W yield recoils at 1073 K due to the increment of O (and BeO) at the surface, as it confirmed by RBS by using incident proton beams (spectra not included in Fig. 6).

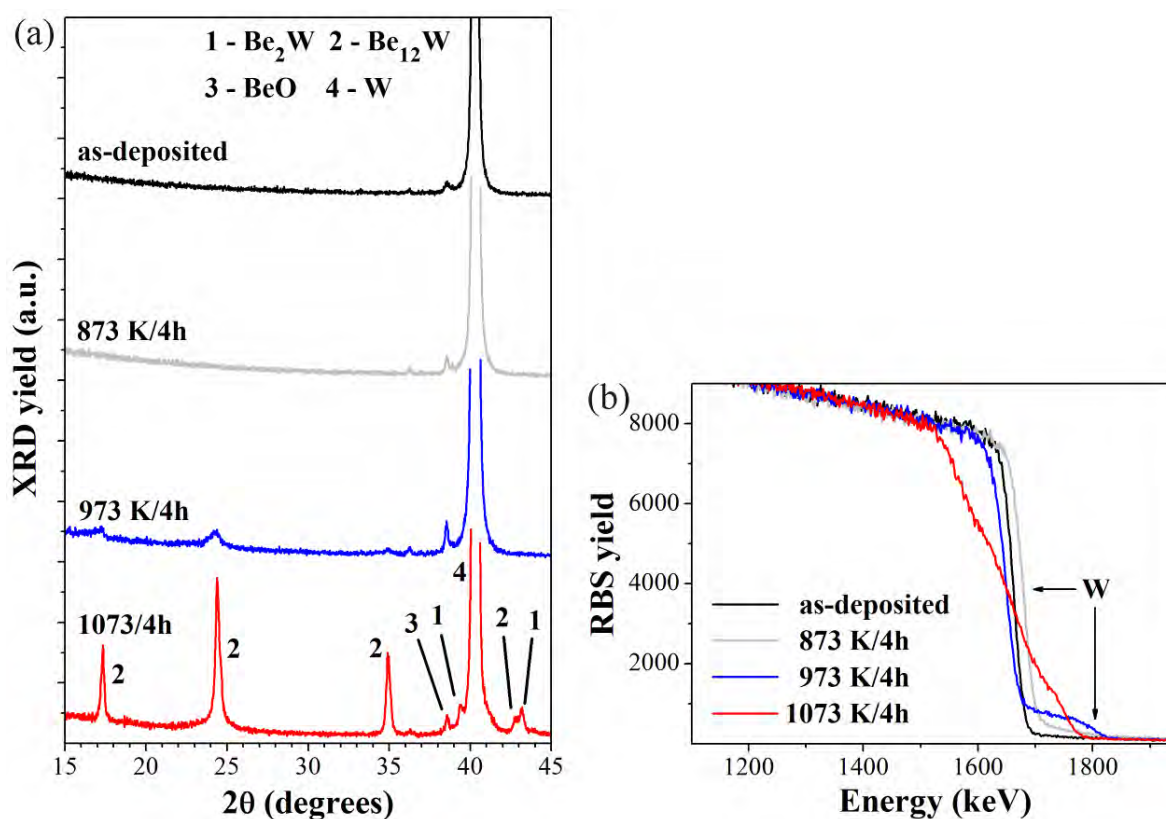


Fig. 6. Study of Be films (100 nm) deposited on W: XRD (a) and respective RBS spectra obtained from 2.0 MeV $^4\text{He}^+$ beams (b).

4. Conclusions

The results of the present work point that the chemical reactivity of re-deposited material with pure PFC may induce by itself the re-emission of dust to the plasma during reactor operation, as in the case of Be deposited on carbon based components and reverse system, due to the simultaneous formation of Be_2C and BeO at temperatures as higher as 873 K. In opposition to this behaviour, the formation of

Be₂W and Be₁₂W intermetallics in the temperature range up to 1073 K improves the toughness of Be-W-O films and mitigates the re-emission of deposits. Moreover, the formation of superficial BeO does not promote the occurrence of delamination events, and the Be-W interdiffusion and reactivity may lead to the recovery of delaminated zones in the deposits.

Acknowledgements

This project was funded by the European Union's Horizon 2020 programme under grant agreement number 633053 and from FCT, Portugal, through project Pest-OE/SADG/LA0010/2013. The opinions expressed herein do not necessarily reflect those of the European Commission.

References

- [1] A.W. Kley, N.J.L. Cardozo, U. Samm, Plasma-surface interaction in the context of ITER, *Phys. Chem. Phys.*, **8** (2006) 1761.
- [2] R.P. Doerner, The implications of mixed-material plasma-facing surfaces in ITER, *J. Nucl. Mater.*, **363-365** (2007) 32.
- [3] V. Philipps, P. Wienhold, A. Kirschner, M. Rubel, Erosion and redeposition of wall material in controlled fusion devices, *Vacuum*, **67** (2002) 399.
- [4] H. Okamoto, L.E. Tanner (Eds.), *Phase diagrams of binary beryllium alloys*, ASM International, Metals Park, Ohio, USA, 1987.
- [5] S.A. Catledge, Y.K. Vohra, Interfacial oxide and carbide phases in the deposition of diamond films on beryllium metal, *Diamond Relat. Mater.*, **9** (2000) 1327.
- [6] S. Zhang, D. Sun, Y. Fu, H. Du, Toughening of hard nanostructural thin films: a critical review, *Surf. Coat. Technol.* **198** (2005) 2.
- [7] C.P. Lungu et al., Beryllium coatings on metals: development of process and characterizations of layers, *Phys. Scr.*, **T128** (2007) 157.
- [8] R. Mateus et al., Formation and delamination of beryllium carbide films, *J. Nucl. Mater.*, **442** (2013) S320.
- [9] R. Mateus et al., Growth of mixed materials in the Be/W/O system in fusion devices, *Microsc. Microanal.*, **21** (2015) 16.

2.5.3 Surface cleaning of beryllium parts from Be-containment dust

**V. Sisenev¹, R. Giniyatulin², L. Gitarskiy¹, A. Milkov¹,
I. Gvozdkov¹, D. Kazakov¹, A. Vdovin¹, A. Gervash²,
I. Mazul²**

¹JSC “Kompozit”, Korolev, RF

²Efremov’s Institute, St-Petersburg, RF
beryllium@kompozit-mv.ru

The total area of the ITER First Wall (FW) panels is about 700 m² and 40% of them are obligation of Russian Federation (RF). About 180 FW panels should be produced by RF in which 7200 heat flux fingers will be coated by 325 000 beryllium tiles. It is well known that beryllium dust is a toxic material and that is why strong requirement for allowable level of Be-containment of FW panels was announced by ITER organization, the upper limit is 10 µg/m².

In order to get this goal it is necessary to develop a technique of cleaning completely finished beryllium products. This technique should provide the minimum surface contamination level of removable beryllium dust and the reproducibility of the cleaning results in a serial production conditions.

Different technics of cleaning beryllium tiles from Be-containment dust were tested. Ultrasonic cleaning with and without surfactant and with mechanical brushing were used. Surface contamination level was determined with a variety of methods such as colorimetric, atomic absorption spectroscopy and mass spectrometry. It was found that the complex cleaning in an ultrasonic bath with multistage rinsing provides best results. At the same time, different smear methods and different analysis methods give a diversity of results which are discussing in the paper.



Surface Cleaning of Beryllium Parts from Be-containment Dust

Radmir Giniyatulin^a, Victor Sisenev^b, Aleksandr Milkov^b

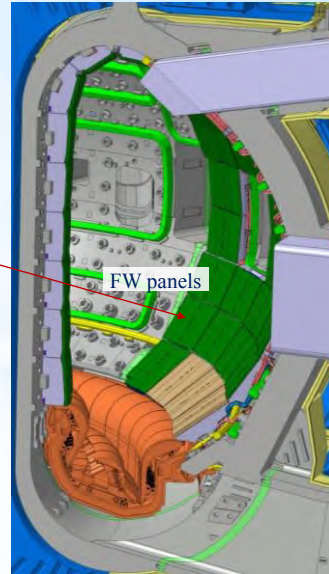
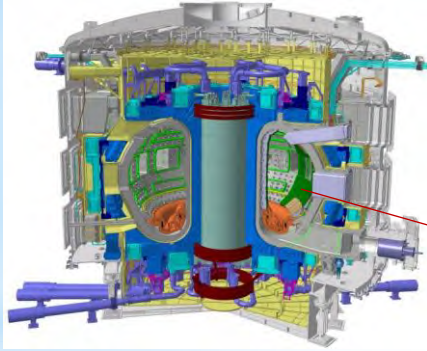
^a*Efremov's Institute, St-Petersburg, RF*, ^b*JSC "Kompozit", Korolev, RF*

12thInternational Workshop on Beryllium Technology, 10-11 September 2015, Jeju Island

Outline

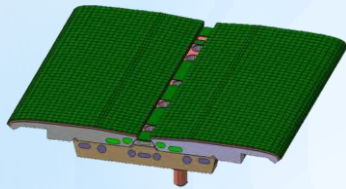
- **Short introduction**
- **Beryllium Safety requirements in RF**
- **Internal Russian Federation cleaning/analyses comparative program**
- Efremov Institute
- JSC "Kompozit"
- FGUP "Bazalt"
- Bochvar Institute
- **Conclusions**

Manufacturing of the ITER FW



Total ITER FW surface $\sim 650 \text{ m}^2$
RF obligation (40 %) $\sim 260 \text{ m}^2$

RF obligation



FW panels 179



HHF absorbing fingers 7200



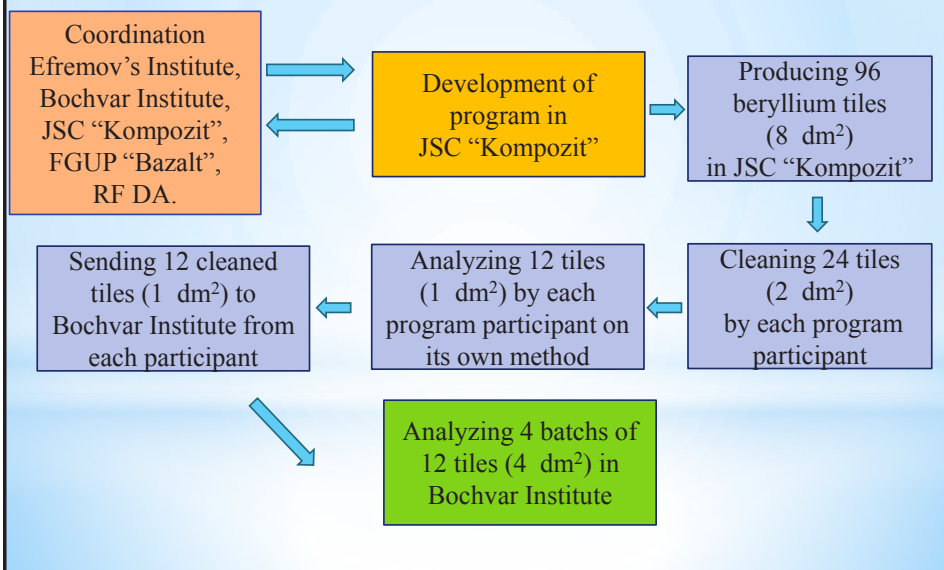
Beryllium tiles $\sim 325\ 000$

Beryllium Safety requirements in RF

	Air, $\mu\text{g}/\text{m}^3$	Surface, $\mu\text{g}/\text{m}^2$
Beryllium working area	1	> 30
Non beryllium area	0,01	≤ 30

- **Planning by IO ITER the requirement on permissible beryllium concentration on surface is $10 \mu\text{g}/\text{m}^2$**
- **This cause optimization of cleaning and analyzing of machined beryllium parts**

Internal Russian Federation cleaning/analysing comparative program 6



7

Efremov's Institute, St-Petersburg

Cleaning method	Ultrasonic cleaning 70°C Deionized water	Rinsing in deionized water 70°C	Air drying 100 ° C
Smear method	Smear with one filter paper moisten in 20 % alcohol		
Analyze method	Filter paper soaks in 10 % HNO ₃ , analyze Atomic Emission Spectrophotometry		

8

JSC “Kompozit”, Korolev

Cleaning method	Ultrasonic cleaning in distilled water 70°C	Rinsing in distilled water with stirring 70°C	Cleaning with brushes
Smear method	Smear with three cotton wool wads (2 moisten in distilled water, 1 dry)		
Analyze method	Cotton wool wads soak in 5 % HCl , analyze photometric method with colorimeter		

FGUP “Bazalt”, Saratov

Cleaning method	Ultrasonic cleaning with detergent 70°C	Ultrasonic cleaning with oil solvent 20°C	Air drying
Smear method	Smear with three cotton wool wads (2 moisted in distilled water, 1 dry)		
Analyze method	Cotton wool wads soak in 5 % HCl, analyze photometric method with colorimeter		

Bochvar Institute, Moscow

Cleaning method	Cleaning with brushes in distilled water 20 °C	Rinsing in distilled water 20 °C	Ultrasonic cleaning in distilled water 20 °C
Smear method	Smear with one filter paper moisten in distilled water		
Analyze method	Filter paper soaks in 10 % HNO ₃ , analyze Atomic Absorption Spectrophotometry		

Range of Be surface concentration ¹¹ on beryllium tiles after cleaning

Organization	Beryllium surface concentration, $\mu\text{g}/\text{m}^2$
Efremov's Institute	10-800
JSC "Kompozit"	30-300
FGUP "Bazalt"	10-350
Bochvar Institute	2-60

Conclusions ¹²

The diversity in results of beryllium surface contamination after cleaning leads to:

1 Optimize in RF a common analyze method for beryllium tiles safety control in a serial production conditions.

2 Continue developing cleaning technology for proving the possibility of reaching surface contamination level in according with ITER requirement of **10 $\mu\text{g}/\text{m}^2$** during serial production: 325 000 beryllium tiles, 7 200 HHF absorbing fingers, 179 FW panels.

3 Start coordination with ITER Organization to get agreement on procedure of safety acceptance of FW panels.

2.5.4 Experimental and calculated data of the beryllium oxide slurry formation process

U. Zhabbasbayev¹, G. Ramazanova¹, B. Assilbekov¹, Z. Sattinova², S. Shakhov³

1 Kazakh-British Technical University, Almaty, Kazakhstan

2 L.N. Gumilyev Eurasian National University, Astana, Kazakhstan

3 Siberian State University of Railway Engineering, Novosibirsk, Russia

Abstract

Results of experiments and numerical simulation of the motion and heat exchange of the beryllium oxide slurry in the annular cavity are presented. The slurry is highly concentrated structured system where the mineral phase is beryllium oxide powder and liquid phase is an organic binder (paraffin, oleic acid and beeswax). The results of experiments and calculations show the process of molding of the slurry in the annular cavity. Calculated data of the isotherms of solidification zone of the beryllium oxide thermoplastic slurry are in agreement with the experimental results.

1. Introduction

The development of new areas of science and directions of technology increases requirements for advanced properties and quality of ceramic fabrications. Products of complex configuration from new non-metallic materials (high thermal conductivity, oxygen-free, superconducting, etc.) are becoming more and more popular. In spite of using isostatic pressing technology of hot casting under pressure [1, 2] remains the basis for the obtaining long-length, multi-channel, complex shaped ceramic fabrications from non-plastic powders.

Nowadays technology of slurry molding (extrusion) is very relevant in connection with intensive development of MIM technology [3-11], where same physical processes take place.

While a lot of attention has been paid to improving of the technology and creation of the new equipment last years, up to now remains unsolved problem of obtaining fault free products by this method. As a result, in practice it does not often achieve the desired quality of moldings and obtaining of acceptable products, which makes this process low profitable. Obtaining of ceramic fabrications by hot molding from dispersion materials with anomalous physical properties, such as BeO is particularly complicated. In this case, the difficulties of obtaining the products of high quality are caused firstly by thermal properties of beryllium oxide, in particular, its unique thermal conductivity [12, 13]. Clearly, it is impossible to eliminate technological limitations and problems without the development based on all experience and knowledge of theoretical representations about regularities and mechanisms of regulation of the thermal regime of the casting on the forming process of molding.

The results of experimental research and the generalization of them by calculations of mathematical model of the thermoplastic slurry of beryllium oxide molding process are presented in this paper.

2. Experimental researches of the solidification process of molding

Experimental research of the effect of casting regimes on the temperature field in the zone of solidification of the molding was made on the experimental bushing (Fig. 1), by measuring the temperature using a thermocouple installed on the different levels by the height of crystallizer. Experimental bushing is structurally closed to the production plant and it is designed for casting of circular tube with the outer diameter 0.02 m and the inner diameter 0.012 m. Material of mandrel and crystallizer is steel of grade X18H10T. The total height of the cylindrical part of the annular cavity is $H = 0.028$ m, the height of the hot zone of the annular cavity is $h_1 = 0.008$ m, the height of the cold zone of the annular cavity is $h_2 = 0.020$ m. Water with the temperature $t_1 = 80$ °C fed to the upper (hot) contour of the crystallizer. Water with the temperature $t_2 = 15 - 20$ °C fed to the bottom (cold) contour. The maximum through put of the crystallizer contours in volume of water is 1500 l / hour.

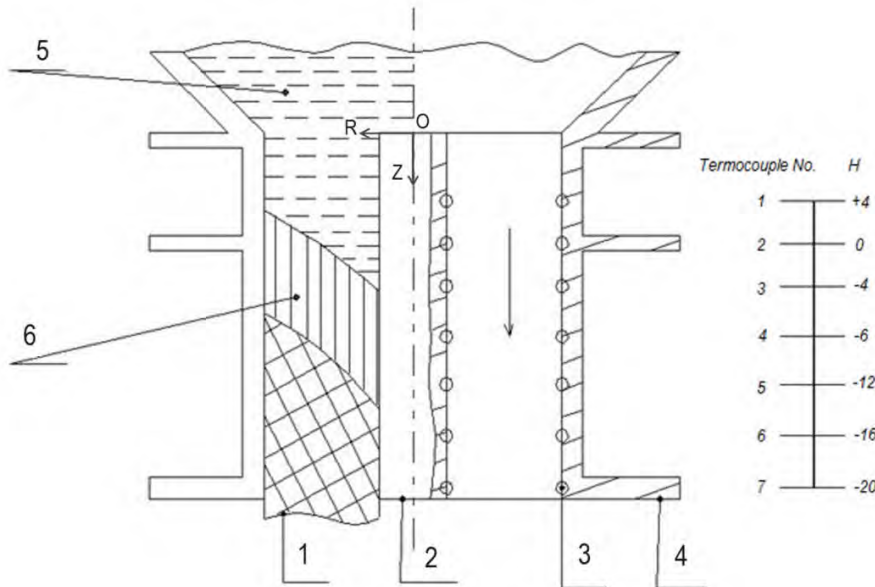


Fig. 1 Scheme of molding solidification process and installation of thermocouple in the bushing: 1 – molding, 2 – mandrel, 3 – thermocouple, 4 – bushing, 5 – liquid slurry, 6 – zone of solidification

Conical input of the bushing is connected with the working tank of casting installation where beryllium oxide slurry is kept. BeO slurry is a high concentrated structured medium. Slurry flows from the tank to the conical inlet of the annular cavity with an initial temperature $t_0 = 80$ °C. During its flow in result of heat exchange with the walls of mandrel and bushing slurry changes its aggregate state and solidifies.

According to the obtained data, dependence of position of the boundary of solidification slurry from different parameters of casting was built. The shape of the curve of surface solidification, which is dependent on the casting parameter, is defined taking into account that the temperature changes linearly by the height and radius of crystallizer on the short segments.

The influence of molding velocity on the thermal regime of the casting was determined in the first series of experiments. The flow rate and temperature values of hot and cold water in the cooling

contours are presented in Table 1. In the experiments molding velocity increases from 20 to 100 mm/min. Fig. 2 shows positions of solidification zones depending on the molding velocity. Isotherm of the AB "solidus" corresponds to the temperature 54°C and isotherm of the CD "solidus" to 40°C (Fig. 2).

Table 1 – Regimes of experiments as a function of the molding velocity

Number of the diagram		1	2	3	4	5
Molding regime	Hot water flow rate, <i>l/hour</i>	500	500	500	500	500
	Cold water flow rate, <i>l/hour</i>	1500	1500	1500	1500	1500
	Molding velocity, <i>mm/min</i>	20	40	60	80	100
	Hot water temperature, °C	80	80	80	80	80
	Cold water temperature °C	20	20	20	20	20

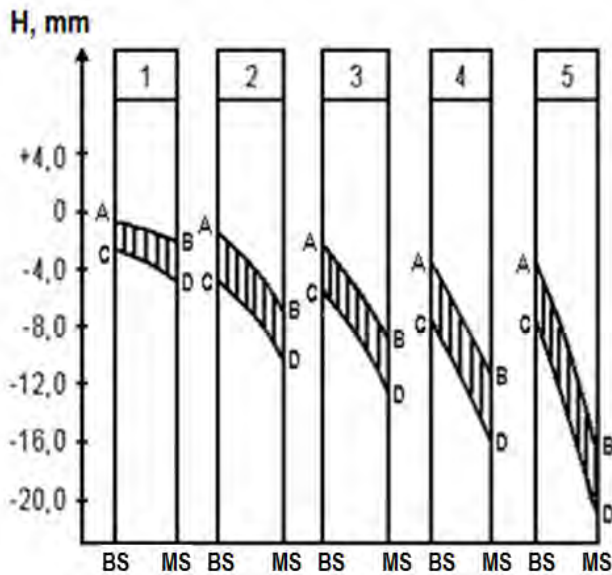


Fig. 2 The position of solidification zone depending on the molding velocity: AB - isotherm "solidus"(54°C), CD - isotherm "solidus"(40°C), BS - the surface of the bushing, MS - the surface of the mandrel

As we see in Fig. 2, the increase of the molding velocity leads to expansion of zone of solidification and its movement to the area of heat extraction of cold contour. It explains that with increasing of molding velocity heat extraction on the walls of the annular cavity does not have time to cool the slurry, and zone of solidification extends, and it moves down towards the molding velocity.

In the second series of experiments the influence of cold water temperature and flow rate on the thermal regime of molding solidification was investigated. Flow rate and temperature of hot and cold water, molding velocity are presented in Table 2. In the experiments the molding velocity is 20

mm/min. Flow rate and temperature of hot water do not change, 500 l/hour and 80°C. Flow rate of cold water changes from 250 to 1500 l/hour, and the temperature from 15 to 20°C.

The results of the second series of experiments are shown in Fig. 3. In the first three regimes cold water temperature is 15°C, and the flow rates are 1000,500 and 250 l/hour, respectively. Solidification zones of molding are located in the area of cold contour, and move downstream with reducing cold water flow rate. Reducing of cold water flow rate leads to reduction of the heat extraction on the wall of bushing (Fig. 3).Therefore, solidification zone of molding is moving down the length of the cold contour.

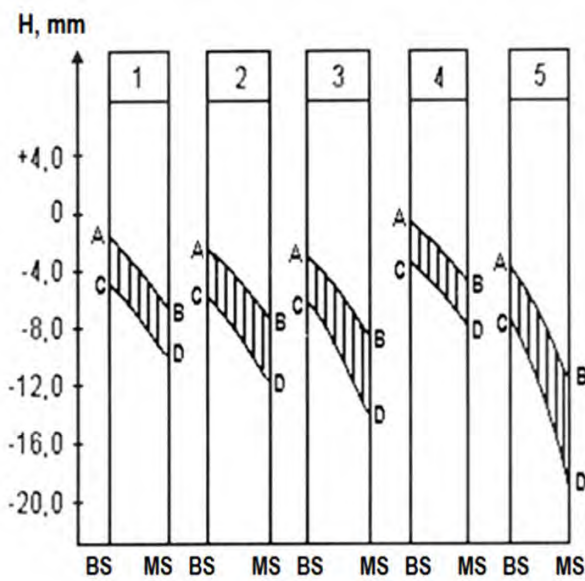


Fig. 3 The position of solidification zone depending on the flow rate and the temperature of cold water: AB - isotherm "solidus"(54°C), CD - isotherm "solidus"(40°C), BS - the surface of the bushing, MS - the surface of the mandrel

Table 2 – Regimes of experiments as a function of the cold water flow rate and temperature

Number of the diagram		1	2	3	4	5
Molding regime	Hot water flow rate, l/hour	500	500	500	500	500
	Cold water flow rate, l/hour	1000	500	250	1500	250
	Molding velocity, mm/min	20	20	20	20	20
	Hot water temperature, °C	80	80	80	80	80
	Cold water temperature °C	15	15	15	20	20

In the last two experiments of this series cold water temperature was 20 °C, and its flow rate was changing from 1500 to 250 l/hour, respectively. In the fourth experiment, the beginning of

solidification zone is located nearer to the hot contour area. Increase of cold water temperature from 15 °C to 20 °C leads to reduction of temperature difference of the hot slurry and cold water. In the conditions of the fifth experiment except increase of cold water temperature takes place reduction of its flow rate from 1500 l/hour to 250 l/hour. Therefore, heat extraction reduces and solidification zone of molding moves down towards motion of the thermoplastic slurry (Fig. 3).

Accordingly, the experimental data show that the thermal regime of molding of the beryllium oxide thermoplastic slurry is sensitive to change of the molding velocity, and to conditions of heat extraction on the walls of the annular cavity.

3. Mathematical model of the process of solidification

Motion and heat exchange of the beryllium oxide thermoplastic slurry in the annular cavity are considered. The slurry flows into cavity with initial temperature of $t_0 = 80^\circ\text{C}$ (Fig. 1). As it moves the slurry is cooled and solidified, and on the output from the cavity it acquires structural form of the tube. The movement of slurry occurs in the laminar regime. Special feature of the slurry beryllium oxide is its high thermal conductivity; however due to high viscosity of thermoplastic slurry Prandtl number is much higher than one. Density of the slurry mass is function of temperature and increases as solidification.

The problem is studied in Cartesian coordinate system with axis z and r . OZ axis coincides with the cavity axis direction, and OR axis is radially directed to it (r_1 – radius of the mandrel, r_2 – radius of the bushing of, $r_2 - r_1$ – thickness of the annular cavity). Molding velocity is directed vertically downward along the OZ axis. Radial component of the velocity originates due to the heat exchange of the slurry with the walls of annular cavity.

Rheological properties of the slurry change with temperature. The heat of phase transition is released during the change of state. Cooling of the slurry may lead to the irregularity of the temperature profile and rheological properties of the pressing molding. Solidification begins at the walls of the annular cavity, while in the central part slurry may be in liquid state. As a result, in-feeding of slurry for the compensation of internal shrinkage of volume in the cooling zone of the cavity may occur.

According to the experimental data the slurry solidification occurs at the temperature range from 54 to 40 °C. Binder of the slurry is in the amorphous state and passes from the liquid amorphous state to the solid-plastic amorphous state in the zone of solidification [12, 14, 15]. The total amount of heat released per unit mass of the slurry mass is determined by the change of enthalpy ΔH at the phase transition zone.

Heat capacity of the slurry changes in the transition zone. Increase of the enthalpy during the phase transition can be determined by the apparent heat capacity method [16-21]. In this method, the latent heat is taken into account by increasing the heat capacity in the phase transition zone. Changing of heat capacity can be represented as [16-18]:

$$c_p = \begin{cases} c_s, & t < t_s & \text{solid phase} \\ c_{in}, & t_s \leq t \leq t_l & \text{transition zone} \\ c_l, & t > t_l & \text{liquid phase} \end{cases} \quad (3.1)$$

where $c_{in} = \left\{ \int_{t_s}^{t_l} c(t) dt + H_{1 \rightarrow 2} \right\} / (t_l - t_s)$, $H_{1 \rightarrow 2}$ – the phase transition specific enthalpy of beryllium

oxide slurry with binder mass fraction of $\omega = 0,117$ is determined by experimental data and is equal to $H_{1 \rightarrow 2} = 7800$ J/kg [22].

In [19, 20] it is believed that the temperature in the transition zone changes linearly, the expression of the specific heat is defined as:

$$c_p = c(t) + H_{1 \rightarrow 2} \frac{\partial f_{sl}}{\partial t} \quad (3.2)$$

$$f_{sl} = \begin{cases} 0, & t < t_s & \text{solid phase} \\ \frac{t - t_s}{t_l - t_s}, & t_s \leq t \leq t_l & \text{transition zone} \\ 1, & t > t_l & \text{liquid phase} \end{cases}$$

In COMSOL Multiphysics [21] phase transition function $\alpha(\bar{t})$ is introduced to the transition zone to consider the latent heat, and changing of the slurry heat capacity is expressed by:

$$c_p = c_s \cdot (1 - \alpha(\bar{t})) + c_l \cdot \alpha(\bar{t}) + H_{1 \rightarrow 2} \frac{d\alpha}{dt} \quad (3.3)$$

where c_s – specific heat of the slurry in the solid state, c_l – specific heat of the slurry in the liquid state, $\alpha(\bar{t}) = 0$ for the pure solid slurry and $\alpha(\bar{t}) = 1$ for the pure liquid slurry, \bar{t} – dimensionless temperature of slurry.

According to the experimental data of beryllium oxide slurry with binder mass fraction of $\omega = 0,117$ function $\alpha(\bar{t})$ takes a form $\alpha(\bar{t}) = 5.712 \cdot \bar{t} - 2.8544$.

The equations (1) – (3) of the method of apparent heat capacity include the latent heat of the phase transition, and are convenient for calculations. For convenience position of the transition zone is not known in advance and is determined as a result of the calculations.

The rheological properties of the slurry for binder mass content $\omega = 0.117$ depend on temperature, and expressed by empirical formulas [23]:

$$\mu(t) = 293.6259 \cdot \exp(-0.05816 \cdot t), (Pa \cdot s) \quad (3.4)$$

$$\tau_0(t) = 11.4 + 11.41 \cdot \exp\left(-\frac{(t - 70.05)}{5.47}\right), (Pa) \quad (3.5)$$

Density of the thermoplastic slurry is defined by the concentrations of the beryllium oxide powder and the binder:

$$\rho = \frac{\rho_{BeO} \cdot \rho_{bin}}{((1 - \omega)\rho_{bin} + \omega \cdot \rho_{BeO})}, (g/cm^3) \quad (3.6)$$

where ρ_{BeO} is the density of the beryllium oxide powder, ρ_{bin} is the density of the binder, ω is relative mass content of the binder in the fractions.

The density of the binder where $\omega = 0.117$ is determined by Eq. (7):

$$\rho_{bin}(t) = 0.852 + 0.0725 \cdot \cos(0.0561 \cdot (t + 273.15) - 16.7361), (g/cm^3) \quad (3.7)$$

The density of the beryllium oxide is $\rho_{BeO} = 3.02 g/cm^3$. The density of the binder ρ_{bin} in the range of temperature from $t = 80 - 40$ °C changed within 0.7797 to 0.9010 g/cm^3 and the density of the thermoplastic slurry during solidification increases from 2.2457 to 2.3553 g/cm^3 for this fraction $\omega = 0.117$.

Thermal conductivity of the slurry depends on the temperature, and for $\omega = 0.117$ it has the following form [22]:

$$\lambda = 1.6 + 4.8 \cdot \exp(-0.017 \cdot t), W/(m \cdot ^\circ C) \quad (3.8)$$

In the experiments [12, 15] beryllium oxide slurry shows thixotropic properties of non-Newtonian fluid, and is described by Shvedov-Bingham rheological model [24]. The motion of the slurry in annulus is considered to be steady-state and the system of equations in the narrow channel is used for its study [23, 25]:

$$\rho u \frac{\partial u}{\partial z} + \rho v \frac{\partial u}{\partial r} = -\frac{dp}{dz} + \frac{1}{r} \frac{\partial}{\partial r} \left(r \mu \frac{\partial u}{\partial r} \right) - \frac{1}{r} \frac{\partial}{\partial r} (r \tau_0) \quad (3.9)$$

$$\frac{\partial \rho u}{\partial z} + \frac{1}{r} \frac{\partial r \rho v}{\partial r} = 0 \quad (3.10)$$

In the limit of solid-plastic state of the slurry the motion equation (9) expresses the squeezing-out of the molding from the cavity and takes the form:

$$-\frac{dp}{dz} = \frac{1}{r} \frac{\partial}{\partial r} (r \tau_0)$$

In contrast to the motion equation (9) conduction heat transfer along the OZ axis is substantially due to solidification of the slurry, and heat of phase transition is determined by the apparent heat capacity

method (3). In the steady-state solidification process of slurry energy equation can be written as [19-21]:

$$\rho u c_p \frac{\partial t}{\partial z} + \rho v c_p \frac{\partial t}{\partial r} = \frac{\partial}{\partial z} \left(\lambda \frac{\partial t}{\partial z} \right) + \frac{1}{r} \frac{\partial}{\partial r} \left(r \lambda \frac{\partial t}{\partial r} \right) \quad (3.11)$$

The following notes are used in the Eqs. (9)–(11): z, r – axial and radial coordinates; u, v – components of the velocity vector; $p, \rho, T, \tau_0, c_p, \mu, \lambda$ – pressure, density, temperature, shear stress, coefficients of thermal capacity, viscosity and thermal conductivity of the slurry, respectively.

In the Eq. (11) temperature is calculated on the Celsius scale for convenience in comparison with experiment.

Condition of the mass flow rate conservation determines the pressure gradient for thermoplastic slurry extrude from the annular cavity [25]:

$$2\pi \int_{r_1}^{r_2} \rho u r dr = \pi(r_2^2 - r_1^2) \rho_0 u_0 \quad (3.12)$$

where r_1, r_2 – the radius of the mandrel and bushing, respectively.

Distributions of the velocity and the temperature at the inlet of the cylindrical portion are constant along the cross section of the annular cavity; respectively, all the thermo-physical properties of the slurry are constant:

$$u = u_0, \quad v = 0, \quad t = t_0, \quad (3.13)$$

if $z = 0$.

On the cavity walls in the area of the liquid slurry state for velocity are put conditions of sticking:

$$u_i = v_1 = 0, \quad i = 1, 2 \quad (3.14)$$

if $z > 0, \quad r = r_i$.

In solid–plastic state they are conditions impermeability and slip:

$$v_1 = 0, \quad \left(\frac{\partial u}{\partial r} \right)_{r_i} = 0 \quad (3.15)$$

if $z > 0, \quad r = r_i$.

The assumption is that the heat from the hot slurry is transferred to the walls of bushing and mandrel.

Then, condition of heat exchange can be applied to the surface of the mandrel [26]:

$$\lambda \frac{\partial t}{\partial r} = \alpha_d (t_c - t_d), \quad (3.16)$$

if $z > 0, \quad r = r_1$.

where α_d – coefficient of heat exchange between the slurry and the wall of the mandrel, t_d – the temperature of the wall of mandrel, t_c – the average temperature of slurry in cross-section of the annular cavity.

If we mark temperature of the water in the hot and cold contours as t_1, t_2 , we can put the boundary conditions on the wall of bushing as:

$$-\lambda \frac{\partial t}{\partial r} = k(t - t_i), \quad i = 1, 2 \quad (3.17)$$

if $z > 0, r = r_2$.

where k is the coefficient of heat transfer on the wall of *bushing*.

At the outlet section of the cavity for temperature are put the following condition:

$$\frac{\partial t}{\partial z} = 0 \quad (3.18)$$

if $z = l$.

Eqs. (9)–(12) and boundary conditions (13) – (18) are presented in the dimensionless form for the convenience. Coordinates z, r are divided by r_1 , velocity components u and v – by u_0 , pressure p – by the value of dynamic head $\rho_0 u_0^2$, temperature t – by t_0 , density, yield point, coefficients of thermal capacity, viscosity, and thermal conductivity – by their values at the temperature t_0 . The equations in the dimensionless form include Reynolds number Re , Prandtl number Pr , and Eckert number Ec .

Set of Eqs. (3)–(12) is solved numerically at boundary conditions of Eqs (13)–(18) [25]. The considered zone is divided into elementary cells with sides $\Delta z_i, \Delta r_j$. Different analogues of the motion equation (9) and energy (11) were obtained by the Crank–Nicolson method of the second order precision, but different analogue of Eq. (10) was obtained by two layer scheme of the second order precision [25]. Pressure gradient is defined by the splitting method [25] from the condition of conservation of mass flow rate (12).

4. Determination of the coefficient of heat transfer on the cavity walls

Coefficients of heat exchange α_d and heat transfer k on the walls of the annular cavity dependent on conductive and convective heat flows, molding velocity, temperature and flow rate of water in the cooling circuits. Heat exchange on the mandrel wall α_d and heat transfer on the bushing wall k were determined by experimental and calculated data comparison. Generalization of experimental and calculated data gives the possibility to determine the dependence of the coefficients of heat transfer and heat exchange from the molding velocity. Dependence of dimensionless coefficients of heat transfer and heat exchange on the walls of the annular cavity from molding velocity is built in Fig. 4. Coefficient of heat transfer on the wall of the bushing at the low molding velocities has great values, it decreases with increasing of molding velocity and it approaches to the limiting value. Coefficient of heat exchange on the wall of the mandrel has a few smaller values to compare with the wall of the bushing and it decreases with increasing molding velocity (Fig. 4).

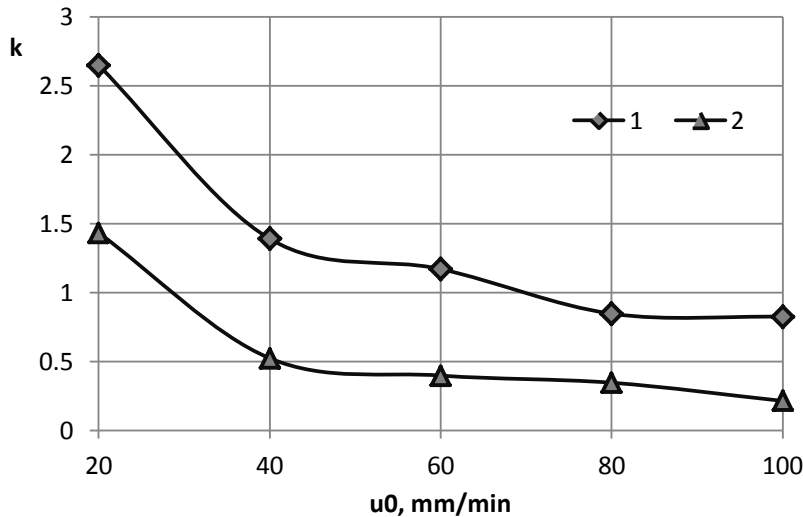


Fig. 4 The dependence of coefficient of the heat transfer on the wall of bushing (1) and heat exchange (2) on the wall of mandrel upon the slurry molding velocity

5. Results of calculations and comparison with experimental data

The calculation is performed under the same regime parameters and conditions as of the experiments. Calculated data by distribution of temperature in an annular cavity according to the conditions of the first series of experiments are demonstrated in Fig. 5 (Table. 1). As we stated above, the effect of molding velocity on the position of zone solidification was investigated in the first series of experiments.

At the inlet of the cylindrical part of the annular cavity the temperature of the slurry is constant and equal to $t_0 = 80^\circ\text{C}$. In the area of hot contour isolines (isotherms) of the temperature show the zones of the constant values of the temperature and parameters of the slurry mass is in liquid state. In this part the temperature of the slurry and the hot water is the same, heat transfer practically does not occur on the bushing wall.

Cooling of the slurry mass starts in the area of cold contour. Difference of the temperature of the slurry mass and cold water leads to an intensive heat transfer in the second cooling contour, and to reduction of the temperature and to change of rheological properties of the slurry.

The slurry temperature field is variable and changes from 80 to 54°C in the beginning of the second contour.

Isotherm with the temperature 54°C expresses upper bound of solidification zone of the slurry mass, and isotherm 40°C expresses the lower bound of the solidification zone. In the area of solidification between isotherms 54 and 40°C the slurry passes from the liquid (viscous-plastic) state to solid-plastic state. The experimental data of isotherms "solidus" AB (54°C) and "solidus" CD (40°C) are shown in Fig. 2 and 3. It may be noticed an agreement between the calculated data and experiments of positions of isotherms AB and CD .

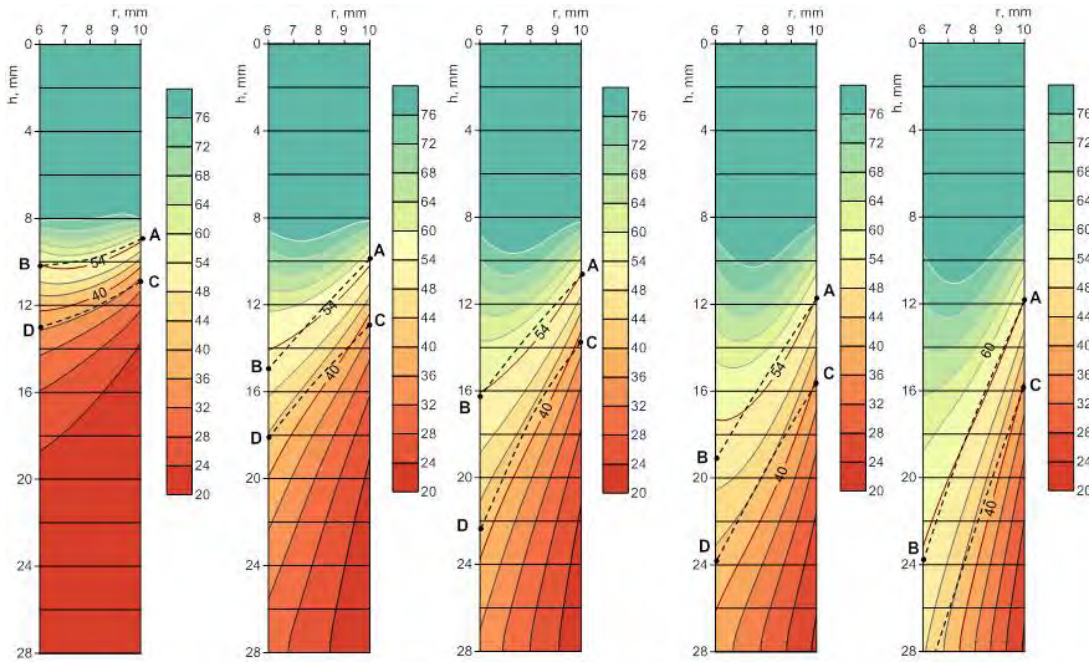


Fig. 5 Comparison of the calculated and experimental data of distribution of the temperature depending on the molding velocity (Table. 1)

At the value of the molding velocity of $u_0 = 20 \text{ mm/min}$ position of the transition zone of the slurry from the liquid (viscous-plastic) state to solid-plastic state is located closer to the beginning of the cold contour of cooling. With increasing molding velocity from 40 to 100 mm/min the position of the transition zone begins to pull down towards movement of the molding and takes extensive areas. It explains that with increasing of molding velocity convective component of heat flow of the slurry mass increases. The position of the transition zone increases and it covers all length of the mold cavity (Fig. 5).

The effect of flow rate and temperature of cold water on the position of the transition zone of the molding by conditions of the experimental researches were determined in the second series of calculations (Table. 2). Calculation data of the temperature distribution and the position of the transition zone of molding, limiting by isotherms "solidus" AB and "solidus" CD are shown in Fig. 6. In the first three cases, the temperature of cold water is 15°C , and its flow rate reduces from 1000 to 250 l/hour , respectively. Reducing the temperature of cold water increases the intensity of heat extraction and reducing of its flow rate and vice versa, it slows down the process of heat extraction. Increasing the temperature of cold water till 20°C , as well as reducing of its flow rate leads to a reduction of heat extraction.

The calculated temperature data are in agreement with the experiment results (Fig. 6).

The experimental and calculated data show that beryllium oxide thermoplastic slurry solidification process can be controlled by adjusting the flow rate and temperature of the cold water.

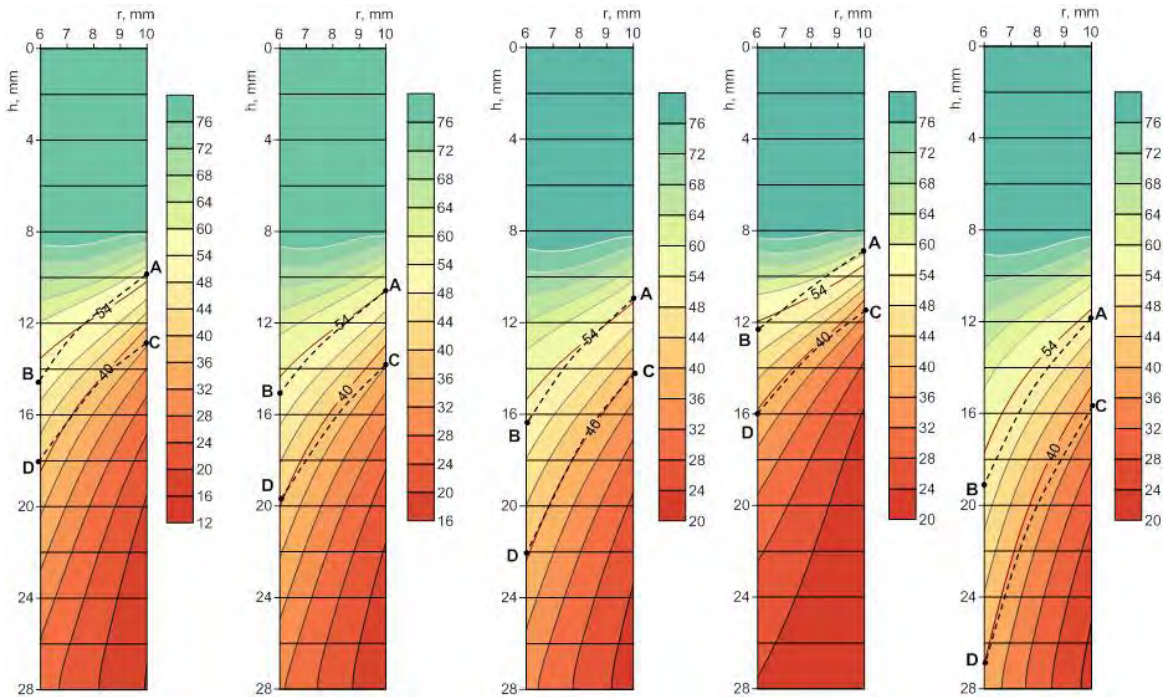


Fig. 6 Comparison of the calculated and experimental data of distribution of the temperature depending on the flow rate and the temperature of cold water (Table. 2)

6. Conclusion

During two series of experiments of the research on the effect of casting regimes on the temperature field in the solidification zone of the molding were identified the followings:

- the position of solidification zone of the slurry mass when molding velocity changes from 20 to 100 mm / min;
- the position of solidification zone of the slurry mass in the form-building cavity depending on the water flow rate and the temperature in the cold contour of cooling.

The upper bound of the solidification zone was estimated by isotherm "solidus" (54°C), and the lower bound – by isotherm "solidus" (40°C).

Temperature distribution, estimated during the experiments, in the form-building cavity of bushing depending on the molding velocity and heat extraction conditions on the walls of form-building of annular cavity lets us determine the transition from liquid (viscous-plastic) state to solid-plastic one.

The experiment results were analyzed and generalized using mathematical model of the thermoplastic slurry molding process. The latent heat of the phase change has been accounted by the apparent heat capacity.

The mathematical model includes the equations of the law of conservation of mass, momentum and energy of non-Newtonian fluid with the Shvedov-Bingham's rheological model. Rheological and thermo-physical properties of the slurry were found on the basis of experimental data and express dependence on the temperature. The coefficients of heat exchange and heat transfer on the walls of the

annular cavity were determined by comparison of experimental and calculation data. The temperature field of the slurry in liquid (viscous-plastic) and solid-plastic states were obtained in the calculations. The positions of isotherm "solidus" (54 °C) and "solidus" (40 °C), expressing the upper and lower boundaries of the solidification zone position were determined.

The results of calculation are in agreement with the experimental data, and they show physical validity of the proposed mathematical model of the molding process of the beryllium oxide thermoplastic slurry.

References

- [1] Gribovsky P.O., Hot casting of ceramic fabrications, Energoizdat, Moscow, 1961 [in Russian].
- [2] Dobrovolskii A.G., Slurry Casting, Metallurgiya, Moscow, 1977 [in Russian].
- [3] German R.M., Bose A., Injection molding of metals and ceramics, Princeton, New Jersey, USA, 1997.
- [4] Parkhomenko A.V., Amosov A.P., Samboruk A.R., Antipova A.A., Kobzeva N.V., Casting powder formation of Metal Parts, *Metallurgy Engineering*, **Vol. 3** (2012) 39-42 [in Russian].
- [5] US Patent. 1998; No. 5, 744, 532. [in Russian]
- [6] EP Patent. 2006; No. 0206685 [in Russian].
- [7] EP Patent. 1992; No. 0465940 [in Russian].
- [8] US Patent. 1992; No. 5, 145, 900 [in Russian].
- [9] EP Patent. 1994; No. 0595099 [in Russian].
- [10] US Patent. 2000; No. 6, 051, 184 [in Russian].
- [11] US Patent. 2005; No. 6, 939, 488 [in Russian].
- [12] Shakhov S.A., Bitsoev G.D., Application of Ultrasound in the Manufacture of High Thermal Conductivity Ceramic Articles, EKTU, Ust'-Kamenogorsk, 1999 [in Russian].
- [13] Akishin G.P., Turnaev S.K., Vaispapis V.Ya., Gorbunova M.A., Makurin Yu.N., Kiiko V.S., Ivanovskii A.L. Thermal conductivity of beryllium oxide ceramic, *Refractories and Industrial Ceramics*, **Vol. 50** (2009) 465–468.
- [14] Shakhov S.A., Controlling the deformation behavior of thermoplastic slips with ultrasound, *Glass and Ceramics*, **Vol. 64** (2007) 354-356.
- [15] Shakhov S.A., Gagarin A.E., Rheological characteristics of thermoplastic disperse systems treated with ultrasound, *Glass and Ceramics*, **Vol. 65** (2008) 122-124.
- [16] Voller V.R., Prakash C.A., Fixed grid numerical modeling methodology for convection-diffusion mushy region phase-change problems, *International Journal of Heat and Mass Transfer*, **Vol. 30** (1987) 1709-1719.
- [17] Voller V.R., Swaminathan C.R., Thomas B.G., Fixed grid techniques for phase change problems: a review, *International Journal of Numerical Methods in Engineering*, **Vol. 30** (1990) 875-898.

- [18] Hu H., Argyropoulos S.A., *Mathematical modeling of solidification and melting: a review*, *Modelling Simul, Mater. Sci. Eng.*, **Vol. 4** (1996) 371-396.
- [19] Moraga N.O., Andrade M.A., Vasco D.A., *Unsteady conjugated mixed convection phase change of power law non Newtonian fluid in a square cavity*, *International Journal of Heat and Mass Transfer*, **Vol. 53** (2010) 3308-3318.
- [20] Carbona M., Cortes C. *Numerical simulation of a secondary aluminum melting furnace heated by a plasma torch*, *Journal of Materials Processing Technology*, **Vol. 214** (2014) 334-346.
- [21] COMSOL. Inc. URL: <http://www.comsol.com/> [accessed: August/12/2014]
- [22] Dvinskikh Yu.V., Popil'skii R.Ya., Kostin L.I., Kulagin V.V. *Thermophysical properties of thermoplastic casting slips of some high-refractory oxides*, *Ogneupory*, **Vol. 12** (1979) 37–40 [in Russian].
- [23] Zhabbasbayev U.K., Ramazanova G.I., Sattinova Z.K., Shabdirova A.D., *Modeling of the beryllia ceramics formation process*, *Journal of the European Ceramic Society*, **Vol. 33** (2013) 1403–1421.
- [24] Wilkinson W.L., *Non-Newtonian fluids. Hydrodynamics, mixing and heat transfer*, Mir, Moscow, 1964. [Russian translation].
- [25] Anderson J.D., Tunnehill J.C., Pletcher R.H., *Computational fluid mechanics and heat transfer*, Mir, Moscow, 1990. [Russian translation].
- [26] Cebeci T., Bradshaw P., *Physical and Computational Aspects of Convective Heat Transfer*, Mir, Moscow, 1987 [Russian translation].

2.6 Technical session 4 : Health and safety issues

2.6.1 Working environment control in Beryllium handling area

K. Yonehara¹, Y. Natori¹, K. Tatenuma¹, M. Nakamichi²

¹ *Kaken Inc., 1044 Hori, Mito, Ibaraki 310-0903, Japan*

² *Sector of Fusion Research and Development, Japan Atomic Energy Agency, 2-166, Omotedate, Obuchi, Rokkasho, Kamikita, Aomori, 039-3212, Japan*

Abstract

Beryllium (Be) and its intermetallic compound (beryllide) are recommended from Japan as the most promising solid neutron multiplier for nuclear fusion power plant. The shape as the neutron multiplier is small sphere (pebble), and the mass production technology of it must be developed urgently. Beryllium is the substance regulated by the law of Ordinance on Prevention of Hazards Due to Specified the Chemical Substances Control. We'll report on a way of the operational environmental management to make a safe Be handling area for the Be handling researchers and workers.

1. Introduction

Beryllium is a regulated substance as specific chemicals in a law, and it's necessary to operate at the facilities approved from government.

Kaken has the Be Laboratory facilities to develop a neutron multiplier material for the nuclear fusion.

Fig. 1 shows the location of the Be Laboratory building at Kaken in Ibaraki of Japan, and the first Be handling facility was established in 2009.

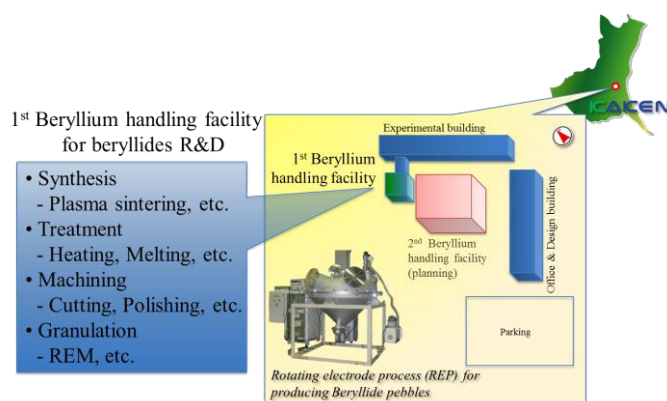


Figure 1 Hokota Functional-Material Developmental Center, KAKEN

Fig. 2 shows the room schematic of Be handling facility of Kaken. Beryllium handling facility consists of the area of 3 sections, which are Be handling area, entrance area, and chemical analysis and inspection area.

The exhaust ports of Be using equipment in the Be handling area are connected to a duct of a local exhaust device and excreted by an exhaust fan finally through HEPA filter (high-efficient particle air filter), and it's maintained simultaneously a negative pressure of the facilities.

Maximum Be concentration in the air inside the Be-Lab is <math><0.001\text{mg/m}^3</math>.

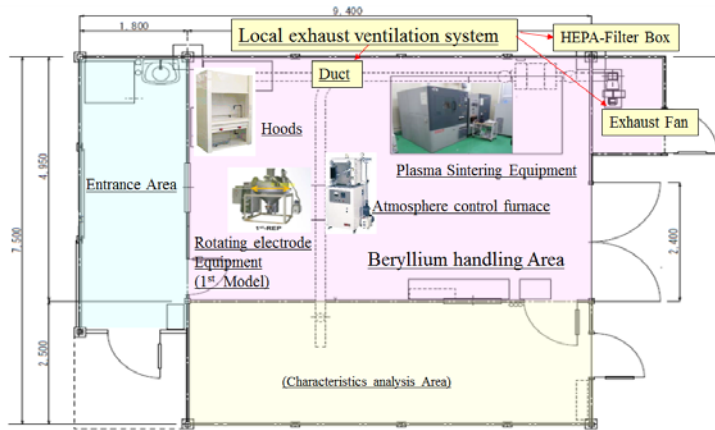


Figure 2 Beryllium handling facility at KAKEN

2. Method of working environment control

Fig. 3 indicates a procedure of working environmental management.

The periodic environment measurement in Be facilities and the check of the condition of local exhaust device are performed once every six months and one time a year, respectively.

Kaken has the license of environmental measurement; Japanese registration number is 08-9.

The process of environmental measurement and evaluation consists of 4 stages as shown in Fig. 4, which are design, sampling, measurement (chemical analysis) and evaluation of the working environment.

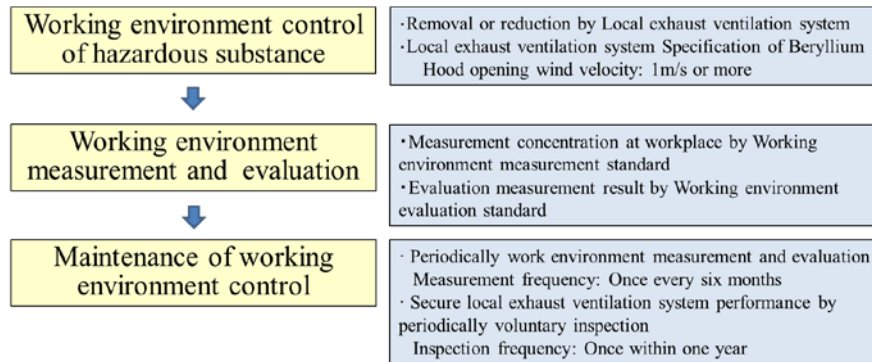


Figure 3 Working environment control of Beryllium

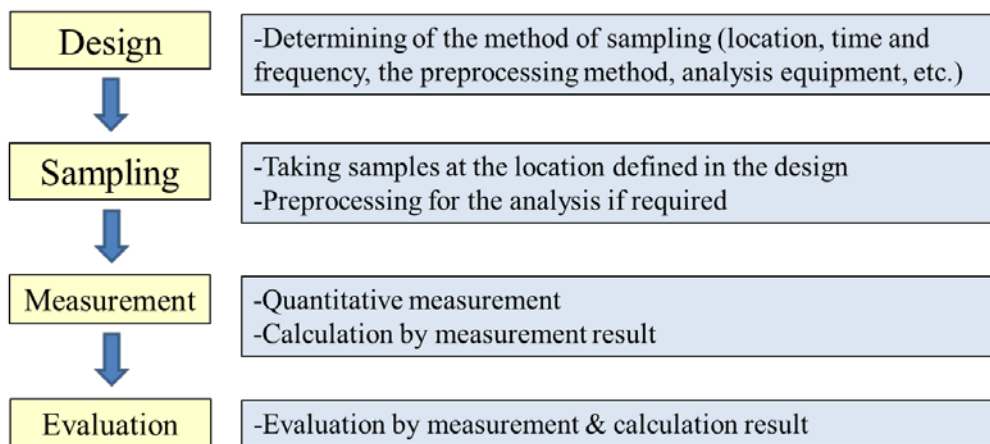


Figure 4 The working environment measurement and evaluation

A general design example of sampling positions is indicated in Fig. 5 and a design example of Be handling facility of Kaken is indicated in Fig. 6.

The A sampling points to measure the average concentration and the B sampling point as the most high concentration inside the facilities are set.

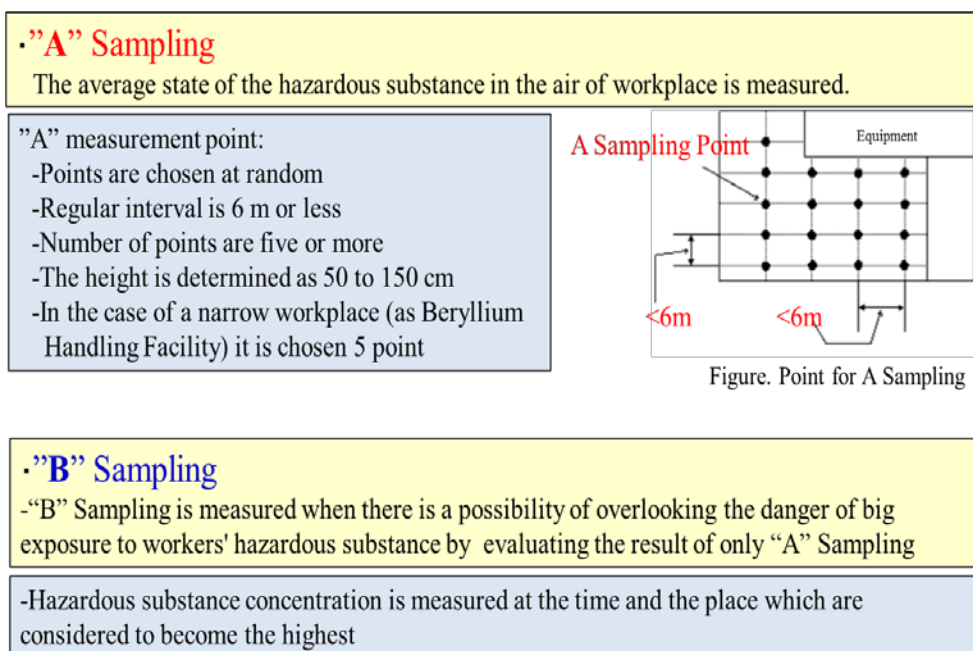


Figure 5 Design of sampling points

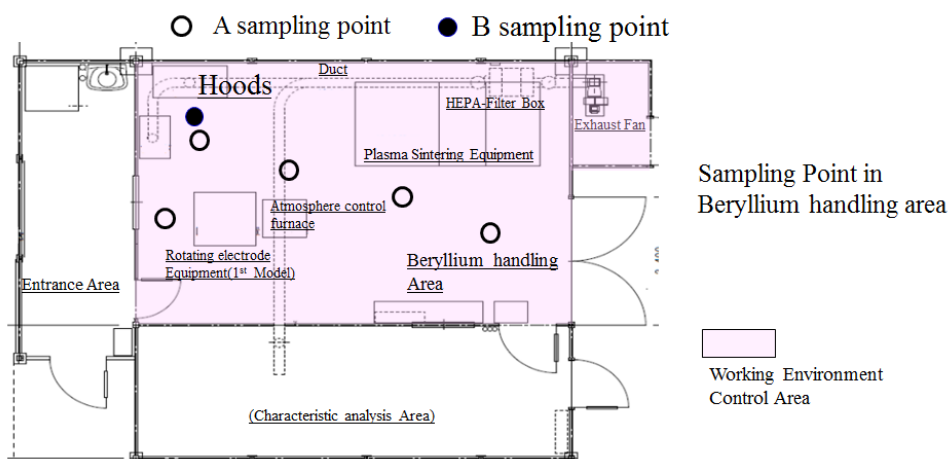


Figure 6 Design of Beryllium handling facility at KAKEN

The methods of sampling and measurement are indicated in Fig. 7.

It's sampled using a filter of pore size 0.45 μm by suction speed 5L/min for 20 min. After sampling, suction filter paper is treated by acid and the Be concentration measured by ICP-AES (inductivity coupled plasma atomic emission spectroscopy).

Sampling



Air Sampler KAS-10A(KAKEN Inc.)

Filtration sampling method : This method is such that an amount of sample air is sucked through a filter (limited to such a filter capable of collecting more than 95% of particles of 0.3 micron) and substances to be measured are gathered by filtration.

Filter specification

Filter	material	Hole diameter	size
Membrane filter	Glass fiber	0.45μm	φ47mm

Sampling condition

material	Administrative control level	Sampling method	Sampling condition	Lower limit of quantification
Be and its compounds	0.001mg/m ³ (Be)	Filtration sampling	5L/minx20min =100L	0.0001mg/m ³

Quantitative measurement



ICP-AES

Measurement method

Measurement method	Equipment	model number/ maker
Inductively Coupled Plasma(ICP) Atomic Emission Spectroscopy	ICP-AES equipment	Optima 7300DV/ PerkinElmer, Inc.

Figure 7 Sampling & Measurement method

The concrete evaluation of the working environment is indicated as follows.

The following EA1 and EA2 are calculated by sampling point “A” concentration, and CB is concentration of “B” sampling point. The values of EA1 and EA2 are calculated by following equation. E is the administrative control level.

$$EA1(1^{st} \text{ evaluation value}): \log EA1 = \log M1 + 1.645 \sqrt{\log 2\sigma1 + 0.084}$$

$$EA2(2^{nd} \text{ evaluation value}): \log EA2 = \log M1 + 1.151(\log \sigma1 + 0.084)$$

M1: geometrical mean value

$\sigma1$: geometrical standard deviation

E: administrative control level = 0.001 mg/m³

The working environment level is determined 3 classes as indicated in Table-1.

If $EA1 < E$ and $CB < E$ is satisfied, the workplace defined at control class I. This class shows that working environment control is appropriate and continuously working environment control is required.

If $EA2 \leq E$ and $CB \leq 1.5E$ is satisfied, the workplace defined at control class II. There is necessity for improvement in the working environment control. Inspection of equipment, improvement of working methods, etc. are required.

If $EA2 > E$ and $CB > 1.5E$ is satisfied, the workplace defined at control class III. At the control class III, working environment control is not appropriate. The inspection of equipment, improvement of working methods is immediately required. In this case, the workplace has to be changed to control class I or control class II.

Table-1 Workplace Control Class by working environment evaluation

Control class	Evaluation	Reaction
Control class I	- $EA1 \& C_B < E$ (Administrative control level) -Working environment control is appropriate	-Continuously working environment control
Control class II	- $EA2 \leq E \& C_B \leq 1.5 \times E$ -There is necessity for improvement in the working environment control	-Check of equipment and work methods -Change of equipment or improvement of working methods, etc.
Control Class III	- $EA2 > E \& C_B > 1.5 \times E$ -Working environment control is not appropriate	-Check of equipment, work methods, immediately -Changing of equipment or improvement of working methods, etc. to change to Control Class I or Control class II

The result of Be handling environment measurement in Kaken Be-Lab is shown in Table-2.

By the result, $EA1 < E$ and $CB < E$. The Be handling facility of Kaken is evaluated as control class I, therefore working environment control is appropriate.

By the above-mentioned method and periodical voluntary inspection, the workplace can be managed as safe working environment.

Table-2 Measurement & Evaluation result in Beryllium handling facility at KAKEN Inc.

Measurement result			Calculation result				
Material name		Beryllium and its compound	A measurement	item	1 day	M and σ	
Administrative control level		$E=0.001\text{mg}/\text{m}^3$		Geometrical mean value	$M_1 =$	0.0001	$M =$ 0.0001
A Sampling point	1	<0.0001		Geometrical standard deviation	$\sigma_1 =$	1.00	$\sigma =$ 1.95
	2	<0.0001		1st evaluation value	$E_{A1} =$	0.0003	
	3	<0.0001		2nd evaluation value	$E_{A2} =$	0.0001	
	4	<0.0001					
	5	<0.0001					
B Sampling point C_B		<0.0001	B measurement	$C_B =$	0.0001		

Evaluation result

Evaluation result	administrative control level	$E = 0.001$	(mg/m^3)	
	A measurement result	$E_{A1} < E$	$E_{A1} \geq E \geq E_{A2}$	$E_{A2} \geq E$
	B measurement result	$C_B < E$	$E \times 1.5 \geq C_B \geq E$	$C_B > E \times 1.5$
	Control Class	I	II	III

As another example of the Be handling facility at JAEA-IFERC is shown in Fig.8, the facility is controlled to class I without problem.

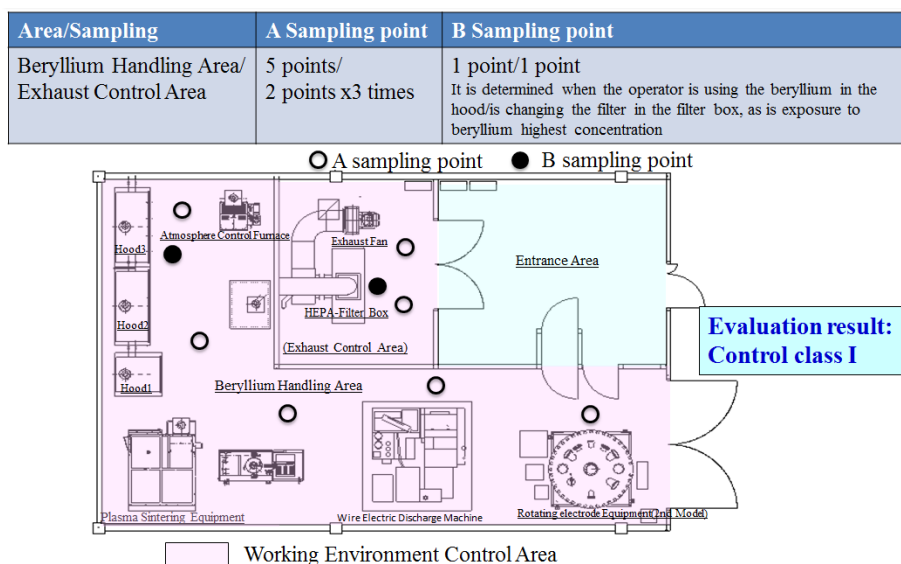


Figure 8 Sampling points at Beryllium handling facility of IFERC

3. Summary

The operational environmental management practice of Be handling area is summarized as below.

- The operational environment management of the Be concentration in air can be achieved by the specification of the Be operational equipment and working methods.
- As the main specifications of the Be facility, the Be handling area should be sealed from outside, the dust generation should be prevented, and the exhaust of Be equipment should be connected to the local exhaust device.
- The Be handling operator must master its adequate handling technique.
- The Be operational environment concentration must be measured every 6 months, and the working environmental condition can be estimated by the result of measurement.

The above mentioned operational environmental management can manage as a safe Be working place.

Reference

- [1] Safety Handling Procedures of Beryllium Intermetallic Compound on Fusion Blanket Study, SHIBAYAMA et al., J. Plasma Fusion Res. Vol.87, No.4 (2011)259-267.
- [2] Industrial Safety and Health Law, Law No. 57 of June 8, 1972.
- [3] Ordinance on Prevention of Hazards Due to Specified Chemical Substances, Ministry of Labor Ordinance No. 39 of September 30, 1972 .
- [4] Working Environment Measurement Standards, Ministry of Labor Notification No. 46 of April 22, 1976.
- [5] Working Environment Evaluation Standards, Ministry of Labor Notification No. 79 of September 1, 1988.

2.6.2 An Overview of Current Beryllium Environmental, Health, and Safety Regulatory Activities

T.M. Civic, T.L. Knudson, and C.K. Dorn

Materion Corporation

6070 Parkland Boulevard, Mayfield Heights, Ohio 44124-4191 U.S.A.

E-mail: terence.civic@materion.com

The current Occupational Exposure Limit (OEL) of $2.0\mu\text{g}/\text{m}^3$ that exists in many countries for beryllium metal is under review in the United States and in the European Union. Ireland, Poland, and Spain have adopted an OEL of $0.2\mu\text{g}/\text{m}^3$, and the U.S. OSHA (Occupational Safety and Health Administration) is expected to include this limit in the proposed beryllium standard that will be issued this year. Germany is advocating a lower limit that is not supported by industry, end-users, or the scientific evidence.

REACH (Registration, Evaluation, Authorization, and Restriction of Chemicals) testing results have shown that the current classification for beryllium metal is not correct and needs to be changed. The most recent and relevant studies demonstrate that beryllium should not be classified as causing cancer.

The method of measuring beryllium in workplaces differs from country to country, such that a measured exposure in the EU using an inhalable sampler would yield a result 3 times higher than what would be measured using a closed-face filter cassette, the sampling method employed in the United States.

This paper will present an overview of these issues as well as how the beryllium industry and other trade associations are working together to address them.

**12th International Workshop on
Beryllium Technology
Jeju Island, Korea**



**AN OVERVIEW OF
CURRENT BERYLLIUM
ENVIRONMENTAL, HEALTH
& SAFETY
REGULATORY ACTIVITIES**

Terence Civic
Theodore Knudson
Christopher Dorn

Materion Beryllium & Composites
Mayfield Heights, Ohio, U.S.A.

September 2015

Materion Beryllium & Composites

Beryllium EH&S Overview – BeWS-12, Korea

Presentation Outline

- Brief Background on Beryllium
 - Naturally Occurring Element
 - Where Commonly Found
 - Understanding CBD Basics
- Beryllium Occupational Exposure Limits
 - Establishment of “BeST” Consortium
 - Current & Proposed U.S. OSHA Change
 - Status of Standards within the EU
- Other Current Beryllium EH&S Issues
 - REACH & RoHS Directives
 - Beryllium as a Carcinogen
 - Measuring Airborne Beryllium
- Summary & Conclusion



Beryllium EH&S Overview – BeWS-12, Korea

A Naturally Occurring Element

- Found at 0.5 to 2.5ppm or higher in soils and rocks throughout the world
- Commonly found in coal, wood, and gemstones such as aquamarine and emerald
- Occurs naturally in ground and surface water
- Beryllium has been measured at ppb levels in most plants and vegetables, for example:



- Rice: 72µg/kg
- Lettuce: 16µg/kg
- Peas: 109µg/kg
- Potatoes: 0.59µg/kg
- Kidney Beans: 2200µg/kg (Fresh Weight)



Beryllium & Composites

3

Beryllium EH&S Overview – BeWS-12, Korea

Beryllium Also Found in Household & Construction Products

- Ceiling Tiles
- Fertilizers
- Detergents
- Charcoal
- Cat Litter
- Concrete Blocks
- Concrete Floors
- Metals
- Roofing Materials



Beryllium & Composites

4

Beryllium EH&S Overview – BeWS-12, Korea

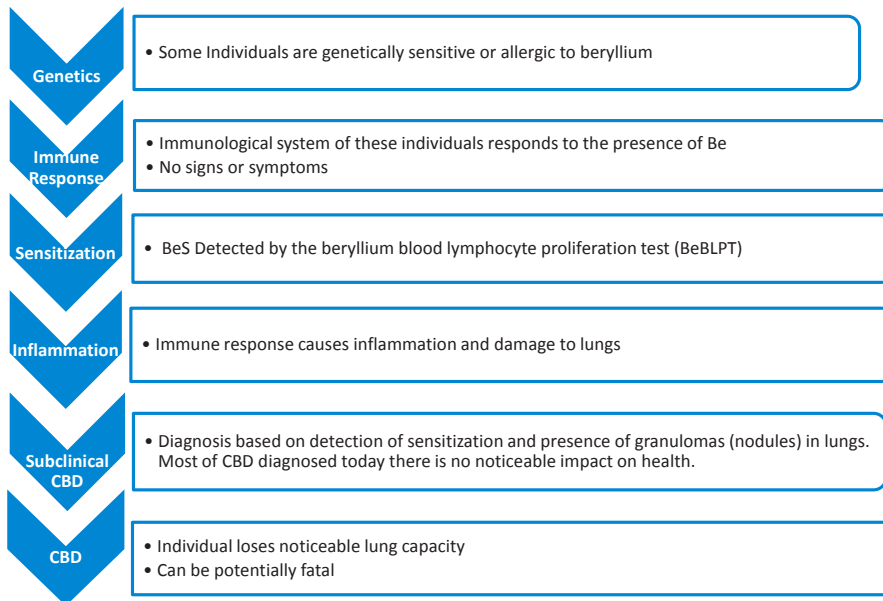
Health & Safety: Chronic Beryllium Disease (CBD)

- Necessary Conditions to get the Disease:
 - An individual must be **allergic or genetically sensitive to beryllium**
 - And
 - Be exposed to **respirable beryllium particulate** in the form of a dust, fume, or mist, less than 10µm in size, roughly one-tenth the diameter of a human hair.
- **Both Conditions are Required!**
 - CBD is a disease which affects the lungs – it cannot be contracted by ingestion or skin contact
 - Beryllium in solid form poses no special health risks
- **Most end-users will never handle beryllium in ways which will generate respirable dust, fume, or mist.**



Beryllium EH&S Overview – BeWS-12, Korea

How Does an Individual Get CBD?



Beryllium EH&S Overview – BeWS-12, Korea

What is the Beryllium Science & Technology Association (BeST)?

- Founded in September 2011
- Non-Profit Organization based in Brussels, Belgium
- Origin: REACH Beryllium Consortium
- Represents Manufacturers, Suppliers, and Users of Beryllium
- Members
 - Materion (U.S.A.)
 - NGK Berylco (France)
 - Schmelzmetall (Switzerland)
 - TROPAG Oscar H. Ritter Nachf. (Germany)



Beryllium Science & Technology Association



Beryllium & Composites

7

Beryllium EH&S Overview – BeWS-12, Korea

The BeST Mission Statement

- To promote sound policies, regulations, science, and actions related to the use of beryllium and to serve as an expert resource for the international community on the benefits and criticality of beryllium applications.



Beryllium Science & Technology Association



Beryllium & Composites

8

Beryllium EH&S Overview – BeWS-12, Korea

Exposure to Airborne Beryllium

- Official Occupational Exposure Limit (OEL) for airborne beryllium is still $2.0\mu\text{g}/\text{m}^3$ as an 8-hour, time-weighted average in the U.S. and other countries
- Materion & BeST recommend an OEL of **$0.2\mu\text{g}/\text{m}^3$**
- Recommended Exposure Guideline (REG) was based on a decade of research with the U.S. Government Agency NIOSH (National Institute for Occupational Safety & Health)
- Industry advocating a global OEL of $0.2\mu\text{g}/\text{m}^3$
 - Already adopted by Spain, Ireland, and Poland
 - U.S. OSHA will finally propose a $0.2\mu\text{g}/\text{m}^3$ OEL this year (2015)
 - Materion has worked with trade unions in the U.S.A. to establish this limit



Beryllium & Composites

9

Beryllium EH&S Overview – BeWS-12, Korea

Potential Beryllium OEL Regulatory Issue

- Bundesanstalt für Arbeitsschutz und Arbeitsmedizin (BAuA) in Germany
 - Advocating EU-wide Standard Beryllium OEL
 - REACH Authority used to Conduct Beryllium Study
 - Notified Beryllium Industry of “Results” Sep-2014
 - Now Pushing for OEL for airborne beryllium of $0.06\mu\text{g}/\text{m}^3$ first for Germany and then for the EU
- Major Issues with BAuA’s Proposal
 - Lack of Scientific Justification
 - Economic Impact
 - Technical Feasibility



Beryllium & Composites

10

Beryllium EH&S Overview – BeWS-12, Korea

Other Beryllium-Related Regulatory Issues

- REACH – Registration, Evaluation, Authorization, and Restriction of Chemicals
 - Most recent and relevant studies demonstrate that beryllium is not a carcinogen (cancer causing)
 - Current classification for beryllium needs revision
 - Beryllium does not meet REACH criteria
 - Recent studies show that recycling of electronics waste containing beryllium presents no health risk to workers



Beryllium EH&S Overview – BeWS-12, Korea

Other Beryllium-Related Regulatory Issues

- RoHS – Restriction of Hazardous Substances
 - Began in the EU in 2003 for electronics and electrical equipment
 - Beryllium not included in RoHS and should remain so
- Measuring of Airborne Beryllium Particulate
 - Different Sampling Methods between U.S. and EU
 - EU Method shows Levels that are 2.88x Higher than U.S.



Beryllium EH&S Overview – BeWS-12, Korea

Summary & Conclusion

- Beryllium is Commonly Found in Nature & Everyday Materials
 - Solid Form Poses No Special Health Hazard
 - Uniquely Breathing Hazard from Airborne Particulate
- Occupational Exposure Limits for Beryllium are Changing
 - Generally Positive as Old OEL was not Protective
 - Potential Impact on ITER & Fusion of BAuA Proposal
- Beryllium Science & Technology Association (BeST)
 - Working towards Scientific Evidence-Based Regulatory Decisions
 - Standardization of Testing & Measurement Methods Needed



Beryllium & Composites

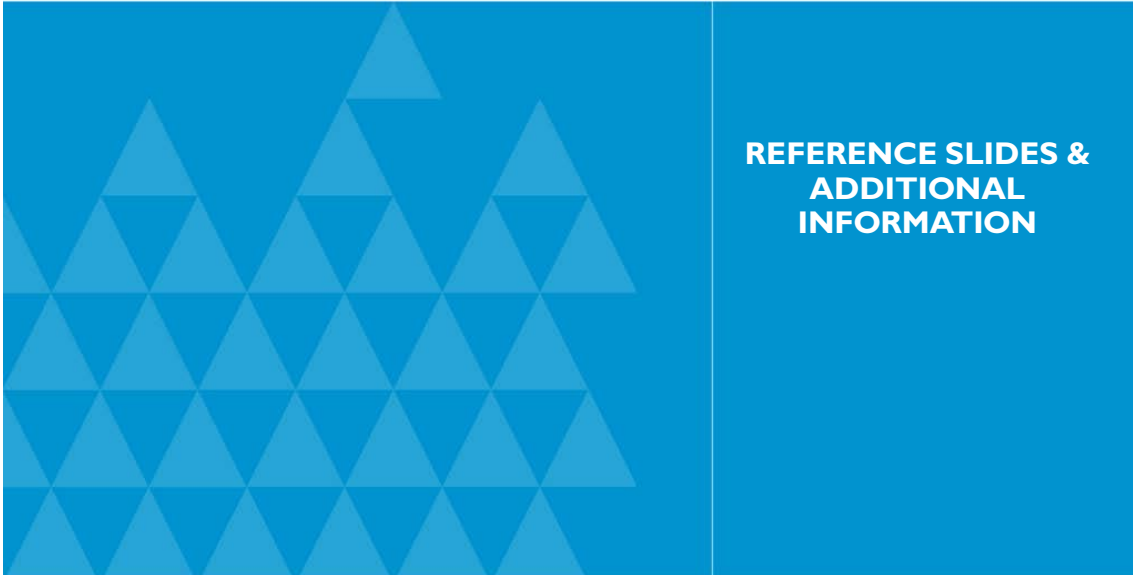
13



MATERION BUSINESSES

Advanced Chemicals
Barr Precision Optics & Thin Film Coatings
Brush Beryllium & Composites
Brush Performance Alloys
Ceramics
Electrofusion
Large Area Coatings
Microelectronics & Services
Natural Resources
Technical Materials

www.materion.com

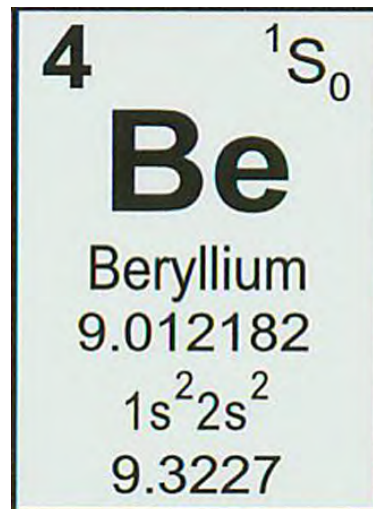


Materion Beryllium & Composites

Beryllium EH&S Overview – BeWS-12, Korea

Physical Properties of Beryllium

- Density
- Modulus
- Thermal
- Melting Point
- Nuclear
- Acoustic
- Optical
- Electrical
- Magnetic



Beryllium & Composites

Beryllium EH&S Overview – BeWS-12, Korea

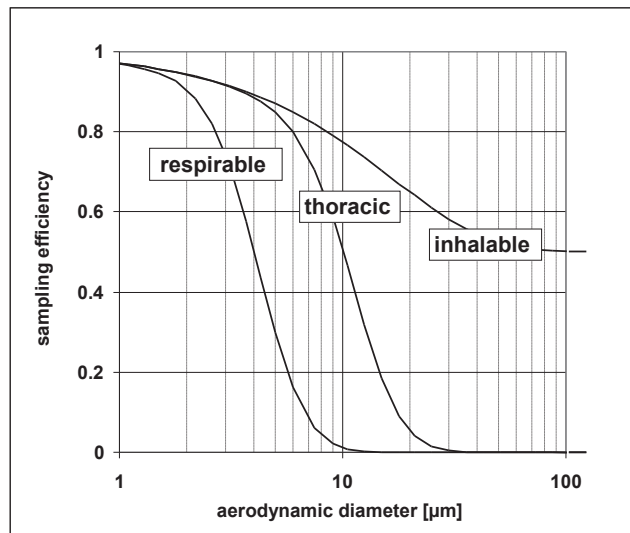
Environmental, Health & Safety (EH&S) Basics

- All Beryllium Materials Must Be Treated Alike
- Solid Forms Pose No Special Hazards
- Necessary Conditions
 - Allergic Reaction
 - Airborne & Ultra-Fine
- All Materials Recyclable
 - Buy-Back Program



Beryllium EH&S Overview – BeWS-12, Korea

Sampling Conventions



Beryllium EH&S Overview – BeWS-12, Korea

Inhalable Samplers

- GSP (Gesamtstaubprobe) is a collection device with a cone-shaped inlet section (CIS)
- A filter capsule containing a 37 mm filter is placed inside the sampler for particulate sampling
- The GSP is operated at a flow rate of **3.5 liters/min**



GSP



IOM

**Typical Inhalable Samplers
Used in Europe**

Beryllium EH&S Overview – BeWS-12, Korea

Total Particulate Samplers

- The **37mm closed-face filter cassette** is equipped with a 4mm inlet hole holding a 37mm filter
- Sampling flow rate is **2.0 liters/min**
- The closed face filter cassette samples **total particulate**



CFC Filter Cassette

**Typical Total Particulate Sampler
Used in U.S.A.**

2.6.3 Recent achievements and related safety issues concerning Beryllide applications

Aniceto Goraieb¹, Christopher Dorn², Petr Kurinskiy³, Sören Müller⁴

¹Karlsruhe Beryllium Handling Facility (KBHF GmbH), Herrmann-von-Helmholtz-Platz 1, D-76344 Eggenstein-Leopoldshafen, Germany, goraieb@kbhf.org

²Materion Beryllium & Composites, 6070 Parkland Blvd., Mayfield Heights, Ohio 44124-4191 U.S.A.,

³Karlsruhe Institute of Technology, Institute for Applied Materials, P.O. Box 3640, D-76021 Karlsruhe, Germany,

⁴TU-Berlin, Extrusion Research and Development Center (FZS), 13355 Berlin

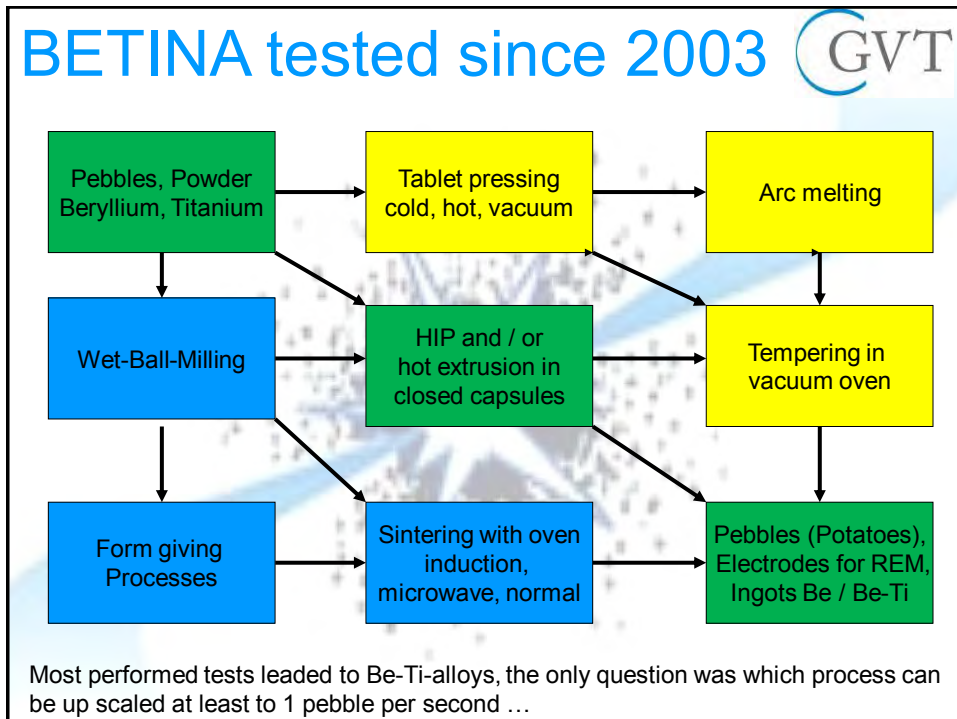
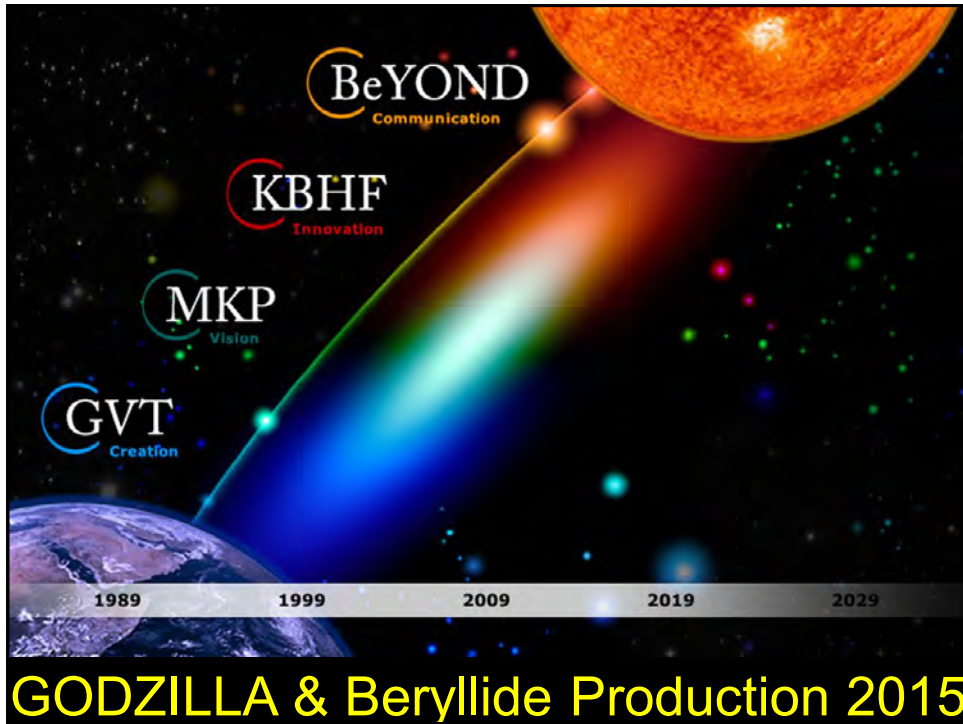
Karlsruhe Institute of Technology (KIT) has one of the leading positions in the development of materials for the Helium Cooled Pebble Bed Blanket (HCPB). Lithium orthosilicate Li_4SiO_4 and beryllium (or titanium beryllide Be_{12}Ti) pebbles, as foreseen, will play a roles of tritium breeder and neutron multiplier, accordingly. Pilot production facilities were built up by the company GVT (former Goraieb Versuchstechnik) to produce several kilograms of lithium- and beryllium-based pebbles.

About 150 kg of breeder and 300 kg of multiplier are required for the ITER Solid Breeder Test Blanket. Therefore, an appropriate process is needed that allows the production with the efficiency of about a pebble per second. This amount of material is beyond a laboratory-scaled production but not of a great interest for the industrial application. Compared to ITER design, the amount of blanket materials in DEMO will be significantly higher. By this reason, the recycling is needed to be taken into account what makes the handling of the blanket materials under nuclear conditions to be considered as well.

Therefore, KIT and GVT decided to build up the Karlsruhe Beryllium Handling Facility (KBHF) at the North Campus (former Research Center Karlsruhe) as a "Spin In". The goal of this cooperation is to run a model for a possible future ITER Blanket Handling Facility (IBHF). "Beryllium Safety" was build up with the support of the Institute for Material Handling and Logistics (IFL) and the Company HIMA (Bruehl, Germany).

In cooperation with the Institute for Applied Materials- Applied Materials Physics (IAM-AWP), the world market leader for beryllium Products, MATERION (Ohio, USA) and the Research Center for Hot Extrusion (FZS) located at Technical University of Berlin, the KBHF qualifies new production methods of beryllium-based materials.

Our presentation gives an overview concerning the recent achievements and related safety issues.



HIDOBE samples 2004



Production of Be₁₂Ti specimens for HIDOBE:

- Wet ball milling of Be and Ti powder together using alkane
- Drying and tablet fabrication by cold vacuum pressing
- Arc melting of the tablets and machining (ultrasonic drill)

HIDOBE: The samples behaved very good at 740 K under high-dose neutron irradiation ($6,94 \times 10^{25} \text{ n/m}^2 > 1 \text{ MeV}$)

Now looking for an industrial version of the process ...

**Handling conditions necessary to produce this samples:
Powder production under wet conditions in a glove box with inert gas atmosphere**



Test production pebbles

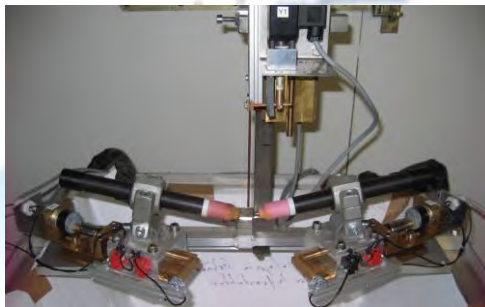


Test production of Ti pebbles:

- Melting of vibrating or rotating wire between two electrodes*
- Cold extrusion of wet powder at TU-Berlin (Bachelor-Thesis)
- Fast pressing of wet powder direct or indirect after extrusion
- Wet processing with mixer/dryer/spheronizer from EIRICH
- Microwave sintering of pebbles from wet powder processing

None of these methods seemed to be useful for up-scaling and REM was already working in Japan

**independence from resistivity*



Up-scaling the process



GODZILLA High Safety Laboratory for Beryllium Handling

Hazards and Risks



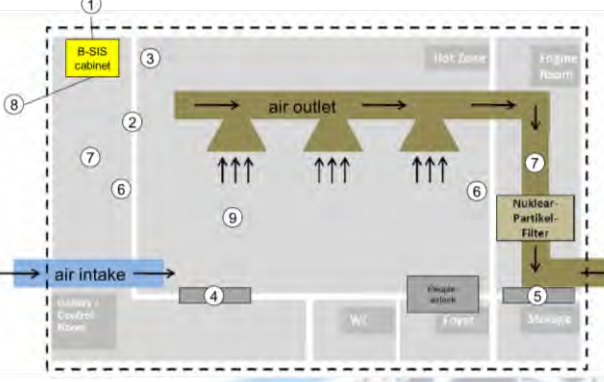
Hazardous event	Building / System	SIL
Defect in the gas line	Building 453, Glove box system	SIL 2
Flammable solids, liquids and Gases can ignite	Building 453, Building 454	No SIL
Undue high-pressure (1) in the glove box (15 mbar > Prel > 0 mbar)	Glove box system	SIL 2
Undue high-pressure (2) in the glove box (Prel > 15 mbar)	Glove box system	SIL 2
Undue low-pressure in the glove box (Prel < -15 mbar)	Glove box system	SIL 2



Definition of Hazards and Safety Integrity Levels (SIL), with the support of IFL Institute and the company HIMA (Brühl, Germany)

Outer containment





The diagram illustrates the outer containment system. It shows an air intake on the left leading into a laboratory area. From the laboratory, air is drawn through three air outlets. The air then passes through a nuclear particle filter and is exhausted. Various sensors and components are indicated by numbered circles (1-9) corresponding to the legend.

- (1) B-SIS Safety PLC
- (2) Laboratory pressure sensor
- (3) Laboratory oxygen sensor
- (4) Emergency exit status
- (5) Material lock status sensor
- (6) Emergency stop buttons
- (7) Smoke and fire detection
- (8) Touch panel visualization
- (9) Visual and acoustic alarm

Building Safety System (B-SIS)
 The building safety system B-SIS observes the critical conditions in the laboratory e.g. oxygen level and ventilation. In addition it helps to save energy by lowering the air flow in absence of persons and under safe conditions of all glovebox systems.



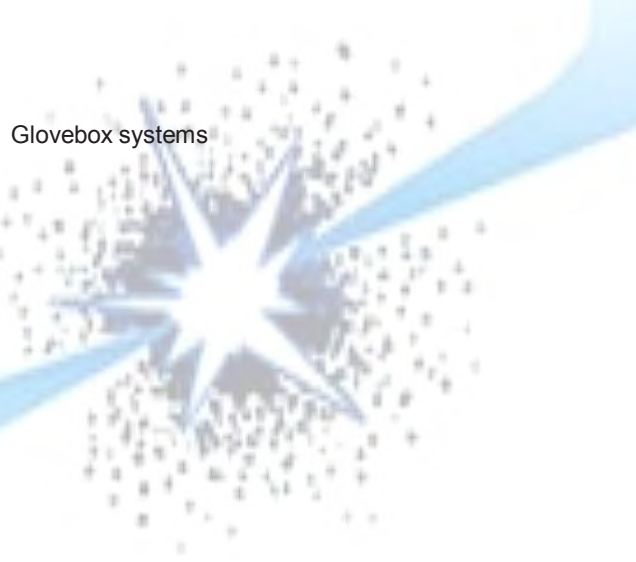
A second containment beside the gloveboxes is required for powder handling in bigger quantities

Inner containment



14 Bachelor- and Master-Thesis lead to the here shown design. Together with the students the GVT stuff has realized this complex system. Nevertheless it is an ongoing process to develop "health and safety" conditions for a future IBHF (ITER Blanket Handling Facility)

Glovebox systems





Equipment

Lab in building 453
(Machining Unit)

KBHF GmbH



Lab in building 454 (Powder Handling Unit)
Personal air lock that has been installed

GVT Some examples for the build up equipment in the KBHF Laboratory on the KIT Campus

Research Center Extrusion



- Cooperation since 2011
- Wet extrusion of Ti-powder
- Hot-Extrusion at 500 - 1000 °C
- More than 30 tests performed

- **Open handling conditions therefore:**
- **Pre tests with Ti-powder performed**
- **Double containment necessary**
- **Respirator masks have to be worn**

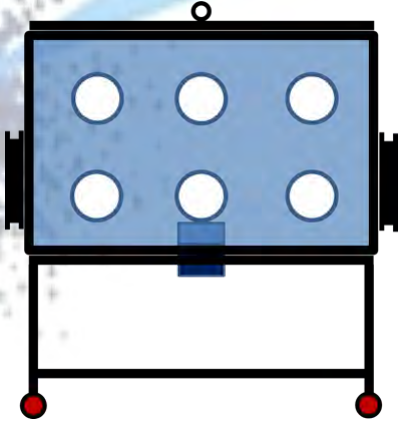


GVT

Research Center Extrusion



During the hot extrusion process the sample can brake. Therefore a special equipment was build. We have called it Catcher. It is a tube that is connected to the mouth of the press.



A blower with filter sucks the air coming out through a barrel filled with water. In a next step a glovebox will be mounted to this device.



Hot extrusion at TU-Berlin



Outer container, requirements:

- It serves as a lubricant during extrusion
- It keeps the temperature constant inside during hot extrusion (tool temperature max. 500 ° C)
- It should have deformation characteristics similar to those of the inner container and the metal powders
- *Best Results with Cu-Cr-Zr alloy (no welding)*

Inner container, functions:

- To make the handling in the in glove-boxes under inert gas atmosphere easier
- Vacuum in the capsule keeps the powder from oxidizing
- **Double containment fulfills high safety issues**
- The inner capsule helps to dismantle the rod after the hot extrusion process
- *Best Results with Niobium capsule (TIG-welding)*

Hot extruded "Trumpets"

KBHF GmbH

Pre tests performed with pure Ti-powder

"Trumpet" of sample 3 after electrical wire cutting.
Titanium powder, filled under argon atmosphere in steel tube with titanium cladding



Titanium cylinder with approx. 95% T.D.



GVT

Results with Beryllium

KBHF GmbH

Production of electrodes for REM:

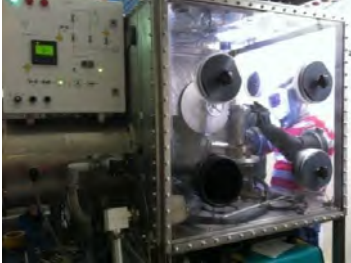
- Finally this year we have got promising results
- We came a long way over "eggs" of "trumpets"
- Still fine tuning of the production process necessary
- Influence of powder sizes on the density
- Influence on pressing angles on the material flow
- Does it work for other beryllides, as well?
- **And if, can we solve possible handling problems**

So next stop Be₁₃Zr ...

An impression of "eggs" and "trumpets" ...

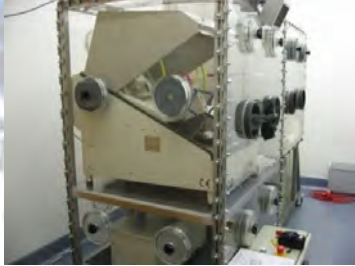


Welding and dismantling



Different other Equipment for:

- TIG-welding of capsules
- Evacuating and closing
- Cutting and dismantling
- Polishing and screening
- Determination of resistivity



GVT All handling is taking place in gloveboxes with inert gas atmosphere to protect workers and material

Powder processing



Wet ball milling device optimized with the help of the Company NETZSCH, Germany

Prototype of a infrared heated mixer/dryer/spheronizer has been build in a glovebox with the support of EIRICH



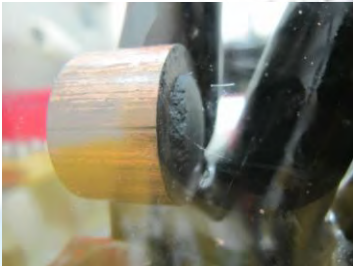
Titanium stator

NETZSCH All machines are prototypical because they have to be build in gloveboxes



Sintering



By hot extrusion we achieved a Be-Ti-compound with densities of about 80%

Next steps should now be:

- To get a Be-Ti-alloy
- To higher the density of the samples
- To compare different routes

Tests performed showed:

- Free vacuum sintering leads to low densities
- Density lowers even in capsule
- “pressurized” sintering is equal to a HIP-Process





Be has high vapor pressure therefore the oven unit is a double tube version connected to a glovebox

Hot isostatic pressing



- Good results were gained 2003 to 2006
- BODYCOTE in Europe now refuses to use Be
- No other facility was available for the tests

Therefore:

- HIP-Facility has been build up in the laboratory
- But experience is needed to run the equipment
- First tests with titanium have been performed
- A new heating rod was designed with the support of the company CREMER
- We now hope to perform tests with Beryllium in the near future





To get a permission to use this equipment, a lot of changes in terms of safety were necessary



Thermoprozessanlagen GmbH

Outlook



Further development of fabrication of beryllide rods is planned:

- 1) Hot extrusion tests with different core temperatures between 670° C and 730° C, to find out if the inhomogeneous material flow depends on this parameter
- 2) Hot extrusion tests with different pressing angles (45° , 60° and 90°) to find out if better material flow and higher density can be achieved
- 3) Further tests with different powder sizes, to improve the beryllide formation during annealing at different temperatures
- 4) Hot isostatic pressing (HIP) of the samples after hot extrusion, to gain a higher density (Fig. 13)
- 5) Test of the possibility to use this method also for other beryllides Be_nX , $Be_nX_mY_o$

X = Ti, Zr, Cr Y = V, Li



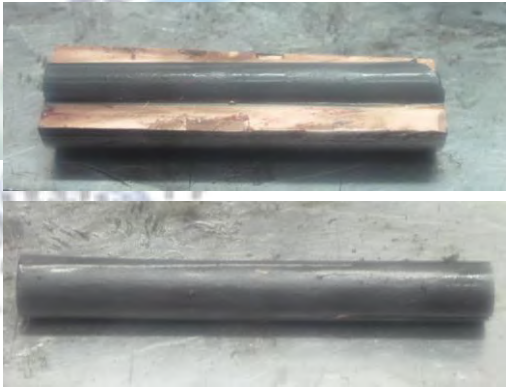
Be-Ti pebbles have been successfully produced in Japan by using electrodes fabricated like discribed

Latest results, September 2015



- 3 cylinders were successfully pressed
- One with Be-Ti powder sizes 32 - 45 µm
- One with Be-Ti powder sizes < 32 µm
- One using first time Be-Zr powder!**
- Successfully dismantled yesterday
- The rod seems to be very stable

- Zr has high chemical reactivity
- Especially with gases like H and O
- Therefore Zr Handling conditions:
- Only under inert gas atmosphere
- Gloveboxes with gas cleaning systems necessary





Breeder Ceramics



Developed by **IAM-WPT** in cooperation with **GVT**

Raw materials

- LiOH·H₂O
- SiO₂
- TiO₂

Preparations

- Mixing
- 2-step drying

Melt-based process

- Process temperature: 1300 to 1450° C (2372 to 2642° F)
- Generation of a thin melt jet (200 to 400 μm)
- Autonomous decay into droplets
- Active LN₂ cooling

Pebbles

- Li₄SiO₄ + max. 30% Li₂TiO₃
- Fine-grained



Also for this prototype facility a Hazards and Safety Integrity Levels (SIL) was defined (in construction)

"Always aim for the Moon, even if you miss, you'll land among the stars." *Friedrich Nietzsche*



Artificial Star Fuel

I was attending nearly every Beryllium workshop since I started in this field 1989
 What I can see today is that it is about **time now to put together the TBM** components
 Therefore I want to encourage You to **think beyond ITER** with the eyes of an engineer
 We build a **DEMO Blanket** with 300 t of Beryllium pebbles and 150 t of Lithium ceramics
 What are the conditions that are expectable in this scenario (for example uranium content)
BeYOND will take place in Berlin on the 1st and 2nd September 2016 (before SOFT)
 We can start the discussion now but please let me give You some homework for BeYOND

2.7 Technical session 5 : Beryllide applicatoin

2.7.1 Recent progress on R&D of beryllides as advanced neutron multipliers for DEMO blanket in the Broader Approach activities

Masaru Nakamichi, Jae Hwan Kim

Japan Atomic Energy Agency, Aomori, Japan

Fusion reactors require advanced neutron multipliers with high stability at high temperatures. The fundamental granulation technique for beryllides as advanced neutron multipliers has been established. However, the homogenized Be_{12}Ti pebbles indicated increase of hydrogen generation reactivity because of the increased specific surface area of the homogenized Be_{12}Ti pebbles. To prevent the increase of hydrogen generation reactivity associated with the increased specific surface area, granulation experiments of prototypic pebbles of the $\text{Be}_{17}\text{Ti}_2$ and Be_{12}V compositions without peritectic reaction were carried out. Prototypic beryllide pebbles 1mm in diameter composed of single phase $\text{Be}_{17}\text{Ti}_2$ and Be_{12}V were successfully fabricated directly by granulation using the rotating electrode method without homogenization treatment. Analysis revealed that these prototypic pebbles of the $\text{Be}_{17}\text{Ti}_2$ and Be_{12}V compositions demonstrated a good oxidation property more than pure Be pebbles.

1. Introduction

Beryllium metal is candidate material as neutron multiplier. In the case of the demonstration fusion power plant (DEMO) blanket design, there are some requirements as follows.

- A lot of neutrons needs for the higher TBR,
- Reduction of the number of cooling pipes for preventing neutron loss by neutron absorption with cooling pipe or coolant,
- High-temperature-tolerant multipliers as the result of cooling pipe reduction.

Therefore, advanced neutron multipliers with high stability at high temperatures are desirable for the pebble bed blankets of DEMO instead of pure beryllium (Be) metal. Beryllium intermetallic compounds (beryllides) are the most promising advanced neutron multipliers [1,2]. Development of the advanced neutron multipliers has been started between Japan and the EU in the DEMO R&D of the International Fusion Energy Research Centre (IFERC) project as a part of the Broader Approach (BA) activities. In Japan, beryllides fabrication R&D has been carried out in the DEMO R&D building at IFERC, Rokkasho. The Beryllium (Be) Handling Room has been installed in the DEMO R&D building. In this facility, synthesis, treatment, machining and characterizations of beryllides and its pebbles are being performed (see Fig.1).

2. Beryllide synthesis method

Beryllides are too brittle to allow production of the pebbles. Therefore, establishment of synthesis and granulation techniques for beryllides is a key issue for development of the advanced neutron multipliers. Conventional syntheses of the beryllides such as a powder metallurgy process involving a hot isostatic

pressing (HIP) method and a melting process such as a casting method, an arc-melting method, a high-frequency heating method. However, there is some issues in these conventional synthesis methods such as complicated process, contamination of impurities, brittleness of synthesized material, difficulty in composition control and low reproducibility. Therefore, these previous synthesis methods were not suitable for beryllides fabrication.

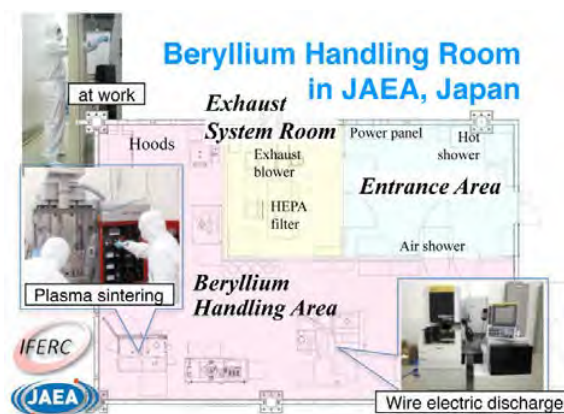


Fig.1 Layout of the Beryllium Handling Room in the DEMO R&D building.

On the other hand, a plasma sintering method has been proposed as a new technique for beryllides synthesis because this method results in powder surface activation that enhances powder particle sinterability and reduces high temperature exposure. It has no affect of the oxidation layer on the surface of raw powders. The plasma sintering process consists of 1) uniaxial pressure, 2) plasma generation for powder surface activation, and 3) resistance heating (see Fig.2). From the results of beryllide synthesis experiments, it was clarified that the not only disk type but rod type of beryllide has been successfully fabricated by the plasma sintering method.

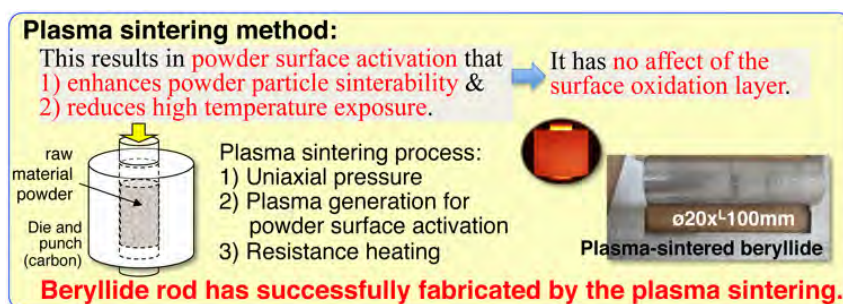


Fig.2 Outline of the plasma sintering method.

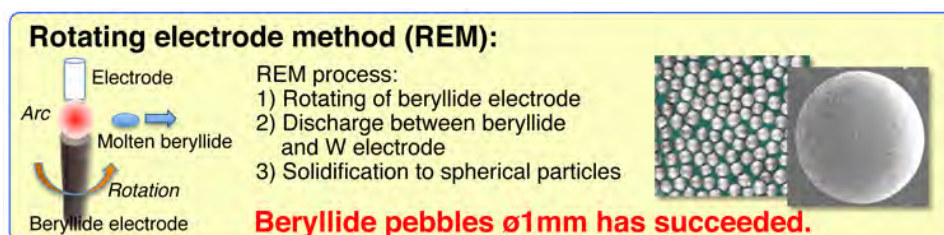


Fig.3 Outline of the rotating electrode method.

3. Beryllide granulation method

To fabricate the prototypic beryllide pebbles using the plasma-sintered beryllide rod, the rotating electrode method (REM) was selected. This method has a lot of the experience base for granulation of not only pure Be metal pebbles but also metallic pebbles. The REM process consists of 1) rotating of beryllide electrode, 2) discharge between beryllide and tungsten (W) electrode, and 3) solidification to spherical beryllide particles. The trial result of beryllide granulation revealed that the prototypic beryllide pebbles 1 mm in average diameter were successfully fabricated using the plasma-sintered beryllide electrode (see Fig.3).

4. Homogenization treatment by annealing

The beryllide of Be_{12}Ti is one of the candidate structural compositions of beryllides. In the case of Be_{12}Ti beryllide granulation, compositional structure was changed by a peritectic reaction caused by remelting under the REM granulation process [3]. For homogenization to Be_{12}Ti phase of beryllide pebble composition, a previous study [4] established that the homogenization treatment of the as-granulated Be-7.7 at% Ti pebbles resulted in the successful fabrication of single phase Be_{12}Ti pebbles that exhibited a higher

degree of porosity than the as-granulated Be-7.7 at% Ti pebbles (see Fig.4).

5. Hydrogen generation reaction with water vapor of as-granulated and homogenized Be-Ti beryllides pebbles

To evaluate the reactivity of the beryllide pebbles, hydrogen generation reaction experiments were performed at 1273 K in Ar gas with a H_2O concentration of 10000 ppm by thermal gravimetry and gas chromatography. Figure 5 shows the results of the hydrogen generation reactivity of several kinds of beryllides pebbles such as as-granulated Be-7.7 at% Ti pebbles, homogenized Be_{12}Ti pebbles, as-granulated $\text{Be}_{17}\text{Ti}_2$ pebbles and as-granulated Be_{12}V pebbles compared with pure Be pebbles.

The homogenized Be_{12}Ti pebbles exhibit higher reactivity with water vapor than the as-granulated Be-7.7 at% Ti pebbles. From the results of the comparative evaluation of the specific surface area, it was clarified that increased reactivity was caused by increased specific surface area of the homogenized Be_{12}Ti pebble [5].

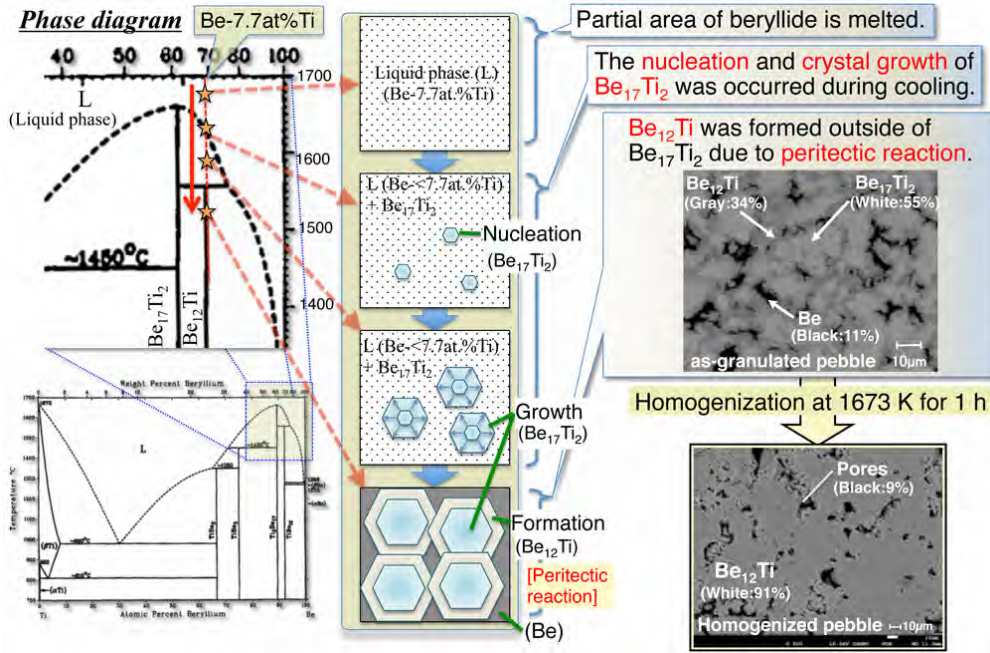


Fig.4 Crystal growth diagram under cooling process of the REM granulation in the case of Be₁₂Ti composition.

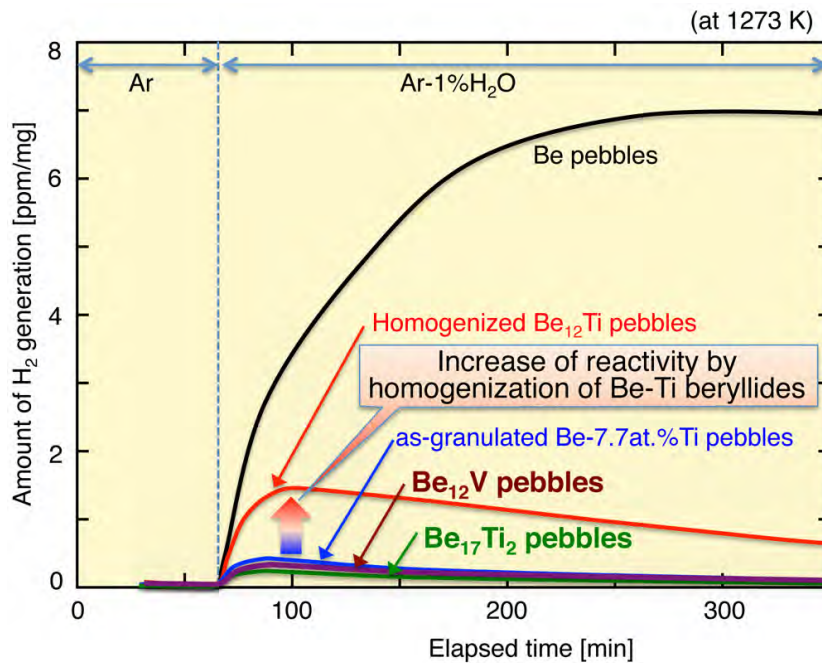


Fig.5 Hydrogen generation reaction of beryllides pebbles with water vapor of 10000 ppm at 1273 K.

6. Granulation without homogenization treatment of single phase pebbles of beryllides except Be₁₂Ti composition

To avoid the observed increase in the specific surface area of single phase Be₁₂Ti pebbles induced by homogenization treatment, and the resulting increase of hydrogen generation, other structural compositions of beryllides such as Be₁₇Ti₂ and Be₁₂V except Be₁₂Ti were

evaluated. The structural composition of Be₁₇Ti₂ was selected because this composition has not only no peritectic reaction during the cooling process from the liquid phase, but also high Be density next to Be₁₂Ti composition. Furthermore, the structural composition of Be₁₂V has not only no peritectic reaction but also similar nuclear property to Be-Ti beryllides.

The raw electrodes for granulation of Be₁₇Ti₂ and Be₁₂V were synthesized in the same manner as for the

fabrication of Be_{12}Ti . Prototypic pebbles of $\text{Be}_{17}\text{Ti}_2$ and Be_{12}V were granulated in the same manner as for the fabrication of Be_{12}Ti without the homogenization treatment. From the compositional analysis results of these pebbles, prototypic beryllide pebbles 1 mm in diameter of $\text{Be}_{17}\text{Ti}_2$ and Be_{12}V single phase were successfully fabricated directly by granulation of the REM without homogenization treatment [5,6].

7. Hydrogen generation reaction with water vapor of $\text{Be}_{17}\text{Ti}_2$ and Be_{12}V beryllides pebbles

Figure 5 also provides results of the hydrogen generation reactivity of $\text{Be}_{17}\text{Ti}_2$ and Be_{12}V pebbles without homogenization, presented in conjunction with the results of as-granulated Be- 7.7at% Ti and homogenized Be_{12}Ti pebbles. These results show that prototypic pebbles of the $\text{Be}_{17}\text{Ti}_2$ and Be_{12}V compositions have a good oxidation property similar to pebbles of the as-granulated Be- 7.7at % Ti pebbles.

8. Conclusions

The fundamental granulation technique for beryllides as advanced neutron multipliers has been established by a combination process comprised of the following: 1) plasma sintering for beryllide electrode fabrication, 2) the rotating electrode method using the plasma-sintered electrode for pebble fabrication by granulation, and 3) the homogenization treatment by annealing. However, the homogenized Be_{12}Ti pebbles indicated increase of hydrogen generation reactivity because of the increased specific surface area of the homogenized Be_{12}Ti pebbles.

To prevent the increase of hydrogen generation reactivity associated with the increased specific surface

area, granulation experiments of prototypic pebbles of the $\text{Be}_{17}\text{Ti}_2$ and Be_{12}V compositions without peritectic reaction were carried out. Prototypic beryllide pebbles 1mm in diameter composed of single phase $\text{Be}_{17}\text{Ti}_2$ and Be_{12}V were successfully fabricated directly by granulation using the rotating electrode method without homogenization treatment. Analysis revealed that these prototypic pebbles of the $\text{Be}_{17}\text{Ti}_2$ and Be_{12}V compositions demonstrated a good oxidation property more than pure Be pebbles.

References

- [1] M. Nakamichi, K. Yonehara, Sintering properties of beryllides for advanced neutron multiplier, *Journal of Nuclear Materials* 417 (1-3) (2011) 765-768.
- [2] M. Nakamichi, J. H. Kim, Fabrication of beryllide pebble as advanced neutron multiplier, *Fusion Engineering and Design* 89 (7-8) (2014) 1304-1308.
- [3] M. Nakamichi, J. H. Kim, K. Yonehara, Novel granulation process of beryllides as advanced neutron multipliers, *Fusion Engineering and Design* 88 (2013) 611-615.
- [4] M. Nakamichi, J. H. Kim, Homogenization treatment to stabilize the compositional structure of beryllide pebbles, *Journal of Nuclear Materials* 440 (1-3) (2013) 530-533.
- [5] M. Nakamichi, J. H. Kim, Fabrication and hydrogen generation reaction with water vapor of prototypic pebbles of binary beryllides as advanced neutron multiplier, *Fusion Engineering and Design*, 98-99 (2015) 1838-1842.
- [6] M. Nakamichi, J. H. Kim, M. Miyamoto, Fabrication and characterization of advanced neutron multipliers for DEMO blanket, *Journal of Nuclear Materials and Energy*, to be submitted, (2015).

2.7.2 Extrusion of Be-Ti powder at 650 °C

P. Kurinskiy^{1*}, A. Moeslang¹, D. Klimenko², S. Mueller³, A.A. Goraieb⁴

¹ - Karlsruhe Institute of Technology, Institute for Applied Materials- Applied Materials Physics (IAM-AWP), P.O. Box 3640, 76021 Karlsruhe, Germany

² - Karlsruhe Institute of Technology, Institute for Neutron Physics and Reactor Technology (INR), P.O. Box 3640, 76021 Karlsruhe, Germany

³ - Extrusion Research and Development Center, TU Berlin, Sekr. TIB 4/1-2, Gustav-Meyer-Allee 25, 13355 Berlin, Germany

⁴ - Karlsruhe Beryllium Handling Facility (KBHF GmbH), Herrmann-von-Helmholtz-Platz 1, 76344 Eggenstein-Leopoldshafen, Germany

Be-Ti rods could be used as initial material for fabrication of Be₁₂Ti pebbles by rotating electrode method.

It is known that the process of extrusion in double-walled containers is very promising from the point of view of production of long Be-Ti rods. The use of containers is determined, from one hand, by high toxicity beryllium and, on the other hand, it prevents direct contact of the extruded material with tools and ambient atmosphere.

Be-30.8 wt.% Ti powder mixture having the equivalent sizes of particles of 32-45 µm was extruded using inner and outer capsules from niobium and CuCrZr alloy, accordingly. Extrusion was performed at 650 °C with an extrusion ratio of 7:1. Influence of working temperature on the stability of material flow as well as the phase composition of produced Be-Ti rods was studied in this work.

Keywords: titanium beryllide, Be-Ti rods, wet milling process, hot extrusion.

1. Introduction

The process of extrusion of blended Be-Ti powder is considered to be very attractive for the fabrication of rods used by rotating electrode method (REM). Due to a high toxicity of beryllium and its compounds, double-walled containers were used for material encapsulation. Be-Ti powder having the composition of Be-30.8 wt% Ti corresponding to stoichiometric content of Be₁₂Ti intermetallic phase was in the process of extrusion.

Extrusion of encapsulated powder was performed at the Extrusion Research and Development Center located at Technical University of Berlin. After the removal of jackets, produced Be-Ti rods were cut into pieces for further investigation of their microstructural properties by means of X-Ray diffraction analysis and optical microscopy.

Since Be-Ti rods are planned to be melted by REM using electric current, the values of electric resistance are the matter of a great interest. Four-point measurement method was used for the evaluation of characteristics of the electric resistance of rods.

The impact of temperature on characteristics of microstructure of produced rods and material flow during the extrusion process is discussed in this paper.

2. Experimental

2.1 Initial materials

Be-30.8 wt% Ti blended powders with the equal sizes of particles of 32-45 µm were used in the process. Beryllium and titanium powders were supplied by Materion Inc. and Alfa Aesar GmbH, accordingly. Operation of vibrational sieving was used for the extraction of the needed powder fractions.

Niobium and the copper-based CuCrZr alloy with the small additives of chromium and zirconium were used as encapsulating materials by the extrusion. The chemical composition of CuCrZr is shown in Table 1.

Table 1: Chemical composition of CuCrZr alloy

Alloying elements, wt%		
Cu	Cr	Zr
balance	0.6-0.8	0.07-0.15

author's email: petr.kurinskiy@kit.edu

2.2 Powder encapsulation and extrusion

Jackets made from CuCrZr alloy and having outer and inner diameters of 83 and 45.2 mm, respectively, were used as the outer encapsulating.

Niobium inner jackets with the outer diameter of 45 and the wall thickness of 2 mm were used for Be-Ti powder canning. After the Be-Ti powder outgassing at 120 °C, niobium capsules were inserted into CuCrZr jackets and sent to Extrusion Research and Development Center located at Technical University of Berlin.

Before the extrusion, the double-walled containers with Be-Ti powder inside were heated in a furnace in air up to 650 °C and held for 2 h at this temperature while the process tools (extrusion die, etc.) were heated up to 500 °C in ambient atmosphere in another furnace.

As in the previous experimental works [1,2], 8 MN extrusion press with the constant velocity of the ram displacement of 10 mm/s was used by the material processing. The diameter of produced rod (together with Cu-Cr-Zr jacket) was 32 mm and the calculated extrusion ratio was 7:1.

Fig. 1 shows encapsulated Be-Ti rods after their cutting by a disc saw.



Fig. 1 Encapsulated Be-Ti rods after their cutting by disc saw

2.3 Density measurements

Density values of six Be-Ti rods having the regular geometric shapes were calculated. The estimated values were in the range of 2.09...2.20 g/cm³. It should be noted that the density of the Be-30.8 wt% Ti compositional mixture (beryllium and titanium do not solve in each other) is 2.65 g/cm³. Therefore, the densities of obtained Be-Ti rods correspond to 79...83% of their theoretical values. Some deviation in density values can be explained by a certain inhomogeneity of material flow during the extrusion process. Noteworthy, pure Be₁₂Ti phase has a density of 2.26 g/cm³ [3].

2.4 Measurements of electric resistance of extruded Be-Ti rods

The four-point method of measurement of electric resistance (Fig. 2) was applied for the evaluation of ohmic characteristics of fabricated Be-Ti rods. Direct current (DC) in the range of 5...10 A and additional shunt having the resistance of 1 kOhm were applied in the circuitry. Taking into account that the resistance of fabricated rods will be low, the electric shunt was switched into a circuitry for the precise determination of the electric current. Investigated rod was placed in the glove-box and the voltmeter outside showed the potential difference between the ends of the rod. Thus, the electric resistivity was calculated by dividing of the voltmeter values by the current values on the shunt.

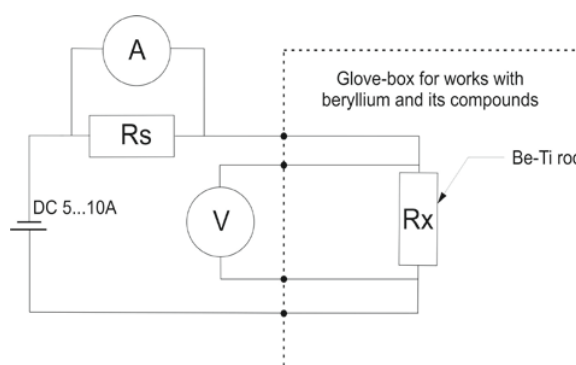


Fig. 2 Electric circuitry used by measurements of electric resistivity of Be-Ti rods

Electric resistivity of six Be-Ti rods (active measured length is 90 mm) was measured and all obtained values lie in the range of 26.3...31.2 μOhm. Observed difference could be determined by a slight variation between diameters and porosities of produced rods.

3. Study of microstructure of extruded Be-Ti rods

3.1 Optical microscopy

Discs cut from Be-Ti rod were embedded and then its surface was ground and polished in the direction which was transverse with the respect to an extrusion axis. KEYENCE VHX 500 optical digital microscope was used for study of microstructure of Be-Ti rod.

It was found that pores having the average sizes of about 20-30 μm are distributed not homogeneously within the whole volume of the rod: the central inner part is characterized by a bigger porosity while the peripheral outer part has a higher density. Fig. 3 and Fig. 4 show, accordingly, microstructure of the outer and inner parts of Be-Ti rod.

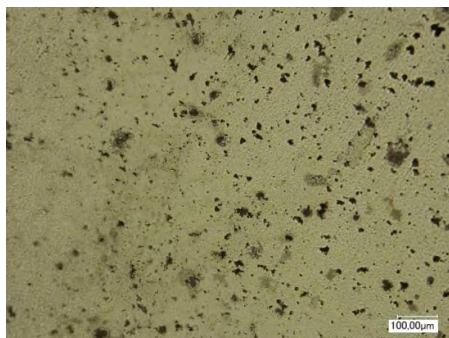


Fig. 3 Microstructure of peripheral outer part

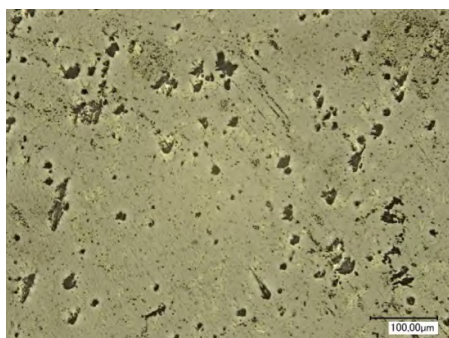


Fig. 4 Microstructure of the inner part of Be-Ti rod

3.2 X-Ray diffraction (XRD) analysis

Three pieces cut, accordingly, from the head, middle and end parts of Be-Ti rod were investigated by means of XRD. All three X-Ray patterns were identical and showed no evidence on the presence of any intermetallic phases (Fig. 5): only pure α -Be and α -Ti phases were detected by XRD measurements.

Obviously, processing temperature of 650 °C is not high enough for the intensive formation of Be-Ti intermetallic compounds.

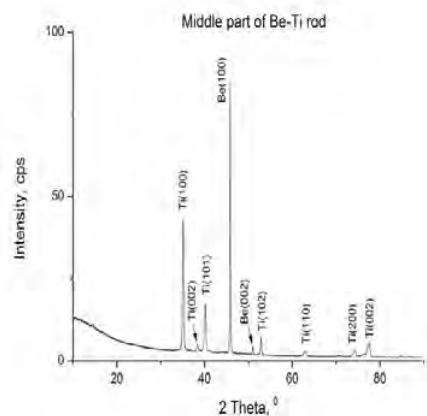


Fig. 5 X-Ray diffraction pattern of Be-Ti rod (middle part)

4. Summary

A phase composition of extruded powders has a big influence on homogeneity of material flow during an extrusion process. According to XRD results, the formation of brittle Be-Ti intermetallic phases has been avoided what contributed to an enhanced plasticity of Be-Ti powder mixture at processing temperature. On the other hand, the intensive formation of Be_{12}Ti phase leads to a volume increase of Be-Ti compositional mixture what is, obviously, accompanied by formation of the multiple pores and cracks.

A proper correlation between mechanical properties of encapsulating materials as well as of the extruded material contributes to smooth processing without a rupture of capsules or cores [4]. Niobium and CuCrZr alloy have yield strength values at 650 °C of approx. 100 and 130-140 MPa, accordingly. It is quite difficult to make an accurate statement corresponding to mechanical properties of the stab which was sintered at 650 °C out of blended beryllium and titanium powders. In any case, some acceptable ratio between mechanical properties of the core and capsules was achieved what lead to a fabrication of Be-Ti rods having the lengths of about 1.5 m.

From the point of view of safety by working with highly toxic beryllium, the structural integrity of capsules remained intact. So, one could conclude that niobium and CuCrZr alloy selected as materials of inner and outer capsules, accordingly, can be further used as encapsulating materials by extrusion of beryllium-based rods.

The influence of the particle sizes of initial Be-Ti powder on the process flow still needs to be investigated. Obviously, this factor has a great impact on mechanical performance of Be-Ti rod inside of capsule and a intensity of formation of possible intermetallic phases by the processing at elevated temperatures.

References

- [1] P. Kurinskiy, A. Moeslang, H. Leiste, A.A. Goraieb, Characterisation of Be-Ti rod fabricated by extrusion at 900 °C, Proceedings of 11th IEA Int. Workshop on Beryllium Technology, (2015) 57-63.
- [2] P. Kurinskiy, H. Leiste, A.A. Goraieb, S. Mueller, Hot extrusion of Be-Ti powder, Fusion Engineering and Design, 98-99 (2015) 1817-1820.
- [3] Ch. Dorn, W. Haws, E. Vidal, A review of physical and mechanical properties of titanium beryllides with specific modern application of TiBe_{12} , Fusion Engineering and Design 84 (2009) 319-322.
- [4] K. Mueller et al., Grundlagen des Strangpressens, Renningen-Malmsheim: Expert Verlag, (1995) 222-230

2.7.3 Ab-initio simulations of intrinsic defects in Be₁₂X (X=Ti,V,W,Mo)

Matthew L. Jackson¹, Patrick Burr, Robin W. Grimes

*¹Imperial College London, London, United Kingdom
E-mail: Matthew.jackson1809@imperial.ac.uk*

Be₁₂X, where X is a transition metal, is a promising family of materials for the first wall and neutron multiplying material in future nuclear fusion reactors owing to their low atomic number, high beryllium content and improved thermo-mechanical properties over pure beryllium. This study employs ab-initio simulations to investigate the accommodation and migration of intrinsic defects across this family of materials to inform predictions of the evolution of the microstructure and accordingly thermo-physical properties under conditions expected in a future fusion reactor.



Ab-initio simulations of intrinsic defects in Be_{12}X ($\text{X} = \text{Ti}, \text{V}, \text{W}, \text{Mo}$)

Matthew Jackson*, Patrick Burr, Robin W. Grimes

*Email : mj1809@ic.ac.uk

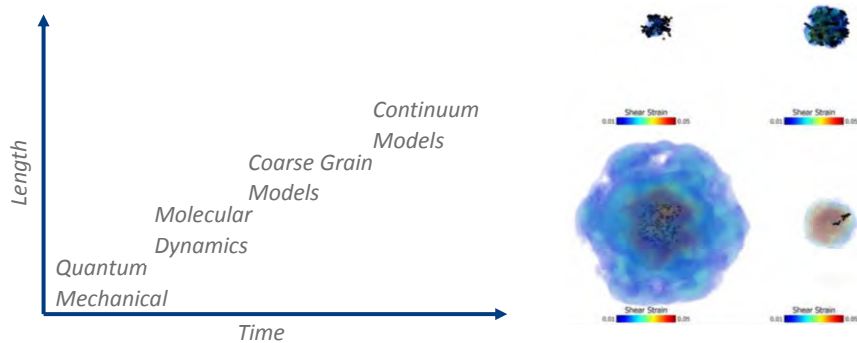


Overview

- Motivation
- Computational Methodology
- Crystal Structure & Defect Morphology
- Defect binding energies
- Migration

Motivation

- All materials originally investigated as candidates for neutron multipliers, Be₁₂Ti favourite, Be₁₂W formed in diverter anyway.
- Multiscale modelling approach ultimately aims to model microstructural evolution over lifetime of a component



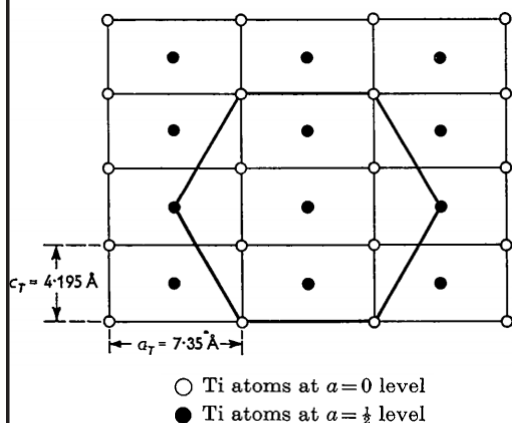
Computational Methodology

All simulations performed using the castep code utilising **Density Functional Theory (DFT)**

DFT solves an approximation of the ground state Schrödinger equation (albeit with several assumptions)

Very computationally expensive – Limited to small cells (250 atoms) with periodic boundary conditions

Crystal Structure



Gillam, E., Rooksby, H. P. & Brownlee, L. D. Structural relationships in beryllium-titanium alloys. *Acta Crystallogr.* **17**, 762-763 (1964).

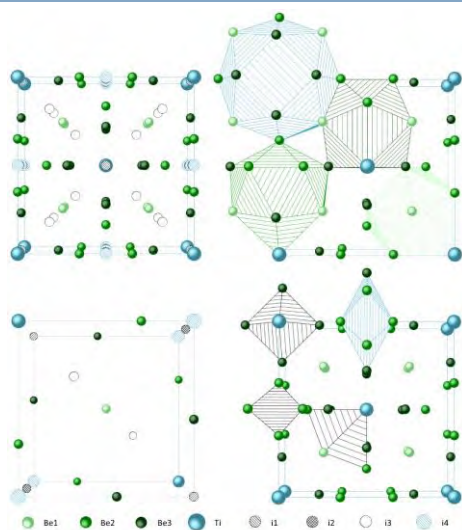
Crystal structure of Be_{12}V , Be_{12}Mo , Be_{12}W is I_4/mmm tetragonal

Be_{12}Ti variously reported as P_6/mmm Hexagonal & I_4/mmm tetragonal

The two phases are closely related, main difference is shift of Ti site, give similar diffraction patterns

Preliminary simulations show I_4/mmm stable ~ 1.2 eV/formula unit at 0K, currently extending to finite temperature.

Interstitial Sites



- 3 Be sites labelled 1 - 3
- 4 stable interstitial sites labelled i1-i4
- i4 site only stable for X species, Be relaxes to i2 site
- Sites i4 and i3 have high multiplicity

Intrinsic defects

E _f /defect (eV)					
Defect	Be ₁₂ V	Be ₁₂ Ti	Be ₁₂ Mo	Be ₁₂ W	Be ₁₂ W ^a
V _{Be1}	1.59	1.60	1.59	1.38	1.38
V _{Be2}	1.48	1.43	1.34	1.20	1.14
V _{Be3}	1.64	1.53	1.66	1.47	1.48
Be _{i1}	2.95	3.19	3.54	3.81	-
Be _{i2}	2.03	1.86	2.37	2.50	-
Be _{i3}	3.54	3.69	3.92	4.14	-

E _f /defect (eV)					
Defect	Be ₁₂ V	Be ₁₂ Ti	Be ₁₂ Mo	Be ₁₂ W	Be ₁₂ W ^a
V _X	3.37	4.10	3.61	3.16	3.25
X _{i1}	4.81	5.37	7.25	8.11	-
X _{i2}	4.79	5.10	5.59	6.47	-
X _{i3}	5.59	7.47	8.79	10.10	-
X _{i4}	4.69	4.19	4.83	5.22	-

- V_{Be2} lowest energy vacancy for all materials
- Be_{i2} by far lowest energy interstitial site in all materials
- X_i and V_X have considerably higher E_f than Be_i and V_{Be}
- X_{i4} site lowest energy site for all materials (approximate position of X site in hexagonal P₆/mmm pseudocell)

^a - Allouche, A., Fernandez, N. & Ferro, Y. Hydrogen retention and diffusion in tungsten beryllide. *J. Phys. Condens. Matter* **26**, 315012 (2014). (DFT data)

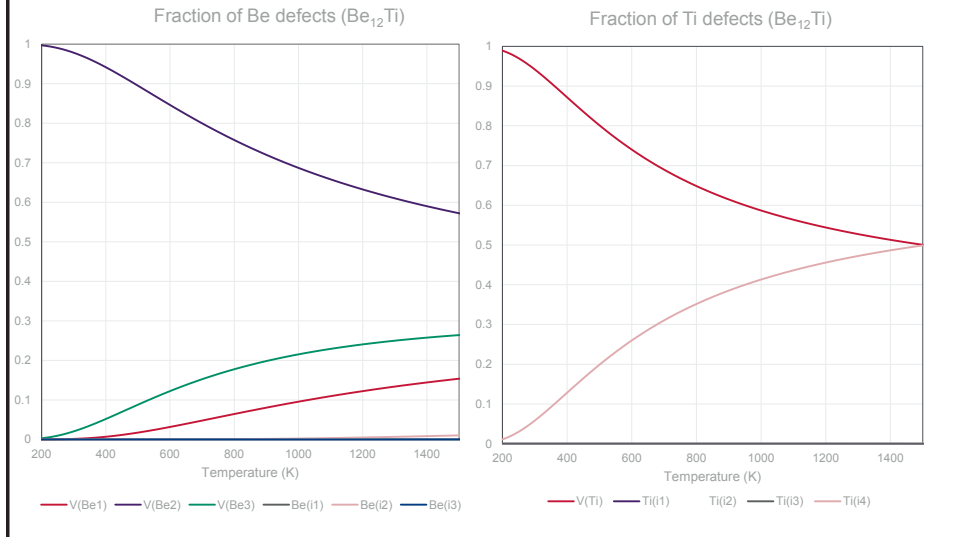
Intrinsic defect processes

defect	E _f /defect (eV)			
	Be ₁₂ V	Be ₁₂ Ti	Be ₁₂ Mo	Be ₁₂ W
Be Frenkel	1.76 - 2.59	1.64 - 2.65	1.86 - 2.79	1.85 - 2.80
X Frenkel	4.03 - 4.48	4.15 - 5.73	4.41 - 6.86	4.55 - 6.63
Schottky	1.63 - 1.77	1.63 - 1.79	1.51 - 1.81	1.35 - 1.60
Anti-site	1.91 - 2.97	2.25 - 3.41	2.33 - 3.62	3.28 - 3.60

Schottky disorder lowest energy defect process

Frenkel disorder similar in Be₁₂Ti and Be₁₂V

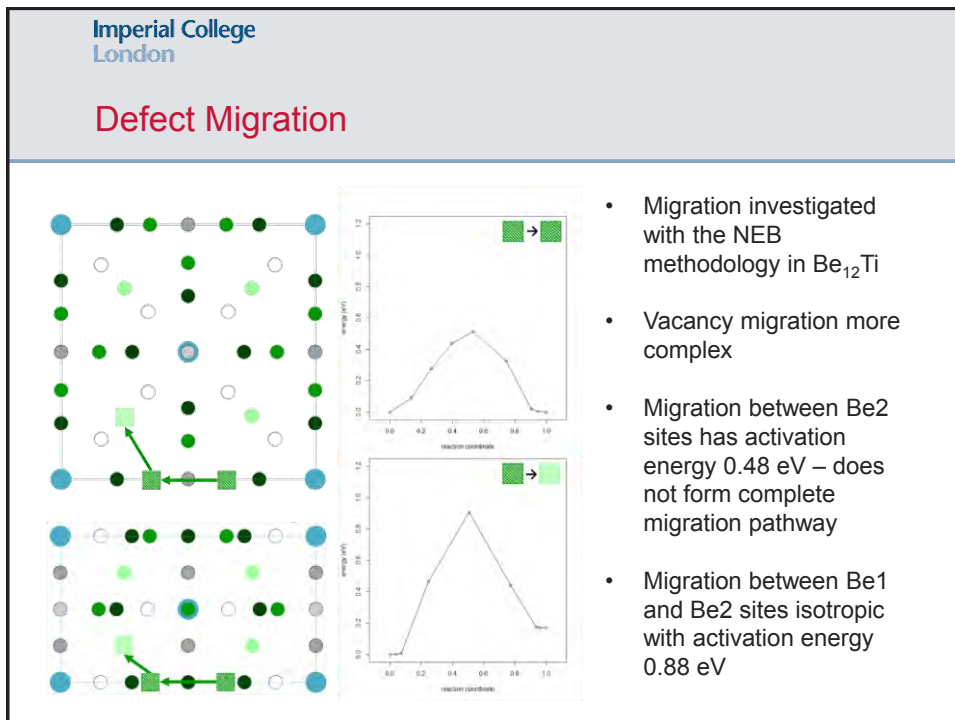
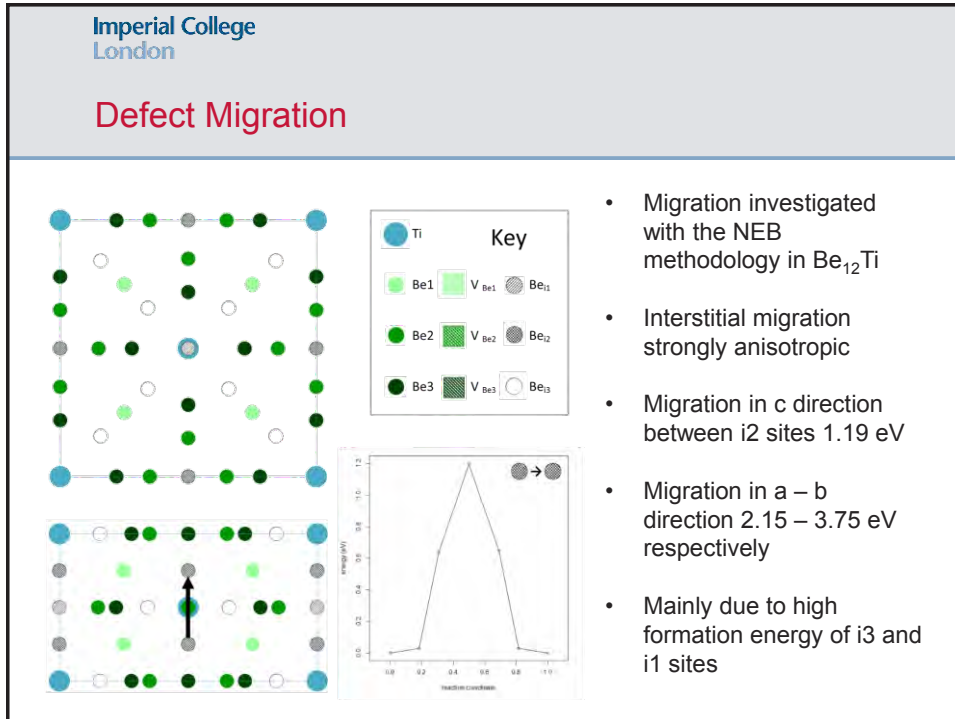
X metal intrinsic defects



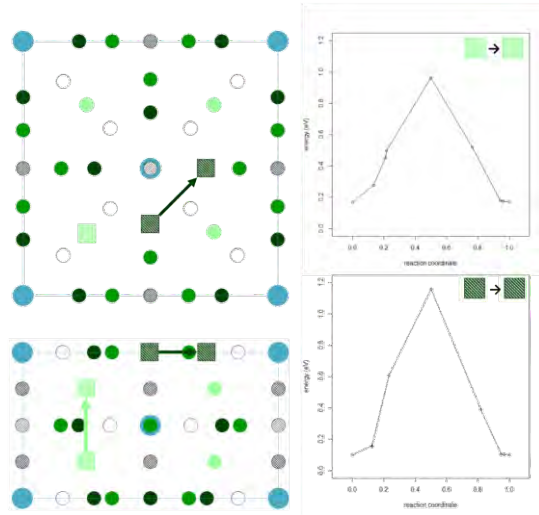
Defect binding energies

defect	E _B (eV)			
	Be ₁₂ V	Be ₁₂ Ti	Be ₁₂ Mo	Be ₁₂ W
V _{Be} V _{Be}	-0.21 - 0.37	-0.22 - 0.45	-0.09 - 0.35	-0.02 - 0.74
V _X V _X	0.75	0.5	0.58	0.72
V _X V _{Be}	-0.50 - 0.11	-0.32 - 0.07	-0.40 - 0.26	-0.34 - 0.14
Be _i Be _i	-0.10 - 1.96	-0.10 - 2.50	0.08 - 2.18	0.09 - 2.32

- Binding energy of vacancies ranges from slightly negative to very positive – most stable are bound Be2 vacancies
- Binding energy of V_XV_{Be} mostly negative – driving force for void nucleation?
- Binding energy of interstitials slightly negative only for two Be interstitials on a single i4 site
- More work needed to explore larger clusters



Defect Migration



- Migration investigated with the NEB methodology in Be_{12}Ti
- Migration between Be1 sites in c direction has activation energy 0.78 eV – thus vacancy migration is slightly anisotropic
- Migration between Be3 sites in a-b plane has activation energy 1.19 eV

Summary

- Tetragonal phase stable for Be_{12}Ti
- Be2 lowest enthalpy vacancy site and i2 lowest enthalpy interstitial site, vacancies dominate on Be sublattice, less so on X sublattice.
- Weak negative binding energy for certain divacancy combinations.
- Schottky lowest energy defect process
- Interstitial migration strongly anisotropic, vacancy migration lower energy and weakly anisotropic.

2.7.4 Synthesis of Beryllides Powder for Advanced Neutron Multiplier

Y. Natori¹, Y. Minagawa¹, K. Yonehara¹, K. Tatenuma¹, M. Nakamichi²

¹ *Kaken Inc., 1044 Hori, Mito, Ibaraki 310-0903, Japan*

² *Sector of Fusion Research and Development, Japan Atomic Energy Agency, 2-166, Omotedate, Obuchi, Rokkasho, Kamikita, Aomori, 039-3212, Japan*

Abstract

Beryllium metal is the candidate neutron multiplier in the pebble bed type of test blanket modules for ITER. On the other hand, advanced neutron multiplier with a higher stability at high temperature is required in pebble bed blankets, which would have a big impact on the DEMO design, especially the blanket operating temperature. Beryllium intermetallic compounds (beryllides) are the most promising advanced neutron multipliers. The establishment of fabrication techniques for beryllides is a key issue in the advanced neutron multiplier development. In this study, we report on the synthesis results of beryllides. The synthesis examination of several kinds of beryllides powder for the raw material of advanced neutron multiplier fabrication was carried out by a powder calcination process.

1. Introduction

In this synthesis examination, the target powdery beryllide compounds were selected as Be₁₂Ti, Be₁₃Zr, Be₁₂V, Be₁₂W, Be₁₂Ta, Be₁₂Mo, and Be₁₂Nb. Synthesis of beryllides was carried out using mixed pure Be and metal powders as stoichiometric value. These mixed powders were sintered in an inert gas atmosphere.

After calcination of mixed raw powder for Be₁₂Ti beryllide synthesis, beryllide powder consolidation was evaluated by X-ray Diffraction (XRD) and Electron Probe Micro Analyzer (EPMA) for structural analysis. From the result of XRD measurement, the formation of Be₁₂Ti as Be-Ti intermetallics was identified by calcination at 1373-1473 K for 24 h in Ar gas flow. Furthermore, other beryllides powders could be synthesized by the similar powder calcination process.

It was revealed that a wide variety of beryllides powder can be easily synthesized by the powder calcination process at a temperature lower than the melting point. The synthetic technology of this study is suitable for mass-production of beryllides powder. We'll also indicate about an improved powdery quality by this beryllide processing.

2. Experimental/Methodological

2.1 Powder Synthesis of Beryllium Intermetallics Compounds¹⁻³⁾

As a method of producing beryllide powders, a simple calcination method was considered. The examined powdery beryllide compounds which were carried out by calcination method are Be₁₂Ti, Be₁₃Zr, Be₁₂V, Be₁₂W, Be₁₂Ta, Be₁₂Cr, Be₁₂Mo, and Be₁₂Nb. The synthesis method is calcination in an inert gas atmosphere: two kinds of metallic powder (Be+Metal) which serves as materials of beryllide are mixed by stoichiometry value. The properties of beryllide powders synthesized by calcination were then evaluated. The physicality and melting point of the target beryllide compounds are shown in Table 1. The case of Be-Ti is shown for the synthetic method of the examined beryllide powder as an example. As shown in Fig.1, The case of Be₁₂Ti which is one of the candidate material, mixture value of Be and Ti powder were 69.3wt%Be – 30.7wt%Ti. Next, the mixed powders are sintered in an inert gas atmosphere in an alumina crucible. Then, Be₁₂Ti could be synthesized. The most important point of this method is that calcination temperature

should be lower than the melting point. The aim of this study is that the synthesis of beryllide powders at lower temperature without melting.

Table 1 Target beryllides

	Target Beryllide	Density [g/cm ³]	Be content [wt%]	Melting point [K]
Be-Ti	Be ₁₂ Ti	2.26	69.30	1,823
Be-Zr	Be ₁₃ Zr	2.72	56.22	2,200
Be-V	Be ₁₂ V	2.37	67.98	1,973
Be-W	Be ₁₂ W	4.57	37.04	2,020
Be-Ta	Be ₁₂ Ta	4.18	37.41	2,123
Be-Cr	Be ₁₂ Cr	2.44	67.53	1,610
Be-Mo	Be ₁₂ Mo	3.02	45.52	1,973
Be-Nb	Be ₁₂ Nb	2.88	53.79	1,945

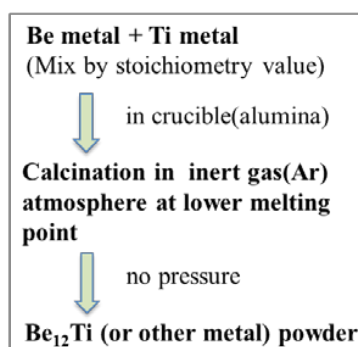
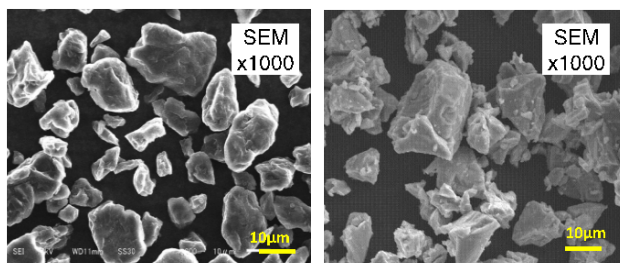


Fig.1 Synthetic method of powdery beryllides

2.2 Be-Ti Intermetallic Compound^{1~3)}

The synthesis of Be₁₂Ti powder was examined using mixed powders of Be and Ti. The purities of Be and Ti powder used in this study, were 99.6% and 99.9%, respectively and their particles of 45 micrometers or smaller were used as shown in Fig. 2. The result of thermogravimetry and differential thermal analysis (TG-DTA) of mixed Be and Ti powders is shown in Fig. 3. From the TG-DTA data, it is surmised that the conversion to beryllide compound occurs at the point of exothermic peak at 1373K. Based on this effect, the calcination temperature was decided at 1373 K.



Be powder
<45µm

Ti powder
<45µm

Fig.2 Raw materials of Be and Ti powders

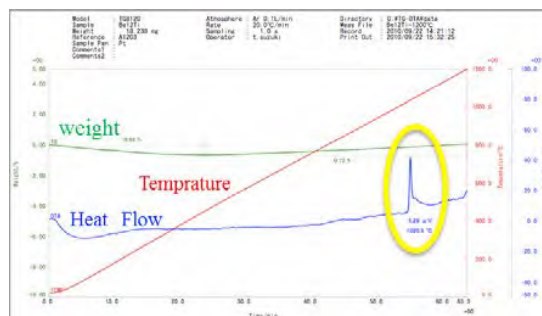


Fig.3 TG-DTA of Be+Ti
rt~1473K(20K/min) in Ar(0.1L/min)

The SEM photographs and X-ray diffraction (XRD) measurement after calcination of the mixed powders at 1373K for 24 h under Ar are shown in Fig. 4 and Fig. 5, respectively. From the result of a crystal structure analysis by using the XRD, the formation of Be_{12}Ti as Be-Ti intermetallics was identified. Therefore it was obvious that Be_{12}Ti powder could be synthesized by calcination at 1373 K.

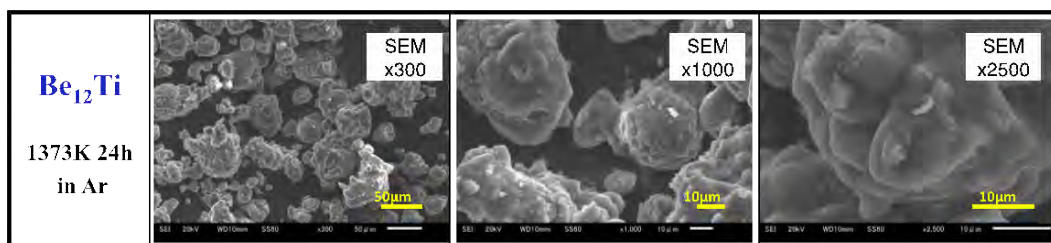


Fig. 4 SEM photograph after calcination of Be+Ti powders at 1373K for 24h in Ar

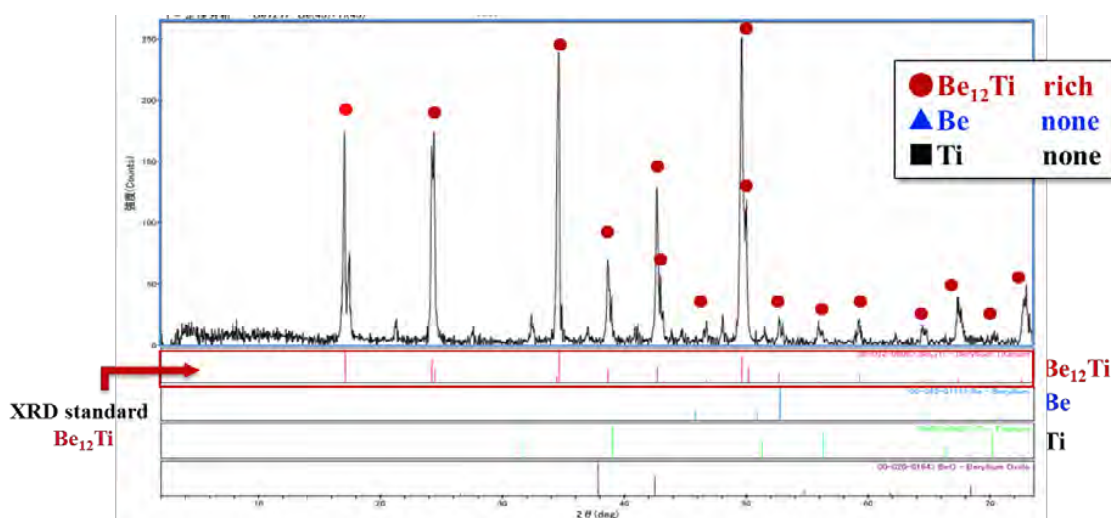


Fig. 5 XRD result of 12Be+Ti powders treated at 1373K for 24h in Ar

To investigate the effect of the calcination holding time, we carried out the calcination at 1373K for 0, 3, 12, 24 and 48 h. The structural analyses using XRD and the electron probe micro analyzer (EPMA) were conducted. From To investigate the effect of the calcination holding time at 1373K as shown in Fig.6, some parts of Be may be remained and unreacted if the holding time is less than 3h, but Be_{12}Ti beryllide synthesis could be mostly completed by more than 12 h at 1373K.

The EPMA and SEM photographs of the calcination holding time of 0, 3, 12, 24 and 48h after reached to 1373K are shown in Fig.7. The beryllide powder is composed of two colors, black and white area which corresponds to beryllide and unreacted Be. By the result of increase of Be_{12}Ti area with long holding time, Be_{12}Ti seems to have increased with holding time in proportion. In Fig. 8, the line graph shows the relation between the growth of Be_{12}Ti and the holding time. By judging from the data of EPMA and XRD, it is assumed that the growth of Be_{12}Ti was mostly completed more than 12h, because this graph shows that the conversion from Be and Ti to Be_{12}Ti is mostly saturated over 12 h.

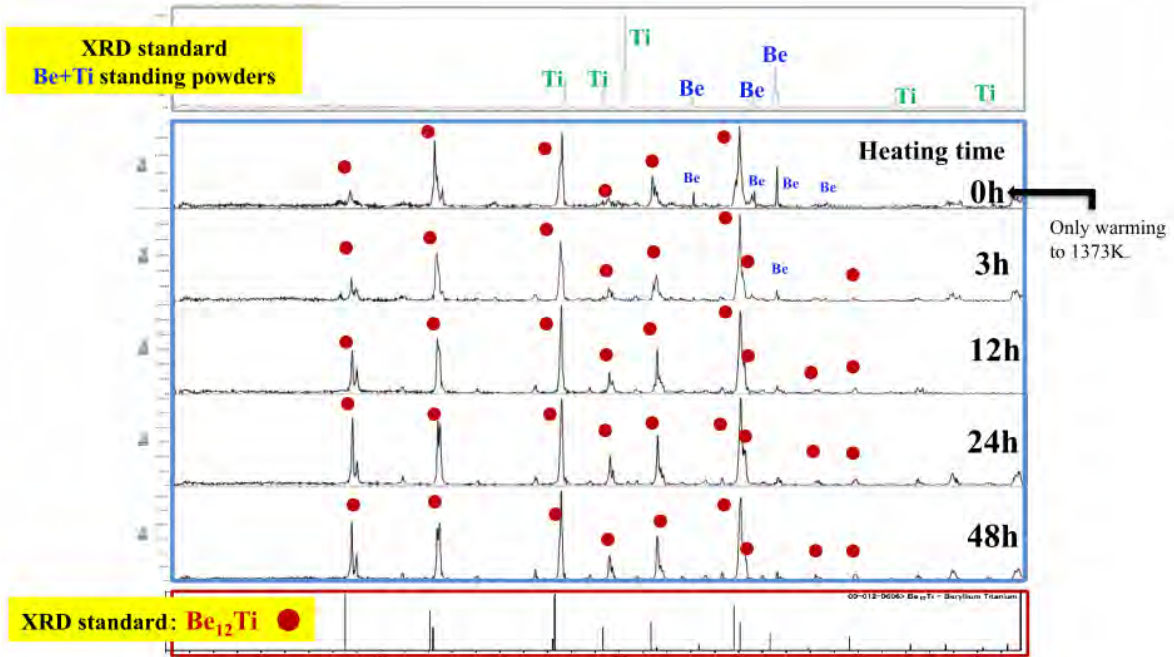


Fig. 6 Effect of calcination holding time of 12Be+Ti at 1373 K

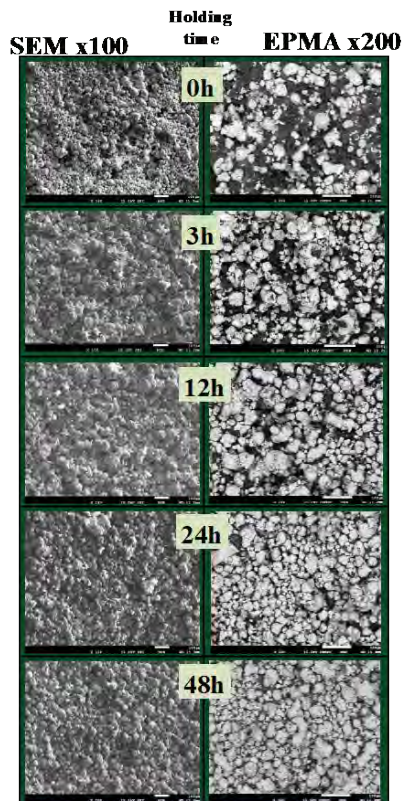


Fig. 7 EPMA and SEM photographs of calcination holding time of 12Be+Ti at 1373K
White area in EPMA is $Be_{12}Ti$ and Black is unreacted Be.

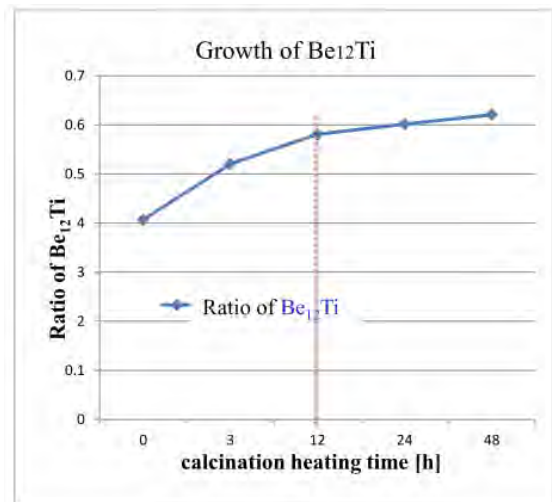


Fig. 8 Relation between the $Be_{12}Ti$ growth and calcination holding time at 1373K

2.3 Other beryllium intermetallic compounds^{1~3)}

As the other synthesis example of Be intermetallic compounds of Be-Zr, Be-V, Be-Ta and Be-W those examination results are indicated.

At first, in the case of the powder of Be and Zr mixed by the ratio of 13 mol and 1 mol, the data of XRD after calcination at 1473K for 24 h under Ar is shown in Fig. 9. From the result, the formation of Be₁₃Zr as Be-Zr intermetallic compound was identified as single phase mostly. Synthesized Be and Zr compound are exactly fitted to Be₁₃Zr peaks with its XRD-standard.

Next, in the case of the powder of Be and V mixed by the ratio of 12 mol and 1 mol, the data of XRD after calcination at 1473K for 24 h under Ar is shown in Fig. 10. From the result of a measurement of XRD, the formation of Be₁₂V as Be-V intermetallics was identified. Some parts of Be seems to remain as it unreacted.

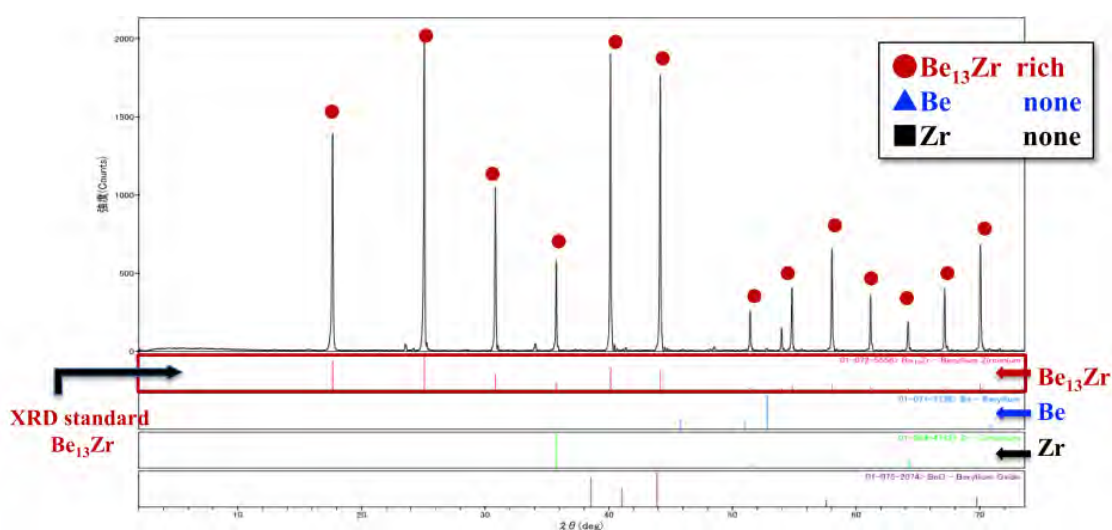


Fig. 9 XRD result after calcination of Be+Zr powders at 1473K for 24h in Ar.

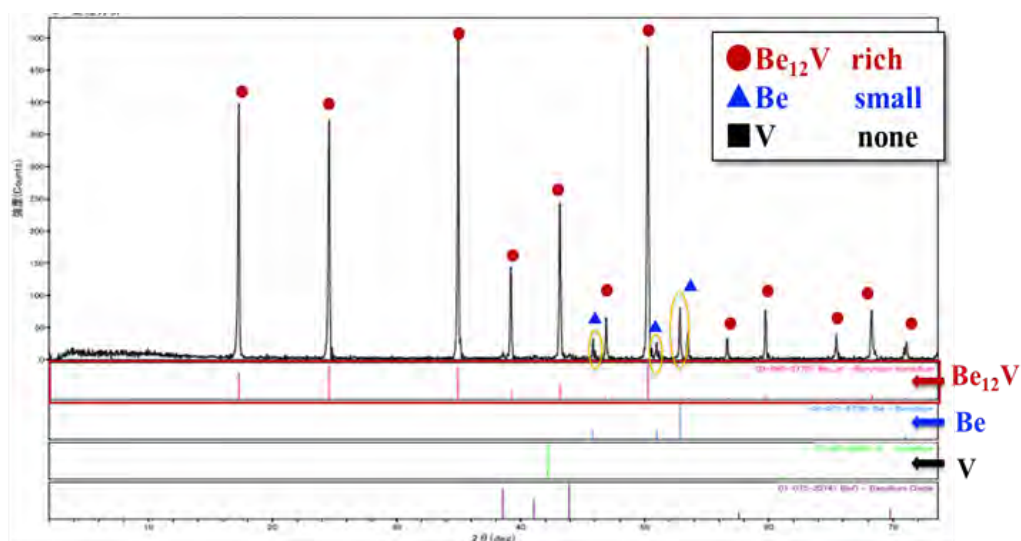


Fig. 10 XRD result after calcination of Be+V powders at 1473K for 24h in Ar.

In the case of the powder of Be and Ta mixed by the ratio of 12 mol and 1 mol, synthesized at 1473K for 24 h under Ar, three kinds of multi-phase mixture of Be_{12}Ta , $\text{Be}_{17}\text{Ta}_2$, Be_3Ta , Be_2Ta were identified as shown in Fig. 11.

And, in the case of powder of Be and W mixed by the ratio of 12 mol and 1 mol, by synthesized at 1473K for 24 h under Ar. The XRD result indicated that two phases of Be_{12}W and Be_{22}W as Be-W intermetallic were identified (Fig.12). Regarding to Be-W intermetallic compound, it is necessary to find out sintering condition in more detail.

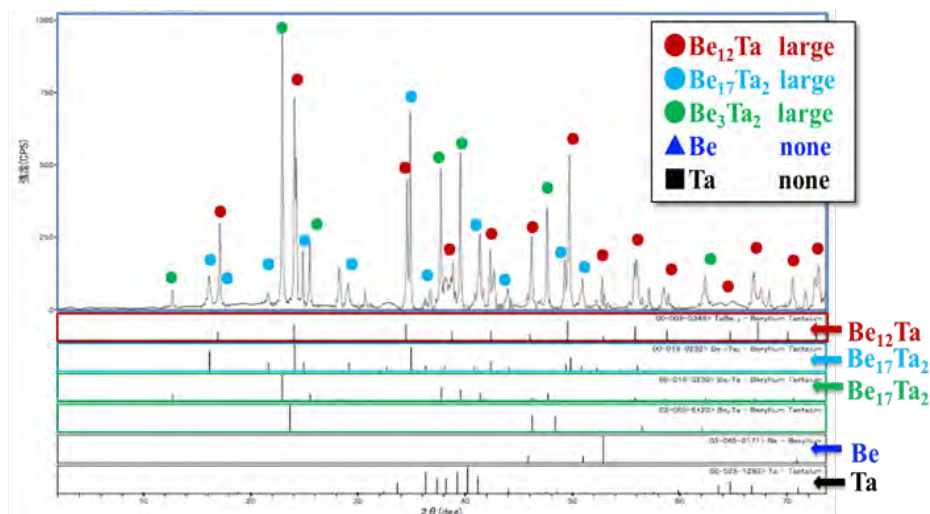


Fig.11 XRD result after calcination of 12Be+Ta Powders at 1473K for 24h in Ar.

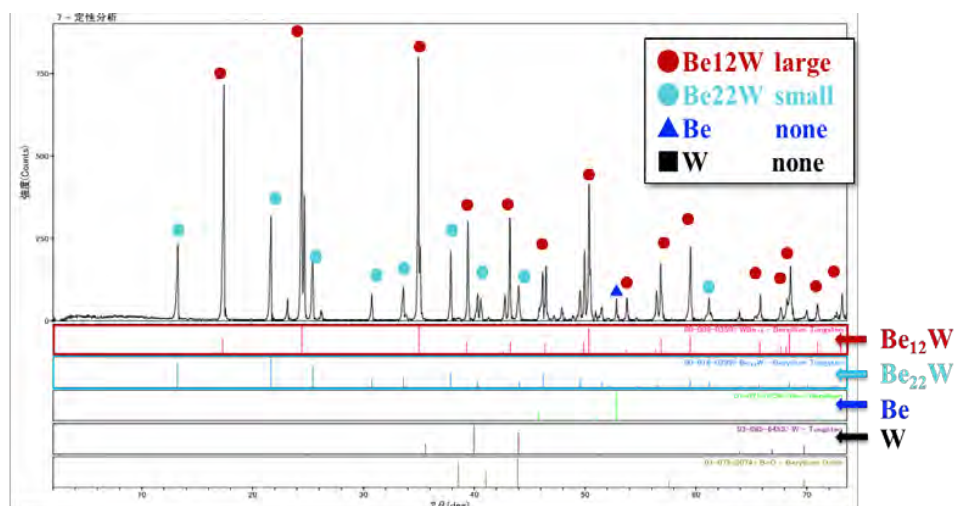


Fig.12 XRD result after calcination of 12Be+W Powders at 1473K for 24h in Ar.

3. Summary

The target beryllides and their synthesis conditions are shown in Table 2. As the panoptic result of this study, it is possible to fabricate wide variety of beryllide powders by the calcination only using mixed powders of Be and another metal. This method is very simple, by calcination in inert atmosphere only. Because Be-W and Be-Ta are composed of multi-phase compositions, however, it is needed to determine an optimum condition to make a single phase of Be_{12}Ta and Be_{12}W . In a future, the detail examination of calcination temperature and holding time is required.

Table-2 Calcination conditions for synthesizing beryllides powder by mixed elemental powers of Be and metals.

Target Beryllide		Synthesis condition
Be-Ti	Be_{12}Ti	1373~1473K, 24h in Ar
Be-Zr	Be_{13}Zr	
Be-V	Be_{12}V	
Be-W	Be_{12}W	
Be-Ta	Be_{12}Ta	
Be-Cr	Be_{12}Cr	
Be-Mo	Be_{12}Mo	
Be-Nb	Be_{12}Nb	

4. Conclusion

The calcination experiments showed that the intermetallic compound beryllide can be directly synthesized by only calcination from mixed elemental powders of Be and Ti (or, others) at a relative lower temperature than the melting point. It is necessary to find out the optimum conditions of the heat-treatment according to the kind of various beryllium intermetallic compounds.

In conclusion, these are the main results of this study, beryllium intermetallic compounds can be directly synthesized by only heating. The synthetic process is very simple and easy to control. And, the beryllide powders can be synthesized with a high reproducibility. On the other hand, as a next step, two additional examinations will be conducted as following: one is to find out the optimum conditions of the heat-treatment. Another is to examine how particle size of the raw materials affects. As a future plan, the fabrication technology of wide variety of beryllide powders with a high quality as single phase will be developed, and the adequate mass-production technology of beryllide powders for advanced neutron multiplier fabrication will be realized.

REFERENCES

- [1] Proceedings of the Sixth IEA International Workshop on Beryllium Technology for Fusion, JAERI-Conf 2004-006, pp.172-183.
- [2] H. Okamoto and L. Tanner, Phase diagrams of Binary Beryllium Alloys, ASM International, Materials Park OH, (1987), p.211.
- [3] H. Okamoto, Desk Handbook Phase Diagrams for Binary Alloys, ASM International (2000), pp.138-139.

2.7.5 Preliminary characterization of Beryllides as advanced neutron multiplier

J-H. Kim, S. Nakano, M. Nakamichi

¹ *Sector of Fusion research and Development, Japan Atomic Energy Agency, JAEA,*

2-166, Omotedate, Obuchi, Rokkasho, Kamikita, Aomori, 039-3212, Japan.

E-mail: kim.jaehwan@jaea.go.jp

Abstract

DEMO reactors require advanced neutron multipliers that have higher stability at high temperature. Beryllium intermetallic compounds (beryllides) are the most promising advanced neutron multipliers. Development of advanced neutron multipliers has been started between Japan and the EU in the DEMO R&D of the International Fusion Energy Research Centre (IFERC) project as a part of the Broader Approach activities. We suggested a new beryllide granulation process, which was combinational process with a plasma sintering method and a rotating electrode method (REM). The plasma sintering is simple, easy to control and can reduce the time of the beryllide electrode fabrication by approximately 30 %, compared to the hot isostatic pressing method as conventional methods. Moreover, the REM has a lot of experiences for not only beryllium granulation in the fusion field but fabrication of metallic pebble in industry in general. The prototypic beryllide pebbles were successfully fabricated by the REM using the plasma-sintered beryllide electrode.

In this report, the preliminary characterization of Be-Ti beryllides was carried out such as reactivity with water vapor, microstructure analysis by ion irradiation effect and deuterium retention property compared with beryllium (Be) metal. From the result of the preliminary characterization, it revealed that plasma sintered Be-Ti beryllide sample has a good performance as a neutron multiplier. This beryllide sample has enough oxidation resistance, high radiation resistance and low deuterium retention property more than Be metal.

1. Introduction

Beryllium intermetallic compounds (beryllides) have attracted great attention owing to stability at high temperature as well as swelling property. Development of advanced neutron multipliers has been started between Japan and the EU in the DEMO R&D of the International Fusion Energy Research Centre (IFERC) project as a part of the Broader Approach activities. In this study, fabrication and characterization of Be-Ti beryllides with different chemical composition will be introduced.

2. Experimental/Methodological

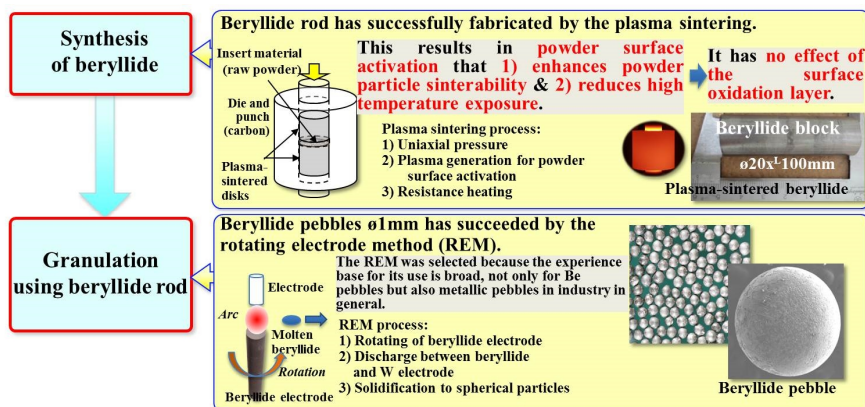


Fig.1 Necessity of advanced neutron multiplier

A combinational process (Fig.1), plasma sintering and rotating electrode method (REM) was applied for the granulation of beryllides with different chemical composition. Prior to the REM for granulation, beryllide rods with different titanium content were sintered under same conditions, which the plasma sintering temperature used in the experiments was 1,073 K while the sintering times were 2 min and 30 sec with heating and cooling rates of 100 and 200 K/min, respectively. To investigate the effect of Ti content on mechanical property and reactivity in beryllide pebbles, the powder composition was varied among 3, 5, 6, 7, 7.7, 9 and 10.5 at. % Ti. In order to understand the mechanical property of the beryllide pebble, compression test (Autograph, AG-X10kNX, Shimadzu, Japan) was carried out with test speed of 0.5 mm/min. Additionally, The reactivity of the beryllides with 1 % H₂O was examined using a thermo-gravimetric apparatus (TG-DTA, TG-8110, Rigaku,CP- Japan), connected with a gas chromatography unit (GC,4900, Agilent, USA). This analyzed the H₂ gas generated by the reaction between beryllides pebble and Ar gas containing 1% water vapor. The experiment was carried out using a temperature ramp of 100 K/min. For clarity, Ar gas with 1% H₂O was introduced (HUM, Rigaku, Japan) at the test temperatures at 1273 K while a flow of Ar gas (99.9999%) was present during temperature ramping.

3. Results and discussion

Fig.3 shows the surface and cross sectional SEM images of the beryllide pebbles with different Ti content, demonstrating in the surface image that Be phase on surface exists in 3 and 5 at.% Ti beryllide pebbles while there was no Be phase on the surface in 7, 7.7, 9 and 10.5 at. % Ti beryllide pebbles. As shown in cross-sectional SEM images, however, it was obvious that the beryllide pebbles with 3 to 9 at.% Ti contain Be phase with different area fraction. EPMA qualitative analysis inferred that the beryllide pebbles with 3 and 5 at.%Ti consisted of two phases, Be and Be₁₂Ti, whereas those with 6 to 9 at. % Ti did three phases, Be, Be₁₂Ti and

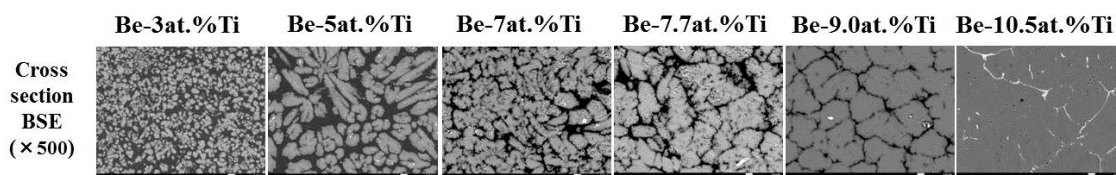


Fig.3 Cross-section SEM images of the pebbles

Fig.4 depicts load and displacement of the pebbles as function of Ti content during the compressive test and fracture SEM images. It demonstrates that the lower Ti content the pebble contains the longer displacement it indicates while the higher collapse load it shows. As mentioned in the SEM observation, this variation can be explained by the fact that the pebbles with higher Ti were mainly consisted of larger fraction of Be_{12}Ti and $\text{Be}_{17}\text{Ti}_2$ phase which are much more brittle than Be phase. These mechanical properties are thought to be considerably dependent on how many ductile and brittle phases contained in the pebbles. As results of area fractions in the beryllide pebbles with different Ti content, accordingly, it is inferred that the pebble with larger fraction of the Be phase showed not only the higher collapse load but the longer displacement.

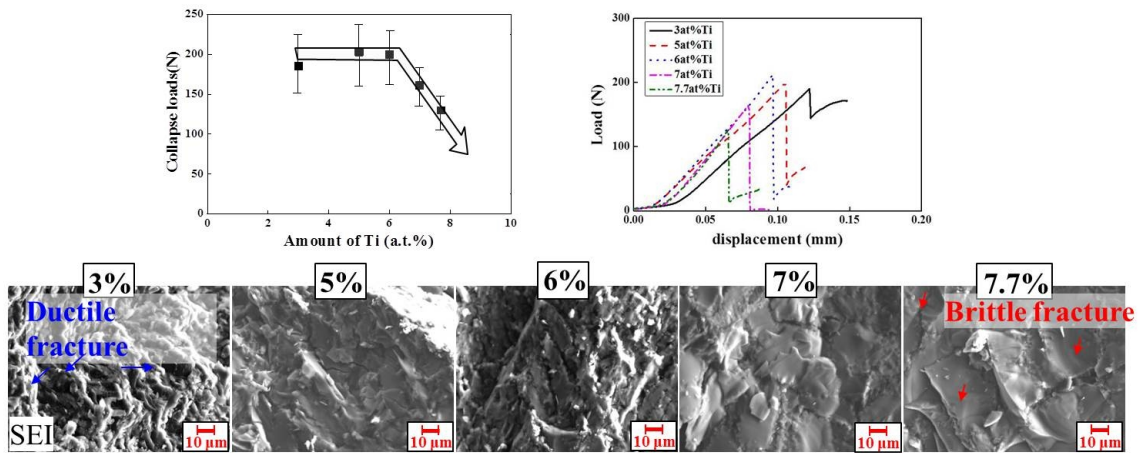


Fig.4 Collapse load/displacement and surface SEM images of the Be-Ti pebbles

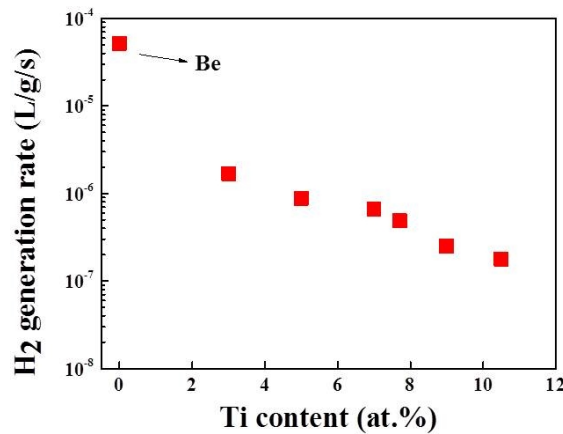


Fig.5 H_2 generation rate of the pebbles

Fig.5 indicates H_2 generation rate of the pebbles with different Ti amount, demonstrating that as Ti contents increased in Be-Ti beryllide, generated H_2 amount (including H_2 generation rate) as well as weight gain (not shown here) decreased because this is associated with decrease of Be phase fraction.

Accordingly, existence and fraction of Be phase in the beryllide pebbles resulted in variation of not only mechanical properties but also reactivity

4. Conclusion

We suggested and established a fabrication process of beryllide pebble, combined with plasma sintering for rod materials and rotating electrode method for granulation. Using this method, not only Ti beryllides pebbles with different Ti contents but Be_{12}V pebble (undergoing for Be_{13}Zr pebbles) were successfully fabricated.

In the Be-Ti beryllides, with increase of Ti contents, Be phase fraction decreased. This decrease is closely associated with decrease of weight gain as well as generated H_2 amount.

Single-phased Be_{12}V and $\text{Be}_{17}\text{Ti}_2$ pebbles were successfully fabricated by two steps, plasma sintering method and rotating electrode method (no homogenization treatment). These pebbles indicate much more resistant to H_2O than Be pebble.

Collaborative studies in Japan have been extensively undergoing with several Universities.

2.7.6 Synthesis and characterization of ternary beryllide

J.-H. Kim, M. Nakamichi

Sector of Fusion Research and Development, Japan Atomic Energy Agency, Japan

Corresponding author's e-mail: kim.jaehwan@jaea.go.jp

Abstract

Beryllium intermetallic compounds (beryllides) such as Be_{12}Ti and Be_{12}V are the most promising advanced neutron multipliers in demonstration fusion power reactors. Advanced neutron multipliers are being developed by Japan and the EU as part of their Broader Approach activities. It has been previously shown, however, that beryllides are too brittle to fabricate into pebble- or rod-like shapes using conventional methods such as arc melting and hot isostatic pressing. To overcome this issue, we developed a new combined plasma sintering and rotating electrode method for the fabrication of beryllide rods and pebbles. In this study, $\text{Be}_{12}\text{Ti}_{1-x}\text{V}_x$ ($x=0.0\sim 1.0$) was successfully synthesized using these methods. We reported on not only preliminary synthesis of the ternary beryllide block but also ternary beryllide pebbles with different chemical compositions.

1. Introduction

Beryllide pebble with a Be-7.7at.%Ti composition as the stoichiometric value of the Be_{12}Ti phase consisted of $\text{Be}_{17}\text{Ti}_2$ and Be phases along with the Be_{12}Ti phase as the result of a peritectic reaction due to re-melting during granulation using the rotating electrode method. This Be phase was found to be highly reactive with oxygen and water vapor. Accordingly, to investigate the Be phase reduction and applicability for fabrication and granulation of beryllide electrodes, Be-Ti-V ternary beryllides were synthesized using the plasma sintering method and then granulated using the electrode. Herein we report the synthesis of Be-Ti-V ternary beryllides prepared using the plasma sintering method prior to fabrication of ternary beryllide pebbles and the effect of the phase composition on their reactivity behavior.

2. Experimental/Methodological

As starting materials for a granulation, Be, Ti, and V powders with purities of 99.5%, 99.9%, and 99.0% and particle sizes less than 45, 45, and 75 μm , respectively, were used. The powders were mixed with compositions $\text{Be}_{12}\text{Ti}_{1-x}\text{V}_x$ ($x=0.1, 0.3, 0.5, 0.7, 0.9, \text{ and } 1.0$) using a mortar (RM200, Retsch, Germany) for 1 h and then loaded into a graphite punch and die for cold compaction. Prior to sintering, an alternate current of 200 A was applied for 30 s as an activation of the powder surfaces. Sintering was conducted at 973 K for 2.5 min using heating and cooling rates of 100 and 200 K/min, respectively. After the plasma sintering, the rods were machined to cylindrical dimension of 50 \times 15 mm in length and diameter for the sake of clarity and set on the rotating electrode machine (REM) after polishing. To identify the phase compositions, scanning electron microscope images of the surfaces and cross-sections were obtained by using an electron probe micro analyzer (EPMA, JXA-8530F, JEOL, Japan) with backscattered electrons and point analysis of each phase by wavelength

dispersive x-ray spectrometer. As an evaluation of mechanical properties, crush strength (Autograph, AG-X10kNX, Shimadzu, Japan) of the granulated pebbles was investigated. Furthermore, to evaluate reactivity of the pebbles at high temperature, the weight gain and H₂ generation rate were measured at 1073, 1273, and 1473 K for 24 h in 1% H₂O/Ar atmosphere using thermal gravimetry (TG-DTA, TG-8110, Rigaku, CP- Japan) and gas chromatography (GC,4900, Agilent, USA), respectively. After reactivity test of the pebbles, cross-sectional observation was performed to confirm phase stability of the pebbles.

3. Results and discussion

In the previous study, Be phase in the beryllide pebbles was found out to be associated with reactivity of the pebbles at high temperature. To clarify the phase variation as a function of V content in the ternary beryllide pebbles, cross sectional images of the pebble with Be₁₂Ti_{1-x}V_x as shown in Fig.1, indicating that Be₁₂Ti_{0.9}V_{0.1}, Be₁₂Ti_{0.7}V_{0.3}, Be₁₂Ti_{0.5}V_{0.5} pebbles consisted of Be₁₂Ti, Be₁₂V, and Be (see area analysis results) while Be₁₂Ti_{0.3}V_{0.7} and Be₁₂Ti_{0.1}V_{0.9} did Be₁₂V and Be₁₂Ti. Accordingly, because Be₁₂Ti_{0.3}V_{0.7} pebble does not contain Be phase not only on the surface but inside of the pebble, it can be highly resistant to oxidation. On one hand, finer grain size on the surface may be associated to easier release of tritium, compared to single-phase Be₁₂V. With regard to mechanical stability, on the other hand, crack formation on the surface of Be₁₂V pebble can be problematic. Accordingly, Be₁₂Ti_{0.3}V_{0.7} and Be₁₂Ti_{0.1}V_{0.9} pebbles seem to be a good candidate as advanced neutron multiplier since no Be phase existed and no crack on the surface found.

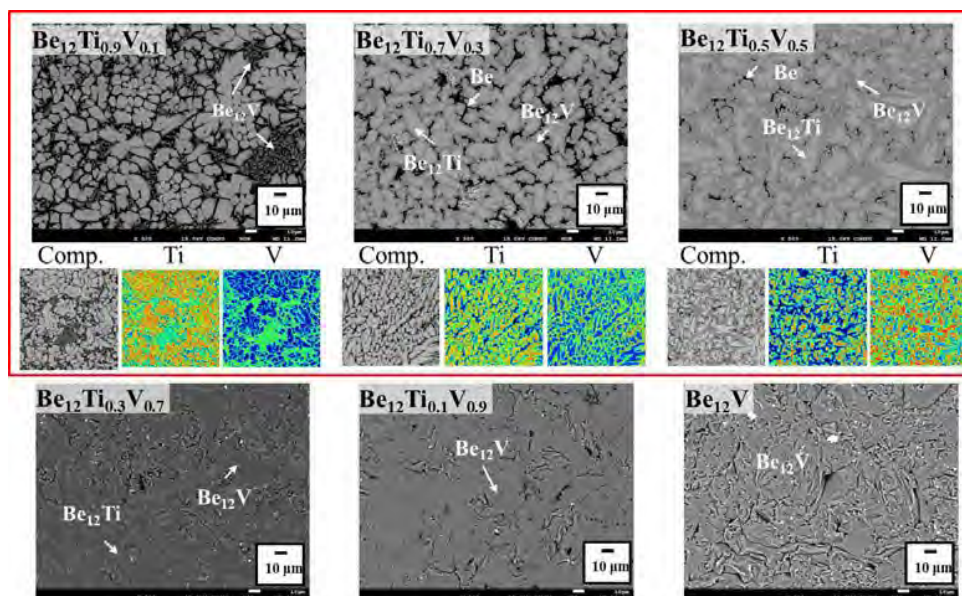


Fig. 1 SEM images and area analysis of ternary beryllide pebbles

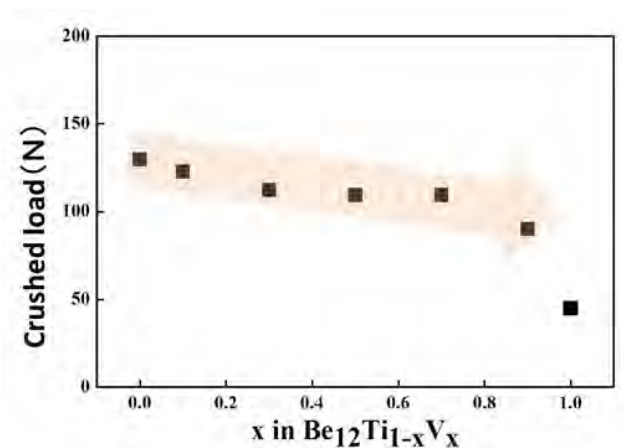


Fig. 2 Crushed load of ternary beryllide pebbles [1]

As an evaluation of mechanical property, compression test of each pebble was carried out at room temperature.

Fig. 2 indicates crushed load of the pebbles as a function of V content. In Be_{12}Ti pebble, the load value was approximately 130 N, while others slowly decreased up to $\text{Be}_{12}\text{Ti}_{0.3}\text{V}_{0.7}$. This decrease is thought to be closely related to decrease of Be fraction, which is relatively ductile compared to beryllides. In turns of displacement, identical tendency was confirmed, revealing that it slightly decreased with increase of V content in $\text{Be}_{12}\text{Ti}_{1-x}\text{V}_x$. Compared to $\text{Be}_{12}\text{Ti}_{0.3}\text{V}_{0.7}$ and $\text{Be}_{12}\text{Ti}_{0.1}\text{V}_{0.9}$ pebble, the crushed load of Be_{12}V pebbles were considerable low. In specific, its sharp decrease of the Be_{12}V pebble can be explained by the fact that some cracks on the pebble surface, generated during the granulation by the REM, identified, which it led to decrease of crush load.

To investigate reactivity of the pebbles with 1% $\text{H}_2\text{O}/\text{Ar}$ with assumption of loss of coolant accident (LOCA), hydrogen generation properties of the pebbles were examined as shown in Fig. 3 with reference of Be blocks and pebbles. From the result of this, it obviously reveals that with increase of V content in $\text{Be}_{12}\text{Ti}_{1-x}\text{V}_x$ pebbles,

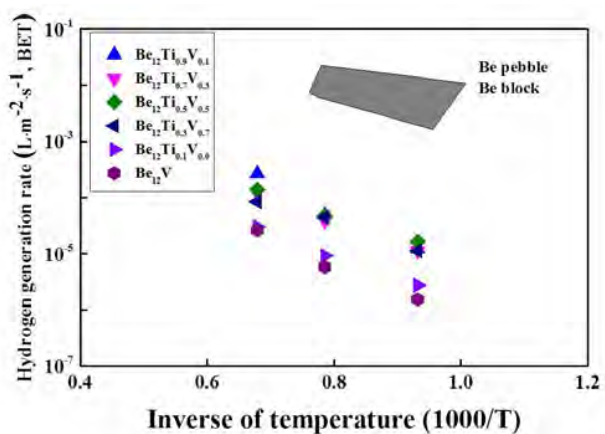


Fig.3 H₂ generation rate of the pebbles [1]

hydrogen generation rate decreased while the rates of all ternary pebbles was lower by approximately two or three digits than that of Be pebble. Furthermore, it was clear that Be_{12}V pebbles seem to be the most stable material among $\text{Be}_{12}\text{Ti}_{1-x}\text{V}_x$ pebbles although crush load of the pebble indicated the lowest value. With regards of reactivity according to V content, it is obvious that as V content increases, the hydrogen generation rate decreases.

4. Conclusion

R&Ds of Be-Ti-V ternary beryllides have been started to overcome some issues when binary pebbles are fabricated. The ternary pebbles with not only disk [2] but pebble [1] were successfully fabricated using plasma sintering and rotating electrode methods to investigate the effect of V content in titanium beryllide pebbles on characterizations and phase stability. Surface observation results reveal that as V content increases, surface structure becomes finer because structure size decreased by hindrance of Be_{12}Ti phase grain growth due to formation of Be_{12}V phase in the pebbles. Besides, cross-sectional analyses proved that as V content increases, area fraction of Be phase decreases while that of Be_{12}V phase increases. It was clearly observed that $\text{Be}_{12}\text{Ti}_{0.3}\text{V}_{0.7}$ and $\text{Be}_{12}\text{Ti}_{0.1}\text{V}_{0.9}$ pebbles composed of Be_{12}Ti and Be_{12}V without Be phase. Accordingly, this variation of Be phase in the ternary pebbles led to decrease of crush strength and displacement when collapsed because Be phase is ductile. With regards to reactivity with 1 % $\text{H}_2\text{O}/\text{Ar}$, it was obvious that the higher V contents they have the lower weight gain as well as hydrogen generation rate they show. It was contributed to decrease of Be fraction, which is much more reactant with H_2O than beryllides. In one hand, no phase variation of the pebbles occurred at 1073 and 1273 K. At 1473 K, on the other hand, Be phase is diffused to beryllides phase and became pores in the pebbles, $\text{Be}_{12}\text{Ti}_{0.9}\text{V}_{0.1}$, $\text{Be}_{12}\text{Ti}_{0.7}\text{V}_{0.3}$, and $\text{Be}_{12}\text{Ti}_{0.5}\text{V}_{0.5}$ while $\text{Be}_{12}\text{Ti}_{0.3}\text{V}_{0.7}$, and $\text{Be}_{12}\text{Ti}_{0.1}\text{V}_{0.9}$ pebbles showed no phase variation and no pore formation, corresponding to high phase stability.

References

- [1] Jae-Hwan Kim, Masaru Nakamichi, Fusion Engineering and Design, in press, doi:10.1016/j.fusengdes.2015.09.015 (2015)
- [2] Jae-Hwan Kim, Masaru Nakamichi, Journal of Alloys and Compounds 640 (2015) 285-289

2.7.7 Long-time Exposures of Be₁₂Ti to 1% Water Vapor at 1273 K

Kenzo MUNAKATA¹ Jae-Hwan KIM² and Masaru NAKAMICHI³.

¹*Faculty of engineering and resource science, Akita university,
1-1, Tegatagakuen-cho, Akita, 010-8502, Japan*

²*Sector of Fusion Research and Development, Japan Atomic Energy Agency,
2-166, Omotedate, Obuchi, Rokkasho, Kamikita, Aomori, 039-3212, Japan*

E-mail: kenzo@gipc.akita-u.ac.jp

Titanium beryllides such as Be₁₂Ti have lots of advantages over beryllium from the perspectives of higher melting point, lower chemical reactivity, lower swelling and so forth. Therefore, Be₁₂Ti material has attracted attention as an alternative of beryllium, and could be used as an advanced neutron multiplier in the advanced fusion reactor blankets. Nakamichi et al. have developed a new synthesis route of Be₁₂Ti material called "plasma-sintering method". This process consists of loading of raw material powder in the punch and the die unit, direct current pulse plasma generation to activate the surface of powder particles, and uniaxial pressing to enhance the sinterability. In this study, we investigated interaction of water vapor with titanium beryllide at temperatures as high as 1273 K. In the experiments Be₁₂Ti samples were placed under 1% H₂O/Ar gas for 100 h. The result shows that no chaotic breakaway oxidation reactions take place during its 100 h exposure to water vapor, indicating that Be₁₂Ti is extremely durable to oxidation by water vapor at high temperatures.

Long-time Exposures of Be₁₂Ti to 1% Water Vapor

Kenzo MUNAKATA^{a,*}, Jae-Hwan KIM^b and Masaru
NAKAMICHI^b

^a*Faculty of engineering and resource science, Akita
university,*

1-1, Tegatagakuen-cho, Akita, 010-8502, Japan

^b*Sector of Fusion Research and Development, Japan Atomic
Energy Agency,*

*2-166, Omotedate, Obuchi, Rokkasho, Kamikita, Aomori,
039-3212, Japan*

Introduction

- Beryllium is considered as a candidate material for the neutron multiplier loaded in water or helium cooled solid breeder blankets of future fusion reactors.
- In these blankets, beryllium (neutron multiplier) would be placed under the condition of high neutron flux and high temperature.
- Beryllium is highly reactive with water vapor and oxygen at high temperatures, which produces hydrogen that may lead to accidents due to H₂ gas explosion and hazardous beryllium oxide.

Introduction

- Titanium beryllides such as Be_{12}Ti have advantages over beryllium from the perspectives of higher melting point, lower chemical reactivity, lower swelling, etc.
- Therefore, Be_{12}Ti material has attracted attention as an alternative of beryllium, and could be used as an advanced neutron multiplier in the fusion reactor blankets.

2

Introduction

- Titanium beryllides have been fabricated by various methods. Oxidation behavior of the Be_{12}Ti samples prepared by the HIP method was previously studied.
- More recently, Nakamichi et al. have suggested new synthesis process of beryllides material called “plasma-sintering method”.
- This process consists of loading raw material powder in the graphite punch and die unit, applying an on-off electric direct current, uniaxial-pressing for cold compaction, and resistance-heating for sintering.
- The peculiar feature of this process is of less time-consuming and of less cost compared with previous fabrication processes of beryllide.

3

Reaction of beryllium with water vapor

- With regard to beryllium, Yoshida et al. carried out thermo-gravimetric measurements in the temperature range 823 - 1023 K under helium gas flow containing water vapor of 1% and 0.1%.
- The test samples were prepared from commercially available hot-pressed and hot-rolled beryllium plates.
- Linear and parabolic rate laws were found for the dominant reaction steps in the preceding period of the breakaway reaction. Microstructure of the surface reaction layer formed in all exposure conditions revealed brittle structure, which was composed of blister and microcracks.

4

Reaction of beryllium with water vapor

- Druyts et al. used a thermogravimetric analysis to determine the reactivity of beryllium in steam as a function of temperature, irradiation history and porosity of the samples.
- It has been reported that kinetics are parabolic for all tested beryllium types at 873 K. At 973 K, kinetics is parabolic for the unirradiated and irradiated 99.9% dense beryllium, and accelerating/linear for the irradiated 97.2% material. At 1073 K, all samples showed accelerating/linear behavior.

5

Reaction of beryllium with water vapor

- Druyts et al. used a thermogravimetric analysis to determine the reactivity of beryllium in steam as a function of temperature, irradiation history and porosity of the samples.
- It has been reported that kinetics are parabolic for all tested beryllium types at 873 K. At 973 K, kinetics is parabolic for the unirradiated and irradiated 99.9% dense beryllium, and accelerating/linear for the irradiated 97.2% material. At 1073 K, all samples showed accelerating/linear behavior.

6

Reaction of beryllium with water vapor

- These results suggest that catastrophic breakaway oxidation reactions on the surface of beryllium take place under the conditions of high temperature and high water vapor pressure after parabolic oxidation or slow oxidation period.

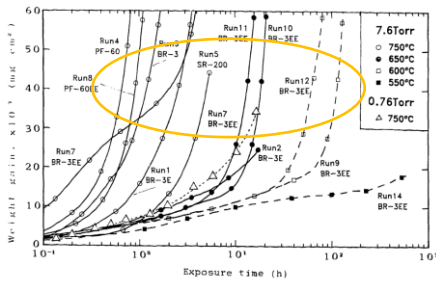


Fig. 7 Time dependence of weight gain during exposure to water vapor

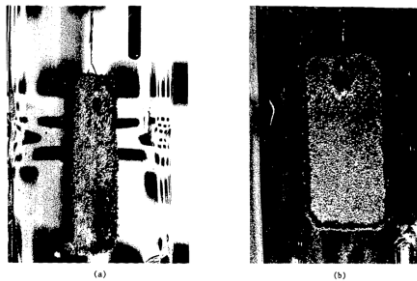


Fig. 12 Macroscopic appearance of test sample after breakaway reaction (Run-1: BR-3, 750 °C, 7.6 Torr, 9.9 h)

7

Motivation of this study

- The present authors have reported results on H₂ generation caused by interaction of water vapor with beryllide prepared by the plasma sintering method and its high durability to steam.
- In these previous works, the beryllide samples were exposed to 1% H₂O/Ar gases, and temperature was raised up to 1273 K; the previous experiments were stopped when generation of hydrogen was not observed.
- However, as mentioned above, chaotic breakaway reactions on the surfaces of beryllium appear to start after parabolic oxidation or slow oxidation period (preceding period). Hydrogen generation from beryllide samples was modest in the past experiential runs of which experimental time that ranged from 24 to 40 h.
- However, there is a possibility that breakaway reactions take place if Be₁₂Ti is interacted with steam for longer periods. Thus, in this study, Be₁₂Ti samples were placed under 1% H₂O/Ar gases for 100 h and their durability was examined.

8

Beryllide sample

- Powders of Be and Ti (<45μm particle size, >99.5% purities) were mixed for 60 min in a mortar grinder (RM200, Retsch, Germany).
- The atomic ratio of the mixture was adjusted to the stoichiometric composition of Be₁₂Ti (69.3:30.7 wt.%). After mixing, the powder was packed in a plasma electrical discharge sintering device (KE-PAS III, KAKEN, Japan).
- The beryllide disc with 20 mm in diameter and 5 mm in thickness, was synthesized by sintering for 40 min at a temperature of 1273 K under pressure of 50 MPa. Then the disc was cut into several small samples (3×3×4 mm) by wire electrical discharge machining. Then, the samples were mechanically polished with a #2400 SiC abrasive paper.

9

Beryllide sample

- The surface morphology of the beryllide samples was examined by secondary electron microscopy (SEM) combined with the electron probe microanalysis (EPMA, JXA-8230, JEOL, Japan).
- The results of EPMA analysis demonstrate that the plasma sintered beryllide is composed of four different phases such as Be, Be₁₂Ti, Be₁₇Ti₂, and Be₂Ti with different fractions.

10

Beryllide sample

- According to image analysis, the representative area fractions for each phase were given in table1. In this work, two Be₁₂Ti samples (3×3×4 mm) were used in experiments. Their composition is slightly different, but their major constituent was Be₁₂Ti. As seen in the table, the fraction of Be phase in the sample (A) is slightly larger than that in the sample (B).

Table 1 phase composition of beryllide samples

	Be	Be ₁₂ Ti	Be ₁₇ Ti ₂	Be ₂ Ti
Sample A	0.246%	90.653%	8.616%	0.775%
Sample B	0.635%	92.964%	6.500%	0.356%



(a) before experiment

11

Experimental

- A Schematic flow diagram of apparatus for a measurement of the hydrogen generation rate is shown in Fig. 1.
- The Be₁₂Ti sample was wrapped by platinum mesh to avoid direct contact with the test tube made of quartz, and then placed between silica wools.

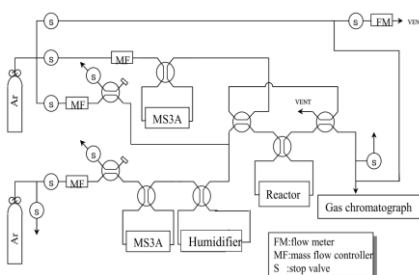


Fig. 1 Flow diagram of experimental apparatus

12

Experimental

- A humidifier (HUM, Rigaku, Japan) was used to enable longer period experiments. The 1% H₂O/Ar gas was introduced to the test tube with a flow rate of 300 cm³/min.
- An electric furnace was used to heat the test tube. The test tube was heated at the rate of 5 K/min, and a temperature inside the tube was finally raised up to 1273 K. This temperature was kept constant for about 100 h.

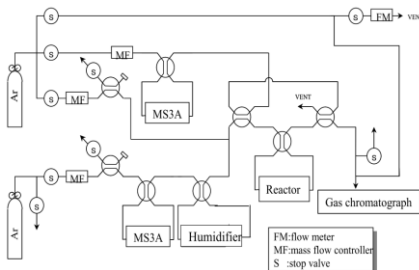


Fig. 1 Flow diagram of experimental apparatus

13

Experimental

- Two runs of experiments were performed using Ar gases with different purity. One was a usual Ar gas with 99.99% purity (sample A) and the other was a high grade Ar gas with 99.9999% purity (sample B). Concentrations of hydrogen in the outlet stream of the reactor were measured with a gas chromatograph (GC-8A, Shimadzu, Japan).

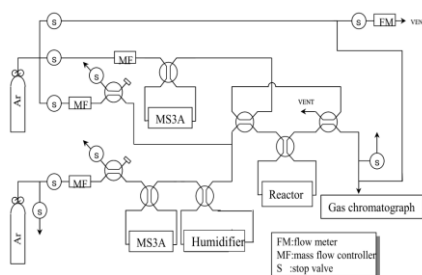


Fig. 1 Flow diagram of experimental apparatus

14

Result and discussion

- Figs. 2 (a) and (b) shows changes in hydrogen concentrations in the outlet stream of reactor charged with sample (A). Fig. 2 (a) shows change in concentration of hydrogen as the full time scale 100 h, and that of close-up in the initial 12 h is shown in Fig. 2 (b). In this case, a 99.99% Ar gas was used as a process gas, which contained 1% of water vapor.
- The total amount of hydrogen generated was 1.3×10^{-4} mol/cm².

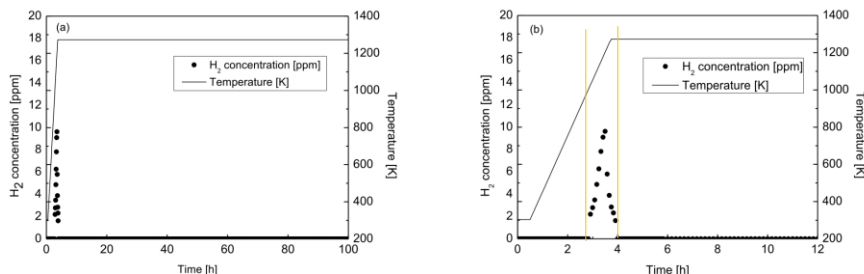


Fig.2 Change in concentration of hydrogen in outlet stream of reactor charged with Be₁₂Ti sample (A) after 1% H₂O/Ar (99.99%) was introduced, (a) full experimental time (100h), (b) initial 12h

Result and discussion

- Figs. 3 (a) and (b) shows changes in hydrogen concentrations in the outlet stream of reactor charged with sample (B) when the 99.9999% Ar gas was used as a process gas. A 1% H₂O/Ar gas was generated with the humidifier, as well.
- The total amount of hydrogen generated was 5.3×10^{-4} mol/cm².

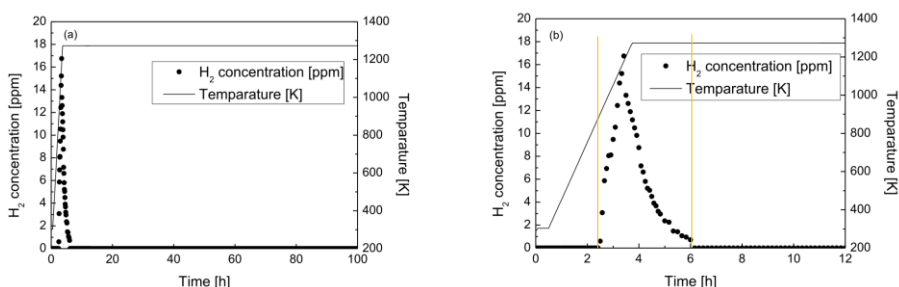


Fig.3 Change in concentration of hydrogen in outlet stream of reactor charged with Be₁₂Ti sample (A) after 1% H₂O/Ar (99.99%) was introduced, (a) full experimental time (100h), (b) initial 12h

16

Result and discussion

- As shown in Figs. 2 and 3, chaotic breakaway reaction did not take place and hydrogen was generated only the initial period of the experiments.
- In the case of 99.99% Ar gas and beryllide sample (A), the amount of hydrogen generated was smaller. This is probably due to impurities contained in the gas such as oxygen and carbon dioxide. Another reason could be difference in Be contents in the beryllide samples.
- Anyhow, two runs of experimental results indicate that transition of oxidative reaction to chaotic breakaway reaction, which has been reported for beryllium metal, never took place within the experimental time (100 h) of this work. Thus, it can be stated that Be₁₂Ti is extremely resistant to oxidation by water vapor at high temperatures.

17

Result and discussion

- Photographic views of the Be₁₂Ti samples before and after the experiments are shown in Fig. 4.
- Before the experiments, the surface of the samples possessed metallic luster whereas white and grey parts arose on the surfaces after the experiments (exposure to steam), which could be the trace of occurrence of oxidative reaction on the surfaces.

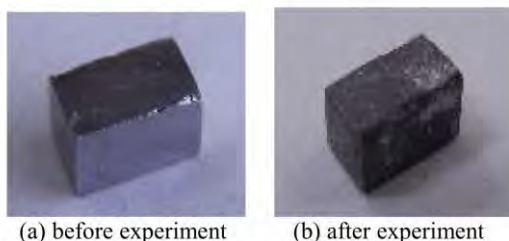


Fig. 4 Photographic views of Be₁₂Ti samples of (a) before experiment and (b) after experiment of 100 h exposure to steam

18

Result and discussion

- The XRD analysis was also performed for the samples. Fig. 5 shows the results of XRD analysis.
- Before the experiments (Fig. 5 (a)), the Be₁₂Ti sample exhibited a representative XRD pattern of Be₁₂Ti.
- After the experiments, as seen in Figs. 5 (b) and (c), the peaks corresponding to BeO arose for both of the samples (A) and (B), which indicates that formation of BeO took place on the sample surfaces.
- However, the experimental results shown in Fig. 3 clearly suggest that the formation of BeO by steam is limited only on the surface.

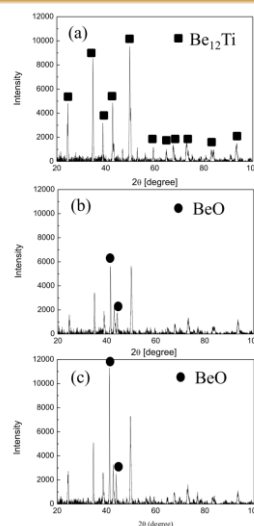


Fig. 5 XRD pattern of Be₁₂Ti samples
 (a) typical XRD pattern of as-received sample
 (b) XRD pattern of Be₁₂Ti sample A after experiment
 (c) XRD pattern of Be₁₂Ti sample B after experiment

19

Conclusion

- A beryllide disc was synthesized by the plasma sintering method and cut into several small samples (3×3×4 mm), which was used in experiments. In the experiments, the beryllide samples were interacted with 1% H₂O/Ar gases at temperatures elevated up to 1273 K.
- Small amounts of hydrogen were generated during initial period after commencement of the experiments, however no chaotic breakaway oxidation reactions take place during 100 h (4 days) exposure of the Be₁₂Ti to water vapor. The experimental results indicate that Be₁₂Ti is extremely resistant to oxidation by water vapor at high temperatures

2.7.8 Comparison of Tritium Release Behavior of Different Beryllium Materials

Vladimir Chakin¹, Rolf Rolli¹, Anton Moeslang¹, Petr Kurinskiy¹, Pavel Vladimirov¹, Christopher Dorn², and Igor Kupriyanov³

¹Karlsruhe Institute of Technology, Institute for Applied Materials, Hermann-von-Helmholtz-Platz 1, 76344 Eggenstein-Leopoldshafen, Germany

²Materion Beryllium & Composites, 6070 Parkland Boulevard, Mayfield Heights, Ohio 44124-4191 U.S.A.

³Bochvar Russian Scientific Research Institute of Inorganic Materials, Rogova str., 5, 123098 Moscow, Russia

Abstract

Comparison of different beryllium samples on tritium release and retention properties after high-temperature loading by tritium/hydrogen gas mixture and following temperature-programmed desorption (TPD) tests has been performed. The best tritium release properties showed the I-220-H grade produced by hot isostatic pressing (HIP) having the smallest grain size, the pebbles of irregular shape with the smallest grain size (10-30 μm) produced by the crushing method (CM), and the pebbles with 1 mm diameter produced by fluoride reduction method (FRM) having a highly developed inherent porosity. Grain size can be considered as a key structural parameter for comparison and ranking of different beryllium materials on tritium release and retention properties.

1. Introduction

It is planned for beryllium to be used as the neutron multiplier material in the European Helium Cooled Pebble Bed (HCPB) concept for a breeding blanket design for DEMO [1]. Tritium release and retention properties are the key issues for successful application of beryllium in the blanket. Under neutron irradiation, large amounts of tritium and helium are produced in beryllium. Clearly, the best possibility in current conditions to simulate fusion relevant parameters is performing an irradiation test with investigated materials in a materials testing reactor. There is, however, another method which allows the saturation of beryllium samples by tritium without neutron irradiation [2]. It is a high-temperature loading of the samples in a tritium/hydrogen gas mixture. By using this method, it is possible to investigate and to rank advanced beryllium materials on tritium release and retention behavior without irradiation and, accordingly, with comparatively lower time costs. In this study, a wide range of beryllium materials is investigated by using the loading method and following temperature-programmed desorption (TPD) tests.

2. Experimental/Methodological

Several kinds of beryllium materials have been investigated. Beryllium grades I-220-H, O-30-H, and S-65-H have been consolidated by hot isostatic pressing (HIP) by Materion Beryllium & Composites (MBe&C), U.S.A. The samples were prepared as cylinders with dimensions of 4 mm in diameter and 2 mm in height. These beryllium grades differ from each other by grain size and beryllium oxide (BeO) content. The second kind of material is beryllium pebbles with irregular shape produced by Bochvar Institute, Russia by a crushing method (CM) from beryllium pieces with subsequent mechanical processing by an attritor. Three different types of pebbles were tested, with grain sizes of 10-30 μm , 30-60 μm , and >100 μm , respectively. The third kind of material is beryllium pebbles with a regular, round shape, differing by production method and diameter. In particular, pebbles produced by the rotating electrode method (REM) with diameters of 0.5 mm, 1 mm, and 2 mm from NGK Insulators in Japan, and pebbles fabricated by the fluoride reduction method (FRM) with diameters of 1 mm and 2 mm from MBe&C were used. In addition, MBe&C supplied a piece of beryllium single crystal in the form of a 5 mm cube which was also investigated in this study.

The tritium/hydrogen loading of the samples was performed in the $^1\text{H}_2 + 500 \text{ appm } ^3\text{H}_2$ gas mixture at 873 K for 6 h at 4 bar. By performance of the TPD tests, a permanent heating mode with a ramp rate of 0.117 K/s up to 1373 K followed by 3 h exposure at the maximum temperature was used [3]. The gas mixture of high-purity helium with a small addition of hydrogen ($^4\text{He} + 0.1 \text{ vol.}\% ^1\text{H}_2$) was applied as a purge gas to transport the released species from the furnace with the beryllium samples to a proportional counter (PC). A Zn-bed was placed between the furnace and the PC. The Zn-bed was permanently heated up to 663 K which permitted the conversion of tritiated water to tritium gas to avoid the absorption of the tritiated water into the pipes and into the PC. For the same reason, all gas pipes in the manifold were heated up to 573 K during the TPD tests. So, the released tritium reaches the PC mainly in the form of $^1\text{H}^3\text{H}$ [3].

3. Results

3.1. Tritium release and retention

Fig. 1 shows the tritium release rate versus testing temperature for beryllium grades fabricated by HIP as well as for beryllium single crystal. All samples have quite a broad single peak at high temperatures with a long shoulder to lower temperatures. For all materials, the high-temperature peaks are located at 1260-1302 K, and the shoulders begin around 500-600 K.

Fig. 2 shows the total tritium release for HIPed beryllium grades and for beryllium single crystal. I-220-H (the grade with the smallest grain size and highest BeO content) has the greatest amount of total release. Both O-30-H and S-65-H have comparatively lower total release values, and S-65-H has the lowest total release and correspondingly, the largest grain size. This demonstrates, therefore, an inverse dependence of the total tritium release on the grain size for these HIPed beryllium grades. It

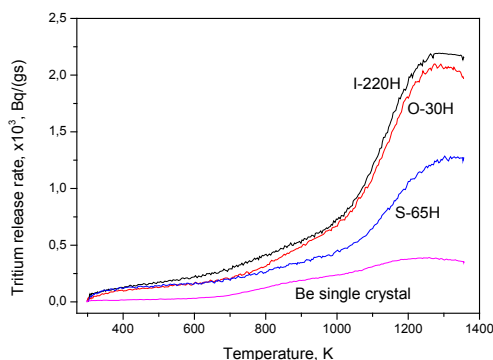


Fig. 1. Tritium release rate for beryllium grades produced by HIP and for beryllium single crystal.

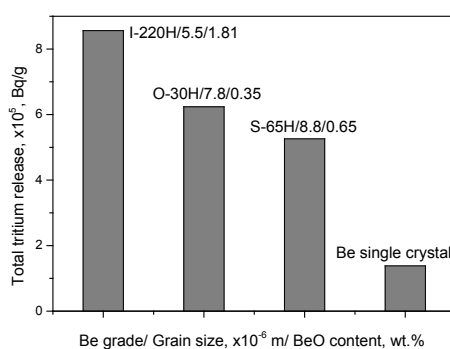


Fig. 2. Total tritium release for beryllium grades produced by HIP and for beryllium single crystal.

seems logical that the beryllium single crystal has the lowest total release, since it has inherently no grain boundaries.

Fig. 3 shows tritium release rates for beryllium pebbles of irregular shape made by CM. The pebbles of grain sizes 30-60 μm and $>100 \mu\text{m}$ have single peaks which are practically coincident with each other, and they are also very similar in shape to the peaks from Fig. 1 for the HIPed beryllium grades. The tritium release rate curve for the pebbles of grain size of 10-30 μm differs significantly from that for the pebbles with the larger grain size. The tritium release starts immediately from the beginning of the TPD test, i.e. from even just a small increment above room temperature after heating, and continues with increasing rate until reaching a broad peak. Despite the difference in the behavior of the release rate for pebbles with grain size of 10-30 μm , however, the peaks for all three pebble types are grouped closely at temperatures in the region of 1251-1308 K.

For the pebbles made by CM, the highest total tritium release detected was for the pebbles with the 10-30 μm grain size, which also happened to be the smallest (see Fig. 4). With increasing grain size, therefore, the total tritium release decreases.

Fig. 5 shows the tritium release rate for beryllium pebbles of different diameters produced by REM. The most facilitated tritium release occurs from the 0.5 mm pebbles where tritium begins to leave the material starting from room temperature at a high rate. For 1 mm and 2 mm pebbles, the release occurs

with close rates up to 650-700 K. Then, at higher temperatures, the release from the 1 mm pebbles is comparatively faster than from the 2 mm pebbles. The major peak for all three pebble sizes is located within the temperature range of 1302-1348 K. It should be noted that there are two additional peaks at lower temperatures for the 0.5 mm pebbles. These peaks occur at ~350 K and ~900 K. For both 1 mm and 2 mm pebbles, the peak at the lowest temperature is absent, and the peak at ~900 K is weakly expressed.

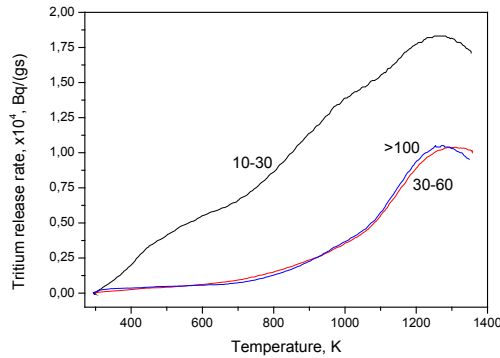


Fig. 3. Tritium release rates for pebbles prepared by CM. Grain sizes are shown in μm .

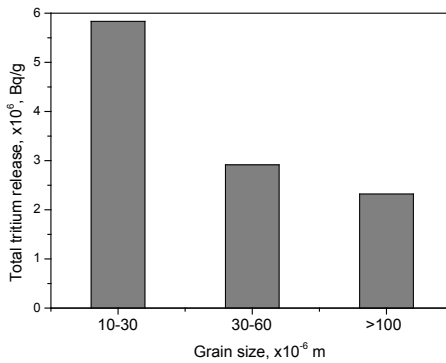


Fig. 4. Total tritium release for pebbles prepared by CM.

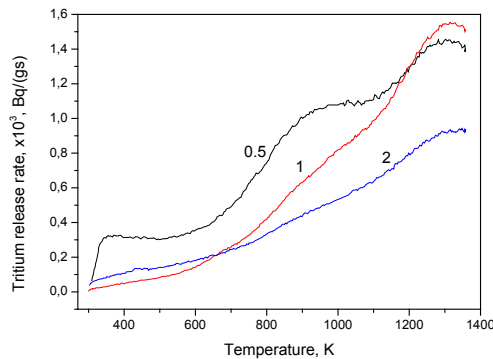


Fig. 5. Tritium release rate for beryllium pebbles with different diameters produced by REM. Diameters are shown in mm.

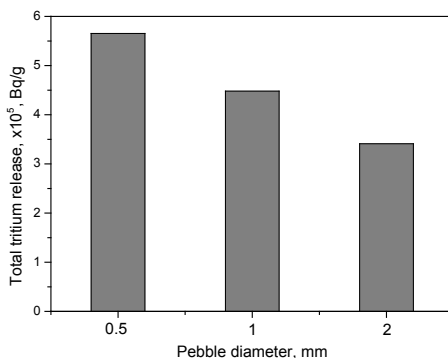


Fig. 6. Total tritium release for beryllium pebbles with different diameters produced by REM.

Total tritium release for the beryllium pebbles produced by REM is strongly dependent on the pebble diameter (see Fig. 6). Specifically, the highest total tritium release is from the 0.5 mm pebbles, and, therefore, the lowest release is from the 2 mm pebbles.

It would be interesting to compare 1 mm-diameter pebbles produced by different methods, since the 1 mm beryllium pebbles produced by REM are currently considered as the reference material for HCPB breeding blanket concepts for fusion reactors. The comparison of 1 mm pebbles produced by REM and FRM on tritium release behavior is represented in Fig. 7. The REM batch with greater content of porosity (see Section 3.2) demonstrates a most facilitated tritium release starting immediately from room temperature. For temperatures higher than 1000 K, however, the release occurs comparatively faster from the FRM pebbles. In addition, the major peak for the FRM pebbles is at the lower temperature (1269 K) compared to that for the REM pebbles (1315-1323 K).

Fig. 8 shows total tritium release for the 1 mm beryllium pebbles produced by REM and FRM. The highest total tritium release is from the FRM pebbles, but for the REM pebbles with the higher amount of porosity, the total release amount is close to that of the FRM pebbles.

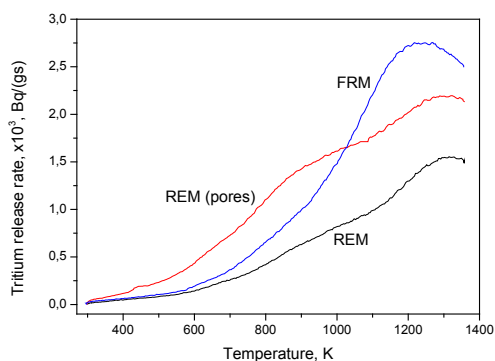


Fig. 7. Tritium release rate for 1 mm-diameter beryllium pebbles fabricated by REM and FRM. “REM (pores)” indicates the presence of a higher relative density of pores compared to the “REM” batch with a significantly lower amount of pores.

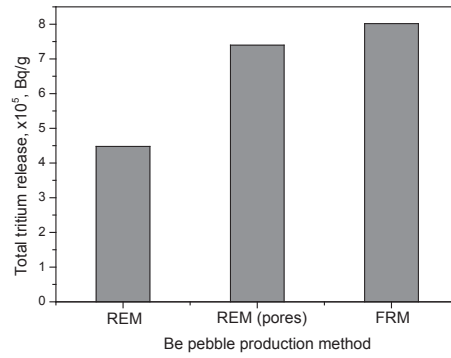


Fig. 8. Total tritium release for beryllium pebbles of 1 mm diameter produced by REM and FRM.

3.2. Microstructure

Fig. 9 shows the microstructure of I-220-H beryllium grade. There are visible fine grains (Fig. 9a) and numerous inclusions (most likely BeO particles) which are located primarily in the grain boundaries (Fig. 9b).

The O-30-H beryllium grade was consolidated by HIP from atomized powder (Fig. 10). This explains the presence of spherical grains and low BeO content in the microstructure. There is a very high degree of variation in the grain sizes. Some individual grains are up to 60 μm in diameter, and numerous fine grains around the larger grains are smaller than 10 μm.

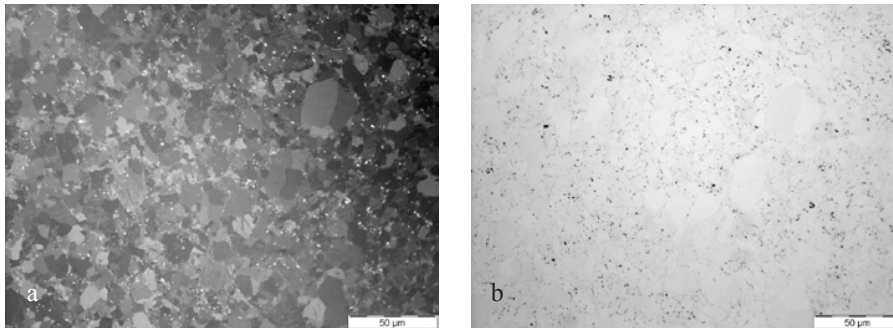


Fig. 9. Optical micrograph of a cross-section of I-220-H beryllium: a) in polarized light, b) the same area, in general light.

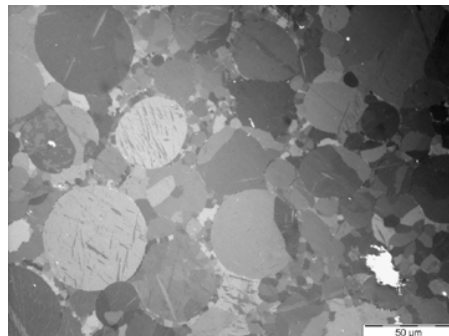


Fig. 10. Optical micrograph in polarized light of cross section of O-30-H sample.

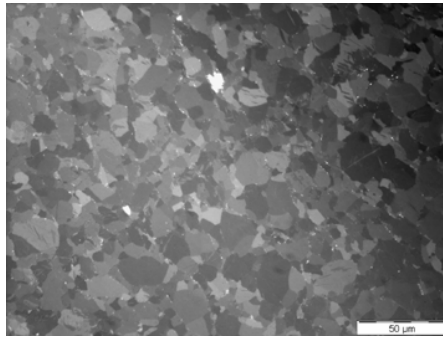


Fig. 11. Optical micrograph in polarized light of a cross-section of S-65-H beryllium.

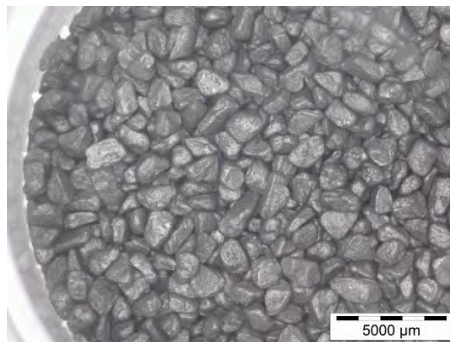


Fig. 12. General view of beryllium pebbles with grain size of 10-30 μm produced by CM.

The microstructure of S-65-H beryllium grade (Fig. 11) is similar to that of I-220-H. S-65-H, however, has comparatively larger grain size, and the amount of BeO particles is considerably less than that in I-220-H.

Fig. 12 shows a general view of beryllium pebbles produced by CM. The pebbles have an irregular, “potato-like” shape. The sizes of the pebbles are mainly between 1 mm and 2 mm.

Fig. 13 shows the microstructure of beryllium pebbles produced by CM with grain size of 10-30 μm. The grains have an elongated or irregular shape. The pebble surface has rough pitted relief. Pores and cracks are visible in the near-surface regions.

A general view of beryllium pebbles with a diameter of 1 mm produced by REM is shown in Fig. 14. In appearance, these pebbles have been selected to have the closest to a true spherical shape with a smooth, shiny surface.

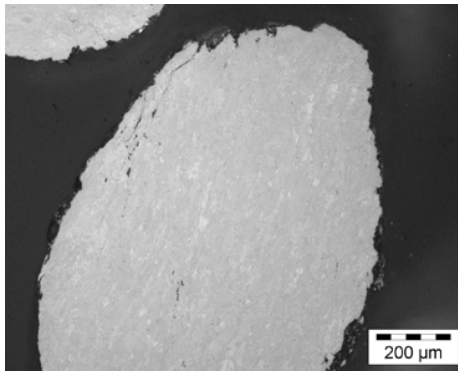


Fig. 13. Optical micrographs in polarized light of the cross-section of a beryllium pebble produced by CM with grain size of 10-30 μm .

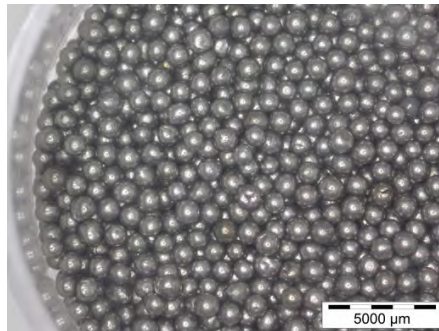


Fig. 14. General view of beryllium pebbles of 1 mm diameter produced by REM.

Fig. 15 shows a cross-sectional image of a 1 mm pebble produced by REM. The main feature of the pebble's microstructure is the presence of coarse grains.

There is one batch of 1 mm REM beryllium pebbles which was made by using a variety of production parameters (Fig. 16) that resulted in much higher porosity in the pebbles' microstructure. As a rule, these pebbles have a large amount of shrinkage in areas close to the pebble's center and many pores more or less uniformly distributed in the coarse grains as well. It should be noted that all uses of the term "porosity" in this paper refer to presence of pores in materials due to their manufacturing processes. This is not to be confused with radiation-induced porosity, which, as the term suggests, is found in the material as a result of its exposure to irradiation.

Fig. 17 presents a general view of 2 mm beryllium pebbles produced by FRM. In contrast to the REM pebbles, they do not have a true spherical shape, and the surface is matte and frequently with indentations. Cross-sections of several FRM pebbles (Figs. 18-19) also demonstrate that the shape of the pebbles is not always perfectly spherical, as well as the presence of numerous pores. The pores are arranged in chains or large conglomerates, or uniformly distributed in the microstructure.

Fig. 20 shows the microstructure of the FRM pebbles in polarized light. There are coarse grains similar to the grains in the REM pebbles (see Fig. 16). The FRM pebbles have, however, comparatively many more pores and a more developed twinning structure. The twins are mainly located near to the external surface of the pebbles and look like parallel or intersecting lines.

Loading of the FRM pebbles with tritium/hydrogen gas mixture at 873 K for 15 h leads to microstructural changes (Fig. 21). The twins almost disappear. The coarse grains are converted in the smaller grains. The loading temperature is more than half the melting point of beryllium, therefore permitting recrystallization to start and inducing the transformation of the grain boundary structure.

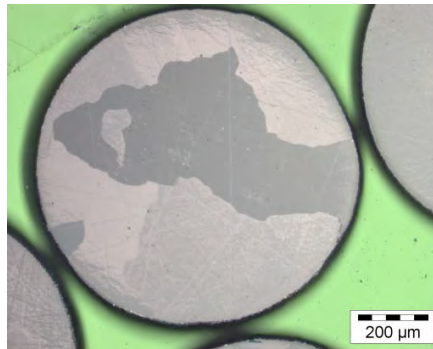


Fig. 15. Optical micrograph in polarized light of the cross-section of a beryllium pebble of 1mm diameter produced by REM.

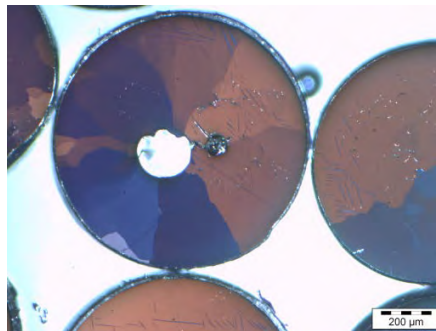


Fig. 16. Optical micrograph in polarized light of the cross-section of beryllium pebbles of 1 mm diameter produced by REM from a batch with comparatively higher porosity.

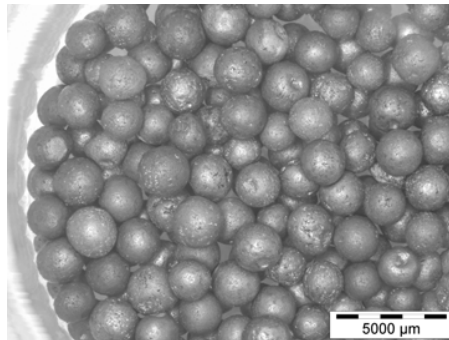


Fig. 17. General view of beryllium pebbles of 2 mm diameter produced by FRM.

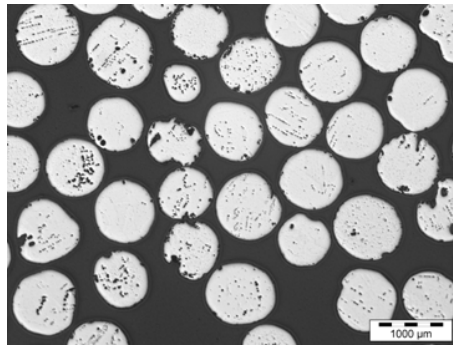


Fig. 18. General view of cross-sections of beryllium pebbles of 1mm diameter produced by FRM.

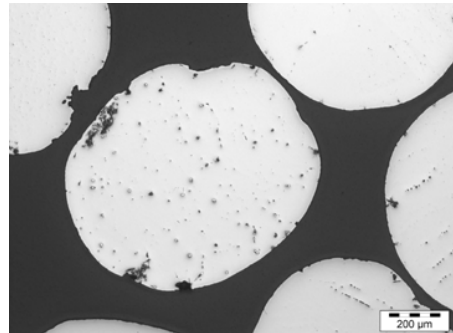


Fig. 19. Optical micrograph of cross-sections of beryllium pebbles of 1 mm diameter produced by FRM. The presence of numerous inherent pores can be seen in the microstructure.

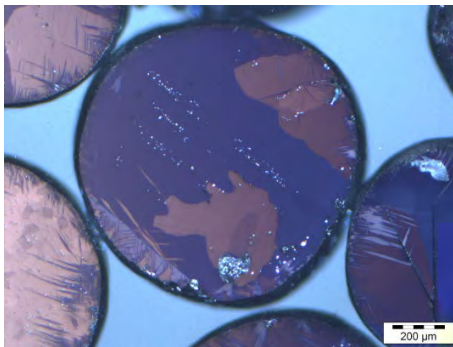


Fig. 20. Optical micrograph in polarized light of cross-sections of beryllium pebbles of 1 mm diameter produced by FRM.

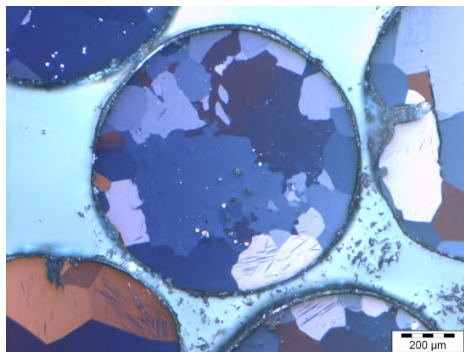


Fig. 21. Optical micrograph in polarized light of cross-sections of 1 mm diameter beryllium pebbles produced by FRM after loading with tritium/ hydrogen gas mixture at 873 K for 15 h.

4. Discussion

High-temperature loading with the tritium/hydrogen gas mixture occurs through the outer surface of a beryllium pebble (or cylinder-sample, as applicable) either directly through the bodies of first-layer grains or along the boundaries which come to the surface (Fig. 22a). Clearly, the mobility of tritium atoms (and hydrogen atoms, of course) moving along boundaries is comparatively much higher than that through the grain body. Only a short time after starting the loading, therefore, the tritium atoms can penetrate along the boundaries into the whole pebble volume reaching the presence of the tritium at the boundaries in sufficient amounts to start the motion of these atoms into the grain bodies. As a result, the possible negative impact of the BeO layer, which is always present on the beryllium sample's surface, is not considered. After dissociation of the tritium molecules outside the pebble, the tritium atoms penetrate through the BeO layer to start their movement into the beryllium pebble. Thickness of the BeO layer can be up to $0.15\mu\text{m}$ [2]. The BeO layers on the beryllium samples in this study have approximately equal thickness. The time of penetration through the oxide layer is, therefore, about the same for each sample. Another point worth noting regards the state of the tritium in the grains after saturation of the beryllium sample by tritium/hydrogen. The tritium and hydrogen should form small bubbles in the beryllium as was observed in the near-surface layers after implantation of deuterium [4-6]. So, as a result of loading at the same parameters, the beryllium samples end up with a similar microstructure with their primary defects being gas bubbles which differ by their size and density according to the grain size in each sample.

Another possible outcome for the moving tritium is for it to be captured by the pores in the beryllium microstructure. These pores already exist in the pebbles after their production and have comparatively larger sizes (see Figs. 16, 18-21) than the bubbles which are formed after tritium/hydrogen saturation. The single major peak in the TPD testing is caused by release of trapped tritium/hydrogen from the small bubbles and pores. So, the total tritium release value is defined by the amount of tritium/hydrogen which penetrated the bubbles/pores under the loading and then, accordingly, left the bubbles/pores as well as the pebbles during the TPD testing. In other words, the total tritium release is the result of a beryllium sample's ability to both absorb and retain the loaded tritium.

Fig. 23b shows a schematic for possible paths of tritium/hydrogen inside the pebbles during the TPD test. Most likely, the tritium leaving the bubbles/pores and reaching the nearest grain boundary prefers to move further along the boundary to the outer surface of the pebble. In that case, a key structural parameter for characterization of this motion can be considered as $r_1 \sim D_{\text{gr}}/2$ where D_{gr} is the average grain size. It can be supposed, however, that the tritium may also leave the pebble by moving directly to the outer surface, bypassing the available boundaries. In this case, the key parameter is $r_2 \sim D_{\text{peb}}/2$ where D_{peb} is the pebble diameter. The essential point is whether r_1 or r_2 defines the ability of a beryllium piece (pebble, sample, etc.) to retain its tritium.

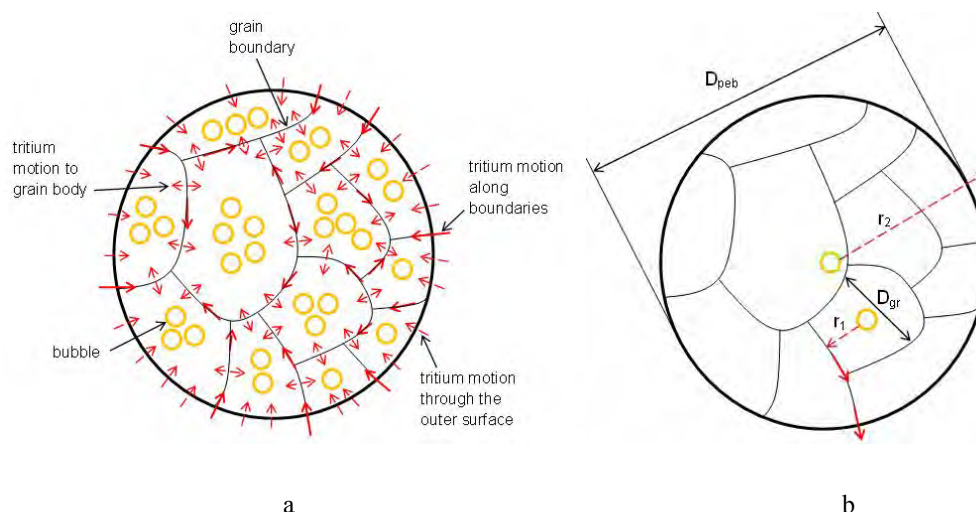


Fig. 22. Possible paths of tritium/hydrogen atoms into a beryllium pebble during thermal loading (a) and their outward motion during the TPD test (b).

Generally speaking, if the tritium atoms freed from structural traps take a two-stage path (in the beginning, a slow path to the nearest boundary, then a faster path along the boundaries to the surface of the piece), it would indicate that the r_1 parameter (or the grain size) is more important for comparison of different beryllium forms/grades. Alternatively, one may also consider a case in which the r_2 parameter (or the characteristic size, e.g. the pebble diameter) is more preferable for this purpose.

In this study, the results permit the assumption that the r_1 parameter plays a more significant role in this matter compared to r_2 . This assumption, however, demands more experimental substantiations. At least, comparing the I-220-H sample ($r_1 = 2.75 \mu\text{m}$, $r_2 = 1 \text{ mm}$), the 10-30 μm CM pebble ($r_1 \approx 20 \mu\text{m}$, $r_2 = 0.5\text{-}1 \text{ mm}$), the 0.5 mm REM pebble ($r_1 = 100\text{-}250 \mu\text{m}$, $r_2 = 0.25 \text{ mm}$), and the 1 mm FRM pebble ($r_1 = 100 \mu\text{m}$, $r_2 = 0.5 \text{ mm}$), a conclusion in favor of the r_1 parameter can be made. In particular, for the highest retention samples such as the I-220-H and the 1 mm FRM pebble, the I-220-H has comparatively much smaller grain size (5.5 μm to 200 μm). At the same time, the I-220-H has the larger overall size compared to the FRM pebble (height of 2 mm vs. 1 mm diameter, respectively). Intuitively, it seems that smaller grain size is the more important factor than the overall size, although it is impossible to say that at this point in full confidence.

Potential impact of BeO content in the beryllium samples on tritium release/retention was not considered in the discussion up to this point. According to Scaffidi-Argentina, the chemical trapping of tritium/hydrogen at BeO inclusions with formation of beryllium hydroxide in beryllium is possible [7]. Data from Fig. 2 for O-30-H and S-65-H grades, however, did not confirm possible influence of BeO content on tritium retention. In particular, despite its comparatively lower BeO content, O-30-H showed a higher total tritium release than S-65-H. There is, therefore, a greater likelihood that the more significant factor in this case is the differing grain size of the beryllium grades.

5. Conclusions

After high-temperature loading of various beryllium grades with different sample shapes with a tritium/ hydrogen gas mixture, and following the subsequent TPD tests, some conclusions can be suggested as follows:

1. Among the beryllium grades produced by hot isostatic pressing (HIP) by Materion Beryllium & Composites, the I-220-H has the best tritium release and retention properties. That characteristic is most likely defined by the smaller grain size of I-220-H compared to other grades.
2. Among the pebbles of irregular shape with various grain sizes produced by the crushing method (CM) by Bochvar Institute, the pebbles with the smallest grain size (10-30 μm) demonstrate the comparatively better tritium release and retention behavior.
3. Among the beryllium pebbles with the regular round shape in diameters of 1 mm made by the rotating electrode method (REM) by NGK Insulators, and by the fluoride reduction method (FRM) by Materion Beryllium & Composites, the FRM pebbles with 1 mm diameter show the better tritium release and retention properties.
4. Grain size can be considered as a key structural parameter for comparison and ranking of different beryllium materials on tritium release and retention properties. In particular, a beryllium grade with smaller grain size has a comparatively higher tritium release and lower tritium retention compared to the grades with larger grain size.

Acknowledgements

This work has been carried out within the framework of the EUROfusion Consortium and has received funding from the Euratom research and training programme 2014-2018 under grant agreement No 633053. The views and opinions expressed herein do not necessarily reflect those of the European Commission.

References

- [1] L.V. Boccaccini, L. Giancarli, G. Janeschitz, S. Hermsmeyer, Y. Poitevin, A. Cardella, E. Diegele, Materials and design of the European DEMO blankets, *Journal of Nuclear Materials* 329–333 (2004) 148–155.
- [2] V. Chakin, A. Moeslang, P. Kurinskiy, R. Rolli, H.-C. Schneider, E. Alves, L.C. Alves, Tritium permeation, retention and release properties of beryllium pebbles, *Fusion Engineering and Design* 86 (2011) 2338–2342.
- [3] V. Chakin, R. Rolli, P. Vladimirov, A. Moeslang, Tritium release from highly neutron irradiated constrained and unconstrained beryllium pebbles, *Fusion Engineering and Design* 95 (2015) 59–66.

- [4] S.P. Vagin, P.V. Chakrov, B.D. Utkelbayev, L.A. Jacobson, R.D. Field, H. Kung, Microstructural study of hydrogen-implanted beryllium, *Journal of Nuclear Materials* 258-263 (1998) 719-723.
- [5] V.N. Chernikov, V.Kh. Alimov, A.V. Markin, A.E. Gorodetsky, S.L. Kanashenko, A.P. Zakharov, I.V. Kupriyanov, Gas-induced swelling of beryllium implanted with deuterium ions, *Journal of Nuclear Materials* 233-237 (1996) 860-864.
- [6] N. Yoshida, S. Mizusawa, R. Sakamoto, T. Muroga, Radiation damage and deuterium trapping in deuterium ion injected beryllium, *Journal of Nuclear Materials* 233-237 (1996) 874-879.
- [7] F. Scaffidi-Argentina, Tritium and helium release from neutron irradiated beryllium pebbles from the EXOTIC-8 irradiation, *Fusion Engineering and Design* 58-59 (2001) 641-645.

Appendix Group Photos

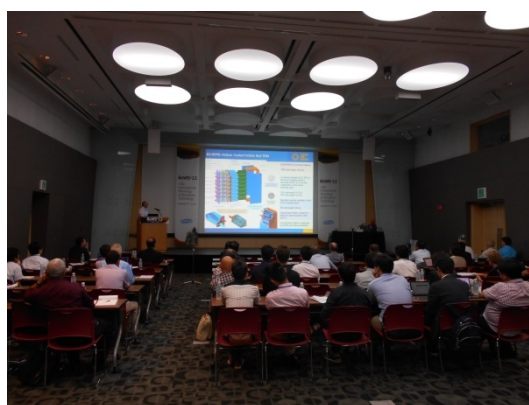


第12回ベリリウム技術に関する国際会議、平成27年9月10日～11日、濟州国際コンベンションセンター（ICCJEJU）

The 12th International Workshop on Beryllium Technology (BeWS-12), 10-11 Sep. 2015, International Convention Center Jeju (ICCJEJU)



パネルディスカッションの様子
Photo of the panel discussion



口頭発表の様子 1
Photo 1 of the oral presentation



口頭発表の様子 2
Photo 2 of the oral presentation



MDDMA 受賞者 (V. Chakin, KIT)
Winner of MDDMA
(Prof. Mario Dalle Donne Memorial
Award)

国際単位系 (SI)

表1. SI 基本単位

基本量	SI 基本単位	
	名称	記号
長さ	メートル	m
質量	キログラム	kg
時間	秒	s
電流	アンペア	A
熱力学温度	ケルビン	K
物質량	モル	mol
光度	カンデラ	cd

表2. 基本単位を用いて表されるSI組立単位の例

組立量	SI 組立単位	
	名称	記号
面積	平方メートル	m ²
体積	立方メートル	m ³
速度	メートル毎秒	m/s
加速度	メートル毎秒毎秒	m/s ²
波数	毎メートル	m ⁻¹
密度, 質量密度	キログラム毎立方メートル	kg/m ³
面積密度	キログラム毎平方メートル	kg/m ²
比体積	立方メートル毎キログラム	m ³ /kg
電流密度	アンペア毎平方メートル	A/m ²
磁界の強さ	アンペア毎メートル	A/m
量濃度 ^(a) , 濃度	モル毎立方メートル	mol/m ³
質量濃度	キログラム毎立方メートル	kg/m ³
輝度	カンデラ毎平方メートル	cd/m ²
屈折率 ^(b)	(数字の)	1
比透磁率 ^(b)	(数字の)	1

(a) 量濃度 (amount concentration) は臨床化学の分野では物質濃度 (substance concentration) ともよばれる。
 (b) これらは無次元量あるいは次元1をもつ量であるが、そのことを表す単位記号である数字の1は通常は表記しない。

表3. 固有の名称と記号で表されるSI組立単位

組立量	SI 組立単位			
	名称	記号	他のSI単位による表し方	SI基本単位による表し方
平面角	ラジアン ^(b)	rad	1 ^(b)	m/m
立体角	ステラジアン ^(b)	sr ^(c)	1 ^(b)	m ² /m ²
周波数	ヘルツ ^(d)	Hz		s ⁻¹
力	ニュートン	N		m kg s ⁻²
圧力, 応力	パスカル	Pa	N/m ²	m ⁻¹ kg s ⁻²
エネルギー, 仕事, 熱量	ジュール	J	N m	m ² kg s ⁻²
仕事率, 工率, 放射束	ワット	W	J/s	m ² kg s ⁻³
電荷, 電気量	クーロン	C		s A
電位差 (電圧), 起電力	ボルト	V	W/A	m ² kg s ⁻³ A ⁻¹
静電容量	ファラド	F	C/V	m ² kg ⁻¹ s ⁴ A ²
電気抵抗	オーム	Ω	V/A	m ² kg s ⁻³ A ⁻²
コンダクタンス	ジーメン	S	A/V	m ² kg ⁻¹ s ³ A ²
磁束	ウェーバ	Wb	Vs	m ² kg s ⁻² A ⁻¹
磁束密度	テスラ	T	Wb/m ²	kg s ⁻² A ⁻¹
インダクタンス	ヘンリー	H	Wb/A	m ² kg s ⁻² A ⁻²
セルシウス温度	セルシウス度 ^(e)	°C		K
光路長	ルーメン	lm	cd sr ^(c)	cd
放射線量	ルクス	lx	lm/m ²	m ⁻² cd
放射性核種の放射能 ^(f)	ベクレル ^(d)	Bq		s ⁻¹
吸収線量, 比エネルギー分与, カーマ	グレイ	Gy	J/kg	m ² s ⁻²
線量当量, 周辺線量当量, 方向性線量当量, 個人線量当量	シーベルト ^(g)	Sv	J/kg	m ² s ⁻²
酸素活性化	カタール	kat		s ⁻¹ mol

(a) SI接頭語は固有の名称と記号を持つ組立単位と組み合わせても使用できる。しかし接頭語を付した単位はもはやコヒーレントではない。
 (b) ラジアンとステラジアンは数字の1に対する単位の特別な名称で、量についての情報をつたえるために使われる。実際には、使用する時には記号rad及びsrが用いられるが、習慣として組立単位としての記号である数字の1は明示されない。
 (c) 測光学ではステラジアンという名称と記号srを単位の表し方の中に、そのまま維持している。
 (d) ヘルツは周期現象についてのみ、ベクレルは放射性核種の統計的過程についてのみ使用される。
 (e) セルシウス度はケルビンの特別な名称で、セルシウス温度を表すために使用される。セルシウス度とケルビンの単位の大きさは同一である。したがって、温度差や温度間隔を表す数値はどちらの単位で表しても同じである。
 (f) 放射性核種の放射能 (activity referred to a radionuclide) は、しばしば誤った用語で"radioactivity"と記される。
 (g) 単位シーベルト (PV, 2002, 70, 205) についてはCIPM勧告2 (CI-2002) を参照。

表4. 単位の中に固有の名称と記号を含むSI組立単位の例

組立量	SI 組立単位		
	名称	記号	SI 基本単位による表し方
粘力のモーメント	パスカル秒	Pa s	m ⁻¹ kg s ⁻¹
表面張力	ニュートンメートル	N m	m ² kg s ⁻²
角速度	ニュートン毎メートル	N/m	kg s ⁻²
角加速度	ラジアン毎秒	rad/s	m m ⁻¹ s ⁻¹ = s ⁻¹
熱流密度, 放射照度	ラジアン毎秒毎秒	rad/s ²	m m ⁻¹ s ⁻² = s ⁻²
熱容量, エントロピー	ワット毎平方メートル	W/m ²	kg s ⁻³
比熱容量, 比エントロピー	ジュール毎ケルビン	J/K	m ² kg s ⁻² K ⁻¹
比エネルギー	ジュール毎キログラム毎ケルビン	J/(kg K)	m ² s ⁻² K ⁻¹
熱伝導率	ジュール毎キログラム	J/kg	m ² s ⁻²
体積エネルギー	ワット毎メートル毎ケルビン	W/(m K)	m kg s ⁻³ K ⁻¹
電界の強さ	ジュール毎立方メートル	J/m ³	m ⁻¹ kg s ⁻²
電荷密度	ジュール毎立方メートル	V/m	m kg s ⁻³ A ⁻¹
電表面電荷	クーロン毎立方メートル	C/m ³	m ⁻³ s A
電束密度, 電気変位	クーロン毎平方メートル	C/m ²	m ⁻² s A
誘電率	クーロン毎平方メートル	C/m ²	m ⁻² s A
透磁率	ファラド毎メートル	F/m	m ³ kg ⁻¹ s ⁴ A ²
モルエネルギー	ヘンリー毎メートル	H/m	m kg s ⁻² A ⁻²
モルエントロピー, モル熱容量	ジュール毎モル	J/mol	m ² kg s ⁻² mol ⁻¹
照射線量 (X線及びγ線)	ジュール毎モル毎ケルビン	J/(mol K)	m ² kg s ⁻² K ⁻¹ mol ⁻¹
吸収線量率	クーロン毎キログラム	C/kg	kg ⁻¹ s A
放射線強度	グレイ毎秒	Gy/s	m ² s ⁻³
放射輝度	ワット毎ステラジアン	W/sr	m ⁴ m ⁻² kg s ⁻³ = m ² kg s ⁻³
酵素活性濃度	ワット毎平方メートル毎ステラジアン	W/(m ² sr)	m ² m ⁻² kg s ⁻³ = kg s ⁻³
	カタール毎立方メートル	kat/m ³	m ³ s ⁻¹ mol

表5. SI 接頭語

乗数	名称	記号	乗数	名称	記号
10 ²⁴	ヨタ	Y	10 ¹	デシ	d
10 ²¹	ゼタ	Z	10 ²	センチ	c
10 ¹⁸	エクサ	E	10 ³	ミリ	m
10 ¹⁵	ペタ	P	10 ⁶	マイクロ	μ
10 ¹²	テラ	T	10 ⁹	ナノ	n
10 ⁹	ギガ	G	10 ¹²	ピコ	p
10 ⁶	メガ	M	10 ⁻¹⁵	フェムト	f
10 ³	キロ	k	10 ⁻¹⁸	アト	a
10 ²	ヘクト	h	10 ⁻²¹	ゼプト	z
10 ¹	デカ	da	10 ⁻²⁴	ヨクト	y

表6. SIに属さないが、SIと併用される単位

名称	記号	SI 単位による値
分	min	1 min=60 s
時	h	1 h=60 min=3600 s
日	d	1 d=24 h=86 400 s
度	°	1°=(π/180) rad
分	'	1'=(1/60)°=(π/10 800) rad
秒	"	1"=(1/60)'=(π/648 000) rad
ヘクタール	ha	1 ha=1 hm ² =10 ⁴ m ²
リットル	L, l	1 L=1 l=1 dm ³ =10 ³ cm ³ =10 ⁻³ m ³
トン	t	1 t=10 ³ kg

表7. SIに属さないが、SIと併用される単位で、SI単位で表される数値が実験的に得られるもの

名称	記号	SI 単位で表される数値
電子ボルト	eV	1 eV=1.602 176 53(14)×10 ⁻¹⁹ J
ダルトン	Da	1 Da=1.660 538 86(28)×10 ⁻²⁷ kg
統一原子質量単位	u	1 u=1 Da
天文単位	ua	1 ua=1.495 978 706 91(6)×10 ¹¹ m

表8. SIに属さないが、SIと併用されるその他の単位

名称	記号	SI 単位で表される数値
バール	bar	1 bar=0.1MPa=100 kPa=10 ⁵ Pa
水銀柱ミリメートル	mmHg	1 mmHg=133.322Pa
オングストローム	Å	1 Å=0.1nm=100pm=10 ⁻¹⁰ m
海里	M	1 M=1852m
バイン	b	1 b=100fm ² =(10 ¹² cm ²) ² =10 ⁻²⁸ m ²
ノット	kn	1 kn=(1852/3600)m/s
ネーパ	Np	SI単位との数値的関係は、 対数量の定義に依存。
ベレル	B	
デシベル	dB	

表9. 固有の名称をもつCGS組立単位

名称	記号	SI 単位で表される数値
エルグ	erg	1 erg=10 ⁻⁷ J
ダイン	dyn	1 dyn=10 ⁻⁵ N
ポアズ	P	1 P=1 dyn s cm ⁻² =0.1Pa s
ストークス	St	1 St=1cm ² s ⁻¹ =10 ⁻⁴ m ² s ⁻¹
スチルブ	sb	1 sb=1cd cm ⁻² =10 ⁴ cd m ⁻²
フオト	ph	1 ph=1cd sr cm ⁻² =10 ⁴ lx
ガリ	Gal	1 Gal=1cm s ⁻² =10 ⁻² ms ⁻²
マクスウェル	Mx	1 Mx=1 G cm ² =10 ⁻⁸ Wb
ガウス	G	1 G=1Mx cm ⁻² =10 ⁻⁴ T
エルステッド ^(a)	Oe	1 Oe _e =(10 ³ /4π)A m ⁻¹

(a) 3元系のCGS単位系とSIでは直接比較できないため、等号「△」は対応関係を示すものである。

表10. SIに属さないその他の単位の例

名称	記号	SI 単位で表される数値
キュリー	Ci	1 Ci=3.7×10 ¹⁰ Bq
レントゲン	R	1 R=2.58×10 ⁻⁴ C/kg
ラド	rad	1 rad=1cGy=10 ⁻² Gy
レム	rem	1 rem=1 cSv=10 ⁻² Sv
ガンマ	γ	1 γ=1 nT=10 ⁻⁹ T
フェルミ	f	1 フェルミ=1 fm=10 ⁻¹⁵ m
メートル系カラット		1 メートル系カラット=0.2 g=2×10 ⁻⁴ kg
トル	Torr	1 Torr=(101 325/760) Pa
標準大気圧	atm	1 atm=101 325 Pa
カロリ	cal	1 cal=4.1858J (「15°C」カロリ), 4.1868J (「IT」カロリ), 4.184J (「熱化学」カロリ)
マイクロン	μ	1 μ=1μm=10 ⁻⁶ m

